

https://dspace.org/

Performance evaluation, exergy analysis and optimization of a natural gas combined cycle power plant retrofitted with pre-combustion capture and power-to-gas

Khesa, Neo

2020
https://hdl.handle.net/10539/31288

Downloaded from a DSpace repository. https://dspace.org/

PERFORMANCE EVALUATION, EXERGY ANALYSIS AND OPTIMIZATION OF A NATURAL GAS COMBINED CYCLE POWER PLANT RETROFITTED WITH PRE-COMBUSTION CAPTURE AND POWER-TO-GAS

Prepared by: Neo Khesa

Student number: 0405717G

Supervisor: Prof. J. L Mulopo

A thesis submitted to the Faculty of Engineering and the Built Environment, University of the Witwatersrand, Johannesburg, in fulfilment of the requirements for the degree of Doctor of Philosophy

10th March 2020

Declaration

I declare that this thesis is my own unaided work. It is being submitted for award of the degree of Doctor of Philosophy to the University of the Witwatersrand, Johannesburg. It has not been submitted before any degree or examination to any other University.



.....

(Signature of candidate)

23 day of October year 2020

Abstract

Carbon capture and sequestration (CCS), fuel switching (switching from coal to natural gas fired power) and renewables are some of the most promising means with which mankind can combat climate change.

Natural gas combined cycle (NGCC) power plants, which make use of both gas fired and steam cycle power generation are the most suitable and efficient fossil fuel power plants that can respond to renewable intermittence. Retrofitting the NGCC power plants with pre-combustion CSS allows the power plant to maintain its flexibility whilst capturing CO_2 because pre-combustion capture occurs upstream; decoupled from the power cycle.

Power to gas (PtG) is a promising technology being developed to overcome renewable intermittence through electrical energy storage (EES). It involves feeding off peak renewable energy to a water electrolyser which splits water into H_2 and O_2 before using the H_2 to valorise CO_2 from an industrial emission source into renewable methane in a methanation unit. The methanation unit is composed of Sabatier reactors that need to have their temperature controlled through recycle of their product gasses. The electrolysis can either be conducted at high temperature using an equimolar feed in water and CO_2 in what is known as high temperature co-electrolysis (HTCE) or it can be conducted at lower temperatures using only water as a feed in what is known as low temperature electrolysis (LTE). A major by-product from both processes is high temperature methanation heat from the Sabatier reactors.

This thesis presents studies on power to gas retrofitted to both LTE and HTCE electrolysers. The two processes were compared on: their ability to produce methane suitable for transportation in natural gas pipelines, their ability to produce renewable methane for onsite storage and their also compared on their energy and exergy efficiency's. The two setups were also retrofitted to a NGCC power plant which itself was retrofitted with a pre-combustion capture sorbent enhanced water gas shift carbon capture and sequestration upstream. No effort is made within the setup to make use of the available heat in the reforming section; with HRSG steam extraction supplying all the required steam for the reformer. This was done with the goal of determining the utility in retrofitting the high temperature methanation heat with the power plant steam cycle for waste heat recovery. The baseline and capture plant efficiencies were also determined and compared with what is stated in the literature.

A novel adaptation to an existing method for determining the physical exergy content of mass streams for flow sheet simulators was developed for ASPEN plus. The fundamental thermodynamic principles were first derived, before being interpreted according to the work of pioneers on the subject and then adapted for use in ASPEN plus. The adaptation involved developing a flow-sheet that could be used to acquire the important stream information from ASPEN plus which could then be used to conduct the calculations using excel or any other software of your choosing. A means of using the flowsheet to determine the thermal and pressure exergy components of the physical exergy of mass streams was also discussed.

Additionally, a novel means for the designing HRSG's for thermal power plants was developed that can be used with flowsheet simulators; a long-standing problem that has made research of power plant setups via simulation somewhat questionable until now. This technique was used to come up with a more accurate estimate for the efficiency penalty associated with pre-combustion carbon capture and sequestration on natural gas power plants. It was also used to determine the mechanical work that could be generated upon heat integration between the NGCC capture plant and the PtG retrofits. The technique developed could be implemented on a thermal power plant setup generating electricity from any hydrocarbon feed or waste heat stream with single or multi-pressure HRSG's. It will especially prove useful for fossil fuel power plants that utilise HRSG steam extraction to provide the necessary steam for their CCS retrofits as well as geothermal, and combined heat and power plants. It can also be used to determine the efficiency of nuclear power plants with greater accuracy through simulation.

The baseline NGCC power plant was simulated successfully and found to have a higher heating value [HHV] and lower heating value [LHV] efficiencies of 53.52% and 59.32% respectively which matched what is reported in the literature. Then the pre-combustion capture NGCC power plant was simulated and found to have lower than expected HHV and LHV efficiencies of 29.92% and 33.17% respectively. The LHV efficiency was 13.83% lower than what is reported in the literature of 47% and the HHV efficiency was 12.48% lower than what is reported in the literature of 42.4%. This disparity was attributed to the fact that a steam cycle flow-sheet for an NGCC pre-combustion capture power plant fitted with SEWGS is yet to be modelled in as much detail as it has in this thesis. This observation is backed by the exergy analysis (developed near the end of the study) conducted on the capture plant which found that the steam extracted for providing the necessary energy for the pre-combustion capture retrofit possess 35 MW of exergy. This amounts to 29.19% of the exergy available within the steam

that reports to the turbines which explains the larger than expected efficiency penalty. The accuracy with which the exergy analysis was able to account for the drop in power production proves that the method proposed for conducting exergy analysis for flow-sheet simulators works. There is much potential to improve the performance of the retrofitted plant, with the exergy analysis revealing that there is 42.29 MW in exergy within the mass stream reporting from the SEWGS flash unit within the pre-combustion capture retrofit. The pre-combustion capture retrofit contributes 13% to the irreversibility of the entire capture plant.

The molar composition of the product stream from the HTCE electrolyser is composed of: 38.8% carbon dioxide, 30.96% carbon monoxide and 30.24% hydrogen. This was attributed to the fact that only 48.3% of the water and CO_2 fed was converted in the electrolyser, to produce H_2, CO and O_2 in an equimolar ratio according to the main reaction. When this product is used as feed to the methanation unit only one Sabatier reactor was needed to completely react all the hydrogen that was fed in. The final product failed to meet the specifications for pipeline transport with a methane composition of only 21% and a carbon dioxide composition of 76.53%. The Sabatier reactor reached a temperature of 313℃ at the maximum Sabatier reactor recycle fraction of 0.9.

The composition of the product stream from the LTE electrolyser was composed entirely of hydrogen due to the fact that it had a conversion of 99.99% after being fed a stream composed of 100% water. Since the hydrogen stream reporting from the electrolyser is pure; all the carbon dioxide required for methanation was fed to first Sabatier reactor. To ensure that there was enough CO_2 and CO to satisfy the reaction stoichiometry for complete reaction within the methanation unit; the flow of water to the electrolyser was adjusted so that the molar flow in hydrogen from the unit is 4 times the molar flow of CO_2 added to three times the molar flow of CO coming from the capture plant. The molar composition of methane coming from the first Sabatier reactor was 70.87% and the temperature of the reactor was 436.16℃ at the maximum recycle fraction of 0.9. The product from the second Sabatier reactor was able to reach a composition in methane adequate for pipeline transport of 95 mole% for a recycle fraction of 78% at a reactor temperature of 259℃.

A heat integration study determined that integrating the methanation heat in the HTCE PtG process with the HRSG in the pre-combustion capture NGCC power plant would reduce the LHV efficiency of the power plant by 48.85% to -15.68% whilst storing renewable energy. Another heat integration study determined that integrating the methanation heat in the LTE PtG

process with the HRSG in the pre-combustion capture NGCC power plant would improve the LHV efficiency of the power plant by 6.32% to 39.49% whilst storing renewable energy. The LTE NGCC pre-combustion capture setup was deemed an adequate renewable adaptation to the traditional NGCC peaker plant. HTCE was deemed unsuitable as source of waste heat.

A thermodynamic study determined that the efficiency of the HTCE electrolyser and the entire HTCE PtG processes were 31.49% and 42.21% with methane storage. The same study determined that the efficiency of the entire HTCE PtG processes will be 43.45% when the methane is prepared for pipeline transport instead. The exergy efficiency of the HTCE electrolyser and that of the entire HTCE PtG process were 87.07% and 84% respectively with methane storage. And the exergy efficiency of the entire HTCE PtG processes was 87% when the methane is prepared for pipeline transport. The electrolyser was found to contribute the most to the irreversibility within the retrofit (73%) and as a recommendation it is suggested that the temperature of the processes be lowered.

Another study determined that the efficiency of the LTE electrolyser and that of the entire LTE PtG processes were 83.52% and 55.95% respectively with methane storage. When methane is prepared for pipeline transport instead the efficiency of the entire processes was 56.79%. The exergy efficiency of the LTE electrolyser and that of the entire LTE PtG retrofit were found to be 83.23% and 83.71% respectively with methane storage. The exergy efficiency of the entire processes was found to be 84.30% when the methane was prepared for pipeline transport instead. The electrolyser was again found to contribute most to the irreversibility within the retrofit (91%) and as a recommendation it is suggested that the temperature of the process also be lowered.

Acknowledgements

I would like to thank Professor Mulopo for helping me select this topic, for having faith that I'd eventually be able to complete the work and for all the assistance (both financial and advisory) he gave me along the way. I will also miss the frequent discussions that I had with Ntokozo, which always provided much needed relief from the stress associated with meeting the PhD deliverables. I'd also like to thank the University of the Witwatersrand school of Chemical and Metallurgical Engineering for allowing me to use their world class facilities, the NRF for funding the work, and friends and family who got me over the line with their advice and contributions along the way. I would also like to thank the people of Unihome.

This thesis is dedicated to my late parents; may their souls rest in peace.

Published work

Khesa, N., Mulopo, J, L., Performance evaluation, optimisation and exergy analysis of a low temperature electrolysis power-to-gas process using Aspen Plus. *Submitted to energy conversion and management.*

Khesa, N., Mulopo, J, L., Performance evaluation, Optimization and exergy analysis of a high temperature co-electrolysis power to gas process using Aspen Plus®-a model-based study. *Submitted to Applied Energy.*

ACKNOWLEDGEMENTS VI
PUBLISHED WORK VII
LIST OF FIGURES XII
LIST OF TABLES XV
NOMENCLATURE XVI
1. **INTRODUCTION** 1
1.1. MOTIVATION 3
1.2. RESEARCH QUESTIONS 5
1.3. RESEARCH OBJECTIVES 6
1.4. ORIGINALITY AND CONTRIBUTION TO KNOWLEDGE 7
1.5. SCOPE 9
REFERENCES 11
2. **LITERATURE REVIEW** 13
2.1. **ANTHROPOGENIC CLIMATE CHANGE** 13
2.1.1. FUTURE PROJECTIONS 13
2.1.2. CONTRIBUTION OF ENERGY SECTOR 16
2.1.3. MITIGATION OPTIONS AND SIGNIFICANCE OF $CO2$ 18
2.1.4. SIGNIFICANCE OF COAL NATURAL GAS, CCS & BECCS 22
2.2. **MATERIALS AND METHODS** 27
2.2.1. RANKIN CYCLE PLANTS 27
2.2.1.1. RANKINE CYCLE DESCRIPTION 27
2.2.1.2. RANKINE CYCLE EFFICIENCY 28
2.2.2. AIR HEATER, GAS TURBINE COMBINED CYCLES (AH-GTCC) 32
2.2.2.1 ADVANTAGES & DISADVANTAGES OF AH-GTCC 33
2.2.3. INTERNAL GASIFICATION, COMBINED CYCLE (IGCC) 33
2.2.3.1. IGCC ADVANTAGES & DISADVANTAGES 34
2.2.4. NATURAL GAS COMBINED CYCLE (NGCC) 36
2.2.4.1. NGCC ADVANTAGES 37
2.2.4.2. TRIPLE PRESSURE HRSG 42
2.2.5. CARBON CAPTURE AND SEQUESTRATION (CCS) 44
2.2.6. PRE-COMBUSTION CAPTURE SEWGS ON NGCC POWER PLANTS 46
2.2.7. POWER PLANT MITIGATION COSTS 49
2.2.8 **ELECTRICAL ENERGY STORAGE (EES)** 53
2.2.8.1. HYDROGEN STORAGE 54
2.2.8.2. PUMPED HYDROELECTRIC STORAGE (PHES) 54
2.2.8.3. COMPRESSED AIR ENERGY STORAGE (CAES) 55
2.2.8.4. BATTERY STORAGE 56
2.2.8.5. POWER TO GAS 60

2.2.8.5.1. ELECTROLYSERS 61
2.2.8.5.1.1. ALKALINE ELECTROLYSERS 62
2.2.8.5.1.2. ELECTROLYSER THERMODYNAMICS 63
2.2.8.5.1.3. LOW TEMPERATURE ELECTROLYSIS (LTE) 65
2.2.8.5.1.4. HIGH TEMPERATURE CO-ELECTROLYSIS (HTCE) 65
2.2.8.5.2. METHANATION 67
2.2.8.5.2.1. PROCESS LAYOUT 67
2.2.8.5.2.2. METHANATION REACTION 69
2.2.9. **EXERGY ANALYSIS** 71
2.2.9.1. SIGNIFICANCE OF THE SECOND LAW 71
2.2.9.2. CARNOT EFFICIENCY; EQUILIBRIUM & REVERSIBILITY 71
2.2.9.3. ENERGY BALANCE FOR A CONTROL REGION 72
2.2.9.4. ENTROPY PRODUCTION RATE FOR A CONTROL REGION 74
2.2.9.5. CHEMICAL EXERGY 76
2.2.9.6. PHYSICAL EXERGY 77
2.2.9.7. IRREVERSIBILITY AROUND A CONTROL REGION 77
2.2.9.8. EXERGY AND FLOW-SHEETING SIMULATORS 78
2.2.9.8.1. EXERGY OF MIXING 79
2.2.9.8.2. PHYSICAL EXERGY 79
2.2.9.8.3. CHEMICAL EXERGY 79
2.2.9.8.4. BENEFITS OF THE METHODOLOGY 80
REFERENCES 81
3. **MODELLING, DESIGN, AND OTIMIZATION OF AN NGCC AND NGCC PRE-COMBUSTION CAPTURE POWER PLANT** 86
3.1. **METHODOLGY** 86
3.1.1. NGCC FLOW-SHEET MODEL 86
3.1.1.1. NGCC PROCESS DESCRIPTION 86
3.1.1.1.1. GAS TURBINE AND RANKINE HIERARCHY 86
3.1.1.1.2. STEAM CYCLE AND HRSG HIERARCHY 87
3.1.1.2. NGCC PERFORMANCE SUMMARY AND STEAM CYCLE OPTIMIZATION 92
3.1.1.2.1. NATURAL GAS AND AIR FEED CHARACTERISTICS 92
3.1.1.2.2. COMPUTATIONAL SPECIFICATIONS 93
3.1.1.2.2.1. GAS TURBINE 93
3.1.1.2.2.2. TURBO MACHINERY UNITS 93
3.1.1.3. STEAM CYCLE DESIGN AND OPTIMIZATION 94
3.1.2. **NGCC PRE-COMBUSTION CAPTURE FLOW-SHEET MODEL** 95
3.1.2.1. NGCC PRE-COMBUSTION CAPTURE PROCESS DESCRIPTION 95
3.1.2.1.1. GHR-ATR-SEWGS AND ASU 95
3.2. RESULTS 99
3.2.1. NGCC RESULTS 99

3.2.2. NGCC PRE-COMBUSTION CAPTURE RESULTS 101
3.3. DISCUSSION 105
3.3.1. NGCC RESULTS DISCUSSION 105
3.3.2. NGCC PRE-COMBUSTION CAPTURE RESULTS DISCUSSION 106
REFERENCES 109

4. **MODELING, DESIGN & SIMULATION OF LTE & HTCE POWER TO GAS PROCESSES** 109

4.1. **METHODOLOGY** 110

4.1.1. POWER TO GAS FLOWSHEET MODEL 110
4.1.1.1. POWER TO GAS PROCESS DESCRIPTION 110
4.1.1.1.1. ELECTROLYSER PROCESS DESCRIPTION 110
4.1.1.1.1.1. HTCE ELECTROLYSER CHARACTERISTICS 111
4.1.1.1.1.2. LTE ELECTROLYSER CHARACTERISTICS 112
4.1.1.1.2. METHANATION UNIT PROCESS DECRYPTION 112
4.1.1.1.3. RESULTS 115
4.1.1.1.3.1. HTCE POWER TO GAS RESULTS 115
4.1.1.1.3.2. LTE POWER TO GAS RESULTS 120
4.1.1.1.4. DISCUSSION 126
REFERENCES 128

5. **HEAT INTEGRATION STUDY ON NGCC PRE-COMBUSTION CAPTURE HTCE AND LTE POWER TO GAS SETUPS** 128

5.1. **METHODOLGY** 128

5.1.1. HTCE, POWER TO GAS HEAT INTEGRATION METHODOLOGY 129
5.1.2. LTE, POWER TO GAS HEAT INTEGRATION METHODOLOGY 131
5.2. RESULTS 133
5.2.1. HTCE POWER TO GAS HEAT INTEGRATIONS RESULTS 133
5.2.2. LTE POWER TO GAS HEAT INTEGRATION RESULTS 135
5.3. DISCUSSION 136
5.3.1. HTCE & LTE POWER TO GAS HEAT INTEGRATION RESULTS DISCUSSION 136

6. **PTG - NGCC PERFORMANCE & EXERGY ANALYSIS** 138

6.1. **METHODOLGY** 137

6.1.1. PROPOSED METHOD FOR FLOW-SHEET SIMULATORS 138
6.2. RESULTS 142
6.2.1. NGCC & NGCC PRE-COMBUSTION CAPTURE POWER PLANT EXERGY ANALYSIS RESULTS 142
6.2.2. HTCE POWERT TO GAS PERFORMANCE & EXERGY ANALYSIS RESULTS 146
6.2.3. LTE POWER TO GAS PERFORMANCE & EXERGY ANALYSIS RESULTS 149
6.3. DISCUSSION 153
6.3.1. NGCC & NGCC PRE-COMBUSTION CAPTURE EXERGY ANALYSIS RESULTS DISCUSSION 154

6.3.2. HTCE POWERT TO GAS PERFORMANCE & EXERGY ANALYSIS RESULTS DISCUSSION. 154
6.3.3. LTE POWERT TO GAS PERFORMANCE & EXERGY ANALYSIS RESULTS DISCUSSION. 154
REFERENCES 158
APPENDIX A 157
APPENDIX B 172
APPENDIX C 188
APPENDIX D 194
APPENDIX E 203

List of figures

FIGURE 1: PROJECTIONS OF GREENHOUSE GAS CONCENTRATIONS AND TOTAL RADIATIVE FORCING FOR REPRESENTATIVE CONCENTRATION PATHWAYS 14
FIGURE 2: FIGURE DEPICTING AVERAGE SEA LEVEL RISE BETWEEN THE YEARS 1900 AND 2100 FOR 6 SIMULATED EMISSION SCENARIOS. 15
FIGURE 3: CONTRIBUTIONS MADE OVER FOUR DECADES TO THE CHANGE IN ANNUAL GREENHOUSE GAS EMISSIONS MADE BY: POPULATION GROWTH, GDP PER CAPITA, ENERGY INTENSITY AND CARBON INTENSITY OF THE ENERGY SUPPLY. TOTAL EMISSION CHANGES ARE INDICATED BY THE WHITE TRIANGLE. 17
FIGURE 4: SHARE IN IN GLOBAL PRIMARY ENERGY SUPPLY BETWEEN THE YEARS 1850 AND 2000 FOR BIOMASS, COAL, OIL, GAS, HYDRO, NUCLEAR AND RENEWABLES. 18
FIGURE 5: GROWTH IN TOTAL ANTHROPOGENIC GREENHOUSE GAS EMISSIONS (GT$CO2$EQ/YR) BETWEEN THE YEARS 1970-2010. 19
FIGURE 6: PROJECTED ELECTRICITY GENERATION BY COAL, RENEWABLES, GAS, NUCLEAR AND OIL FROM 1990 TO 2035. OECD STANDS FOR ORGANIZATION FOR ECONOMIC COOPERATION AND DEVELOPMENT, AND INCLUDES MOSTLY DEVELOPED NATIONS FROM AMERICA, ASIA AND EUROPE.. 23
FIGURE 7: INCREASE IN NET PRESENT VALUE OF MITIGATION COSTS BETWEEN 2015 AND 2100 (DISCOUNTED AT 5% PER YEAR) FOR FOUR DIFFERENT SCENARIOS. 24
FIGURE 8: DIAGRAM OF A PULVERISED COAL POWER PLANT. 28
FIGURE 9: IMPROVEMENTS SEVERAL ACTIONS WILL HAVE ON THE OVERALL PLANT EFFICIENCY. 29
FIGURE 10: TEMPERATURE ENTROPY DIAGRAM FOR STEAM AND WATER. 30
FIGURE 11: TEMPERATURE ENTROPY DIAGRAM FOR AN IDEAL AND AN ACTUAL RANKINE CYCLE 31
FIGURE 12: SIMPLIFIED BLOCK FLOW DIAGRAM OF AN IGCC POWER PLANT. 34
FIGURE 13: IDEALISED ENERGY FLOW DIAGRAM FOR IGCC. 35
FIGURE 14: SIMPLIFIED DIAGRAM ON AN NGCC PLANT. 37
FIGURE 15: TEMPERATURE ENTROPY DIAGRAM FOR COMBINED CYCLE PLANT 38
FIGURE 16: EFFECT OF LARGE SCALE WIND ENERGY GENERATION ON DAILY LOAD CURVE 39
FIGURE 17: IDEALISED DAILY LOAD CURVE WITH NGCC OCCUPYING INTERMEDIATE LOAD RANGE. 41
FIGURE 18: COMPARISON OF THE LEVELIZED COST OF ELECTRICITY (LCOE) BETWEEN DIFFERENT POWER PLANT SETUPS. 42
FIGURE 19: FLOW DIAGRAM OF HRSG. 43
FIGURE 20: FIGURE DEPICTING THE THREE PREDOMINANT CCS STRATEGIES AVAILABLE TODAY 46
FIGURE 21: SIMPLIFIED DIAGRAM OF AN NGCC POWER PLANT RETROFITTED WITH PRE-COMBUSTION CAPTURE. 47
FIGURE 22: SIMPLIFIED DIAGRAM OF A PRESSURE SWING ADSORPTION UNIT. 49

FIGURE 23: FIGURE SHOWING HOW EES WOULD AFFECT THE LOAD PROFILE OF A GRID WITH A LARGE SHARE IN RENEWABLES**.** 53
FIGURE 24: SIMPLE DIAGRAM OF PHES FACILITY.....55
FIGURE 25: SIMPLE DIAGRAM OF A CAES PLANT / FACILITY. 56
FIGURE 26: SIMPLE DIAGRAM OF A TYPICAL BATTERY.....58
FIGURE 27: SIMPLE DIAGRAM OF A SODIUM SULPHUR BATTERY. 59
FIGURE 28: SIMPLE BLOCK FLOW DIAGRAM ILLUSTRATING BASIC PRINCIPLE BEHIND PTG.....61
FIGURE 29: ALKALINE ELECTROLYSER DESIGN CONFIGURATIONS: (A) UNIPOLAR ELECTRODE GEOMETRY AND (B) BIPOLAR ELECTRODE GEOMETRY.....62
FIGURE 30: SIMPLIFIED DIAGRAM AN ELECTROLYSER OF BEG.....63
FIGURE 31: GRAPH DEPICTING CHANGE IN TOTAL ENERGY DEMAND (ΔH), FREE ENERGY CHANGE (ΔG) AND HEAT DEMAND ($T\Delta S$) FOR THE ELECTROLYSIS OF $CO2$ (DOTTED LINES) AND WATER (SOLID LINES).....64
FIGURE 32: SIMPLIFIED DIAGRAM OF A CO-COMBUSTION IN SOEC. 67
FIGURE 33: SIMPLE DIAGRAM OF METHANATION UNIT FED BY AN OXY-COMBUSTION POWER PLANT. 69
FIGURE 34: MOVEMENT OF A SYSTEM THROUGH A CONTROL REGION.....73
FIGURE 35: ENTROPY PRODUCTION IN A CONTROL REGION.....75
FIGURE 36: FLOW-SHEET OF NGCC BASELINE POWER PLANT.. 89
FIGURE 37: RANKINE HIERARCHY ASPEN-PLUS FLOW SHEET**.**.....90
FIGURE 38: DIAGRAM OF ASPEN PLUS FLOW-SHEET FOR THE STEAM CYCLE WITHIN THE HRSG HIERARCHY. 91
FIGURE 39: ASPEN FLOW-SHEET FOR AUTO THERMAL REFORMER, GAS HEATED REFORMER SEWGS RETROFIT.....97
FIGURE 40: FLOW-SHEET OF PRE-COMBUSTION CAPTURE NGCC POWER PLANT.....98
FIGURE 41: STEAM CYCLE HEAT LOAD AND TEMPERATURE DIAGRAM FOR THE BASELINE NGCC POWER PLANT.. 100
FIGURE 3.2.2A: REDIRECTED HRSG WATER VERSES GROSS MECHANICAL ENERGY OUTPUT 103
FIGURE 42: STEAM CYCLE HEAT LOAD VERSUS TEMPERATURE DIAGRAM FOR THE PRE-COMBUSTION CAPTURE NGCC POWER PLANT. 104
FIGURE 43: ASPEN FLOW-SHEET WITHIN THE RANKINE HIERARCHY OF THE PRE-COMBUSTION CAPTURE NGCC POWER PLANT. 105
FIGURE 44: GENERIC ASPEN PLUS FLOW-SHEET FOR BOTH THE HTCE AND LTE ELETROLYSER. 111
FIGURE 45: GENERIC DIAGRAM OF THE METHANATION UNIT. 114
FIGURE 46: GRAPH CHARTING SYNGAS CONVERSION AGAINST THE CO, $H2$ AND $CO2$ MOLE FRACTION IN THE PRODUCT STREAM FROM THE HTCE ELECTROLYSER FOR AN EQUIMOLAR FEED IN $H2O$ AND $CO2$.....116
FIGURE 47: GRAPH PLOTTING SABATIER RECTOR RECYCLE FRACTION AGAINST UNIT OPERATION TEMPERATURE AND PRODUCT METHANE COMPOSITION IN THE FIRST AND ONLY SABATIER REACTOR FOR HTCE (UNIT PU-02 IN FIGURE 45). 117

FIGURE 48: FLOW-SHEET FOR HTCE ELECTROLYSER. 118
FIGURE 49: FINAL FLOW-SHEET FOR HTCE PTG RETROFIT. 119
FIGURE 50: FINAL FLOW-SHEET FOR ENTIRE NGCC, CCS POWER PLANT RETROFITTED WITH HTCE, PTG. 120
FIGURE 51: GRAPH PLOTTING SABATIER RECTOR RECYCLE FRACTION AGAINST UNIT OPERATION TEMPERATURE AND PRODUCT METHANE COMPOSITION IN THE FIRST SABATIER REACTOR FOR LTE (UNIT PU-02 IN FIGURE 45).. 122
FIGURE 52: GRAPH PLOTTING SABATIER RECTOR RECYCLE FRACTION AGAINST UNIT OPERATION TEMPERATURE AND PRODUCT METHANE COMPOSITION IN THE SECOND SABATIER REACTOR FOR LTE (UNIT PU-05 IN FIGURE 45). 122
FIGURE 53: THIS GRAPH COMBINES THE RESULTS FROM THE FIRST SABATIER REACTOR (FIGURE 51) WITH THOSE OF THE SECOND ONE (FIGURE 52). 123
FIGURE 54: FINAL FLOW-SHEET FOR THE LTE ELECTROLYSER. **....** 124
FIGURE 55: FINAL FLOW-SHEET FOR LTE PTG RETROFIT 125
FIGURE 56: FINAL FLOW-SHEET OF NGCC POWER PLANT RETROFITTED WITH SEWGS CCS AND LTE PTG. 126
FIGURE 57: GCC FOR PTG HTCE RETROFIT HEAT INTEGRATION WITH NGCC, CCS STEAM CYCLE. 133
FIGURE 58: GCC FOR PTG LTE HEAT INTEGRATION WITH NGCC, CCS STEAM CYCLE HEAT SINKS. 135
FIGURE 59: FIGURE USED TO COLLECT DATA REQUIRED FOR EVALUATING THE EXERGY CONTENT OF A STREAM POSSESSING BOTH LIQUID AND GASEOUS PHASES. 140
FIGURE 60: DISTRIBUTION OF IRREVERSIBILITIES IN THE NGCC POWER PLANT IN FIGURE 36. 143
FIGURE 61: DISTRIBUTION OF IRREVERSIBILITIES IN THE PRE-COMBUSTION CAPTURE NGCC POWER PLANT SEEN IN FIGURE 40. 144
FIGURE 62: PROPORTION IN IRREVERSIBILITY'S AROUND THE PTG, HTCE RETROFIT. 149
FIGURE 63: PROPORTION IN IRREVERSIBILITY'S AROUND THE PTG, LTE RETROFIT. 153
FIGURE 64: DIAGRAM DEPICTING IRREVERSIBLE CHANGE OF STATE 157

List of tables

TABLE 1: COMPARISON OF DIFFERENT POWER PLANT SETUPS ON FLEXIBILITY 40
TABLE 2: KP VALUES FOR SABATIER REACTION BETWEEN THE TEMPERATURES OF $400K$ - $1000K$ .70
TABLE 3: MOLAR COMPOSITION OF METHANE FEED. 92
TABLE 4: MOLAR COMPOSITION OF AIR FEED. 92
TABLE 5: SPECIFICATIONS FOR THE TURBINES AND THE COMPRESSORS....93
TABLE 6: NGCC POWER PLANT PERFORMANCE SUMMARY 101
TABLE 3.2.2A: REDIRECTED HRSG WATER VERSES GROSS MECHANICAL ENERGY OUTPUT 102
TABLE 7: PLANT PERFORMANCE SUMMARY FOR THE NGCC, CCS POWER PLANT 106
TABLE 8: ELECTROLYSER CHARACTERISES FOR HTCE.... 111
TABLE 9: STREAM RESULTS ACROSS HTCE ELECTROLYSER.... 116
TABLE 10: STREAM CHARACTERISTICS OF THE PRODUCT FROM THE FIRST SABATIER REACTOR IN THE HTCE PTG SETUP 118
TABLE 11: STREAM RESULTS ACROSS THE LTE ELECTROLYSER 121
TABLE 12: TABLE CONTAINING THE STREAM RESULT FOR THE PRODUCTS EMANATING FROM THE LTE METHANATION UNIT. 123
TABLE 13: INLET AND OUTLET TEMPERATURES, HEAT DUTIES, COMPRESSION RATIOS, CP VALUES AND COMPRESSION WORK FOR THE PTG COMPRESSOR COMPRESSION STAGES IN HTCE. 130
TABLE 14: INLET AND OUT LET TEMPERATURES, HEAT DUTIES AND CP VALUES FOR ALL THE HEAT SINKS AND HEAT SOURCES IN THE METHANATION UNIT IN HTCE. 130
TABLE 15: INLET AND OUT LET TEMPERATURES, HEAT DUTIES, COMPRESSION RATIOS AND CP VALUES FOR THE PTG COMPRESSOR COMPRESSION STAGES IN LTE PTG RETROFIT. 132
TABLE 16: INLET AND OUT LET TEMPERATURES, HEAT DUTIES AND CP VALUES FOR ALL THE HEAT SINKS AND HEAT SOURCES IN THE METHANATION UNIT IN LTE PTG RETROFIT. 132
TABLE 17: PLANT PERFORMANCE SUMMARY OF PRE-COMBUSTION CAPTURE POWER PLANT UPON HEAT INTEGRATION WITH HTCE PTG RETROFIT 134
TABLE 18: PLANT PERFORMANCE SUMMARY FOR THE PRE-COMBUSTION CAPTURE NGCC POWER PLANT UPON HEAT INTEGRATION WITH ITS LTE PTG RETROFIT.... 136
TABLE 19: EXERGY CONTENTS OF MASS AND WORK STREAMS FLOWING TO AND FROM SYSTEM BOUNDARIES WITHIN THE BASELINE NGCC POWER PLANT DEPICTED IN THE ASPEN FLOW-SHEET IN FIGURE 36. 142
TABLE 20: IRREVERSIBILITYS AROUND SYSTEM BOUNDARIES STEAM CYCLE (SC) AND GAS TURBINE (GT) IN THE BASELINE NGCC POWER PLANT IN FIGURE 36. 142
TABLE 21: IRREVERSIBILITIES AROUND MAJOR SYSTEM BOUNDARIES IN PRE-COMBUSTION CAPTURE NGCC POWER PLANT SEEN IN FIGURE 40.... 144
TABLE 22: EXERGY CONTENTS OF MASS, WORK AND HEAT STREAMS FLOWING TO AND FROM SYSTEM BOUNDARIES WITHIN THE PRE-COMBUSTION CAPTURE NGCC POWER PLANT.... 145
TABLE 23: FIRST LAW THERMODYNAMIC EFFICIENCY OF THE PTG HTCE RETROFIT.... 147
TABLE 24: IRREVERSIBILITY'S AROUND SYSTEM BOUNDARIES WITHIN THE PTG HTCE RETROFIT. .. 148
TABLE 25: EXERGY EFFICIENCY OF THE PTG HTCE RETROFIT.... 148
TABLE 26: IRREVERSIBILITY'S AROUND SYSTEM BOUNDARIES WITHIN THE PTG LTE RETROFIT..... 150

TABLE 27: FIRST LAW THERMODYNAMIC EFFICIENCY OF THE PTG LTE RETROFIT 151
TABLE 28: EXERGY EFFICIENCIES OF THE FOR THE LTE, PTG PROCESS..... 152
TABLE E1: EXERGY ANALYSIS DATA FOR STREAM CC-H2 152
TABLE E2: EXERGY ANALYSIS CALCULATION FOR STREAM CC-H2 152

Nomenclature

P	Pressure
T	Temperature
T_0	Ambient temperature
W	Work
U	Internal energy
W_x	Shaft work
W_{CS}	Work due to volume change
v	Specific volume
C	Velocity
g	Gravitational acceleration
Z	Perpendicular height
$\dot{m}$	Mass flow
h	Enthalpy
S	Entropy
Π	Entropy of an isolated system
Q	Heat flow
T_r	Temperature of a thermal reservoir
$\dot{E}$	Mass stream exergy
$\dot{E}_{ph}$	Mass stream physical exergy
$\dot{E}_{ch}$	Mass stream chemical exergy
$\dot{E}_{mix}$	Mass stream exergy of mixing
$e^0_{ch,i}$	Standard chemical exergy
$\dot{E}^P$	Pressure exergy component
$\dot{E}^T$	Thermal exergy component
F	Molar flow
LHV	Lower heating value
HHV	Higher heating value
V	Vapour fraction
L	Liquid fraction

x	Mole fraction in the liquid phase
y	Mole fraction in the vapour phase

Abbreviations

EES	Electrical energy storage
PtG	Power-to-gas
PHES	Pumped hydroelectric storage
CAES	Compressed air energy storage
UEG	Unipolar electrode geometry
BEG	Bipolar electrode geometry
HTCE	high temperature co-electrolysis
LTE	Low temperature electrolysis
SOEC	Solid oxide electrochemical cell
RWGS	Reverse water gas shift reaction
SEWGS	Sorbent enhanced water gas shift
GHR	Gas heated reformer
ATR	Auto thermal reformer
BECCS	Bioenergy and carbon capture and sequestration
CCS	Carbon capture and sequestration
IGCC	internal gasification combined cycle
NGCC	Natural gas combined cycle
HRSG	Heat recovery steam generator
LCOE	Levelized cost of electricity
PC	Pulverised coal
HP	High pressure
IP	Intermediate pressure
LP	Low pressure
MH	Metal hydride
ASU	Air separation unit

Subscripts

0	Reference state
00	Dead state

1. Introduction

Climate change which comes as a result of global warming is today a critical issue that poses a threat to global food security and the planets biosphere. Global warming being a phenomena whereby average global temperatures rise because of an increase in insulating gases (greenhouse gases) in our atmosphere that trap the suns heat [1].

Rapid industrialisation and population growth have been fingered as the 2 major contributors to the recent exponential increase in greenhouse gases which we know are responsible for global warming. As much as half of the cumulative, anthropogenic CO_2 emissions since 1750 have occurred in the last forty years alone, with a projected 3.7 to 4.8℃ increase in global temperatures by 2100 if the trend continues. Just to keep the global temperature rise below 2℃ by 2100, its been predicted that global greenhouse emissions in 2050 will need to be as much as 40 to 70% lower than those recorded in 2010 [2].

The bulk of all emissions (25%) contributing to global warming were found to be produced by the energy sector in 2010, and the bulk of all growth in emissions (47%) between the years 2000 and 2010 have also been attributed to the energy sector. An explanation for this is that the sector provides primary energy for all other sectors, another explanation for its large contribution is that power generation derived from fossil fuel combustion is the primary means with which man produces power today. Though this means of producing power is mature cheap and reliable, its very carbon intensive: producing a large amount of CO_2 per unit power output. It should come as no surprise then, that it has been found through simulation that decarbonization of the energy sector is pivotal in maintaining greenhouse gas concentrations at a recommended 450 ppm by 2100. [2].

Options available for decarbonisation of the energy sector include: power plant efficiency improvements, fossil fuel switching, fugitive emission reduction during fossil fuel extraction, as well as carbon free energy production (renewables, nuclear energy, carbon capture and sequestration [CCS] and power to gas (PtG) [2], [3].

Though nuclear power plants are a proven, carbon free electricity option; their share in the global energy portfolio has declined over the years. This can be attributed to poor public perception (brought about by disasters such as Chernobyl [1986] and Fukishima [2011]), fears of nuclear proliferation, waste disposal issues and their high upfront cost. This makes them unattractive in liberalized markets which have access to cheap fossil fuel alternatives [2].

An adaptation which could eradicate CO_2 emissions from coal fired powerplants is carbon capture and sequestration (CCS). CCS is a process whereby CO_2 emissions from fossil fuel power stations are captured, transported and stored in geological formations, allowing man to continue using coal and meet future energy demands without all the adverse side effects associated with untreated CO_2 emissions [4]. The reason it's so attractive is the relative maturity of its sub processes [5], and because it extends the life of fossil fuel power plant infrastructure within the mitigation portfolio [6]. This makes CCS the best short term solution for reducing the power sectors emission contribution by the recommended 40 to 70% of 2010 baseline readings provided it does not have a major impact on the retrofitted plants net power output and cost of electricity.

Renewable sources of energy such as wind and solar energy are an ideal solution that emits little to no CO_2, they are the cheapest means of providing decentralised power, their cost is declining and efficiencies improving rapidly. Though renewable energy sources have seen significant efficiency improvements and growth; especially wind (which grew 5 fold) and solar energy (which grew 25 fold) between the years 2005 and 2012. They're not yet competitive. Most of their growth and improvement came about because of massive support through subsidies, feed in tariffs and quota obligations [2]. An added disadvantage is their intermittence (this comes about because renewable sources such as solar and wind energy fluctuate in strength wildly across the course of a day and a year) an attribute which further increases their cost [2], [7].

Fuel switching; specifically switching from coal to natural gas (NG), has the potential to reduce the CO_2 emissions from a fossil fuel power plant by as much as a half for every kilowatt-hour of electricity produced [2], [8], [9]. One reason for this is the lower carbon to hydrogen ratio in natural gas [10], [11]. Another reason is the higher efficiency (around 60%) [9], [12] one gets with natural gas power plants (specifically natural gas combined cycle plants (NGCC)) as opposed to even advanced supercritical coal fired plants (around 45%) [10]. NGCC power plants are also very flexible; an attribute that results from being gas fired [12].

Power to gas (PtG) is an innovative means with which to solve renewable energy intermittence through storage. It involves retrofitting a water electrolyser to a CO_2 emission source (in our case a NGCC power plant retrofitted with sorbent enhanced water gas shift (SEWGS) pre combustion capture) and methanating the CO_2 emissions using the hydrogen produced by the cell. Because the cell is fed renewable energy, this setup provides much needed flexibility to a grid by storing renewable energy during off peak hours as Methane, which can then be

converted back to electricity using the NGCC power plant during peak hours or at a later date [3], [7], [12], [13].

We have chosen to focus on PtG processes that make use of renewable Hydrogen to valorise CO_2 emissions from natural gas power plants into CH_4. The focus on natural gas stems from recent discoveries of the fossil fuel in Mozambique which power South Africa's gas fired power plants [14]. And although renewably acquired H_2 is a clean, high energy density fuel which shows great promise [12], [15]–[17]; the lack of H_2 infrastructure makes CH_4 for the moment more appealing. South African companies such as SASOL also have a great deal of experience in the production of synthetic fuels from syngas feeds. South Africa also has exceptional wind and solar resources which (because they're so intermittent) [2], [7] require increased grid flexibility (via storage) that can be achieved through PtG processes [7] and NGCC power plants [12].

1.1. Motivation

Since there are no commercial scale CCS power plants retrofitted with PtG, their costs for the moment can only be estimated using design studies or the few existing pilot projects. This is important since retrofitting a fossil fuel power plant with both CCS and PtG carries with it additional capital investment, alters the efficiency penalty and affects the cost of electricity (COE) from the said plant. Preliminary performance and cost estimates provide policy makers with the information they need to produce the most cost effective mitigation portfolios and determine appropriate carbon taxes and financial support required to support clean energy projects [2].

Several researchers and institutions have conducted studies that have looked to determine the performance and costs associated with the more popular CCS strategies. Much of this research has focused on PC, IGCC and NGCC plants [8], [9], [18]–[20]. A lot of the time the findings are in disagreement or vary significantly [8], [9], [12], [19], [21]. Several key assumptions that result in dissimilar performance and cost estimates are site specific [2]**,** and time dependant, such as: prevailing exchange rates, ambient conditions, the cost of fossil fuels, discount rates, the cost of materials, cost of labour and the fixed charge factor. Therefore predictions made about the performance and costs associated with thermal plants retrofitted with CCS need constant revision; and are only of real value within the regions the power plants are assumed to have been built. Thus far there are no up to date thermodynamic and economic assessments on thermal setups with the said characteristics (NGCC retrofitted with CCS) within the South

African context. Additionally, the most comprehensive assessments on natural gas capture plants to date have not conducted a detailed design on the characteristics of the power plant steam cycle [12], [18]. Without this, it is impossible to determine things like the magnitude of the capture penalty, the cost of the HRSG, the cost of electricity, and the water consumption with great accuracy.

Very little research has been conducted assessing the economic feasibility of PtG, or attempted to produce detailed process layouts of PtG [13], [22]. Additionally, nothing in the literature suggests that anyone has made an assessment on a power to gas setup together with an NGCC power plant retrofitted with CCS. The two processes complement one another; and we say this because NGCC is for the moment the cheapest means with which to produce electricity from synthetic natural gas. Additionally, NGCC is the most efficient thermal power plant setup that can run on synthetic natural gas. This backs the suggestion made by Hoekman, et al, [26] that the synthetic natural gas from PtG processes could be captured from an NGCC setup and recycled back into the power plant as supplementary fuel. It also backs opinions on NGCC being the ideal setup for providing the grid (once the share of renewable energy is high) with the flexibility it requires within the intermittent (volatile) region of the daily a load curve [12]**.** PtG is also restricted to regions in which there is ready access to CO_2 [3] and as mentioned earlier thermal power plants (such as NGCC) are the primary sources of CO_2 emissions in the world [2], [9]**.** Some have stated that the methanation heat could be used for steam and power generation, which is best achieved with the aid of a detailed steam cycle design which as stated in the paragraph before, was one of the goals set out in this study.

There is no clear consensus as to which is more efficient between LTE or HTCE. Some claim that HTCE (occurring at temperatures between 600℃ and 1000℃ [22]) is more efficient [13], [15]**.** However, many have also reported that the minimum amount of energy required to split water is equivalent to the standard free energy of the reaction taking place in the cell (ΔG°) [15], [16] with the remainder of what is required supplied as heat in order for the cell to achieve thermo-neutral operation (when the cell operates at the standard temperature of 25℃) [15]**.** This would occur at ambient temperature, which is far lower than the temperature at which HTCE or even LTE are reported to occur. There are very few studies providing detailed comparisons between HTCE and LTE electrolyser performances; and the figures i.e.(efficiencies of 70% for LTE [15], [16] and 50% for HTCE [17]) are also seemingly in disagreement with what's been reported.

With this in mind, it is the objective of the research which will be undertaken in this PhD to produce up to date performance assessments on a simulated NGCC power plant retrofitted with pre combustion CCS and a PtG unit producing methane. The system attributes we'll attempt to optimize from a performance standpoint include; the methanation operating conditions such as the optimum CO_2 feed fraction and flow rate, product recycle fractions and Sabatier reactor temperatures. Included will be an assessment on whether HTCE or LTE is superior within the setup. Additionally, an exergy analysis will be conducted comparing power plant layouts on exergy efficiency, and ranking important plant sections according to which have the greatest potential for improvement [23]. This will be done using ASPEN plus models similar to those developed by O'Brien, et al, [17], Redissi and Bouallou [13], Wittebrood, [12], Agerborg and Lingehed [24], Anantharaman, et al, [25], Hoekman, et al, [26] and the National Energy Technology Laboratory (NETL) report, DOE/NETL [27]. The Exergy analysis will be conducted using the method developed by Hinderink, et al, [27]. To accomplish this, the following research questions will need to be answered [24]–[27]:

1.2. Research questions

1. How would the auxiliary loads, gross power outputs, unit and overall efficiencies of a state of the art NGCC power plant be affected by typical Southern African ambient conditions (25℃ and 1 atm) and natural gas?
2. How would the auxiliary loads, gross power outputs, unit and overall efficiencies of this same NGCC power plant be affected when retrofitted with sorption enhanced water gas shift (SEWGS) pre-combustion capture?
3. What are the optimum conditions for the syngas feed to a HTCE and LTE, PtG methanation retrofit which acquires it's CO_2 from this pre combustion capture NGCC plant?
4. If there is ever a need for CH_4 storage how much energy would it require; and how would this effect the overall performance of both the HTCE and LTE, PtG setups?
5. Which is more efficient at producing H_2 of the flowrate and quality required for methanation between LTE and HTCE.
6. How are the auxiliary loads, gross power outputs, unit and overall efficiencies of the NGCC pre-combustion capture plant affected by the PtG methanation retrofit for both

LTE and HTCE when the electrolyser is storing renewable energy and the PtG processes heat is integrated with the pre-combustion capture NGCC power plant.

7. What are the irreversibilities across all major power plant sub sections in all three power plant setups (without taking into consideration heat integration)?

1.3. Research objectives

In order to answer the research questions the following objectives will need to be met:

1. Using Aspen plus, simulate a NGCC power plant using natural gas one would typically find in Southern Africa i.e.(Mozambique), under Southern African ambient conditions.
2. Design a SEWGS pre-combustion capture retrofit for the NGCC power plant using ASPEN plus.
3. Design a PtG methanation retrofit for the capture plant that can process a syngas stream with a flow rate in CO_2 equivalent to that which is produced by the retrofitted plants SEWGS unit.
4. Design a PtG process that accommodates methane storage.
5. Determine if LTE or HTCE is more efficient within the setup.
6. Determine and compare the capture penalties when the pre-combustion capture NGCC power plant is retrofitted to LTE and HTCE PtG (take heat integration into consideration).
7. Determine the exergy losses in all major unit operations and sub sections for the baseline NGCC power plant, the pre-combustion capture NGCC power plant, the HTCE PtG processes and the LTE PtG processes. Determine the exergy efficiencies of the HTCE PtG processes and the LTE PtG processes.

1.4. Originality and contribution to knowledge

The novel contributions made from the research outlined in this thesis are as follows.

i. A novel means with which to design HRSG's for thermal setups using flowsheet simulators was developed. Fixing a long-standing problem that has made research of power plant setups difficult until now. It enables the design of single and multi-pressure HRSG's with and without steam extraction with great accuracy. This technique was used to more accurately determine the efficiency penalty associated with pre-combustion capture sorbent enhanced water gas shift carbon capture and sequestration on an NGCC power plant. The results were also used to accurately evaluate the mechanical energy generated from waste heat recovery in PtG retrofits.

ii. An ASPEN plus process flowsheet was developed that was used to collect the required stream data for determining the exergy contents of material streams using a method developed by Hinderink, et al, [27]. Means with which one could determine the thermal and pressure exergy components of a material stream using the flowsheet were also described.

iii. The HHV and LHV of the baseline NGCC power plant were found to be 53.52% and 59.32% respectively. These were in close agreement with those referenced within the literature of 55.7% for the LHV efficiency and 50.2% for the HHV efficiency. An exergy analysis determined that the gas turbine and the steam cycle were found to be responsible for 84% and 16% of the irreversibility within the setup respectively.

iv. The HHV and LHV efficiencies of the NGCC pre-combustion capture power plant in which there is HRSG steam extraction for the pre-combustion capture retrofit, and no effort is made to utilise the heat evolved in the upstream reformer were found to be 29.92% and 33.17% respectively. The HHV efficiency was found to be 12.48% lower than that of referenced literature (42.4%), and the LHV efficiency was found to be 13.83% lower than that of referenced literature (47%). The disparity was attributed to the comprehensive way in which the steam cycle flow-sheet for the capture plant was modelled in this work. It can be asserted that this was the first study in which the processes was modelled comprehensively (i.e. mimicked the real life situation). An exergy analysis determined that the air separation unit was found to be responsible for 1% of the irreversibility, the steam cycle was found to be responsible for 8% of the irreversibility, the pre-combustion retrofit was found to be responsible for 13% of the

irreversibility, and the gas turbine was found to be responsible for 78% of the irreversibility within the setup.

v. A LTE PtG setup was developed that possessed two Sabatier reactors in its methanation unit. The recycle fraction for the first adiabatic Sabatier reactor was 90%, at a reactor operating temperature of 436.16℃. The recycle fraction for the second Sabatier reactor was 78%, at a reactor operating temperature of 259℃. The final synthetic methane product had a CH_4 composition of 95 mole%, which is suitable for transport and storage in pipeline networks. The first law thermodynamic efficiency of the LTE electrolyser and the entire LTE PtG setup were determined to be 83.52% and 55.95% respectively. The exergy efficiency of the LTE electrolyser and the entire LTE PtG setup were determined to be 83.23% and 83.71% respectively.

vi. A HTCE PtG setup was developed that possesses one Sabatier reactor in its methanation unit. The HTCE electrolyser model, which did not take into consideration the reversible water gas shift reaction (RWGS) produced a product stream composed of 38.80 mole% CO_2, 30.96 mole% CO, and 30.24 mole% H_2. The Sabatier reactor produced a product stream composed of 21.38 mole% CH_4 and 76.53 mole% CO_2 at the maximum recycle fraction of 90%. This was not adequate for transport and storage in pipeline networks. The first law thermodynamic efficiency of the LTE electrolyser and the entire LTE PtG setup were determined to be 83.52% and 55.95% respectively. The exergy efficiency of the LTE electrolyser and the entire LTE PtG setup were determined to be 83.23% and 83.71% respectively.

vii. The LTE PtG processes was integrated with the NGCC pre-combustion capture power plant. The required CO2 feed molar flow to the LTE PtG processes was made to match the CO2 molar flow of the stream produced by the capture plant. It was determined that heat integration between the high temperature Sabatier reactor heat and the pre-combustion capture NGCC power plant HRSG would raise the power plant HHV and LHV efficiencies to 35.62% and 39.49% respectively. It was concluded that the setup would prove useful as a renewable adaptation to a traditional peaker plant.

viii. The HTCE PtG processes was integrated with the NGCC pre-combustion capture power plant. It was found that 75% of the CO_2 fed to the HTCE electrolyser had to be acquired from an external source. This was due to the water feed to the LTE and HTCE electrolyser being used a basis for comparison between the two integrated PtG setups. It was determined that heat integration between the high temperature Sabatier reactor

heat and the pre-combustion capture NGCC power plant HRSG would lower the power plant HHV and LHV efficiencies to -14.15% and -15.68% respectively.

1.5. Scope

The thesis is divided into 6 chapters. Chapter 2 is a literature review, that starts with a review on the current climate crisis, and how it is that global warming brought on by an accumulation of greenhouse gasses in the atmosphere is responsible for this. The chapter also contains findings on the contribution that CO_2 emissions from fossil fuel powerplants have had that lead to the current climate crisis from literature, as well as the most popular means with which these emissions are being eradicated. The second part of the chapter is a review on conventional subcritical, as well as state of the art supercritical coal and natural gas power plants, with special attention being paid to natural gas combined cycle power plants. Also included is the role that combined cycle and conventional coal fired power plants will play in future electricity grids that will have a large share in renewable electricity. There is a review on carbon capture and sequestration strategies on coal and natural gas power plants, as well a section outlining the means with which the power plant CO_2 mitigation costs can be estimated. The chapter also covers various strategies for storing renewable electricity over short and long durations, with special attention being paid to electrolysis and power to gas. The chapter closes with a review on exergy analysis, that outlines how they are performed conventionally, as well as the ideal means with which to perform them when using flowsheet simulators.

Chapter 3 is a report on the modelling of the NGCC and the NGCC pre-combustion capture power plant using ASPEN plus. It contains a detailed description of the power plants, as well as a description on the design and optimization of the gas turbine and the HRSG. The design and optimization of the pre-combustion capture HRSG was of particular importance, as this was the first time that this unit operation was designed in such detail. This enabled the determination of a more accurate efficiency penalty for the capture plant, along with a more detailed heat duty verses temperature diagram for its HRSG.

Chapter 4 is a report on the modelling of LTE and HTCE PtG processes developed for the NGCC pre-combustion capture power plant using ASPEN plus. Detailed flowsheets were developed, and both processes were compared on their ability to produce synthetic natural gas ready for transport and storage in pipeline networks. Chapter 5 contains a report on a heat

integration study conducted on both setups; determining the improvements in efficiency that would come about if the PtG heat were to be utilised in the pre-combustion capture power plant. It was also an opportunity to utilise the more accurate heat duty verses temperature diagrams for the pre-combustion capture power plant HRSG that were produced in chapter 3 to determine the mechanical work that could be generated from heat integration in both cases.

Chapter 6 is a report on the first law and exergy efficiencies determined for the baseline NGCC power plant, the pre-combustion capture NGCC power plant, the HTCE PtG retrofit, and the LTE PtG retrofit. An ASPEN plus flow sheet was developed that could be utilised to collect important stream information required when conducting exergy analysis on ASPEN plus simulations. The flow sheet was developed to make use of a technique specifically developed for determining the physical exergy of mass flows from flowsheet simulators. Additionally, means with which the flowsheet could be used to determine the thermal and pressure exergy components of a stream were outlined.

References

[1] Houghton JT *et al.*, "Climate Change 2001: The Scientific Basis," 2001.

[2] O. Edenhofer *et al.*, "Climate Change 2014: Mitigation of Climate Change," *Work. Gr. III Contrib. to Fifth Assess. Rep. Intergov. Panel Clim. Chang.*, vol. 3, pp. 1–1435, 2014.

[3] M. Bailera, P. Lisbona, L. M. Romeo, and S. Espatolero, "Power to Gas-biomass oxycombustion hybrid system: Energy integration and potential applications," *Appl. Energy*, vol. 167, pp. 221–229, 2016.

[4] B. J. P. Buhre, L. K. Elliott, C. D. Sheng, R. P. Gupta, and T. F. Wall, "Oxy-fuel combustion technology for coal-fired power generation," *Prog. Energy Combust. Sci.*, vol. 31, no. 4, pp. 283–307, 2005.

[5] J. Herold, S. Rüster, and C. Von Hirschhausen, "Carbon capture, transport and storage in Europe: A problematic energy bridge to nowhere?," 2010.

[6] EU Commission, ""Winning the battle against global climate change"," Brussels, 2005.

[7] M. Bailera, P. Lisbona, L. M. Romeo, and S. Espatolero, "Power to Gas projects review: Lab, pilot and demo plants for storing renewable energy and CO_2," *Renew. Sustain. Energy Rev.*, vol. 69, no. October 2016, pp. 292–312, 2017.

[8] E. S. Rubin and H. Zhai, "The Cost of Carbon Capture and Storage for Natural Gas Combined Cycle Power Plants," *Environ. Sci. Technol.*, no. 46, pp. 3076–3084, 2015.

[9] IEAGHG, "CO_2 CAPTURE AT GAS FIRED POWER PLANTS," 2012.

[10] J. M. Beér, "High efficiency electric power generation: The environmental role," *Prog. Energy Combust. Sci.*, vol. 33, no. 2, pp. 107–134, 2006.

[11] South African department of science and technology, "The ten year plan for science and technology," 2008.

[12] B. J. Wittebrood, "System design and thermody namic evaluation of natural gas combined cycle (NGCC) systems including carbon capture & storage (CCS) and metal hydride based hydrogen storage .," 2015.

[13] Y. Redissi and C. Bouallou, "Valorization of carbon dioxide by co-electrolysis of CO_2/H_2O at high temperature for syngas production," *Energy Procedia*, vol. 37, pp. 6667–6678, 2013.

[14] PWC, "The gas equation: An analysis of the potential of the natural gas industry in South Africa," 2012.

[15] P. M. Diéguez, A. Ursúa, P. Sanchis, C. Sopena, E. Guelbenzu, and L. M. Gandía, "Thermal performance of a commercial alkaline water electrolyzer: Experimental study and mathematical modeling," *Int. J. Hydrogen Energy*, vol. 33, no. 24, pp. 7338–7354, 2008.

[16] A. S. Tijani, N. A. B. Yusup, and A. H. A. Rahim, "Mathematical Modelling and Simulation Analysis of Advanced Alkaline Electrolyzer System for Hydrogen Production," *Procedia Technol.*, vol. 15, pp. 798–806, 2014.

[17] J. E. O'Brien, M. G. McKellar, E. A. Harvego, and C. M. Stoots, "High-temperature electrolysis for large-scale hydrogen and syngas production from nuclear energy - summary of system simulation and economic analyses," *Int. J. Hydrogen Energy*, vol. 35, no. 10, pp. 4808–4819,

2010.

[18] DOE/NETL, “Carbon Capture Approaches for Natural Gas Combined Cycle Systems,” 2010.

[19] M. Kanniche, R. Gros-Bonnivard, P. Jaud, J. Valle-Marcos, J. M. Amann, and C. Bouallou, “Pre-combustion, post-combustion and oxy-combustion in thermal power plant for CO_2 capture,” *Appl. Therm. Eng.*, vol. 30, no. 1, pp. 53–62, 2010.

[20] DOE/NETL, “Cost and Performance Baseline for Fossil Energy Plants,” 2007.

[21] J. Amann, M. Kanniche, and C. Bouallou, “Natural gas combined cycle power plant modified into an O_2 /CO_2 cycle for CO_2 capture,” *Energy Convers. Manag.*, vol. 50, no. 3, pp. 510–521, 2009.

[22] Y. Zheng *et al.*, “A review of high temperature co-electrolysis of H_2O and CO_2 to produce sustainable fuels using solid oxide electrolysis cells (SOECs): advanced materials and technology,” *Chem. Soc. Rev.*, vol. 46, no. 5, pp. 1427–1463, 2017.

[23] T. J. Kotas, *The Exergy Method of Thermal Plant Analysis*. Essex: Butterworths, 1985.

[24] J. Agerborg and E. Lingehed, “Integration of Power-to-Gas in Gasendal and GoBiGas,” 2013.

[25] R. Anantharaman *et al.*, “CO_2 Enhanced Separation and Recovery,” 2007.

[26] S. K. Hoekman, A. Broch, C. Robbins, and R. Purcell, “International Journal of Greenhouse Gas Control CO_2 recycling by reaction with renewably-generated hydrogen,” vol. 4, pp. 44–50, 2010.

[27] A. P. Hinderink, F. P. J. M. Kerkhof, A. B. K. Lie, J. De Swaan Arons, and H. J. Van Der Kooi, “Exergy analysis with a flowsheeting simulator - I. Theory; calculating exergies of material streams,” *Chem. Eng. Sci.*, vol. 51, no. 20, pp. 4693–4700, 1996.

2. Literature review

2.1. Anthropogenic climate change

There is strong evidence that the recent increase in global mean temperatures is consequence of recent human industrial activity and its associated greenhouse gas emissions. When the earth receives incoming solar radiation from the sun, a fraction of it is re-emitted from the surface as outgoing solar radiation at longer (infrared) wavelengths. Greenhouse gasses are able to absorb a fraction of the outgoing solar radiation and re-emit it at higher altitudes and lower temperatures. This phenomenon is called positive radiative forcing and tends to warm the lower atmosphere and surface [1]. Typical greenhouse gasses include species such as, CO_2, CH_4, SO_2 and even water vapour just to name a few. Evidence tying human activity to the rise in temperatures has been found from the inspection of atmospheric air bubbles in ice cores drilled from ice sheets in cold regions such as Antarctica and Greenland. These ice sheets are several hundred thousand years old, providing a comprehensive record of atmospheric conditions over these time scales [2]. The exponential increase in greenhouse gas emissions has also been confirmed in studies conducted by the Intergovernmental Panel on climate change (IPCC). According to the (IPCC), half the cumulative anthropogenic CO_2 emissions between 1750 and 2010 have occurred in the last 40years. Results showed that greenhouse gas emissions between the years 2000 and 2010 grew at 1.0gigtonne carbon dioxide equivalent (GtCO_2eq) or 2.2%, whist those between the years 1970 and 2000 grew by only 0.4 (GtCO_2eq) or 1.3% [3].

2.1.1. Future projections

The Intergovernmental Panel on climate change (IPCC) has conducted comprehensive studies forecasting the degree to which average global temperatures will change for several mitigation scenarios. The mitigation scenarios are models that forecast changes in global temperatures with differing assumptions on the degree to which governments take action and collaboratively combat climate change. The mitigation scenarios are called Representative Concentration Pathways (RCPs). There are four predominant Representative Concentration Pathways: (RCP8.5), (RCP6.0), (RCP4.5) and (RCP2.6). RCP8.5 is a worst case scenario in which governments take little action to combat climate change. In this scenario its projected that greenhouse gas concentrations in the upper atmosphere exceed 450 parts per million (ppm) CO_2eq by 2030, and go on to reach up to 1300 ppm CO_2eq by 2100. This will result in an increase in global mean surface temperatures of between 3.7℃ and 4.8℃ compared to pre-

industrial levels. RCP2.6 is a best case scenario in which governments make a concerted effort to combat climate change. It's characterized by greenhouse gas concentrations in the upper atmosphere of around 450 ppm CO_2eq by the year 2100. In this scenario mean surface temperatures grow to less than 2℃ relative to pre-industrial levels. RCP6.0 and RCP4.5 are scenarios that lie between these two extremes [3]. Figure 1 is a graph showing predictions on the projected upper atmosphere greenhouse gas concentrations and total radiate forcing associated with each scenario from 2010 to 2090.

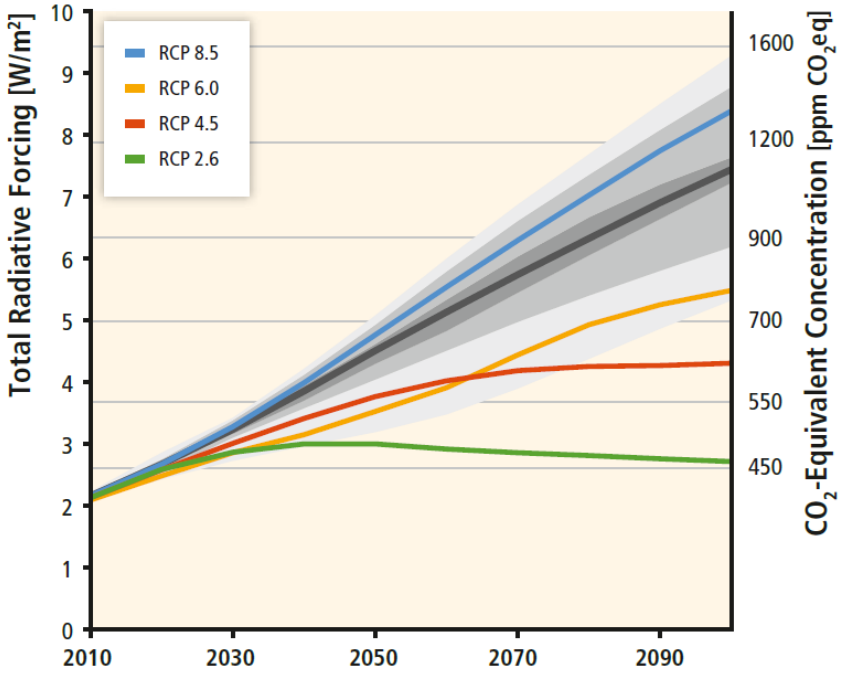


Figure 1: Projections of greenhouse gas concentrations and total radiative forcing for representative concentration pathways between the years 2010 and 2090. The solid lines represent medians, whilst the shading represents the degree of uncertainty or possible deviation [3].

If nothing is done to mitigate the projected high concentration in greenhouse gasses by 2100 (RCP 8.5) , simulations on global climate predict: extreme variations in precipitation, increased drought and flooding, enhanced El Nino, continued glacial retreat and sea level rise [1]. Average water vapor, evaporation and precipitation are expected to increase globally. However the precipitation won't be evenly dispersed, with excesses and shortfalls to usual patterns predicted from region to region. Furthermore, strong correlations have been drawn between seasonal variations and mean precipitation. For example it's projected that while precipitation will increase in both summer and winter in high latitude regions, a decrease in winter rainfall is predicted for Australia, Central America and South Africa. Simulations also predict

reductions in summer precipitation in mid continental areas and that flooding will increase in intensity and frequency across almost all regions. El Nino events, which are associated with an eastward migration in precipitation around the equatorial pacific are likely be enhanced in the event of extreme climate change. This would increase the risk of droughts and heavy flooding associated with these events in many regions. Models also predict an overall continued retreat in glaciers and ice caps, but much like global precipitation, regional discrepancies to the overall trend are predicted. For example while snow cover and sea ice are projected to decrease in the Northern Hemisphere, the Antarctic is projected to gain mass. This overall glacial and ice cap melting will result in notable sea level rise. Models predict this rise in sea level will be anywhere between 0.11m and 0.77m by 2100 (see figure 2) [1].

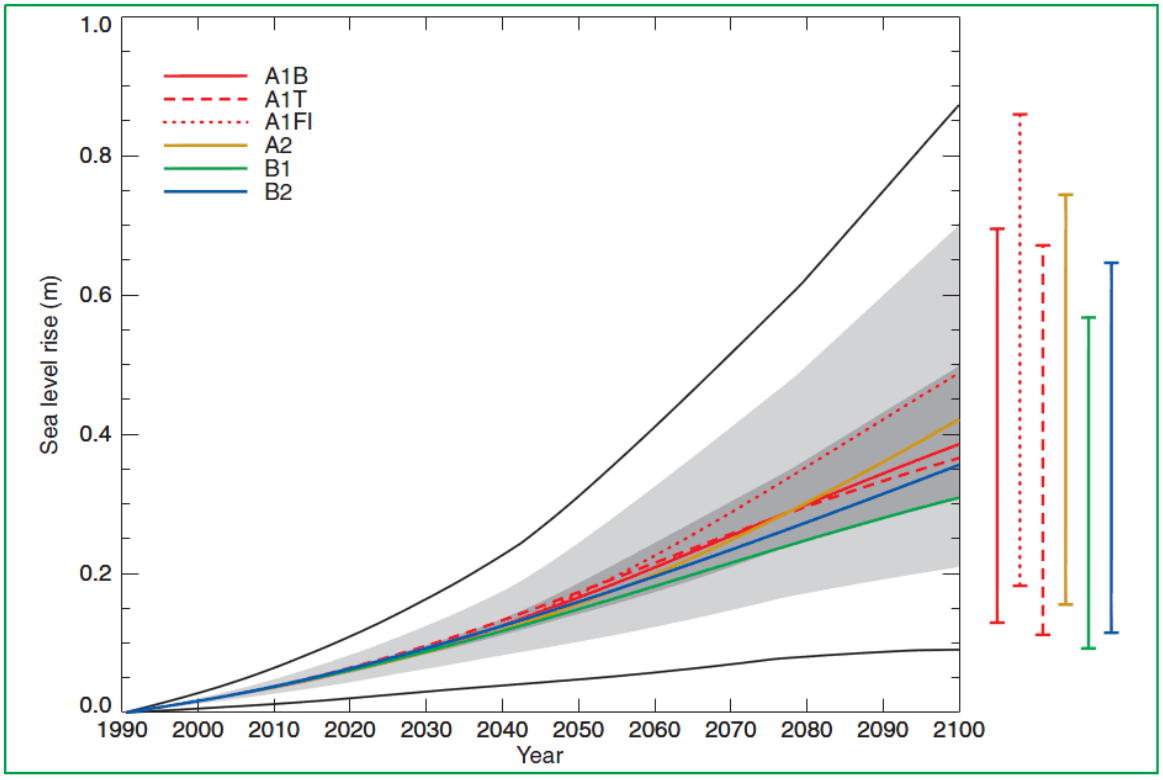


Figure 2: Figure depicting average sea level rise between the years 1900 and 2100 for 6 simulated emission scenarios. Scenario A1F1 assumes a fossil fuel intensive technology emphasis and has the highest predicted atmospheric CO_2 concentrations by 2100. Scenarios A1T and B1 broadly describe a world of reduced fossil fuel usage with greater reliance on clean resources. These two scenarios have the lowest predicted atmospheric CO_2 concentrations by 2100 [1].

These extreme weather patterns will change the prevailing conditions that man has become accustomed to for cultivation; threating sustainable development. These changes also affect

natural systems and the earth's biosphere. Rising sea levels will threaten many coastal regions and low lying islands.

2.1.2. Contribution of energy sector

The energy supply sectors contribution to the increase in annual greenhouse gas emissions between the years 2000 and 2010 was around 47%. This was greater than the contributions made by industry (30%), the transport sector (11%) and the buildings sector (3%) [3]. One of the reasons for its large contribution could be that it supplies much of the primary power to the industrial, building, and transport sectors. Another reason for this is that fossil fuel combustion is the primary means the energy supply sector produces power today. This method of producing power can be very carbon intensive; meaning the ratio of CO_2 emitted per unit of primary energy for it can be very high. Fuels with higher carbon content release a greater amount of CO_2 per unit power output. Two major fossil fuel combustion products are CO_2 and H_2O.

From the year 1850 to around the year 1975, there has been a gradual progression toward fuels with ever decreasing carbon content. From fuels such as biomass and coal with very high carbon content, to natural gas which has a very low carbon content and on to renewables which have near zero carbon content. This trend of gradual decarbonization has not been enough though to mitigate the exponential increase in greenhouse gas emissions in the upper atmosphere. There are several reasons for this, and one of them is population growth, which globally went from around 3billion at the beginning of the 20th century to around 7billion at the turn of the millennium. Its impact has been roughly linear though, with studies estimating that its contribution between the years 2000 and 2010 being roughly identical to those it made in the previous three decades. Another is economic growth, which had a more pronounced contribution with the current rapid economic growth in developing regions such as Asia, South America and the African continent. These two factors have outpaced improvements in energy utilization or energy intensity [3]. Energy intensity is the degree to which economic growth is dependent on energy output, See figure 3.

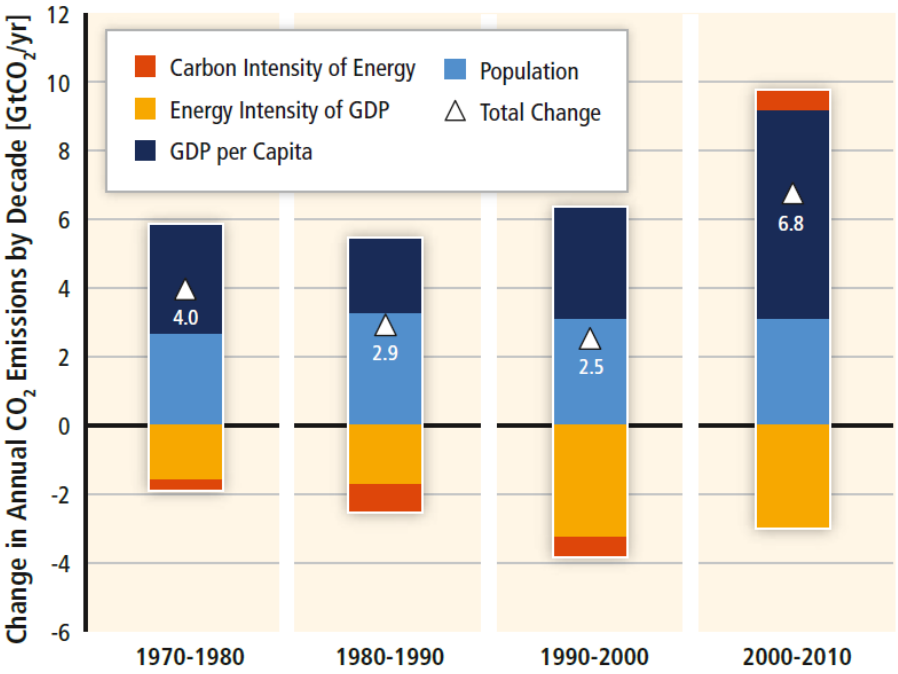


Figure 3: Contributions made over four decades to the change in annual greenhouse gas emissions made by: Population growth, GDP per capita, energy intensity and carbon intensity of the energy supply. Total emission changes are indicated by the white triangle [3].

Finally, fossil fuel combustion of fuels with high carbon content is popular among developing nations as means of producing electricity for their ever growing populations. This is because these nations are under severe pressure to lift large fractions of their population out of poverty and fossil fuels (especially coal) represent the cheapest means of powering their economies. One of the reasons for this is that fossil fuel combustion is a mature and reliable means of producing power today. Another reason is that fossil fuel reserves are also very abundant in these developing regions. For example it's estimated that oil reserves are up to 20,000EJ; about 120 times larger than current global production. Natural gas reserves are up to 120,000EJ; 1300 times larger than current production. While coal reserves are as high as 400,000EJ; 3500 time larger than production. At current rates of extraction these cheaper fossil fuel alternatives will only be depleted many decades from now. These factors have countered the long standing trend of gradual decarbonization of the world's energy supply. The effects of this can be clearly seen on figure 4. From the figure, its clear there has been a rapid decline in the use of non-commercial biomass from 1850 to the year 2000. Coal rose in usage till the year 1910 before declining steadily. This was accompanied by the steady rise of less carbon intensive alternatives such as Nuclear power. However coal has experienced resurgence around the 1980's for reasons outlined above [3].

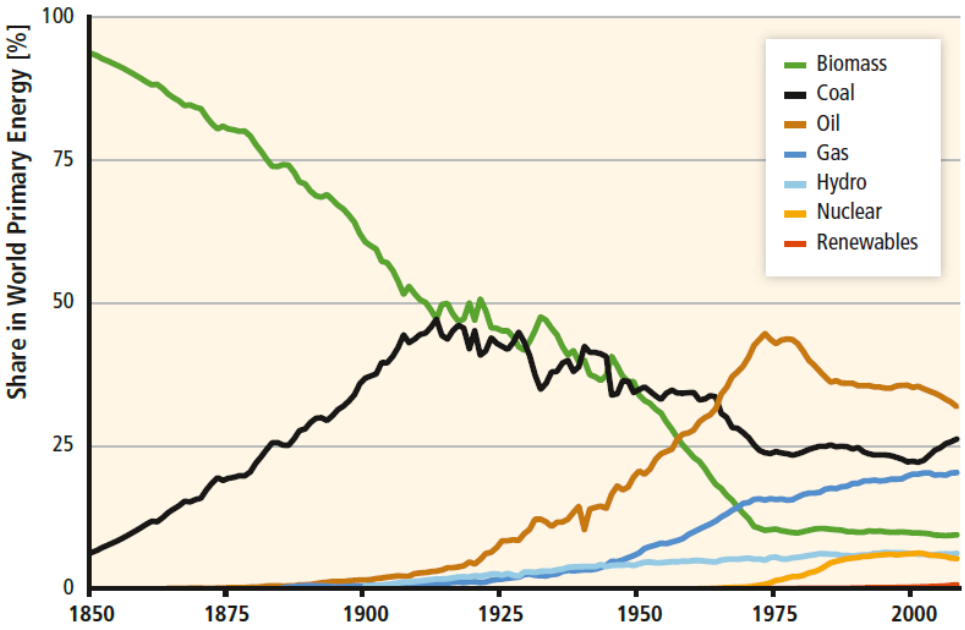


Figure 4: Share in in global primary energy supply between the years 1850 and 2000 for Biomass, Coal, Oil, Gas, Hydro, Nuclear and Renewables [3].

2.1.3. Mitigation options and significance of CO_2

As mentioned in the previous section the majority of the growth in greenhouse gasses in the upper atmosphere from the years 2000 to the present day can be attributed to the electricity sector. Of all the anthropogenic greenhouse gasses CO_2 is emitted the most. This is a long standing trend that has been observed since 1970 in which CO_2 emissions from fossil fuel combustion and industrial processes amount to 78% of all greenhouse gas emission growth from then until 2010 (see figure 5). For reasons stated in the previous section this trend is set to continue, in fact in baseline scenarios were no mitigating action is taken (i.e. RCP8.5), CO_2 emissions from the energy supply sector are projected to double or even triple by the year 2050 compared to the levels they were in 2010, which were around 14.4 (GtCO_2/year) [3].

It should come as no surprise then that in most optimistic mitigation scenarios (such as RCP2.6) decarbonization of electricity generation is considered pivotal in keeping greenhouse gas concentrations at acceptable levels in the upper atmosphere by 2100. These scenarios predict a required 90% reduction below 2010 levels in CO_2 emissions in the energy supply sector between the years 2040 and 2070 [3].

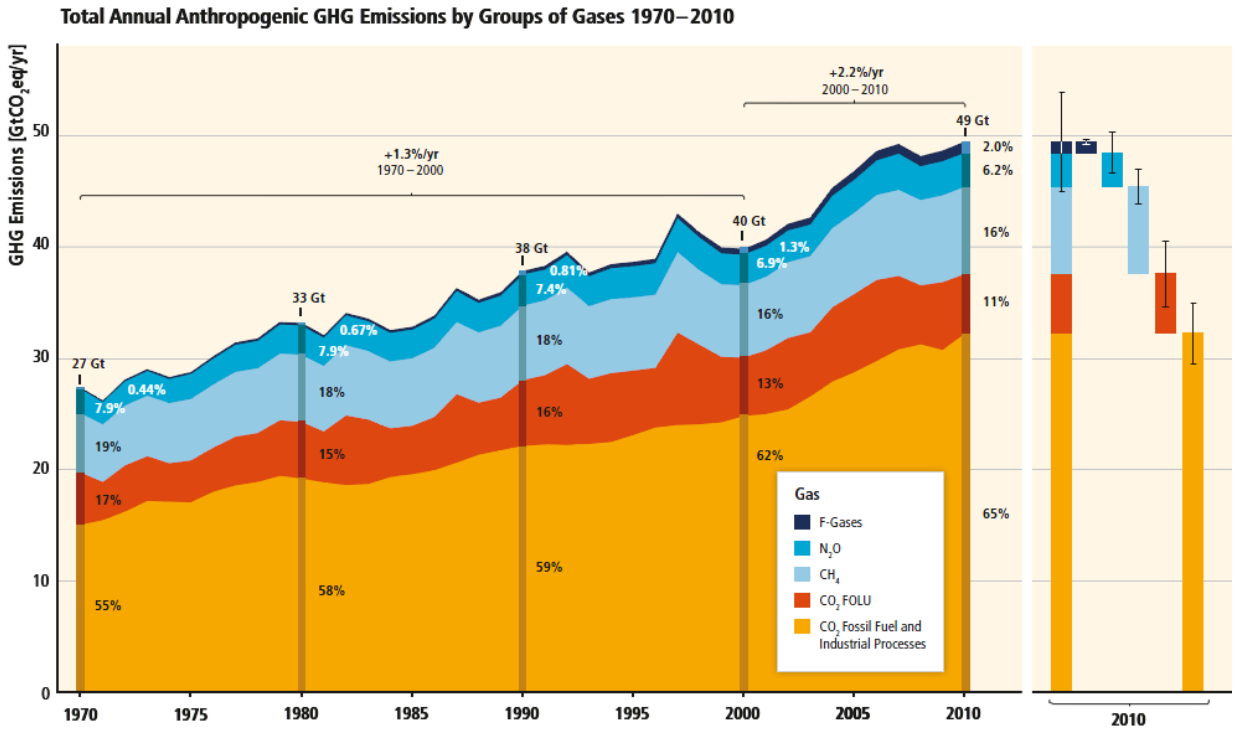


Figure 5: Growth in total anthropogenic greenhouse gas emissions (GtCO_2eq/yr) between the years 1970-2010. CO_2 emissions from fossil fuel combustion and industrial processes are depicted in orange, CO_2 emissions from forestry and other land use are depicted in red, CH_4 emissions are depicted in light blue, N_2O emissions are depicted in sky blue and fluorinated gasses are depicted in dark blue [3].

Decarbonization is also projected to occur more rapidly in the electricity generation sector; outpacing industry, buildings and the transport sectors. Optimistic mitigation scenarios predict that the share of low carbon energy sources (such as renewable energy, nuclear and CCS) will need to increase in share from 30% to more than 80% by 2050. With a complete phase out of fossil fuel power generation without CCS predicted by 2100 [3]. Apart from the sectors large contribution, this finding could be attributed to fact that the sector is a single point source from which all other sectors receive their primary energy.

Several options exist for energy sector decarbonisation: energy efficiency improvements, fossil fuel switching, renewable energy sources (solar energy, wind energy, hydroelectric power etc.), nuclear power, carbon capture and sequestration (CCS) and fugitive emission reductions in fuel extraction [3]. Three that carry the greatest potential to decrease energy sector CO_2 emissions are; renewable energy sources, nuclear power and CCS. Special attention will be paid to fuel switching since South Africa is among a select number of countries that have access to cheap natural gas.

Renewable energy consists of all non-emitting sources that represent an idealized means of achieving the long term emissions targets set in optimistic climate models. What makes them ideal is that many of them are associated with zero emissions and are acquired from non-depleting sources. For instance bioenergy produces liquid fuels from constantly renewable biomass. Hydroelectric power generates electricity from renewable water sources. Wind turbines produce electricity from renewable prevailing winds. Photo voltaic cells generate electricity by converting renewable solar radiation to electricity. Some of the advantages associated with renewable energy include: improved energy security, drastically reduced emissions, sustainable economic growth and improved access to electricity in remote regions where traditional grid extensions would be too costly [4]. Renewable energy sources have improved substantially in performance, availability and cost over the years. Over half of new electricity generation added globally in 2012 was sourced from renewable energy technologies [3]. Despite the global financial crisis of 2008; renewable energy sources experienced rapid growth in 2009 compared to cumulative installed capacity the previous year. Wind power experienced an increase of 32% (38 Gigawatts (GW)), hydropower experienced an increase of around 3% (31 GW), photovoltaics supplying power to the grid experienced a 53% rise (7.5GW), geothermal power 4% (0.4GW added) and solar hot water heating grew by 21% (31GW) [5]. This growth though is reliant on massive subsidies doled out by governments concerned about long term energy security, human health and climate change. It's estimated that over $101 billion was paid in subsidies to renewables in 2012, an increase of 11% to those paid in 2011. Projections predict an increase to over $220 billion in subsidies by the year 2035 [4]. An added disadvantage is their intermittence; (this comes about because renewable sources such as solar and wind energy fluctuate in strength wildly across the course of a day) an attribute which further increases their cost which can be mitigated through electrical energy storage (EES) [3], [6], [7].

Nuclear energy is a mature technology that's already supplying cheap energy to many parts of the world. It could drastically reduce global greenhouse gas emissions if it were widely implemented. This is because it produces no CO_2 emissions. In the European Union for example it's estimated to have displaced around 300million tonnes of CO_2 that would have been emitted from fossil fuel power plants with similar output [8]. However, its share in the global energy mix has declined steadily from around 17% in 1993, to around 11% in 2012 [3]. This can be attributed to a variety concerns centered on: waste disposal, safety, security and poor public opinion. Safety concerns stem from the many nuclear power plant accidents over

the years (such as the Chernobyl disaster (26 April 1986), and the Fukishima disaster (11 March 2011)). These accidents have the potential to render regions in which they occur uninhabitable for thousands of years. Nuclear proliferation is another safety concern that could threaten global security. There are also major waste disposal concerns over the entire nuclear fuel chain, from mining to decommissioning and fuel storage [8]. Ongoing research into new fuel cycles, reactors, waste disposal and safety may make this technology a more viable in the future [3].

Carbon capture and sequestration (CCS) involves capture of carbon dioxide from fossil fuel power plants, compression of the pure carbon dioxide stream followed by storage in geological formations. The methods employed to capture the CO_2 include downstream chemical absorption of the CO_2 from flue gasses using solvents, physical absorption of the CO_2 fraction of a gasification product that's undergone shift reaction and finally combustion of fossil fuel in a near pure oxygen atmosphere to produce a near pure CO_2 flue gas ready for compression and storage. A major advantage associated with these processes is the relative maturity of their subsystems, for example chemical absorption has been used as a means to capture CO_2 emissions from ammonia plants since the 1980's. High temperature fuel combustion in near pure oxygen atmospheres has been used by the glass and steel industries for some decades now [9]. Another major advantage is that it extends the lifespan of fossil fuel power plants within the mitigation portfolio. Providing a relatively affordable climate mitigation option that serves as an energy bridged, that can smooth the transition to renewable forms of non-emitting energy sources [8]**.** A challenge associated with these processes, is that they have yet to be fully implemented on a commercial scale. So many operational issues that can only be identified and solved through experience are unknown. Rules and regulations on CO_2 storage and monitoring in geological formations need to be established. There are also questions on the operational safety and long term integrity of CO_2 storage. The biggest challenge though is finding means of mitigating their associated efficiency penalties relative to their unabated counterparts. Solutions to these challenges are not that far off though. Large scale pilot plants are likely to be built in places such as the United States in the not too distant future. A lot of ongoing research is currently under way that attempts to find means of ensuring the integrity of CO_2 wells. Much research is under way on means of reducing CCS efficiency penalties through well-established methods such as heat integration, exergy analysis and mathematical optimization. Supercritical plants that will have efficiencies high enough to offset the efficiency penalties associated with CCS are already at the demonstration phase. Therefore, CCS is likely to become competitive far sooner than renewables. This is also corroborated by various climate

mitigation models [3]. This makes CCS the best near term climate mitigation option for the global energy sector.

Fuel switching; specifically switching from coal to natural gas, has the potential to reduce the CO_2 emissions from a fossil fuel plant by as much as a half for every kilowatt-hour of electricity produced [3], [10], [11]. One reason for this is the lower carbon to hydrogen ratio in natural gas [3], [12]. Another reason is the higher efficiency (around 60%) [11], [13] one gets with natural gas power plants (specifically natural gas combined cycle power plants (NGCC)) as opposed to even advanced supercritical coal fired plants (around 45%) [12].

2.1.4. Significance of coal Natural gas, CCS & BECCS

Of the fossil fuels that have contributed to the slowing in the decarbonization of the global energy sector, coal is the most abundant. It accounts for over 55% of the world's total fossil fuel reserves. Coal reserves that are economically and technically exploitable at today's prices were determined to be around 1 040 billion tonnes at the end of 2011. These exploitable reserves grew by nearly 35 billion tonnes in 2011, with notable additions coming from countries such as: Australia and Indonesia. Globally, coal reserves and resources are well distributed. Coals low cost and accessibility has resulted in it becoming the fossil fuel of choice in developing regions. This would explain why globally its use has increased substantially, satisfying nearly half of the increase in global energy demand over the decade ending in 2012. This growth in coal use in the developing world is predicted to continue into the near future although at a slightly slower rate than in decades passed. Despite the fact that coal use is decreasing in the developed world (driven by the desire to decarbonize through renewables) it's not enough to offset this continuing growth in the developing world. This explains why projections have indicated that coals contribution to global electricity generation by 2035 will be 33%. This would maintain its position as the leading fuel source for the energy sector (see figure 6) [4].

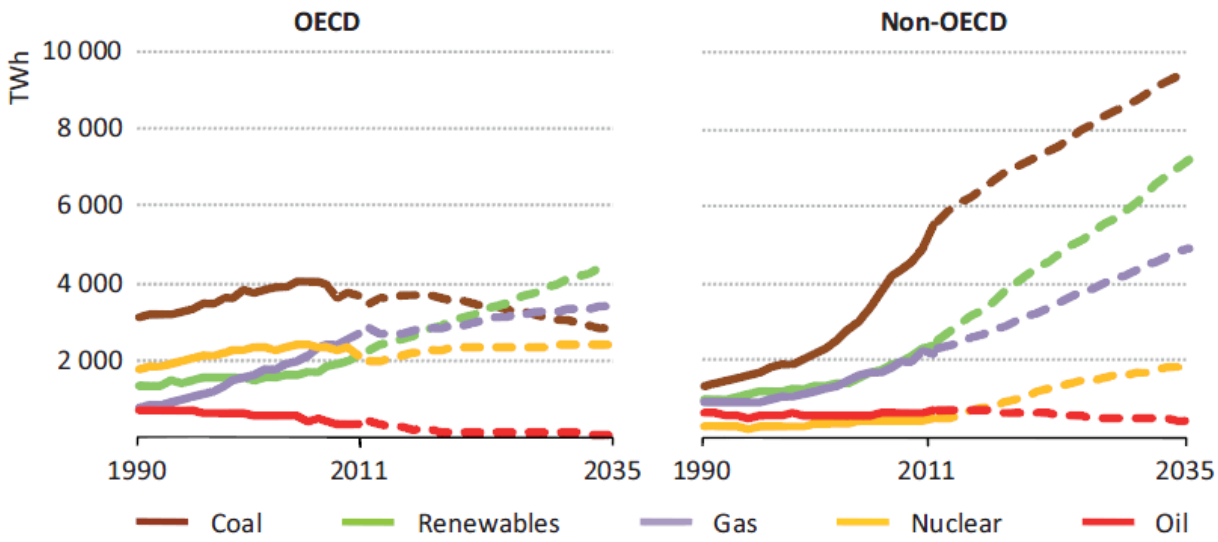


Figure 6: Projected electricity generation by Coal, Renewables, Gas, Nuclear and oil from 1990 to 2035. OECD stands for Organization for Economic Cooperation and Development, and includes mostly developed nations from America, Asia and Europe. This graph was lifted off [4].

Coal use has major drawbacks though. Its high carbon content (highest among all fossil fuels) means it releases a large amount of CO_2 per unit energy released. As a result coal fired power plants are largely to blame for the rising anthropogenic CO_2 emissions that have been recorded over the years. A better alternative would be fuel switching via gas fired power generation, which at present accounts for around 20% of the world's electricity production, and like coal has been a popular means with which to generate electricity the world over [11]. Here, methane is used to generate electricity using a natural gas combined cycle (NGCC) power plant [13]–[16]. One of the reasons it's so much better is the fuel [17]: natural gas with its lower fuel carbon content [3], [12], [18] (15.3gC/MJ compared to 26.2gC/MJ for sub-bituminous coal [3]) emits half the emissions of a coal fired plant per unit work output [3], [10], [18]. For example, if you were to replace a coal fired power plant (emitting around 850-900g/kWh) with an NGCC power plant (emitting around 330-340g/kWh) one would avoid emitting up to 3 million metric tons of CO_2 emission per year for every 1000MW of capacity [11], [18]. The shale gas revolution will see gas play a significant role in the energy mix, with the share of

unconventional gas growing significantly worldwide [3], [11].

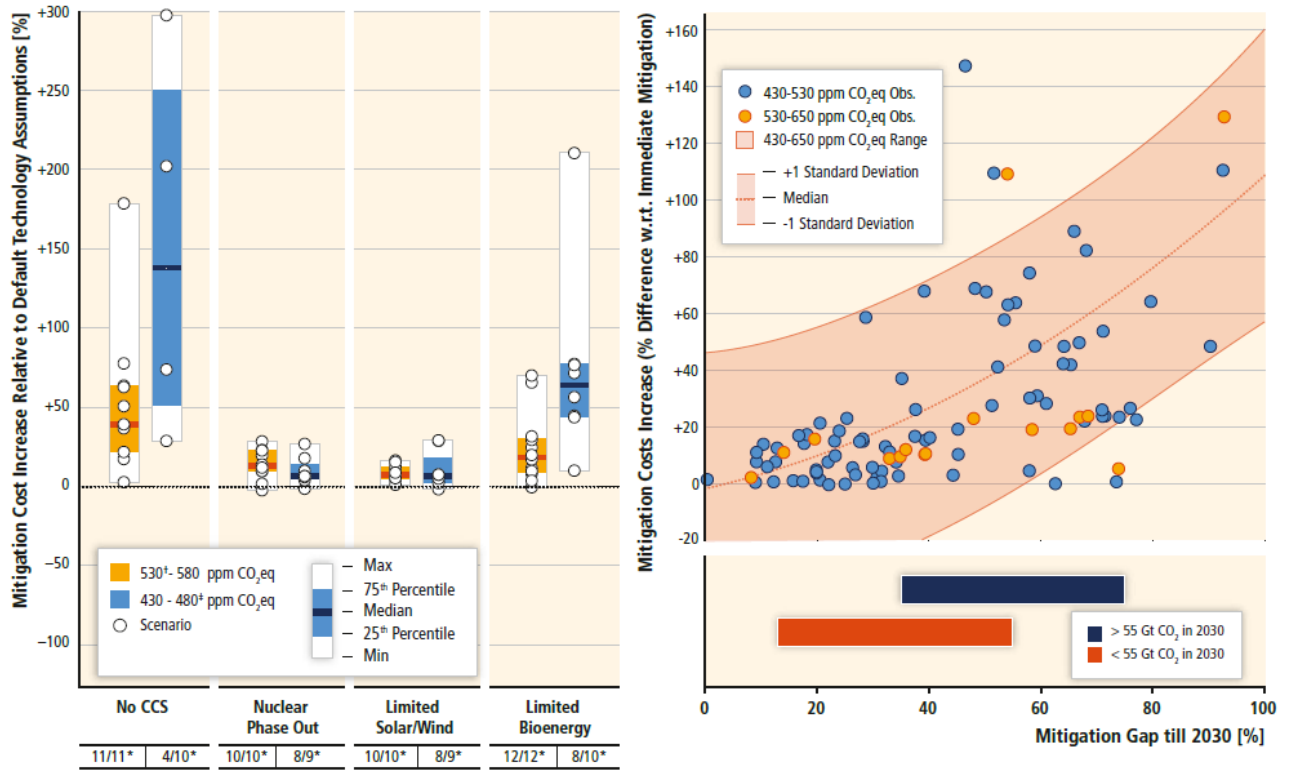


Figure 7: The left panel shows the predicted increase in net present value of mitigation costs between 2015 and 2100 (discounted at 5% per year) for four different scenarios: A scenario with no CCS, a scenario with no Nuclear energy, a scenario with no Solar or Wind energy and a scenario with limited Bioenergy. The right panel charts long term mitigation cost increases against mitigation gap. The mitigation gap defined as the difference in cumulative CO_2 emission reductions between scenarios where mitigation happens immediately and those where it's delayed till 2030. These graphs were lifted from [3].

Among the major contributors to this increase are the United Sates (here the share in unconventional gas more than doubled between the years 2000-2011 reaching 67%), Qatar, Iran, China, Norway and Russia [3]. Additionally, gas supplies are assured in Europe because of planned pipelines from new sources such as the Nord stream and Nabucco as well as supplies form existing natural gas terminals such as those in Rotterdam [18]. This increase in popularity is clearly depicted in figure 6 from 1990 to 2011, and is predicted to increase till the year 2035 [4].

Because CCS can be retrofitted to both new and existing plants, it can be implemented without the need to replace all of the preexisting fossil fuel power generation capacity. This, along with

its relative maturity makes CCS an invaluable low cost option in a world that still requires cheap coal and natural gas fired electricity. In fact it's been determined that CCS could potentially reduce the overall cost of decarbonizing the energy sector by around $1 trillion between the years 2012 and 2035 [4]. The optimistic mitigation scenarios (those that reach atmospheric greenhouse gas concentrations of around 430ppm-480ppm CO_2eq) ran by the IPCC predict that the cost of mitigation could increase by close to 300% in the absence of CCS (see figure 7 left panel).The low cost of CCS also makes it a mitigation option that developing countries can implement fairly quickly. So it can also significantly reduce the costs associated with delayed mitigation. These additional costs are incurred because of things like lack of availability and reduced mitigation time frame. These could be significant as figure 7 (right panel) shows: here, simulation results show that mitigation costs could increase by just over 100% if no action is taken by 2030.

Bioenergy coupled with carbon capture and sequestration (BECCS); a means with which emissions from fossil fuel power generation are reduced through fuel substitution; is considered today as an integral strategy for meeting the projections made by the more optimistic mitigation scenarios simulated in studies by the IPCC to combat climate change [3]. The main reason it's so crucial is because it's a means with which CO_2 can be scrubbed out of the atmosphere through negative emissions [3]. This comes about because the CO_2 sequestered through the growth cycle of the bioenergy production (via photosynthesis) is taken into account when the CO_2 emissions from the processes are determined [3]. Determining emissions in this manner dose have shortcomings as there are no obligatory, comprehensive guidelines that outline how to determine emissions from either carbon capture and sequestration (CCS) or BECCS. Though the newly revised guidelines drawn up by the Intergovernmental Panel on climate Change (IPCC) cover BECCS are yet to be adopted [19]. Additionally, there is also the problem of determining whether the biomass is produced sustainably. An involved process, considering things like; carbon emissions that come about because of possible land use change, water depletion and loss of biodiversity. This is especially challenging when the biomass is imported: for instance, the country from which the biomass is sourced may not produce annual inventories; compromising the accuracy of the assessment. Even if the biomass is sourced from a nation that produces annual inventories; there would still be uncertainty since complete reporting which takes into account things such as land use and land use change and farming are not compulsory [19]. Despite all this, it's been argued (using the Biosphere Carbon Stock Management (BCSM) concept) that it should be technologically easier to combat climate

change through the way we manage land-use than it is to achieve decarbonization of fuel used in the energy sector [20]. This is likely because of the high cost [4] and complexity associated with non-emitting renewables which are heavily dependent on subsidies. When one also considers that BECCS is likely to bolster employment (especially in rural communities) and strengthen rural/agricultural economies by diversifying farm out-put when implemented sustainably [3]; can go about meeting their climate mitigation obligations whilst providing steady employment. Other advantages associated with BECCS include: good public perception (compared to CSS) [20] and its competitiveness relative to other air capture methods such as use of sodium hydroxide [20]. In a study ran to determine the lifecycle global direct climate impact of several biomass fuels, the IPCC found that bioenergy fuels derived from sugarcane, perennial grasses, crop residues and waste cooking oil were the best performers [3]. A major reason crop residues (the biofuel source being investigated in this study) perform so well is that their waste products; and as such are associated with little to no emissions resulting from indirect or direct land use change [3], [20]. Since they are waste products they also don't compete for land with food crops which is a major impediment to the full scale adoption of BECCS. Agricultural residues were found through modelling to have a significant 10-32EJ/year global potential to the year 2050 [21]. Among the most abundant (amounting to 8 900 metric tonnes) agricultural waste products in South Africa are corn residues, which are typically composed of 20% corn cob (residue left after removing the maize grains from cobs during harvesting) and 80% corn stover (which includes the stalk, leaf, tassel and husk) [22]. BECCS for the moment has been implemented in co-firing regimes where biomass is fed along with a conventional fossil fuel feed (which is usually coal) as fuel to a power plant. The main reason this is done is that co-firing is a compromise that allows low energy density biomass to be used in conventional power plants (which are designed to handle high energy density fossil fuel feeds) that operate at high thermal efficiencies. This is a low cost mitigation strategy that preserves current electricity infrastructure; avoiding the added cost that comes with designing, planning and construction of new dedicated plants [20]. An alternative that has the potential to provide the large amounts of biomass needed without competing with food crops is algae; as it grows quickly and requires very little land by comparison. Its drawbacks are its lack maturity and need for further research and development.

2.2. Materials and methods

This section is a review on the means with which society generates power from coal and natural gas. Much of it will focus on advanced cycle, next generation power plants which have efficiencies high enough for carbon capture retrofit. Doing this will give an overview of the industry, and the technology available.

2.2.1. Rankin cycle plants

2.2.1.1. Rankine cycle description

The Rankine cycle is the predominant means with which man has been producing power from coal since 1920's [12]. Today it also forms the bottom cycle of combined Ranking and Brayton cycles in what are often called combined cycle power plants [12], [23]. There is a separation between the working fluid (which is normally water) and the combustion gasses within this cycle; with the combustion gasses transmitting heat to the working fluid through a conducting surface. The working fluid moves through a cycle in which it is converted to vapour in a furnace/boiler by the hot combustion gasses. This vapour then generates electricity by reporting to a turbine train before being condensed and fed back to the furnace/boiler; restarting the cycle. A disadvantage of the cycle is the temperature disparity between the hot combustion flue gasses (around 2000℃) and the high-pressure steam (around 650℃) [23], which results in significant exergy losses [24]. Figure 8 is a diagram of a pulverised coal power plant [25].

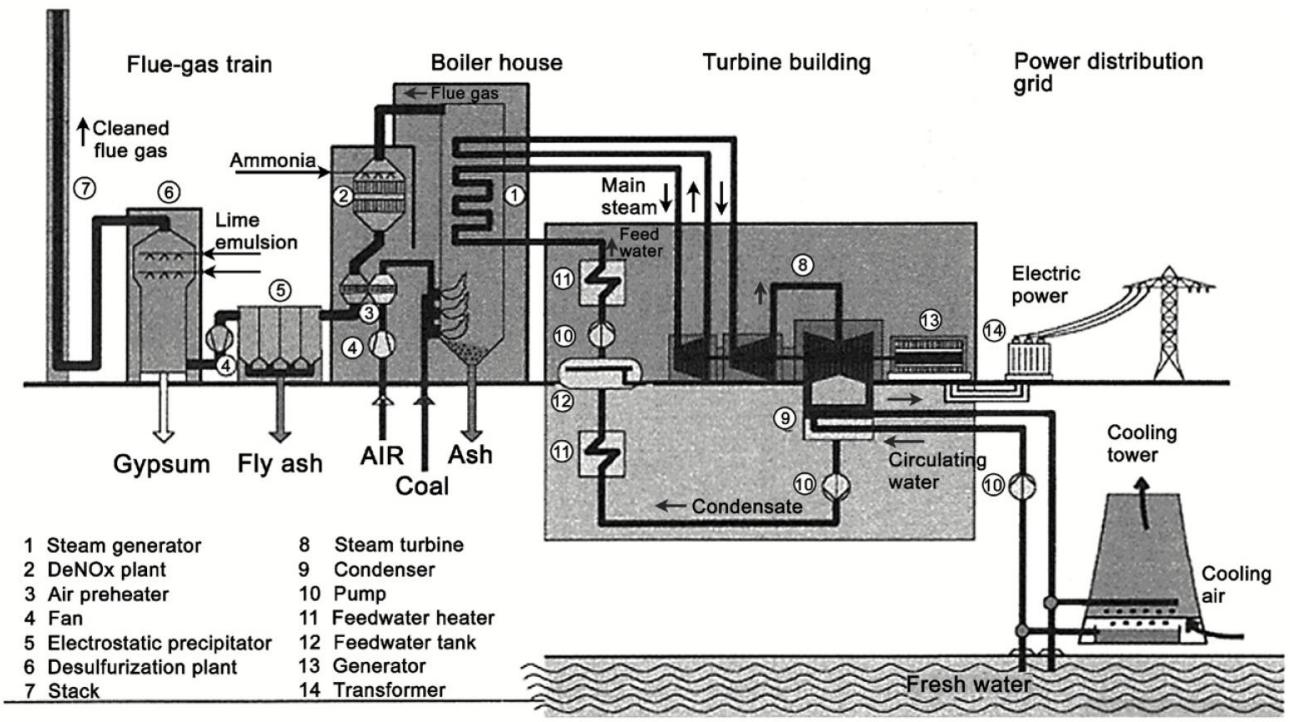


Figure 8: Figure of a pulverised coal power plant [12].

These Rankine cycle coal fired plants can have their efficiencies improved by changing the condition of the working fluid from sub, to super or ultra-supercritical steam. This increases the operating parameters of the steam (temperature and pressure), increasing the energy content of the steam reporting to the turbine. Typical subcritical operating conditions are 163bar and 538℃, those of supercritical plants are 245bar and 565℃ whilst those of ultra-supercritical plants are 300bar and 600℃ [12].

2.2.1.2. Rankine cycle efficiency

Figure 9 illustrates the means with which a supercritical Rankine cycle coal fired plant can have its efficiency improved systematically, with the horizontal axis representing the action taken whilst the vertical axis represents the efficiency improvement this action will have. The efficiency of an idealised sub critical pulverized coal Rankine cycle plant is around 45% [12].

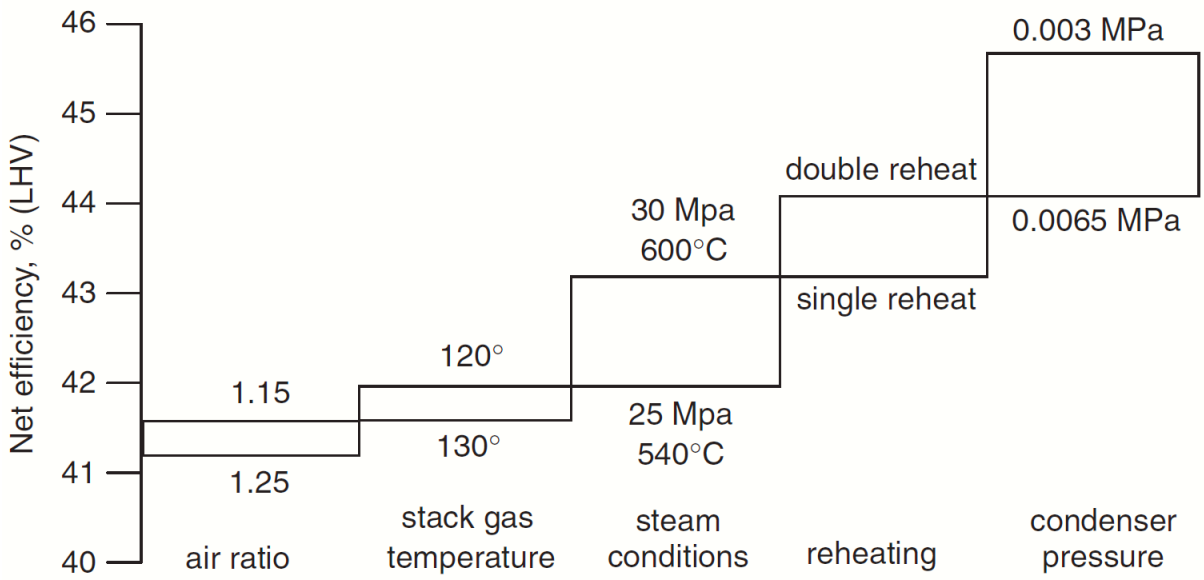


Figure 9: Figure charting the improvements several actions will have on the overall plant efficiency of a coal fired power plant [12].

The air ratio, by definition, is the ratio between the mass of air stoichiometrically required for combustion and the mass of air fed. Inefficient combustion is the reason the air is fed in excess. While feeding in excess air dose increase the likelihood of complete combustion, it increases the flowrate of hot flue gasses leaving the stack. This of course increases heat losses through the stack. A number of actions can be taken to improve combustion efficiency without increasing the air feed such as using finer coal or improving the burner design [12] [26]. Improved heat transfer between the working fluid and the flue gasses should bring closer their approach temperatures when they leave the vessel (much like in a heat exchanger). This might explain why lower stack gas temperatures are associated with improved efficiency. Increasing the number of times the steam goes through reheating reduces the temperature disparity between the flue gasses and the working fluid and improves efficiency.

It is convenient to chart the progress of the working fluid in a Rankine cycle power plant on temperature entropy diagrams such as Figure 10. In Figure 10 the left half of the blue line represents saturated vapor, and the right half represents saturated liquid. The apex of the curve is the critical point, and in the area bound beneath the curve, water is in equilibrium with vapor. To the left of the diagram the working fluid exists as liquid water and to the right its steam [26]. Figure 11 shows the path traced by the working fluid in a Rankine cycle on a temperature entropy diagram. The orange line represents the path taken by an ideal cycle and the green line represents the path taken by a real cycle [23]. Line segment (1-2) represents the path taken by the fluid as it is pumped into the boiler. As the fluid is heated in the boiler it changes phase

from liquid water at point 2 to steam at point 3. It then expands through the turbine from point 3 to point 4 before being condensed back to liquid water from point 4 back to point 1 [27]. These diagrams give an indication of how far the process strays from ideality. As will be mentioned in the section on exergy a process is perfectly efficient or reversible when it goes through series of equilibrium processes between its initial and final sate. This is why in the ideal cycle line segment (4-1) (which represents condensation) and line segment (2-3) (which represents heat addition) are flat. When at equilibrium fluids will change phase at constant temperature when the pressure is held constant. So these segments are isobaric unlike those traced by the green line. Line segments (1-2) and (3-4) represent isentropic compression and expansion in the ideal cycle. Without the generation of entropy these segments are reversible and perpendicular unlike those on the actual cycle.

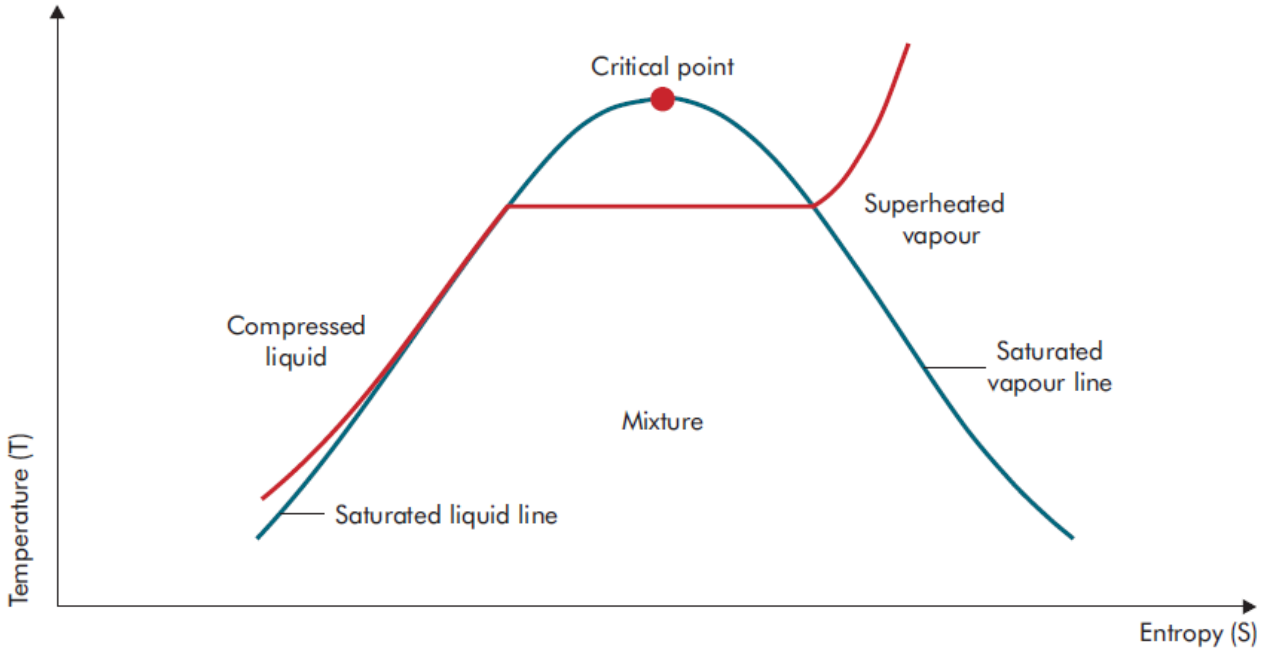


Figure 10: Temperature entropy diagram for steam and water [26].

Pulverised coal plants can also have their efficiencies improved by changing the condition of the working fluid from sub, to super or ultra-supercritical steam. This increases the operating parameters of the steam (temperature and pressure), increasing the energy content of the steam reporting to the turbine. Typical subcritical operating conditions are 163bar and 538℃, those of supercritical plants are 245bar and 565℃ whilst those of ultra-supercritical plants are 300bar and 600℃ [12]. The effect of this can be seen in Figure 11 by the rise in temperature of the working fluid from the horizontal line representing constant temperature heat addition to point 3. As the operating parameters of the steam increase to superheated conditions point 3 is shifted

upward. Superheating the steam also ensures the working fluid remains dry as it expands through the turbine. This extends turbine life by reducing the associated damage caused by water impingement on the turbine blades [27]. Advancements in materials of construction are what have enabled pulverised coal plants to operate at these advanced steam conditions that would otherwise damage units such as the boiler and turbine blades. For example current super alloys and coatings permit turbine inlet temperatures of up to 1290°F, and fourth generation super alloys with Ruthenium mono-crystal structures could potentially increase inlet temperatures to 2010°F in the future [27].

Another parameter that has a major impact on efficiency is the condenser pressure. As the condenser pressure drops, point 4 in Figure 11 shifts downward. This improves efficiency by increasing the pressure drop between point 3 and 4, increasing the capacity for the steam to expand through the turbine [27].

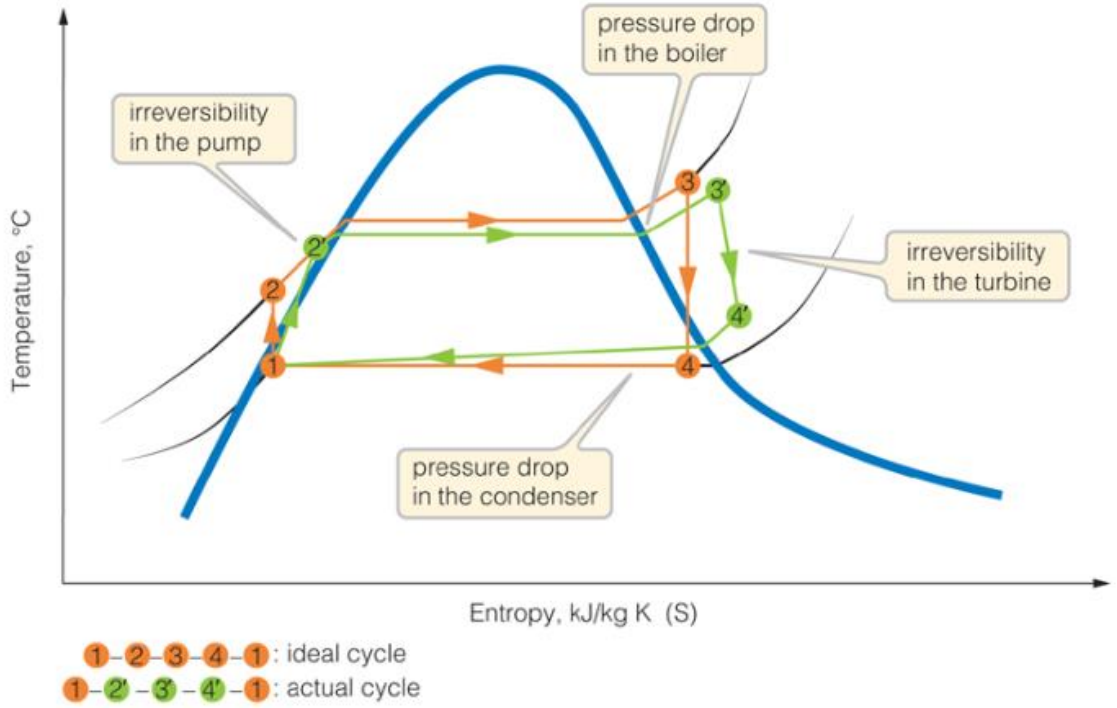


Figure 11: Temperature entropy diagram for an ideal and an actual Rankine cycle [23].

2.2.2. Air heater, gas turbine combined cycles (AH-GTCC)

In this setup, air is first heated by passing it through an active circulating fluidised bed. The furnace uses heat from coal combustion to heat and pressurise the air before feeding it to a gas turbine which produces power for the toping Brayton cycle. The gas turbine generates power before the outgoing hot air is fed into the furnace to act as oxidant for the combustion of the fuel coal which provides combustion heat for a Rankine cycle [12].

In this setup the coal is burned in a fluidised bed; which is a process unit that gives a bed of manufactured or crushed solid particles fluid like characteristics. The particle bed lies on a perforated floor near the base of the unit. The unit is open at either end, with a channel near the bottom to permit the injection of an oxidant (either air or oxygen) at high enough flow-rates to lift and scatter the particles up the length of the unit (In other words enough for the entire mixture to become turbid). This is what gives the bed of particles fluid like characteristics [28].

Removal of NOx and SOx is much simpler and cheaper with this unit. The bed has lower supercritical (SC) combustion temperatures (563℃ - 582℃) than those you would typically find in a SC Pulverised coal facility which inhibits the formation of NOx, this is most likely due to the fact that the unit operates at temperatures lower than is required to overcome the activation energy penalty for the oxidation of nitrogen. This lower temperature also contributes to furnace flexibility, as it inhibits ash fouling along with corrosion of the heat transfer surfaces associated with certain fuels which are difficult to deal with. Removal of 90% to 95% of the SOx emissions can be achieved simply with the addition of limestone [28].

Despite a lower combustion temperature, these furnaces have comparable combustion efficiencies to those of Pulverised coal boilers. This can be attributed to the turbidity within the unit; which improves heat transfer and effectively removes temperature profiles which destroy usable work. The increased reaction surface area (result of crushing coal to finer particles) and turbidity also insure more of the fuel is burned which makes further use of usable work contained within the fuel.

The improved combustion efficiency makes the boiler more flexible and able to deal with fuels of varying quality: from those with low calorific content i.e.(Waste coals and biomass) to those with higher calorific content such as Anthracite [28].

One of the major problems with these units is scale; most of the units are small (≥300MWe) compared to pulverised coal units (>1000MWe) [28] so when scaling up one has to consider the added cost associated with acquiring parts made rare or unique, because their unusually large or bespoke. They also operate at predominantly subcritical conditions because of the lower combustion temperatures; this will make adaptation to super-critical and especially ultra-supercritical operation difficult [25].

2.2.2.1 Advantages & disadvantages of AH-GTCC

Having a fluidised bed, the cycle will inherit all advantages associated with this process unit: Ability to deal with a wide variety of fuel qualities, simple and cost effective removal of SOx and NOx, effective furnace heat transfer along with efficient combustion [28]. The gas turbine operates on the Brayton cycle, whilst the steam turbine operates on the Ranking cycle. Combining the two allows for gas turbine power production; which is much more efficient than using a steam turbine alone, so less of the fuel's energy content is wasted. The initial conditions are also improved i.e.(gas turbine inlet pressure and temperature), and as a result the two cycles effectively enhance each other resulting in a combined efficiency of around 40.4% (LHV) [12], which is much higher than either cycle could achieve alone [29]. Being air fed, the turbine feed need not go through gas cleaning more common with other gas turbine setups [12].

The cycle also inherits all the disadvantages associated with fluidised beds mentioned above: which are lower combustion temperatures that inhibit supercritical and ultra-supercritical operation along with their smaller scale.

2.2.3. Internal gasification, combined cycle (IGCC)

In this setup coal is first gasified in a pressurised fluidise bed gasifier producing syngas and char (in the case of incomplete gasification). The syngas produces power by reporting to a combustion turbine whilst the char is sent to a pressurised fluidised bed combustor (PFBC) which generates power by transmitting the resultant heat to a steam cycle. To increase efficiency and reduce wastage even further; the high pressure, oxygen laced flu gas product fraction from the fluidised bed boiler (After going through gas cleaning for removal of

particulates and alkali at 870℃) also reports to the combustion turbine along with the syngas. See figure 12 for a basic schematic of the process [12].

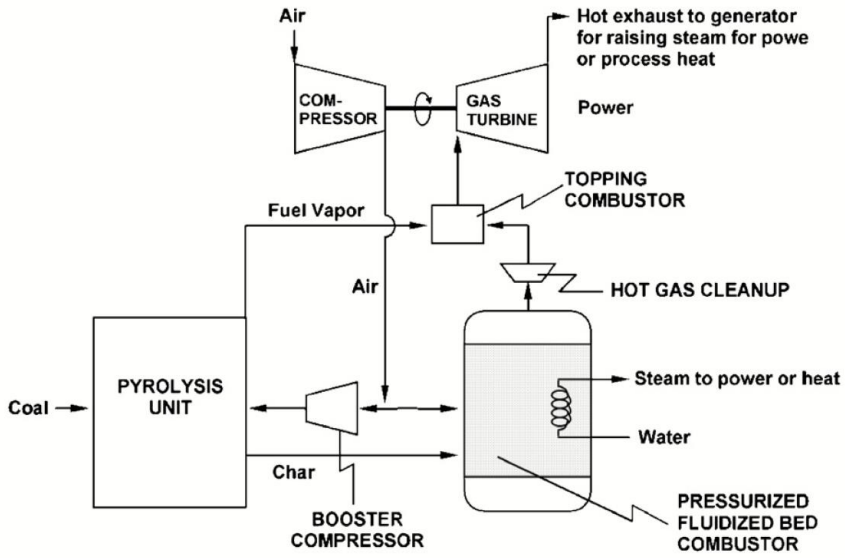


Figure 12: Simplified block flow diagram of an IGCC power plant [12].

2.2.3.1. IGCC advantages & disadvantages

Coal gasification followed by gas turbine combustion is currently the optimal way to generate power from coal; overcoming many of the limitations associated with the Rankine cycle. It represents the best means of reducing global greenhouse gas emissions to 20% of those emitted in 1990 [30], with some stating the technology can potentially reach 60% efficiency and beyond. Currently the net efficiency of existing IGCC plants is around 42%. The paragraphs that follow outline the characteristics that make this possible [12].

Having a circulating fluidised bed furnace results in the setup inheriting all the benefits associated with this combustion unit within the Rankine or steam cycle: ability to handle fuels of varying quality, convenient and inexpensive treatment of SOx and NOx, efficient char combustion and efficient furnace heat transfer.

In IGCC it pays to have syngas with a large chemical energy to sensible heat ratio. This insures that the energy contained in the syngas is perfectly conserved on route to the gas turbine, with less of the available energy reporting as heat to the steam cycle which is a lot less efficient because of the difficulty that comes with transmitting heat. This is because gas turbines are essentially grounded jet engines that inject the gaseous fuel down the length of the turbine Producing heat, and a pressure differential down the length upon ignition (If the fuel possesses

chemical energy). Unlike boiler steam turbine configurations, the heat from combustion is transmitted to the working fluid (which in this case is a mixture of syngas and air) directly, overcoming the transmition restriction associated with boilers when they heat the working fluid (which in that case is water) through a conducing surface (transmition which we know is restricted by the temperature disparity between the hot reservoir and the ambient environment). The nature of the working fluid also contributes: being a gas, there is no need to overcome the sensible heat barrier and destroy work potential, before reaching saturation and producing the vapour that ultimately turns the rotor. So a larger proportion of the heat received increases the working fluid temperature and pressure; improving efficiency and increasing thrust. The fluid can also be compressed using power from the cycle with little chance of condensation; this is advantageous as electricity can be fully converted to work with little loss.

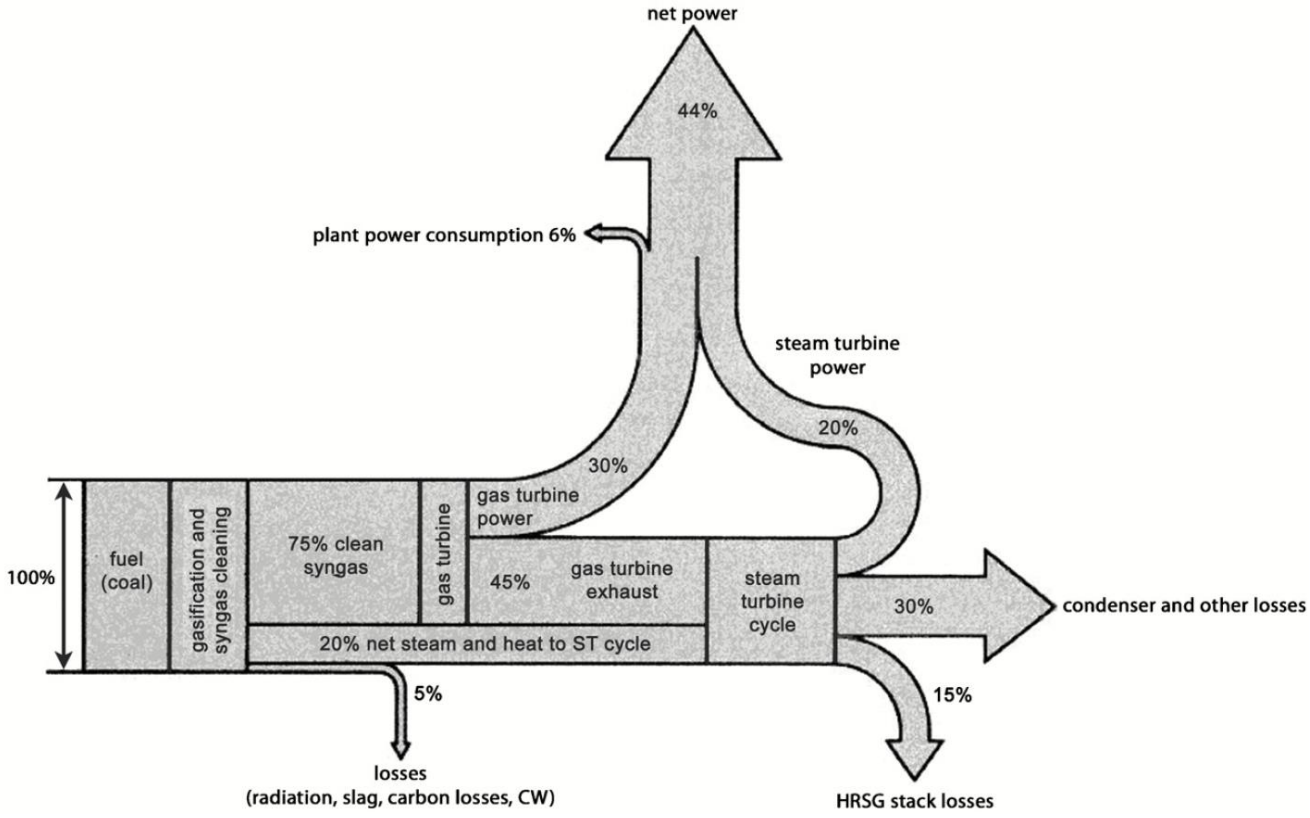


Figure 13: Idealised energy flow diagram for IGCC [12].

The idealised energy flow diagram (Figure 13)

is pictorial confirmation of the superior efficiency associated with gas turbine power generation. Looking at the diagram, 75% of the total fuel energy input which is “labelled 75% clean syngas” reports to the gas turbine as syn-gas, and only 60% of that; 45% of the total fuel

input which is labelled “45% gas turbine exhaust” is wasted by the turbine. Whereas of the total fuel energy reporting to the steam cycle; represented by the sum of the streams labelled “20% net steam and heat to ST cycle” and “45% gas turbine exhaust”, 69.23% is wasted by the steam cycle. These losses being represented on the diagram by the sum of the outgoing streams labelled “condenser and other heat losses” and “HRSG stack losses” which are 30% and 15% of the total fuel energy input respectively [12].

Once carbon capture and sequestration become obligatory, IGCC will become very attractive for newly built coal fired power plants because of the ease with which carbon dioxide can be captured from the setup. This is because carbon dioxide is expelled from the system at high pressures, making capture and compression a lot less energy intensive [12].

Historically IGCC suffered from high capital costs brought on by lack of availability that naturally colligates with all pioneering technology. The lack of reference plants also meant operating risks; maintenance costs and any other unforeseen issues that could only be resolved through experience were unknown [12]. In response to this, various supplier groupings (Very likely incentivised by governments) came together and produced generic IGCC plant designs on a turnkey basis with guarantees on cost, construction time, availability, and efficiency. But despite all this, and the expansive research that has gone into characterizing, developing and optimizing it, the negative perception still persists; with the technology very likely spurned as a result of voluntary and involuntary organizational inertia [25].

2.2.4. Natural gas combined cycle (NGCC)

NGCC is very similar to IGCC; with a topping Brayton cycle working in conjunction with a Rankine cycle. This is enabled by gas fired power generation with the only exception being that the fuel is ready for combustion turbine power generation without need for initial treatment like IGCC. After the natural gas has been utilized by the combustion turbine to generate power; the resulting hot combustion flue gasses then report to a bottom Rankine cycle that makes use of the remaining heat in the hot combustion flue gasses to generate additional power by transmitting it to a steam cycle [11], [13], [14]. Figure 14 is a simplified diagram of a NGCC power plant which uses a triple pressure system that recovers more exergy from the hot exhaust gases than more conventional steam cycle setups. The system produces streams of low pressure (LP), intermediate pressure (IP) and high-pressure (HP) steam separately from one another in heat a recover steam generator (HRSG) to generate power using LP, IP and HP steam turbines

respectively. The cycle has an overall efficiency of around 50% to 60% [11], [13]**;** which is higher than coal fired power generation at 38% and IGCC at 42% [12].

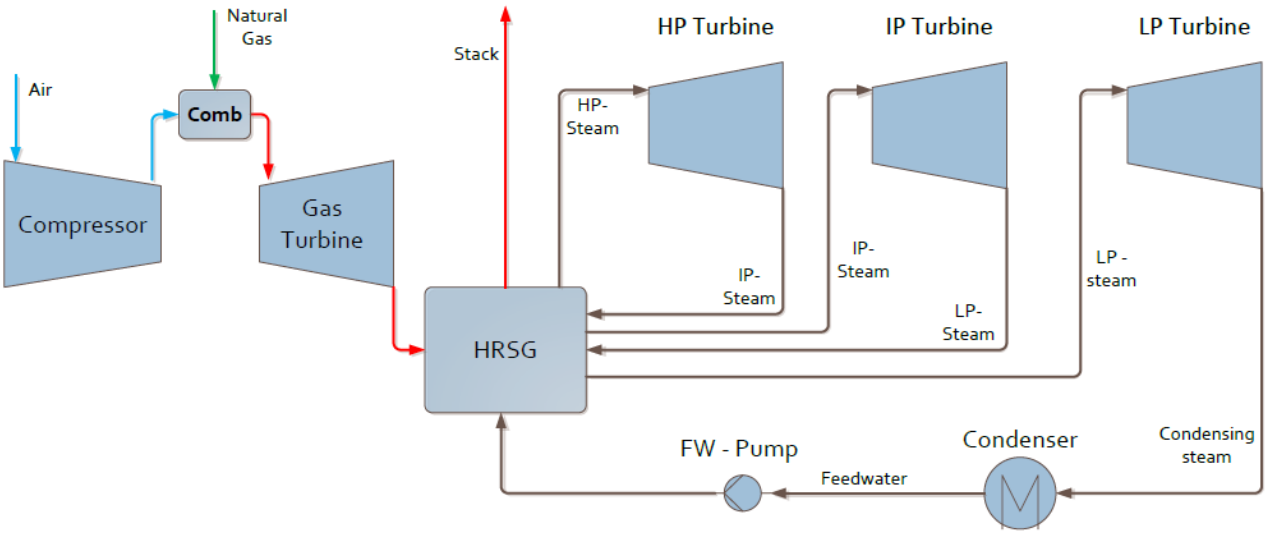


Figure 14: Simplified diagram on an NGCC plant [13].

2.2.4.1. NGCC advantages

The temperature disparity which exists between the combustion gasses and the working fluid is one of the major disadvantages that combined cycle power plants try to overcome. By using the combustion gases as working fluid in a combustion turbine, combined cycles can overcome the exergy losses that come with heat transmition over finite temperature differences which occur within the boiler section of Rankine cycles [23], [31]. Modern gas turbines can operate at these elevated temperatures because of recent developments in high temperature resistant materials such as ceramics. The reason a bottom Rankine cycle is included is because gasses leave the gas turbine at high temperatures (around 500℃) [31]: at these lower temperatures Rankine cycles become feasible. It is the complimentary temperature ranges between the Brayton cycle (1600K-900K) and the Rankine cycle (850K-288K) that make combined cycles so effective; allowing them to make more use of the fuels exergy content [12], [14]. This gives the cycle a high efficiency of between 50%-60% [11], [13]. The utility in including the bottom Rankine cycle is illustrated on the temperature entropy diagram for an NGCC plant in figure 15 [12]. The curved arrows depict heat flows toward and within the setup and the areas bounded represent the amount in exergy one can harness from each cycle. The area of the bolder shape on the bottom end of figure 15 is the exergy one can harness from the bottoming Rankine cycle if it is included.

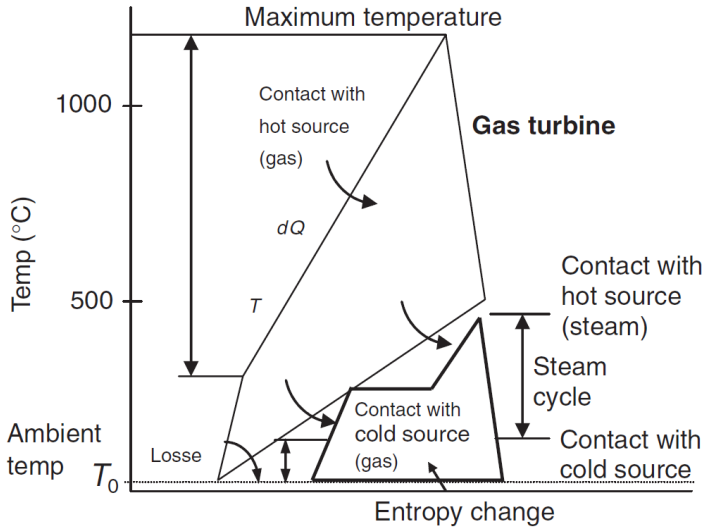


Figure 15: Temperature entropy diagram for combined cycle plant [12].

There are other alternatives for the bottom cycle working fluid: such as the mercury vapour process, various organic fluids and ammonia. The mercury vapour process fell out of favour once conventional steam power plants developed higher efficiencies. Organic fluids and ammonia have advantages over water in the low temperature range such as: reduced volumetric flows and no wetness. The higher volatility of these alternate fluids have the potential of making more use of the heat rejected by the gas turbine, increase work output and improve efficiencies. However, high development costs, complexity and environmental impact make it unlikely that they will ever replace water as a working fluid in the bottom Rankine cycle. Additionally, steam cycles are a mature technology that has proven itself in conventional, single cycle pulverised coal (PC) Ranking cycle plants. And water is an inexpensive widely available medium well suited for medium to low temperature ranges [14].

The adoption of intermittent renewable energy production will require that conventional power plants become more flexible due to the lack of large scale, affordable, long term energy storage [18]. The effect that renewable intermittency will have on the typical daily load curve of a grid with a large share in renewables (specifically wind energy in this case) can be seen in figure 16 [32]. The “Total load” on this curve represents the demand for electricity. The “Minimal output of thermal plants” represents baseload (power plants running at full capacity) fossil fuel electricity production from conventional; predominantly fossil fuel thermal power plants [18].

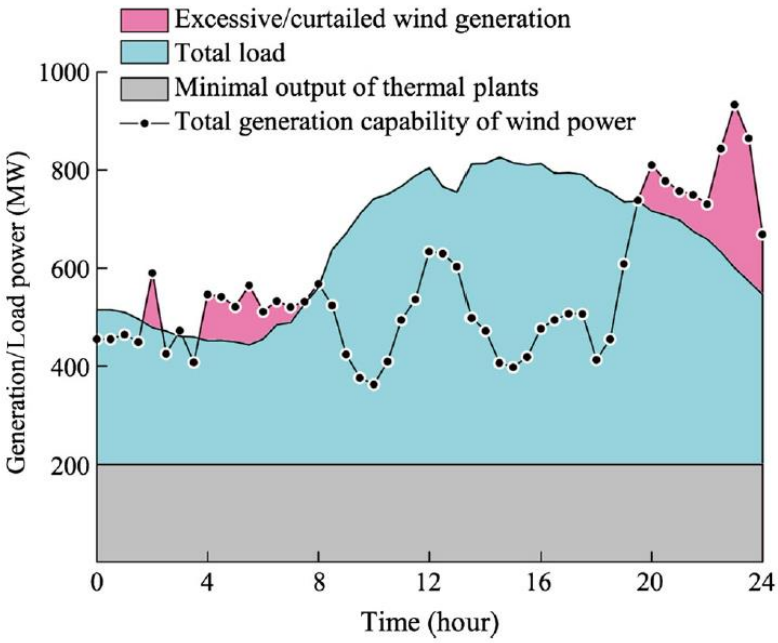


Figure 16: effect of large scale wind energy generation on daily load curve [32].

Power plant setups in future would need to satisfy the shortfall in supply between the eighth and twentieth hour in figure 16. They would also need to completely shut down during periods of peak over production of renewable energy generation as can be seen in the region between hours 2 and 8, as well as hours 20 and 24. Among the consequences for significant overproduction of electricity include negative power prices and grid instability [18].

The best fossil fuel power plant setup that could affordably fulfil these requirements is NGCC [13], [18], and in doing so, it would be best to divide the daily load curve into three regions; with NGCC occupying the more volatile region. The three regions into which the daily load curve is subdivided are: (1) the baseload region (satisfied by nuclear, hydro and coal fired power), (2) the intermediate region (satisfied by combined cycles) and (3) the peak load region (satisfied by hydro and simple cycles) [13]. The reasons NGCC power plants are considered suitable for operating in the intermittent region are: that they have very high part load efficiency, their less complex than other power plant types and their gas powered and don't require warm or hot start up for rapid load change [18]. It is the gas turbine that is mostly responsible for this flexibility and superior part load efficiency, with efficiency reductions of only around 2-3% at 60% part load and increasing gradually until you reach a minimum operating load of approximately 40% [11], [13] or more specifically between 30-50% for an NGCC power plant operating with one gas turbine [18]. The minimum operating load can drop to as low as 15- 25% for NGCC power plants with two gas turbines (see table 1 for statistics

that make NGCC superior at part load compared to other power plant setups) [18]. How this would affect the daily load curve can be seen in figure 17 [18]: here the contribution made by combined cycle power plants is in yellow, with the peaks being satified by pumped storage and aeroderivaties, the regions in green are those satified by intermittent renwable energy and the grey region near the bottom would be satified by by inlfexible baseload power plants (coal, nuclear etc…) [18].

Table 1: Comparison of different power plant setups on flexibility [18].

Table 1. Comparison of operating characteristics of nuclear and fossil-fired power plants

Operating requirement	Nuclear power plant[a]	New coal-fired plant[b]	Combined cycle plant	
			Siemens F-class	Siemens H-class
Average rate of load change in load-follow mode	10%/min at 80 to 100% load, 5%/min at 50-100% load, 2%/min at 20-100% load	3-6%/min at 40-100% load	4-8%/min at 40-100% load[c]	4-9%/min at 40-100% load[c]
Grid frequency control (primary/ secondary)	60%/min at 60-100% load	>60%/min at 40-100% load	180%/min at 50-100% load	180%/min at 50-100% load
Minimum load (% of rated power)	20-30%	20-25% in recirculation mode, 35-40% in once-through mode	30-50% for single-unit plant[c,d] 15-25% for multiple-unit plant (2GTs+ST)[c,d]	
Load rejection to auxiliary power/ island operation (ie capability for sudden large load reduction without trip)	Yes, to turbine bypass mode	Yes, to turbine bypass mode	Yes, to gas turbine operation	Yes, to gas turbine operation
Plant efficiency (100% load)	36-38% (EPR)	45-47%	58-59%	>60-61%
Plant efficiency (50% load)	33-35% (EPR)	42-44%	52-55% for single-unit plant <60% for multiple-unit plant	54-57% for single-unit plant >60% for multiple-unit plant
Specific CO_2 emissions (g/kWh)	None	740	345	330
SO_2 emissions (mg/Nm^3)	None	100-200	approx. 0	approx. 0
NO_x emissions (mg/Nm^3)	None	75-100	30-50	30-50

Notes and sources:

a. AREVA corporate communication 2010.

b. Experience feedback from start-up of coal fired power plants (Paiton, Kogan Creek).

c. With preheating of GT intake air.

d. Technically feasible depending on emission limits.

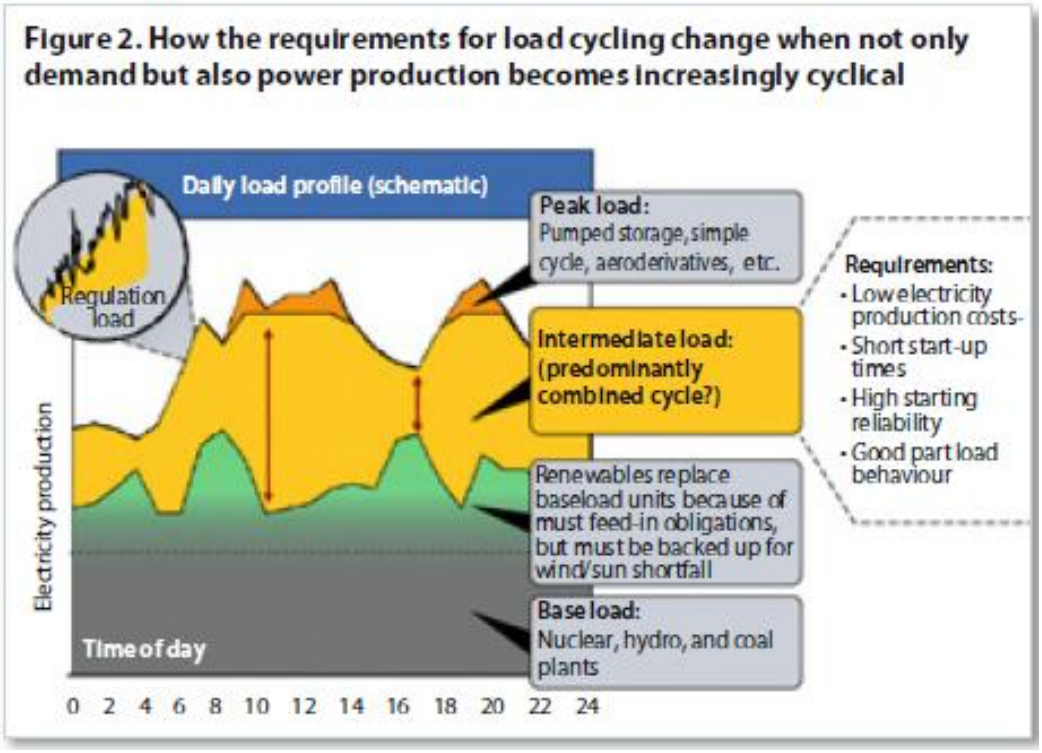


Figure 17: Idealised daily load curve with NGCC occupying intermediate load range [18].

Each attribute that makes NGCC suitable for the intermittent load region of the daily load curve will result in significant cost savings. For instance, apart from the obvious cost savings associated with higher part load efficiencies; there is an additional cost saving associated with the rapidity with which NGCC reaches part load output (a power plant attribute known as rapid load change). Because coal and nuclear power plants are slow to reduce their outputs; they have a far higher associated wastage that will come with producing electricity when there is no demand during periods requiring rapid load change. This is partly because conventional power plants require warm or hot start ups as mentioned before [18] which consume fuel. And since a significant proportion of the cost of electricity is the fuel cost (see figure 18) [11], [33]; this needlessly makes the power plant expensive to run during periods requiring rapid load change [18]. An additional attribute of NGCC power plants that makes them more capable of rapid load change is that their gas fired. This enables their fuel feed rates to be reduced using valves sitauted upstream, and for the fuel gas to be immediately converted to mechaical energy in a combustion turbuine. NGCC powerplant setups are also more scalable than conventional power plants; allowing one to reduce the impact associated with overproduction even further since they can be made much smaller to meet a specific demand. This also makes them ideal as a suppliment for local, decentralised renewbale energy production.

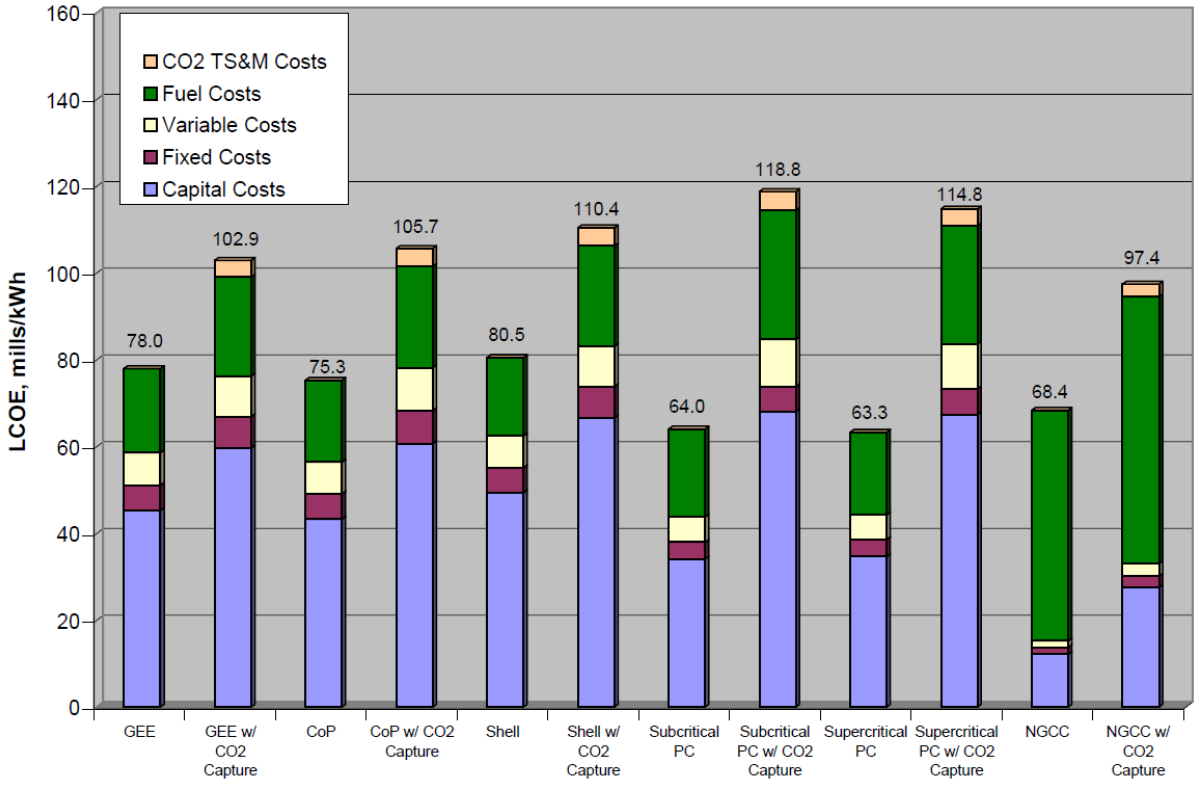


Figure 18: Comparison of the levelized cost of electricity (LCOE) between different power plant setups. The contributions made by the capital costs, fixed operating costs, variable operating costs and fuel costs are indicated [33].

2.2.4.2. Triple pressure HRSG

The steam cycle used in this work is composed of 3 pressurised steam flows (a high pressure (HP), intermediate pressure (IP) and low pressure (LP) stream) that flow counter currently to the flue gas that contains the heat rejected by the gas turbine (see figure 19). Each stream is initially heated by economisers (the high-pressure stream has 3, the intermediate pressure stream has 2 and the low pressure stream has 1) to its saturation temperature at the specified stream pressure. Once that is done the stream then enters an evaporator that vaporises it before reporting to heat exchangers that take it to the final required turbine inlet conditions. The HP and LP streams only report to a super heater and the IP stream has a re-heater (RH) following the super heater before reporting to the turbine. The HP and IP pressure turbine outlet streams then combine with the streams from super heaters at pressure levels immediately below them before reporting to the lower pressure turbine. The steam reporting from the LP turbine then flows to a condenser operating at 48mbar, where the resulting water is then split into three streams which are then pumped to the requisite pressure levels required for feed into the HP,

IP and LP sections of the steam cycle. The three streams are then preheated by the flue gas on its way out the stack before being fed back in to re-initiate the cycle [13].

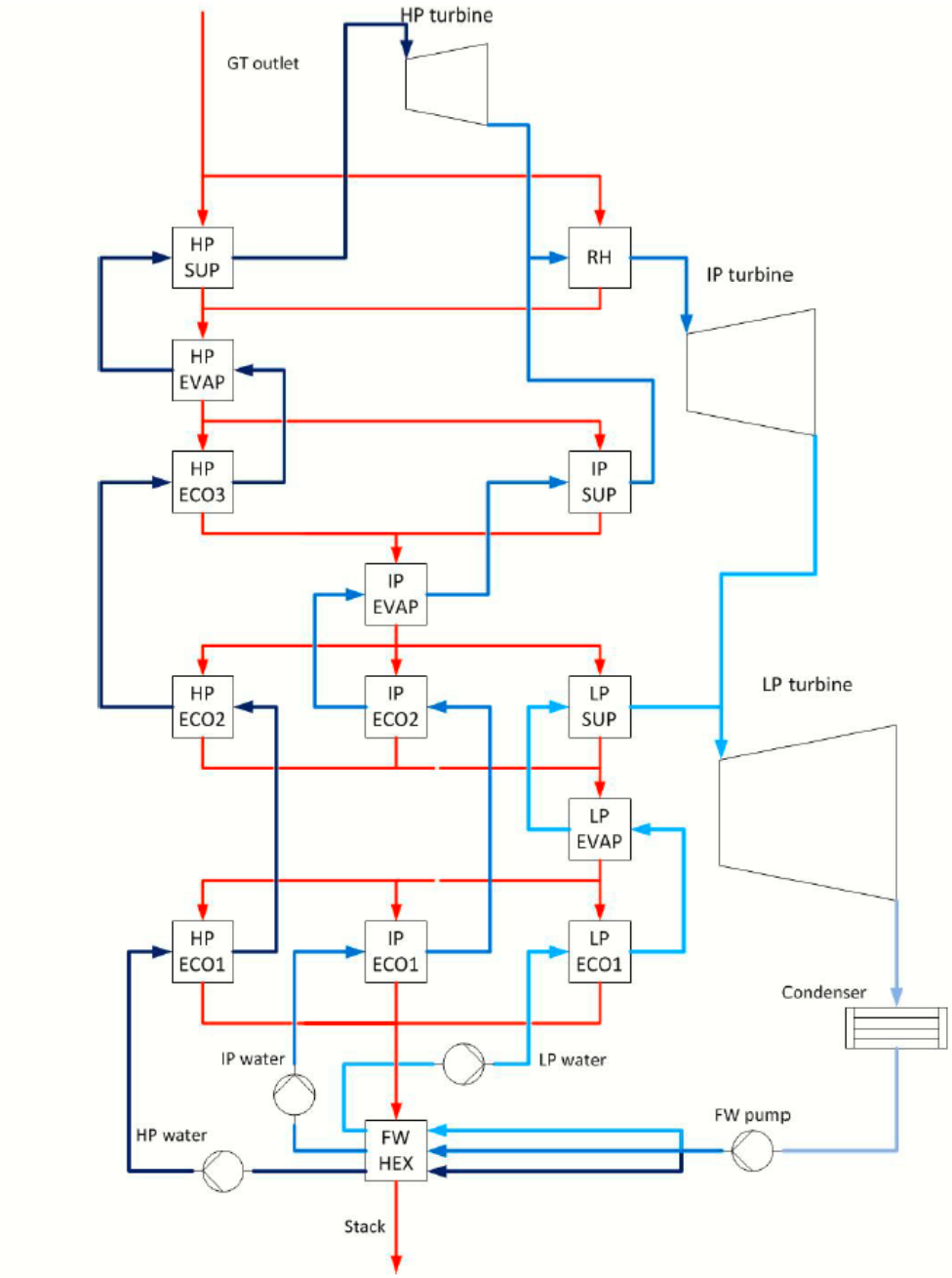


Figure 19: Flow diagram of HRSG [13].

The pressure levels in the HRSG are optimized for exergetic utilisation. The greater the pressure of the high-pressure steam and the lower the pressure of the low pressure steam the greater the overall steam turbine output. However, increasing the pressure level of steam reporting to the HP turbine increases the cost of the HRSG, its piping and the feed-water pumps. An additional constraint is the quality of the water reporting to the condenser, which cannot be lower than 0.88 to avoid erosion of the turbine blades. Another constraint is the pressure level

of the stream reporting to the low pressure evaporator: when it's below 3 bar, equipment costs associated with larger volumetric flows rise to an unacceptable level. Based on the mentioned criteria it was found that the optimal steam pressures for the HP, IP and LP sections should be 120, 32, and 5 bar respectively which fixes the outlet pressures from the HP, IP and LP pumps for the pressure drops they experience according to the literature. Pinch points of 10℃ are set as a design specification by adjusting the mass flow of water to the respective evaporators. The temperatures of the streams reporting to the HP, IP and LP turbines are 550℃ for the HP and IP turbines and 275.2℃ for the LP turbine [13].

2.2.5. Carbon capture and sequestration (CCS)

There are predominantly three means with which CO_2 emissions are captured from both coal and natural gas power plants: Pre combustion capture, oxy-combustion capture and post combustion capture [17], [34]–[36].

Pre combustion capture is implemented on combined cycle plants that make use of both gas and steam turbine power generation. With coal, this would take place in an integrated gasification combined cycle power plant (IGCC). In this setup coal is first gasified in the presence of steam and oxygen (provided by an air separation unit (ASU)) to produce syngas; a mixture of CO and H_2. The CO is then converted to CO_2 via shift reaction before being separated out through physical absorption [37]**.** The hydrogen then reports to a combustion turbine producing power via a topping Brayton cycle. The hot combustion products from the combustion turbine then report to a bottom Rankine cycle that produces power via a steam cycle [25]. Power generation from natural gas has to takes place in combined cycles known as natural gas combined cycle plants (NGCC). Pre combustion capture in NGCC plants is conducted in the same way with the major difference being that natural gas is reformed to syngas [13], [34]**.** Pre combustion capture induces the smallest efficiency penalty (between 7%-8% [13], [15], [16]) (efficiency reduction induced by carbon capture strategy) on both coal [33] and natural gas power plants [15]**.** An additional advantage it has with coal is that it's implemented on IGCC plants which are more efficient than conventional coal fired plants [12]**.** A disadvantage that comes with IGCC is its complexity and high capital cost [25].

Oxy-combustion capture involves using a steady stream of near pure oxygen from an ASU to remove nitrogen from the incoming feed air. All this to simplify separation by producing a flue gas composed of mostly CO_2 and H_2O. The water is easily condensed out before the CO_2 is

compressed for storage [16], [25]**.** The separation takes place downstream from the furnace in a conventional pulverized coal (PC) plant in the case of coal fired power generation [38]**,** and downstream of the heat recovery steam generator (HRSG) of a NGCC power plant [17]. Oxy-combustion on PC plants requires recycling of the CO_2 rich flue gas in order to moderate temperatures in the furnace [39]**.** On NGCC power plants the CO_2 rich flue gas after the HRSG is recycled back in order to regulate temperatures in the gas turbine [34]. The cryogenic air separation unit is the largest energy consumer in both PC and NGCC setups [9], [17]. Oxy-combustion induces an energy penalty on PC plants upon retrofit slightly lower than that of post combustion capture [40] and can be retrofitted to existing PC power plants with little modification. Some of the disadvantages associated with this process include: the need for air leakage prevention which becomes more difficult with plant age and the need for additional flue gas treatment steps if a very pure carbon dioxide stream is required [9]**.** A major disadvantage associated with it on NGCC power plants is that current combustion turbines are not designed to deal with a working fluid composed mostly of CO_2 [37], [41]. The efficiency penalty associated with oxy-combustion capture is around 10% [42].

Post combustion capture involves removal of the carbon dioxide via chemical absorption downstream: which is after the furnace in PC plants and after the HRSG in NGCC plants [34], [35].The most commonly used solvent is monoethanolamine (MEA) [11]. The regeneration of solvent in the stripper following the absorber using steam from the steam cycle is the most energy intensive step within the capture process for both PC and NGCC plants [11], [37]. Other amine based solvents which show promise of reduced regeneration penalties are currently undergoing research and development. Some of the disadvantages to application of the strategy include: highly impure flue gases, use of toxic chemicals, reduced power plant flexibility and a high efficiency loss upon retrofit. Some of the advantages associated with post combustion capture include: that it's the most widely used and mature strategy of the three and that it can be readily retrofitted to existing setups without the need for modification [9]**.**

Figure 20 is a flowsheet that illustrates these three capture strategies pictorially

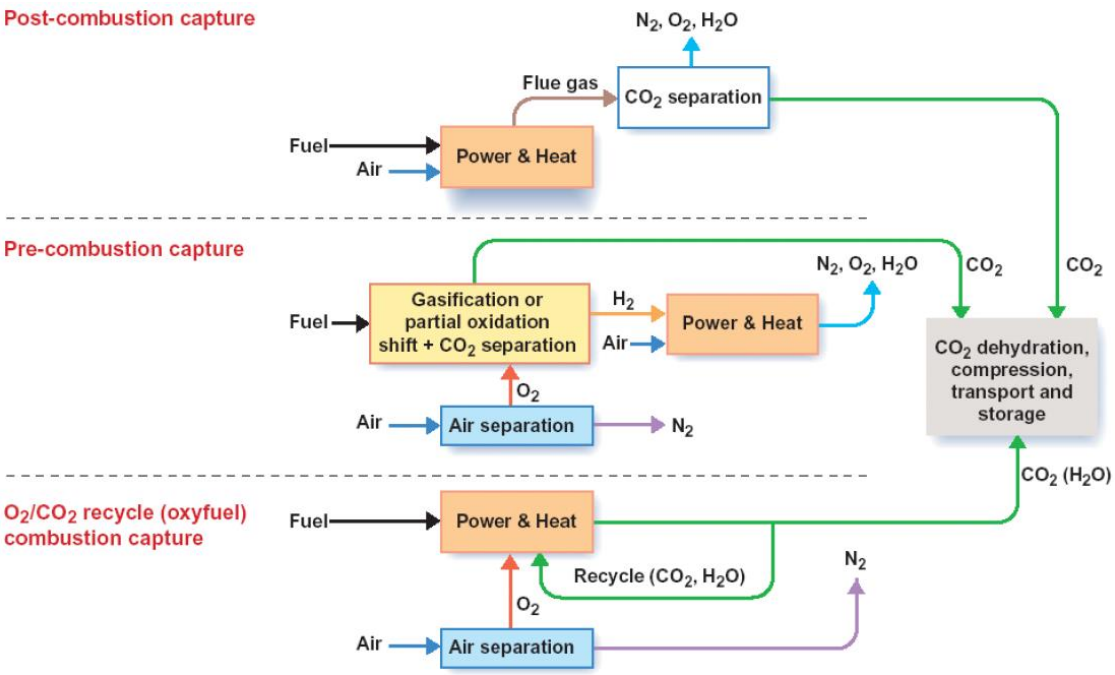


Figure 20: Figure depicting the three predominant CCS strategies available today [43].

2.2.6. Pre-combustion capture SEWGS on NGCC power plants

Figure 21 is a simplified diagram of an NGCC power plant retrofitted with pre-combustion capture sorbent enhanced water gas shift (SEWGS). As mentioned before, pre-combustion capture on NGCC power plants involves reforming the incoming natural gas into syngas (a mixture of CO and H_2). The CO is then fed to a sorbent enhanced water gas shift unit (SEWGS) that converts the CO into CO_2 in the presence of high pressure steam [13].

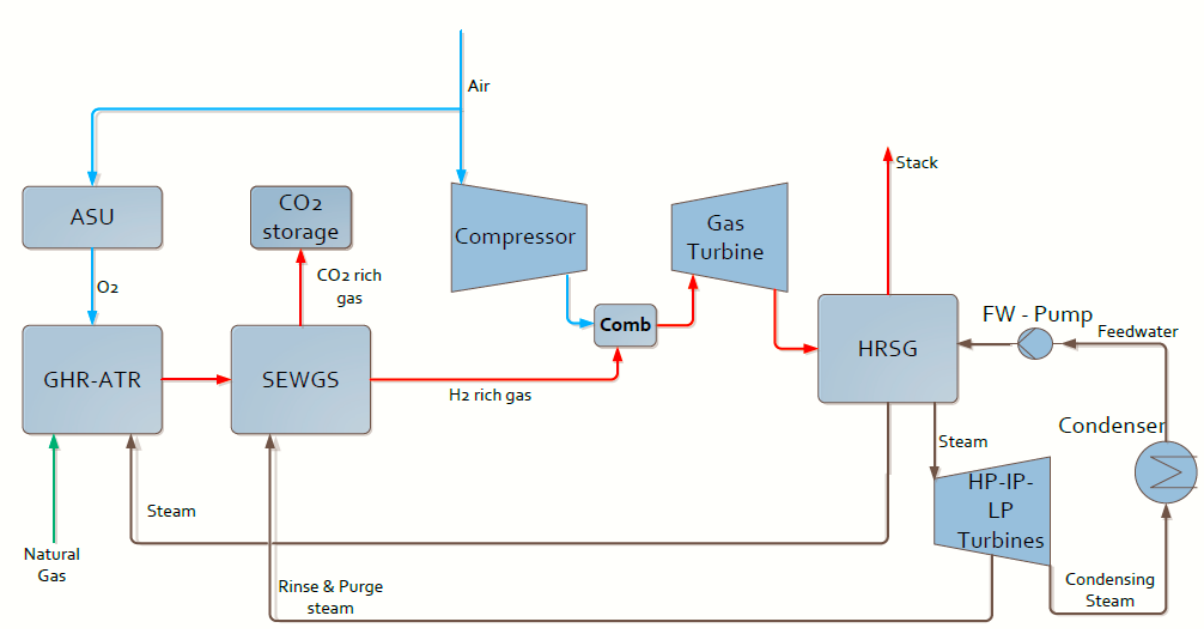


Figure 21: Simplified diagram of an NGCC power plant retrofitted with pre-combustion capture [13].

The setup feeds pure oxygen from an air separation unit (ASU) upstream along with high pressure steam to a Gas Heated Reformer Auto Thermal Reformer (GHR-ATR). The reason the process is fed pure oxygen is to produce a pure stream of H_2 from the SEWGS unit for convenient onsite storage in the event of part load operation, or for the production of fossil fuel derived hydrogen. The GHR-ATR is an innovative heat exchanger type reformer used for reforming natural gas into a highly pure syngas stream suitable for the pre-combustion capture setup. The SEWGS reactors are able to simultaneously enhance the water gas shift reaction whilst capturing CO_2 . Once the CO_2 has been separated out. The resulting hydrogen stream then reports to a gas turbine that generates electricity by combusting the hydrogen fuel in the presence of compressed air [13]. SEWGS uses a multi-bed, pressure swing adsorption (PSA) unit in which each vessel is filled with CO_2 adsorbent [15]. PSA can be used to separate out many different types of multi component gaseous mixtures (such as the separation of water as steam from ethanol [44]) and has the advantage of quick desorption of the adsorbent by depressurisation alone [45]. The GHR-ATR is a heat exchanger type of reactor that uses the exothermic heat from the outlet of the ATR to do preheating in the GHR. The GHR takes preheated natural gas and high pressure (HP) steam from the steam cycle to partially reform the natural gas and steam before the products report to the ATR. The reason the process taking place in the GHR requires heat is because the reaction is endothermic; requiring 206.2 (kJ/mol) of energy as CH_4 and H_2O are reformed into CO and H_2 (see equation 1) [13]. The

partially reformed gas then gets sent to the ATR where together with a stream of pure oxygen it is reformed once more, but this time to completion [13] (see equation 2). The fact that equation 1 is endothermic explains why it is that the GHR needs to be fed a stream of high pressure steam in order to bring the reaction about. The fact that equation 2 is exothermic explains why it is that the heat evolved from the ATR is used to partially heat the GHR. The GHR-ATR operates at a pressure of 25bar and the temperature of the ATR is 1050℃. The syn-gas form the GHR-ATR is then cooled and fed to the HTS reactor at 310℃; which converts the CO present in the stream to CO_2 before feeding the product stream at a temperature of 400℃ [13], [15] to the SEWGS unit. The HTS rector and the SEWGS unit work together to convert the CO within the stream to CO_2 (see equation 3) before separating out the CO_2 for compression and storage, and purifying the H_2 that remains which then reports to the gas turbine.

$$CH_4 + H_2O \rightarrow 3H_2 + CO \quad \left[\Delta H = \frac{206.2kJ}{mole}\right] \qquad \textbf{Equation 1}$$

$$2CH_4 + O_2 \rightarrow 4H_2 + 2CO \quad \left[\Delta H = \frac{-36kJ}{mole}\right] \qquad \textbf{Equation 2}$$

$$CO + H_2O \rightarrow CO_2 + H_2 \quad \left[\Delta H = \frac{-41.1kJ}{mole}\right] \qquad \textbf{Equation 3}$$

The CO_2 is then separated from the hydrogen after SEWGS in multiple PSA units [15], [44]–[47]. The first step in PSA is called the production step; in which hot impure vapour flows up the column and the gaseous species one wants to separate out is physically adsorbed into the pores of the molecular sieves within the bed. The pore size is just large enough for the molecules of the species of interest to fit through; which is why it is that the process has to occur at high pressures [11]. After the production step the bed must be regenerated for the next cycle once the molecular sieves are saturated; this involves depressurisation. Then the bed is re-pressurised and prepared for the next cycle. PSA cycles are composed of two or more beds [15], [44] out of a need for the process to run smoothly without interruption while each bed cycles through production and regeneration: how it works is that as one bed is regenerated the stream that needs to be purified is fed to another bed which has completed its regeneration cycle and is ready for production. The optimal number of beds is usually between six or nine; which is a good compromise between installed cost and efficiency (see figure 22 for a simplified diagram of a PSA operation comprised of 2 units). One of the most important components within SEWGS is the adsorbent; which needs to adsorb and desorb CO_2 with each pressure swing cycle at pressures between 30bar and 1 bar and at operating temperatures within

the range of 350℃ and 550℃. Some of the more important adsorbent characteristics include [15]:

1. High CO_2 capacity and selectivity over H_2.
2. Low water adsorption.
3. Low specific cost.
4. Mechanical stability under pressure and temperature variation.
5. Chemical stability in the presence of impurities.
6. Easy regeneration using steam.

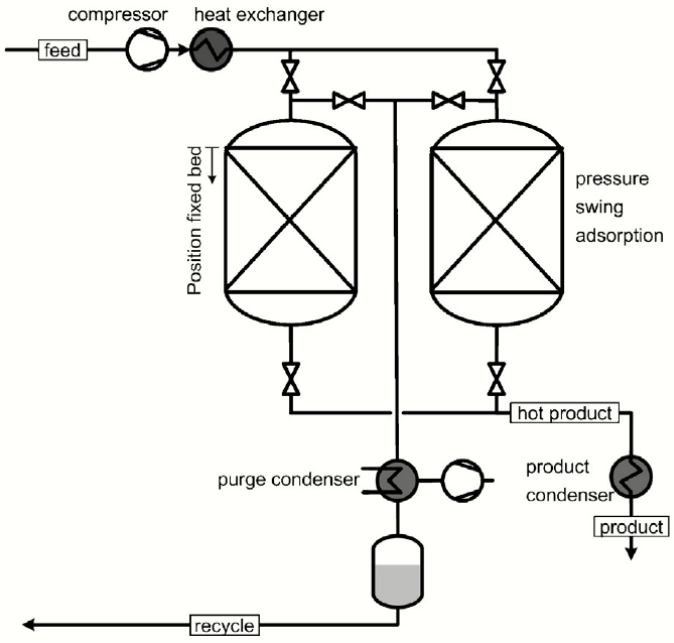


Figure 22: simplified diagram of a pressure swing adsorption unit [46]**.**

2.2.7. Power plant mitigation costs

There are many ways of determining the important cost estimates for a prospective thermal power plant. The method outlined here is that which was employed in the DOE/NETL [16] report; a study conducted by the DEPARTMENT OF ENERGY/NATIONAL ENERGY TECHNOLOGY LABORATORY with the intention of producing up to date performance and cost estimates for natural gas combined cycle power plants with CCS. The cost estimates were based on an earlier study called the Bituminous Baseline Study (BB) [33]. This study was also

conducted by the DOE/NETL with the intention of producing up to date cost estimates for PC, IGCC and NGCC power plants.

The method employed in the DOE/NETL [16] report for costing most pieces of equipment involves using reference costs in the BB study. The cost data from the BB study was used to scale common pieces of equipment. (see equation 3.1):

$$\frac{C_a}{C_b} = \left(\frac{A_a}{A_b}\right)^n \qquad \textbf{Equation 3.1}$$

Where:

- C_a and C_b = Cost of equipment item a and equipment item b
- A_a and A_b = Attribute of equipment item a and b

The value of the cost exponent n will depend on the type of equipment being scaled. Equipment without established exponents were assigned an exponent of 0.7. The attributes used for scaling are different for different categories of equipment. For instance the HRSG is scaled using its heat duty, steam turbines are scaled using their capacity and the air separation unit was scaled according to the power consumption of the main compressor.

For novel or uncommon pieces of equipment correlations such as the one given in equation 3.2 were used.

$$\log_{10} C_p^{\circ} = K_1 + K_2 \log_{10} A + K_3 (\log_{10} 10)^2 \qquad \textbf{Equation 3.2}$$

Where:

- C_p° = equipment cost at ambient operating pressure using carbon steel
- K_1, K_2, K_3 = correlation coefficients (different for differeing types of equipment)
- A = capacity or size parameter of the piece of equipment

The correlation constants relevant to specific pieces of equipment can be found in table A.2 of DOE/NETL [16] report. Equation 3.1 is used to determine the cost price of the specified piece of equipment if it were made of carbon steel and operated at ambient pressure. In order to adapt this estimate to specified operating conditions/materials one would use pressure and material correction factors [16], [48].

Using the correlations mentioned one can get the bear erected cost (BEC) with which you can estimate other important costs. Among these costs are [16]: The total plant cost (TPC), the total overnight cost (TOC), the total as spent capital (TASC) and the operating and maintenance costs. Labour costs were determined using Exhibit 4-2 in the DOE/NETL [16] report and the

variable operations and maintenance costs scaled from the BB study [33]. With these one can determine the cost of electricity using equation 3.3 [16].

$$COE = \frac{(CCF)(TOC)+OC_{FIX}+(CF)(OC_{VAR})}{(CF)(MWH)} \qquad \textbf{Equation 3.3}$$

Where:

- COE = Cost of electricity ($/MWh)
- CCF = Capital charge factor (0.111 for low risk projects and 0.105 for high risk projects)
- TOC = Total overnight capital
- OC_{FIX} = Sum of all fixed anual operating costs
- OC_{VAR} = Sum of all variable annual operating costs, including fuel at 100% capacity factor
- CF = Plant capacity factor (fraction of the year plant will be running)
- MWH = Annual net power output in MWh at 100% capacity factor

All costs in equation 3.3 are expressed in base year dollars (the first year of capital expenditure). The cost of electricity represents the revenue required to recoup all costs of building and operating a plant over a specified period [10]. The cost of electricity and all the variables used to calculate it are assumed to escalate at the nominal annual inflation rate: in other words they remain constant in real terms over the operational period [16].

Using the COE one can then determine the levelized cost of electricity (LCOE) using the levelization factor (LF). Equation 3.4 is used to calculate the LF and equation 3.5 used to calculate the LCOE [16].

$$LF = \frac{\left(1-(1+E)^{T}(1+DR)^{-T}\right)}{\frac{(DR-E)}{\frac{(1+DR)^{T}-1}{DR(1+DR)^{T}}}} \qquad \textbf{Equation 3.4}$$

$$LCOE_T = LF * COE \qquad \textbf{Equation 3.5}$$

Where:

- LF = Levelization factor based on the end of year values
- E = Escalation (inflationary) rate
- DR = Discount rate (assumed to equal required return on equity)
- T = Levelization time (number of years over which evaluation takes place)
- $LCOE_T$ = Levlized cost of electricity over T years, $/MWh

- COE = Cost of electricity, $/MWh
- ROE = Required rate of return on equity

The cost of CO_2 avoided is determined using equation 3.6 [16]:

Equation 3.6

$$Cost\ of\ CO_s avoided = \frac{\left(COE_{with\ removal} - COE_{w/o\ removal}\right)\$/MWh}{\left(CO_2 emissions_{with\ removal} - CO_2 emissions_{w/oremoval}\right) tonnes/MWh}$$

Where:

- $COE_{with\ removal}$ = Cost of electricity with removal
- $COE_{w/o\ removal}$ = Cost of electricity without removal
- $CO_2 emissions_{with\ removal}$ = Mass of CO_2 emissions with CCS
- $CO_2 emissions_{w/oremoval}$ = Mass of CO_2 without CCS

The cost of CO_2 avoided is especially important as it determines the cost of removing CO_2 per unit mass on the sequestration plant. This is the carbon tax that would be required to make the capture plant competitive with its unabated counterparts [10].

2.2.8. Electrical energy storage (EES)

The push for renewable energy requires that we find solutions to the problems that prevent its large scale implementation on the grid [7]. Some of the major issues are: cost, availability and intermittence. Section 2.2.4.1 contains an explanation on how it is that renewable intermittence will affect the daily load curve and the best suited fossil fuel power plant setup (NGCC) that could cope with all the volatility [13], [18]. But this would simply be a means to supply more conventional energy from the combustion of a non-renewable fossil fuel in response to shortfalls; a better alternative that would allow one to use excess renewable energy during shortfalls is storage (or rather electrical energy storage (EES)) [6], [7], [13]. Figure 23 shows how it is that utility scale storage could accomplish this through peak shaving, and load levelling [7].

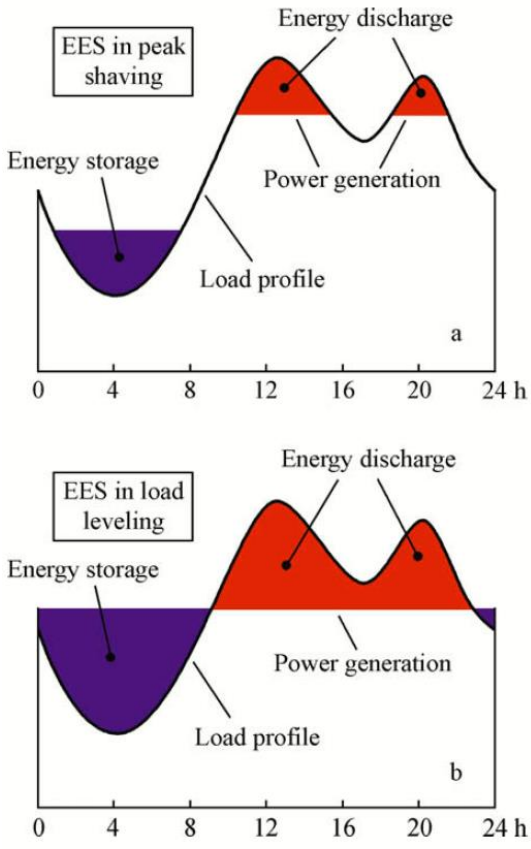


Figure 23: figure showing how EES would affect the load profile of a grid with a large share in renewables; smoothing volatility by providing peak shaving and load levelling [7]. The five most popular EES options are: hydrogen storage, methane storage (through PtG), pumped hydro-electric storage (PHES), compressed air energy storage (CAES) and battery storage [6], [7], [13], [49]–[51].

2.2.8.1. Hydrogen storage

An option for renewable energy storage is hydrogen, which once it has been produced renewably (via electrolysis for example [52]**)** can be stored using three methods: it can be stored at high pressures (up to 800bar), it can be stored as a cryogenic liquid (at 21K), or it can be stored within metal hydrides (MH). Hydrogen can be compressed to pressures between 800-900bar using high strength tanks. Its disadvantages are: the required high pressure vessels are hazardous, hydrogen compression (due to its very low volumetric energy density) is an energy intensive process requiring up to 12 or 16% of the gasses calorific value. Storing the hydrogen as a cryogenic liquid overcomes the problem associated with its low volumetric energy density. The process is very complex and energy intensive though (requiring up to 20-30% of the gasses calorific value). Storage in metal hydrides is able to overcome the difficulties associated with hydrogen's low volumetric energy density with greater efficiency and safety than compression and cryogenics; and this is because the process occurs at reduced pressures and volumes. Additionally, MH materials of construction are abundant and the hydrogen kinetics and cyclability of the selected metal hydride can be improved through use of a catalyst [13].

Additionally, hydrogen is receiving a lot of attention as a promising renewable energy carrier in future: it's safe, it can be used as a clean alternate to conventional liquid fuels in every application requiring liquid fuels today, it can be burned without any emissions, it can be converted to useful forms of energy more efficiently than any existing fossil fuel [53] and renewable hydrogen is receiving ever growing interest as an alternative for refining ever increasingly low-quality petroleum resources [54].

2.2.8.2. Pumped hydroelectric storage (PHES)

Pumped hydroelectric storage (PHES) is the most widely used EES method today [7], [55]. It stores electricity as potential energy of liquid water between reservoirs situated at different heights [7], [51]. Figure 24 is a simplified diagram of a PHES site that illustrates how this would work. Excess renewable energy would be used to pump water from the lower reservoir (at the discharge) to the higher reservoir (at the Intake). When there is demand and a shortage of renewable energy, this water would be released from the Intake and allowed to flow back to the Discharge; generating power as it does by turning turbine blades situated near the lower reservoir [7], [51], [55]. Among its advantages are that it is able to store electricity over long periods [7], and it's a high efficiency; able to regain between 70-85% of the electricity used to

pump the water upstream during the generation cycle [7], [51]. A disadvantage associated with it is scarcity, as it would be limited to sights similar to the one depicted in figure 24. They also have long lead times of up to 10 years and high costs of typically around hundreds to thousands of millions of US dollars [7], [51].

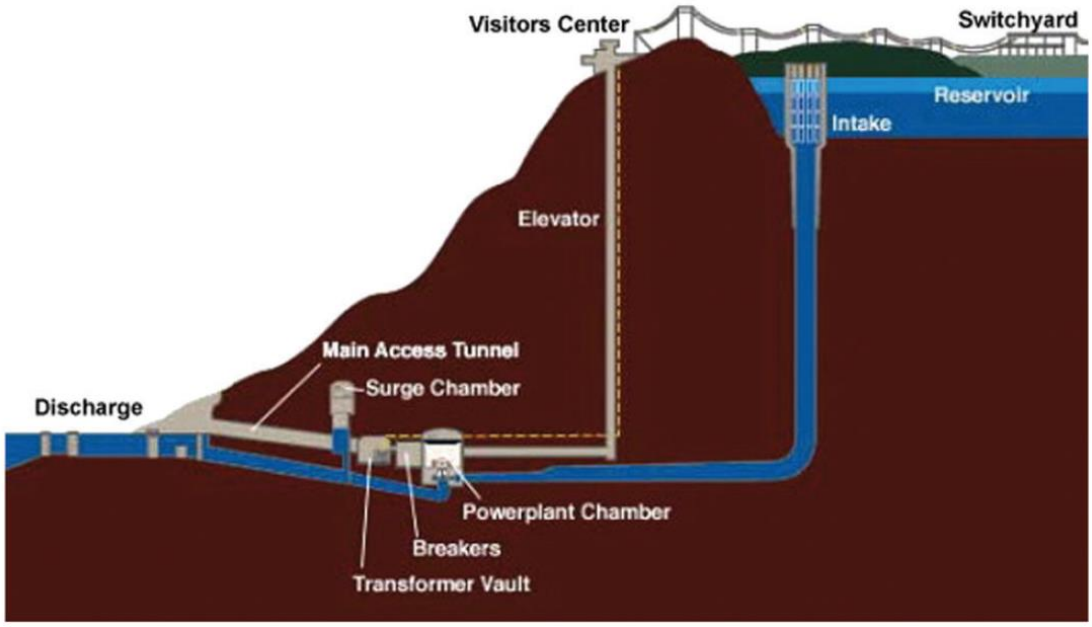


Figure 24: Simple diagram of PHES facility [51].

2.2.8.3. Compressed air energy storage (CAES)

Compressed air energy storage is much like gas turbine power generation, only with the compression and expansion cycles decoupled from one another. The energy is stored in the form of elastic potential energy of the compressed air [7]. When demand is low, renewable energy is fed to a reversible motor / generator that runs a chain of compressors which pump the air into an evacuated space (either a storage vessel, ground tanks or underground caverns [55]) to a high pressure (around 4-8 MPa [7]). When demand returns, the compressed air is then drawn from the storage vessel before being heated using heat recovered from compression or combustion after injecting a small amount of fuel. The hot gasses then report to a low pressure turbine to generate power [7], [55] and the waste heat from compression can be recycled back to a recuperator (see figure 25) [55]. One of the advantages of CAES is its capacity; storing up to 100MW with a single unit much like PHES. It also has very high part load [7], [55] and baseload efficiency (with a baseload efficiency of around 70-89% [7]), has a relatively long storage period (which can be over a year), low capital cost and is

environmentally friendly [7]. They can also be built for small or large scale capacity's [55]. A disadvantage associated with it is site [7], [55]; as it requires geographical locations that have nearby rock mines, salt caverns, aquifers or depleted gas fields that can be used to store the air on a large scale. Another disadvantage is that CAES is dependent on gas fired power generation and as such has to be deployed alongside a gas fired power plant. This fossil fuel combustion requirement produces emissions that make the setup less attractive though this could be overcome through CCS or PtG. As such, research is under way to improve the setup. Some of the proposals include: small scale CAES with fabricated small vessels, CAES with humidification [7] and finally advanced adiabatic CAES (AACAES) [7], [55] which does not require combustion and involves integration with a thermal energy storage system [55].

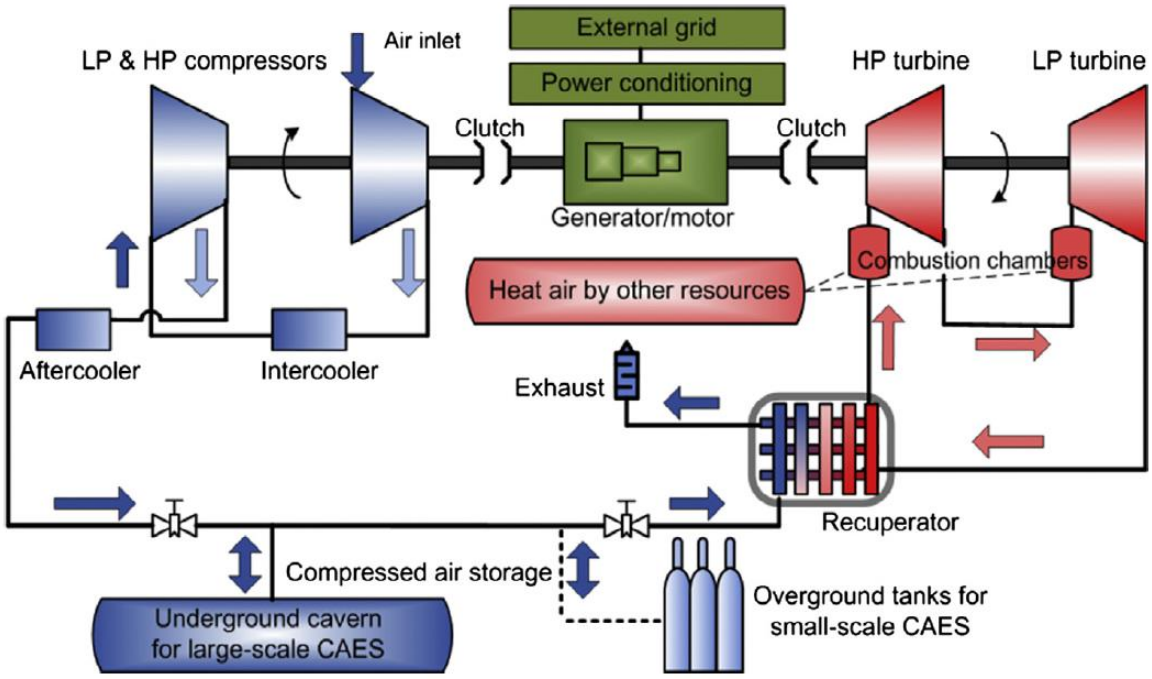


Figure 25: Simple diagram of a CAES plant / facility [55].

2.2.8.4. Battery storage

Batteries are the oldest form of EES that have been used to store electrical energy chemically for everyday appliances [7]. The electricity is stored in the form of electrochemical potential existing between two electrodes (a cathode and an anode) made of differing materials connected by a conductor. The electrodes are placed in an electrolyte which can be liquid, paste or solid electrolyte and the difference in electrochemical potential between the two electrodes is what provides the energy required (potential difference) to drive electrons from the anode to the cathode when discharging. To charge the battery an external potential difference is applied

which forces the electrons to then move in the reverse direction from the cathode to the anode. There also exists some means with which charge can move from one electrolyte compartment to the next (sometimes called a salt bridge); completing the circuit [7], [55]. The batteries most suitable for utility scale application are: the lead acid battery, the nickel cadmium battery, the sodium sulphur battery, the sodium nickel chloride battery and the lithium ion battery [7].

Lead acid batteries were invented in 1859 [7] and are the most widely used rechargeable electrochemical devices today. This battery has an anode made of lead (Pb), a cathode made of lead oxide (PbO_2) and a sulphuric acid electrolyte. Equation 4 and equation 5 are the reactions that occur at the anode and the cathode respectively [7], [55]. As it discharges both electrodes acquire sulphate ions from the electrolyte, turning them into lead sulphate ($PbSO_4$) and leaving the original electrolyte solution as water. The different types of lead acid battery include: the flooded battery which constantly needs to be topped up with distilled water, the sealed maintenance free battery which has a gelled / absorbed electrolyte and the valve regulated battery [7]. Their applications include: powering stationary devices as backup power for data and telecommunication systems, energy management applications and as clean supplementary power sources for hybrid cars [55]. Their advantages include: fast response times, smaller daily life recharge rates (<.0.3%), relatively high cycle efficiencies (63%-90%) and low capital costs (50-600$/kWh). Their disadvantages include: they have yet to find wide use in utility scale application due to their short cycle life (500-1000 cycles), their low energy density (30-50Wh/kg), as well as their short storage durations [7], [55].

$$Pb + SO_4^{2-} \leftrightarrow PbSO_4 + 2e^- \qquad \textbf{Equation 4}$$

$$PbO_2 + SO_4^{2-} + 4H^+ + 2e^- \leftrightarrow PbSO_4 + 2H_2O \qquad \textbf{Equation 5}$$

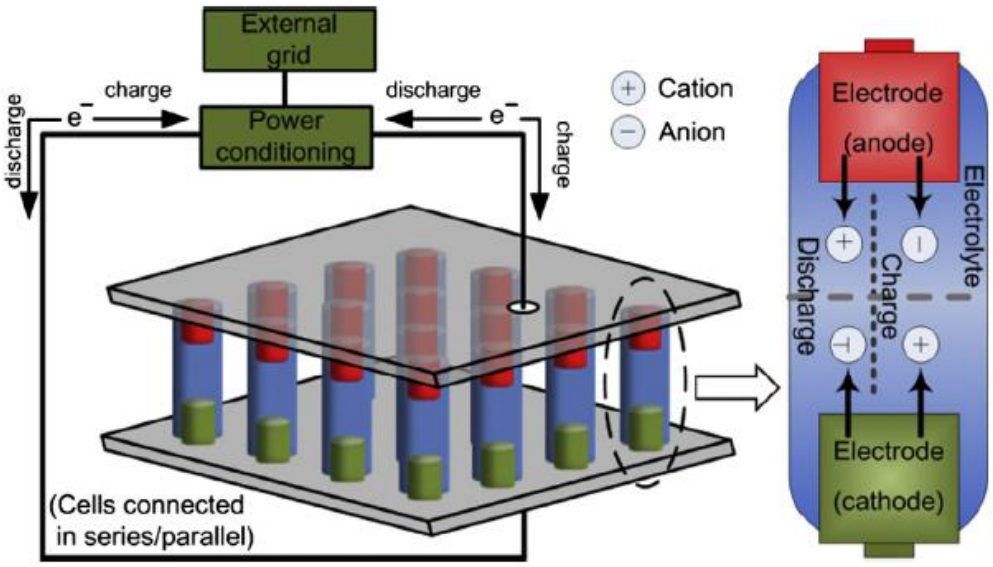


Figure 26: Simple diagram of a typical battery [55].

Nickel Cadmium batteries much like lead acid batteries are mature, and have been in existence for a long time (~100 years) [7]. The battery is made of a nickel hydroxide anode, a metallic cadmium cathode, a separator and an alkali solution serving as electrolyte. The battery is enclosed in a metal case that has a sealing plate with a self- sealing safety valve. The positive and negative electrodes are rolled in a spiral shape with the separator used to keep them apart. Equation 6 is the overall electrochemical reaction taking place within the cell. An advantage associated with these batteries is that their very robust and reliable and have low maintenance costs [7], [55]. The battery is able to deliver rated power at ~27MW for 15 minutes or 40MW for 7 minutes and has a very high efficiency of around 72%-78% at close to ambient operating temperatures of around 233K-323K. These advantages are what made them favoured over lead acid batteries over the years for power tools, emergency lighting, portable devices, UPS, telecoms and generator starting. However, they are environmentally hazardous due to cadmium and nickel being toxic heavy metals. They also suffer from memory effect; which is when the maximum capacity is greatly diminished after being repeatedly recharged when it was only partially discharged [55]. They have however fallen out of favour and been displaced by other more suitable batteries in portable devices such as mobile phones and laptops of late [7].

$$2Ni(OH) + Cd + 2H_2O \leftrightarrow 2Ni(OH)_2 + Cd(OH)_2 \qquad \textbf{Equation 6}$$

Sodium sulphur batteries are composed of a molten sodium negative electrode and a molten sulphur positive electrode and use a solid Bata alumina electrolyte. The need for the electrodes to be molten results in the cell operating at high temperatures of around 574K-624K [7], [51],

[55]. The electrolyte only allows positive ions to flow through it, and so during discharge; sodium ions flow through and react with the sulphur in the cathode compartment creating sodium polysulphide. A simple diagram depicting this setup is shown in figure 27. The battery has a short cycle life of around 2500 cycles, it has a power density of around 150 W/kg - 230W/kg, an energy density of around 150-240W/kg and has a high efficiency of around 75%-90% [7]. This battery is relatively cheap [51], [55], uses non- toxic materials and has a high recyclability of around 99% [55]. Its disadvantages include high annual operating costs (80$/kW.year) and systems required to maintain its high temperature [7], [55].

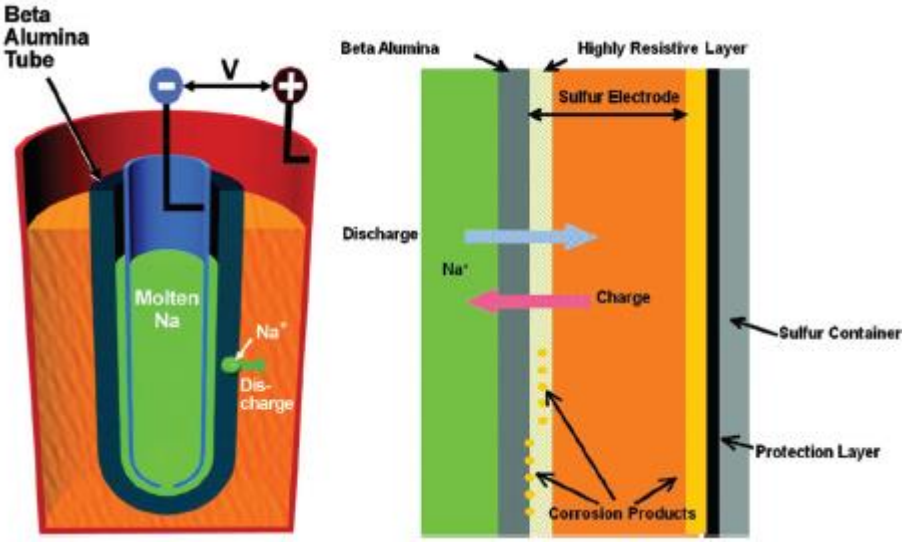


Figure 27: Simple diagram of a sodium sulphur battery [51].

Finally, the lithium ion battery has a cathode composed of a lithium metal oxide ($LiCoO_2, LiMO_2, LiNiO_2$), and an anode made of graphitic carbon with a layering structure. The electrolyte is an aqueous lithium salt that uses organic carbonates as solvent**.** These batteries have high cycle efficiencies of between 97%-100%, high energy densities (75 to 200Wh/kg) [7], [51], [55] and are considered a good candidate for applications in which response time, small dimension and or weight of the equipment is important. Among its drawbacks are the requirement of an on board computer to manage the cycles depth of discharge (DoD) which can affect the Li-ion batteries lifespan and increases the overall cost [55].

2.2.8.5. Power to gas (PtG)

Massive growth in renewables over the last decade has created a demand for an affordable means with which to solve renewable intermittency via storage [6], [50]. PtG achieves this by converting renewable electricity into chemical energy in the form of methane which is easy to store. It was first developed by Koji Hashimoto in 1994 with the intention of being a means with which to transport electricity over large distances [6]. This is partly because the methane product can easily be transported from point to point within pre-existing methane infrastructure [6], [50]. It involves feeding off peak renewable energy to an electrochemical cell which splits water into renewable H_2 and O_2. The H_2 produced is then used to valorise CO_2 emissions into synthetic natural gas [6] via equation 7 in a Methanation unit [6], [49], [56], though the concept (if you use appropriate reactors) could be adapted to produce chemicals (ethanol, methanol, propane), various pharmaceuticals [56] and synthetic fuels [6], [56], [57]. And although the CO_2 would be re-emitted upon combustion of the synthetic fuels when vented; the process would reduce global emissions by having different sectors use fuels derived from CO_2 emissions from other sectors. And the process itself could make any facility it's retrofitted to carbon neutral by re-using the synthetic fuels produced onsite. PtG has a lot of potential to become a feasible option of storing energy over longer (seasonal durations); storing much of the energy that would normally be curtailed during seasonal peaks (like the larger amount in incoming solar radiation that falls to the earth in summer that we would need to dispose of).

It's also a valuable alternative to CCS in regions with little to no CO_2 storage sites. Electrolysis can be conducted at either high (between 600℃ and 1000℃) or low temperature (around 80℃) [49], [52], [54], [57], [58].

$$CO_2 + 4H_2 \rightarrow CH_4 + 2H_2O \qquad \Delta H_{298.15K} = -164.9\ (kJ/mol) \qquad \textbf{Equation 7}$$

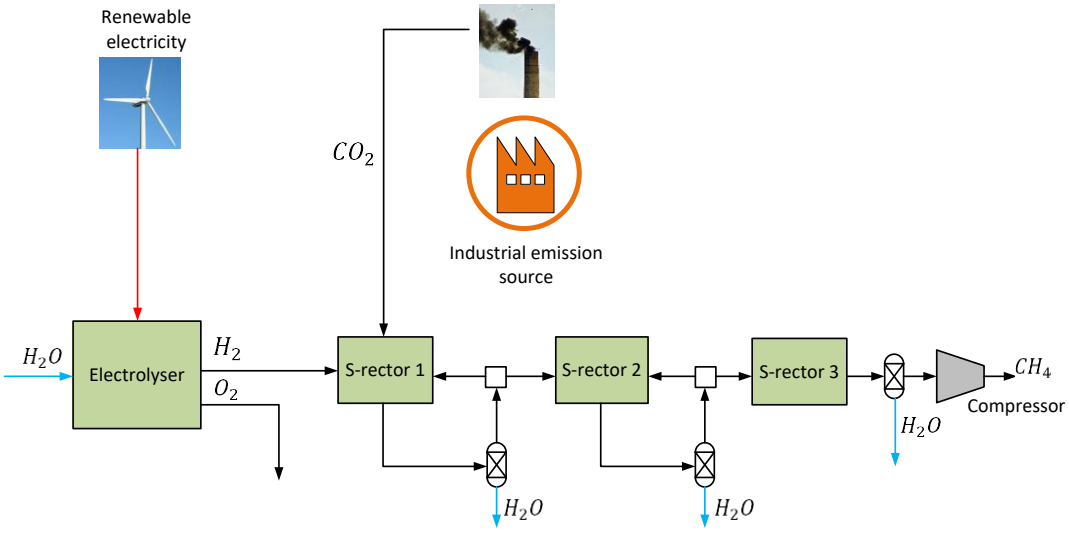


Figure 28: Simple block flow diagram illustrating basic principle behind PtG.

2.2.8.5.1. Electrolysers

Electrolysers are inverted electrolytic cells that instead of supplying electrical energy, are instead fed electrical energy to bring about a non-spontaneous reactions. There are two types of electrolysers in commercial use today: Alkaline electrolysers and proton exchange membrane electrolysers (PEM). PEM electrolysers are composed of a solid electrolyte, are quicker at altering their power consumption and can operate at elevated pressures. Alkaline electrolysers have a liquid electrolyte and are the most commonly used in situations requiring large amounts of hydrogen (such as is required in water electrolysis) because of their lower investment cost [50].

Among the motives for selecting the electrolyser (or rather the electro-chemical conversion of renewable energy and water to hydrogen) are; that the means with which we produce hydrogen today (via Methane reforming) is not ideal from a long-term perspective because methane is a non-renewable resource that we need to wean ourselves from if we are to run our economies sustainably and combat climate change [54]. Electrochemical conversion is efficient (between 50% - 70%) [52]–[54] and convenient; and this is partly because the process is very easy to control using electrode potentials. And lastly, SOEC's can be powered using renewable energy, are very compact, modular and scalable [57]. Although producing hydrogen via electrochemical conversion is for the moment expensive as a stand-alone process; it can become viable as a supplementary source of hydrogen to another process [54]. Such as a

process requiring syngas upgrading [6], [56] or the NGCC pre combustion capture power plant simulated in this work.

2.2.8.5.1.1. Alkaline electrolysers

Alkaline electrolysers typically have an aqueous electrolyte composed of 20-30% KOH (stainless steel has optimal conductivity and corrosion resistance within this concentration range) by mass, with the rest being composed of water. Modern alkaline electrolysers can operate at current densities within the range of 100-400 ($mA.cm^{-2}$), and can have unipolar [53], or bipolar electrode geometry (See figure 29) [52], [53]. With bipolar electrode geometry (BEG), only the cathode and anode end points are connected to the external circuit [52], [53], while in the unipolar electrode geometry (UEG), the electrodes are connected in parallel; with several electrodes connected to the external circuit [53].

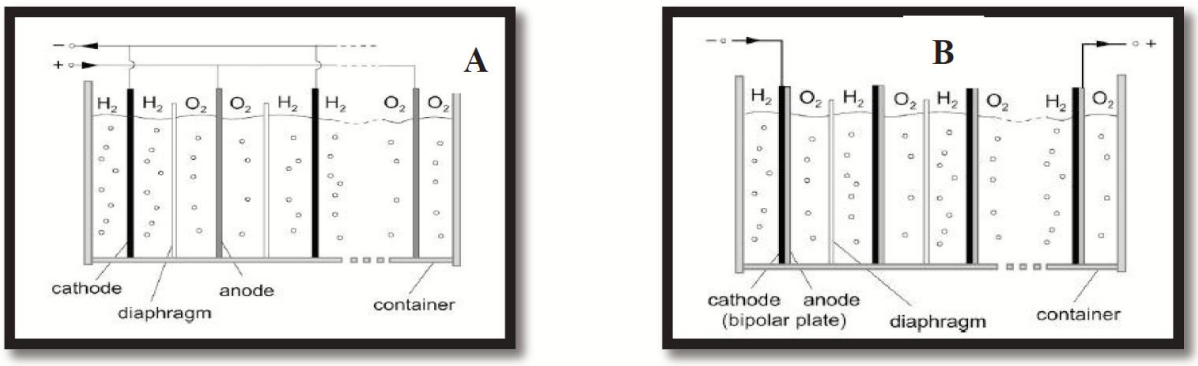


Figure 29: Alkaline electrolyser design configurations: (a) Unipolar electrode geometry and (b) Bipolar electrode geometry [53].

Advantages associated with UEG are; that it's composed of fewer parts and is easy to manufacture and repair [53]. BEG (filter press configuration) has among its advantages; compact design, shorter current paths [52], [53] and the ability to operate at elevated pressures [52]**.** The shorter current paths one gets with BEG are as result of its compact design which reduces losses due to ohmic resistance [52], [53]**;** increasing efficiency [53]. The cell itself is tubular and contains circular electrodes which are separated by a diaphragm or membrane meant to prevent the product gasses from mixing. Part of the reason they're so compact is that the membrane is very thin [52]**,** another reason they're so compact is that the electrodes are placed at either end; reducing cell height. A major disadvantage with BEG is that the unit cannot be repaired without replacing the entire stack [53]. A disadvantage that comes with

today's commercial electrolysers is that in future we will require electrolysers 10 to 100 times the size of today's largest units in order to satisfy demand [52].

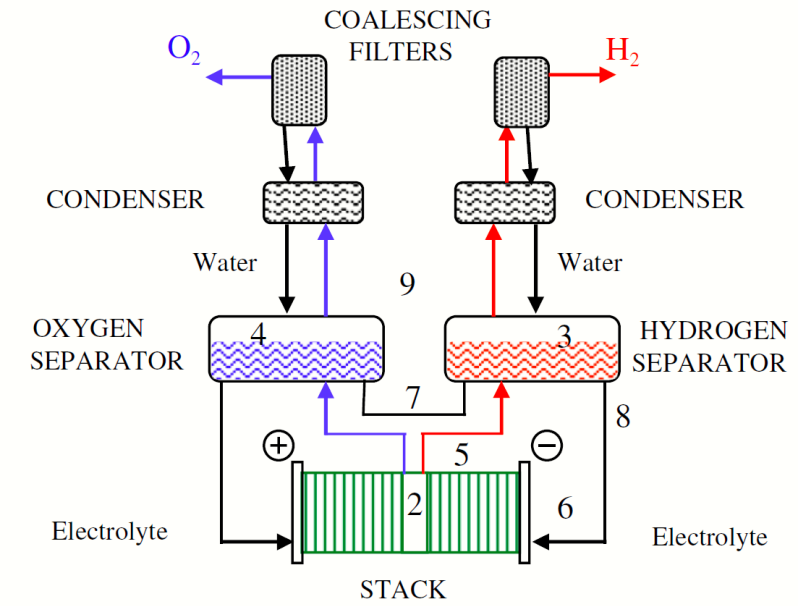


Figure 30: Simplified layout of the main components of a HySTATA™alkaline water electrolyser. Numbers refer to the important components within the unit: (2) this is the electrolyser stack, (3) Hydrogen separator, (4) Oxygen separator, (5) Hydrogen pipe at the stack outlet, (6) electrolyte pipe at the stack outlet, (7) pipe communicating the two gas separators, (8) electrolyte pipe at the hydrogen separator outlet, (9) ambient environment [52].

2.2.8.5.1.2. Electrolyser thermodynamics

Using standard half reactions one can determine the standard enthalpy change that comes with the endothermic decomposition of water into hydrogen and oxygen to be 286 (kJ/mol) or 39.7 (kWh/kgH_2). The standard free energy change of the reaction ΔG^o is 237 (kJ/mol) [52], and one can use it to determine the minimum voltage (reversible potential) that needs to be applied using equation 8 which comes to 1.23V [52], [53].

$$\frac{\Delta G^o}{z.F} = U^o_{rev} = \frac{2.37\times10^8(J/kmol)}{2[9.65\times10^7(C/kmol)]} = 1.23V \qquad \textbf{Equation 8}$$

Where: ΔG^o is the standard free energy change of the reaction, z is the number of electrons transferred, F is faradays constant and U^o_{rev} is the reversible overpotential. U^o_{rev} represents the minimum potential difference needed to upgrade the reactants into products.

The rest of the total energy (ΔH^o) required to bring about thermoneutral potential (ΔU_{th}^o) (this is the potential difference required to bring about the reaction at standard state) can then be supplied as electrical work or heat. This additional energy requirement is represented by the term $T.\Delta S^o$ in equation 10, or one can determine thermoneutral potential directly using equation 9 [52].

$$\frac{\Delta H^o}{z.F} = U_{th}^o = \frac{2.86\times10^8(J/kmol)}{2[9.65\times10^7(C/kmol)]} = 1.48V \qquad \textbf{Equation 9}$$

$$\Delta H^o = \Delta G^o + T\Delta S^o \qquad \textbf{Equation 10}$$

Where: ΔH^o is the standard enthalpy change of the reaction, T is the temperature at which the reaction takes place and ΔS^o is the standard entropy change of the reaction.

As temperature rises, the free energy change (ΔG) across the cell reduces. However, the total energy demand (ΔH) increases gradually with temperature rise. The reason this happens is that entropy change across the unit increases to the point that the increase experienced by the term $T\Delta S$ (which is often called the heat demand) outstrips the reduction in total energy demand (See figure 31).

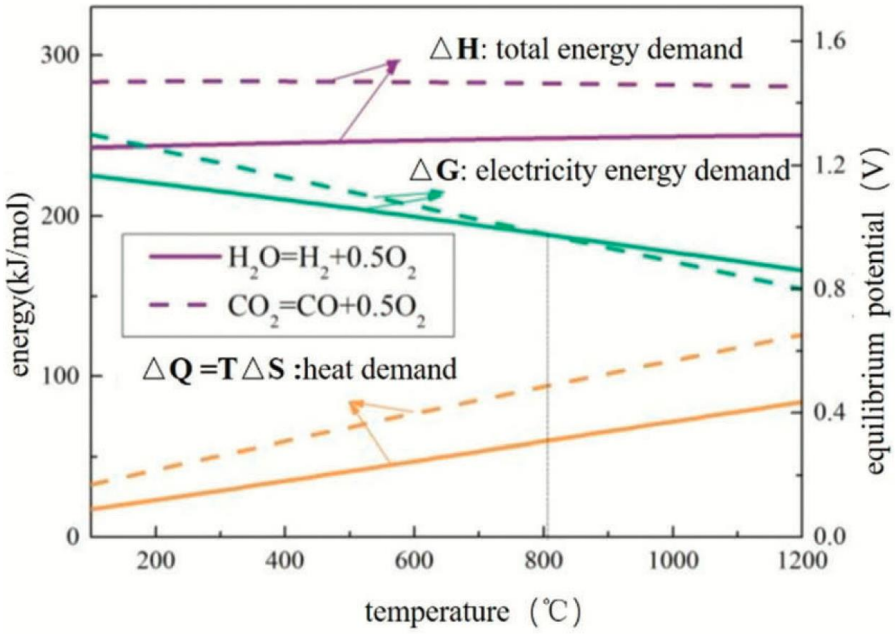


Figure 31: Graph depicting change in total energy demand (ΔH), free energy change (ΔG) and heat demand ($T\Delta S$) for the electrolysis of CO_2 (dotted lines) and water (solid lines) [57].

The voltage drop across the cell (U_{cell}) has several components. Among them are: The reversible potential (U_{rev}), the activation overvoltage (U_{active}) and the ohmic overpotential (U_{ohm}) (see equation 12) [52], [53].

$U_{cell} = U_{rev} + U_{active} + U_{ohm}$ **Equation 11**

The activation overpotential is associated with the potential difference required to overcome the activation energy of the electrochemical processes across the electrodes. This overpotential depends strongly on the electro catalytic activity of the material with which the electrodes are constructed and increases logarithmically with current density. This ohmic overpotential is associated with electrical resistance of the materials with which the cell was constructed such as the membrane and the electrolyte. It is directly proportional to current density, indirectly proportional to the electrical conductivity and indirectly proportional to the distance between the electrodes [52].

2.2.8.5.1.3. Low temperature electrolysis (LTE)

For electrolysis conducted at low temperature the electrolyser is fed only water; which it then splits into H_2 at the cathode (equation 12) and O_2 at the anode (equation 13) [52]. Water conversion is above 99.9% [49].

$Cathode: 2H_2O_{(l)} + 2e^- \rightarrow H_{2_{(g)}} + 2OH^-{}_{(aq)}$ **Equation 12**

$Anode: \ 2OH^-{}_{(aq)} \ \rightarrow 1/2\, O_{2_{(g)}} + H_2O_{(l)} + 2e^-$ **Equation 13**

As mentioned before, the standard enthalpy change when water is split into hydrogen and oxygen is 286 (kJ/mol) [50]. This ideal however is never realised since commercial electrolysers cannot operate at standard conditions because of material constraints. Your typical low temperature electrolysers (LTE) operates at around 80℃ [49], [52]**,** has an energy consumption of around 4.3 (kWh/Nm^3H_2) [49], [52] and has an efficiency of around 70% [52]. Currently, the Norwegian manufacturing company Norsk Hydro manufacture commercial alkaline electrolysers that can produce 380,000 $(kgH_2/year)$, have a power consumption of 2.3MW, a system energy consumption of 53.4 (kWh/kgH_2) at an efficiency of around 73% [52].

2.2.8.5.1.4. High temperature co-electrolysis (HTCE)

For electrolysis conducted at high temperature the electrolyser is co-fed water and CO_2 which are both reduced (reactions 14, 15 and 17) to produce syngas. The oxide ions then migrate through the electrolyte before being oxidised at the anode (reaction 16) [54], [56], [57]. HTCE

was suggested as a means with which one could produce syngas directly, using an electrolyser. The syngas once fed to a Fischer-Tropsch unit could then be used to produce carbon neutral synthetic fuels [54], [57]. Co-electrolysis reaction mechanisms are complicated by the reverse water gas shift (RWGS) reaction (reaction 17) with much debate on whether it is it that is responsible for the majority of the CO released at the cathode or reaction 15 [56]. The RWGS reaction (reaction 17) is an equilibrium reaction which occurs because of favourable thermodynamic conditions. It is endothermic, with a standard enthalpy change of around 41 (kJ/mol). An undesirable side reaction which could hinder the electrolysis process is coke formation (reaction 18). It can hinder the process through carbon deposits on the electrolyser surface and occurs at very high cell voltages. Another undesirable side reaction is reaction 19 which occurs when nickel is used as a catalyst at temperatures lower than $973K$.

$$Cathode: 2H_2O(l) + 4e^- \rightarrow 2H_2(g) + 2O^{2-}(aq) \quad \textbf{Equation 14}$$

$$Cathode: 2CO_2(g) + 4e^- \rightarrow 2CO(g) + 2O^{2-}(aq) \quad \textbf{Equation 15}$$

$$Anode: 2O^{2-}(aq) \rightarrow \ O_2(g) + 4e^- \quad \textbf{Equation 16}$$

$$Cathode\ (RWGS): 2CO_2(g) + H_2 \leftrightarrow \ CO(g) + H_2O \quad \textbf{Equation 17}$$

$$CO \rightarrow C + \left(\frac{1}{2}\right) O_2 \quad \textbf{Equation 18}$$

$$CO + 3H_2 \rightarrow CH_4 + H_2O \quad \textbf{Equation 19}$$

A simple diagram of the cross section of a co-electrolysis electrolyser can be seen in figure 32. Co-electrolysis utilises a solid oxide electrochemical cell [56], [57] composed of a cathode (fuel electrode), an anode (oxygen electrode) and a dense ionic conductor acting as electrolyte [57]. The reduction reaction occurs on the cathode electrode surface which is typically made of porous nickel or an alloy of nickel and yttria stabilised zirconium (YSZ). The anode is the electrode from which oxygen is released; and is typically made of an alloy of lanthanide, strontium and manganese oxide (LSM) [56]. CO_2 and H_2O are fed in, before being reduced, and then released from the cathode as CO and H_2 [57]. Oxide ions (O^{-2}) then migrate across the tight, solid electrolyte before being oxidised at the anode and being released as oxygen [56], [57]. O'Brien, et al, [54] reported that HTCE when retrofitted to a nuclear power plant could have thermal to hydrogen efficiencies of 50% or higher.

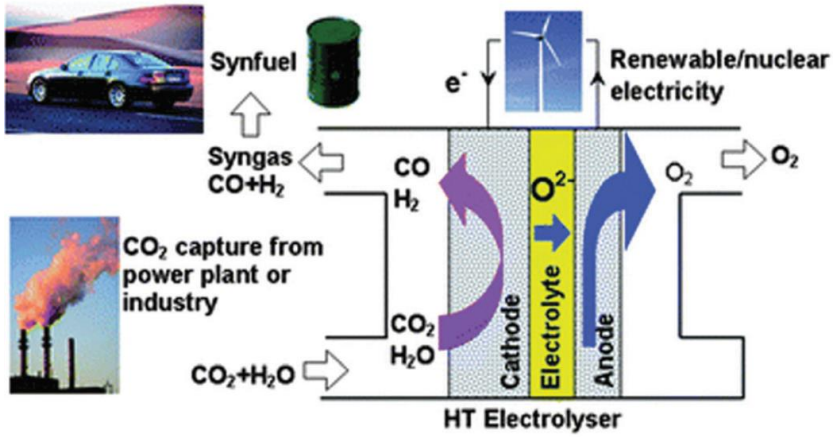


Figure 32: Simplified diagram of a co-combustion SOEC, fed CO_2 and H_2O to produce a syngas mixture which is used to produce synthetic fuels and oxygen [57].

The RWGS reaction (equation 17) products can be determined using the equilibrium constant ($K(T)$) (equation 20). The value of equilibrium constant itself can be determined using equation 21 for varying temperatures [56].

$$K(T) = \frac{(Y_{H_2})(Y_{CO_2})}{(Y_{H_2O})(Y_{CO})} \qquad \textbf{Equation 20}$$

$$\log(K) = -2.4198 + 0.0003855T + (2180.6 / T) \qquad \textbf{Equation 21}$$

Where: $K(T)$ is the equilibrium constant at a specified temperature, Y_{H_2} is the equilibrium mole fraction of hydrogen, Y_{CO2} is the equilibrium mole fraction of CO_2, Y_{H_2O} is the equilibrium mole fraction of water, Y_{CO} is the equilibrium mole fraction of CO and T is the temperature in kelvin [56].

However, HTCE using a SOEC is not yet mature enough for commercialisation; requiring much research and development. Major challenges include: HTCE is not yet commercially viable because of low activation / conversion of carbon dioxide and as well as degradation of the SOEC stacks [57].

2.2.8.5.2. Methanation

2.2.8.5.2.1. Process layout

The methanation unit typically consists of several Sabatier reactors which are fed CO_2 from an industrial emission source and renewable hydrogen from an electrolyser to produce CH_4 (see Figure 28). Both Hydrogen and the CO_2 rich flue gas can initially be compressed to pressures

of around 30bar by compression trains with intermediate intercooling keeping the gasses at 120℃ between each compression stage. The gas temperature is then altered to between 195℃ and 300℃ using a pre-heating stage before entering the reactor. The methanation unit then exothermically converts the incoming syngas into methane [49], [50] via equation 22.

$$Methnation: CO_2(g) + 4H_2 \leftrightarrow CH_4\,(g) + H_2O \qquad \textbf{Equation 22}$$

The reaction temperature must be kept within the range of 200℃ - 450℃ [59] to prevent loss of catalyst active surface area at temperatures above 600℃ [49]**.** The feed to each Sabatier reactor must be heated to around 195℃ and to prevent unacceptably slow reaction rates temperatures must not drop below 200℃ [50]. To achieve this, up to 89% of the reactor product can be recycled back into the reactor [49], [50]. The most common type of catalyst used is the Haldor TopsØe – PK-7R nickel-based catalyst. This catalyst can operate at temperatures within the range of 190℃ - 450℃. For operation at higher temperatures (above 700℃); another catalyst denoted MCR is used. Among the Advantages associated with higher temperature is that there is reduced need for temperature control and increased opportunity for heat integration. But this does come at the expense of hydrogen conversion and increases the metallurgical demands on the materials from which the equipment has been built. Additionally, carbon formation needs to be avoided and H_2S needs to be removed as these degrade the catalyst through fouling and poisoning. There are other catalysts made from Rubidium, Rhodium, Platinum, Iron and Cobalt; though the nickel catalyst is preferred due to its superior selectivity, activity and low cost [50].

It's been reported that for an oxy-combustion retrofit that the temperature of the stream reporting to the third reactor should match that of the first, and to prevent solid carbon formation it's also been reported that the temperature of the intermediate condensation stage needs to be kept above 125.5 ℃ for this same setup (see Figure 33) [49]. Bailera, et al, [49] also reported that the product from the final reactor is typically not recycled as this promotes methane formation. Any oxygen within the feed needs to be removed as it poisons the catalyst, and this places a restraint on the fraction of total flue gasses that are directed to the methanation unit. This percentage can be determined using equation 23. The oxygen is removed by burning it in the presence of Hydrogen [49] until the ratio of $H_2{:}\,CO_2$ is (1:4); satisfying the reaction stoichiometry [49], [53]. The final product has a composition in methane of around 95% [49], [50].

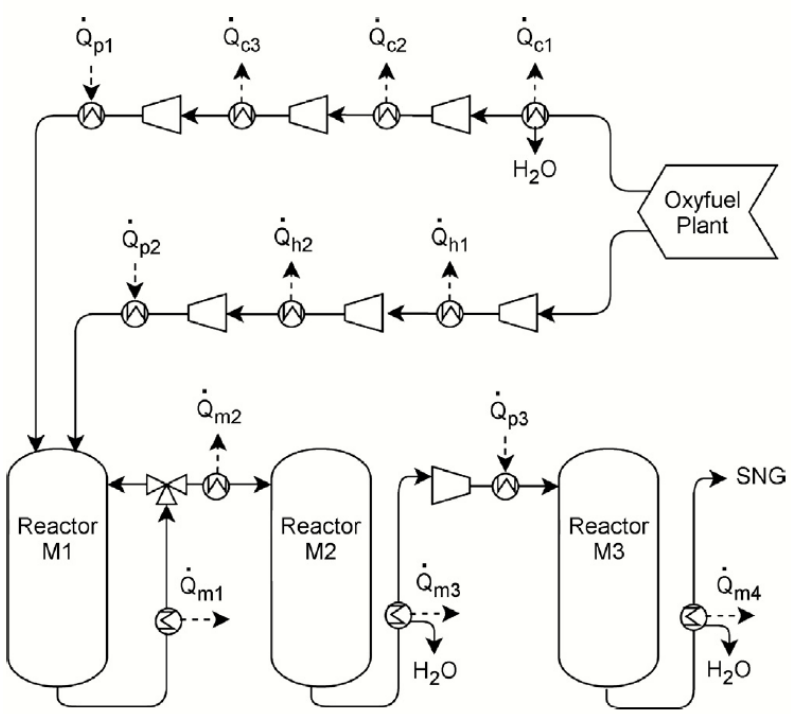


Figure 33: Simple diagram of methanation unit fed by an oxy-combustion power plant [49].

$$\emptyset_{FGM} = \mathbf{100}\left[\left(\gamma_{CO_2,FG} + \frac{1}{2}\,\gamma_{O_2,FG}\right)^{-1}\frac{\left(\frac{1}{4}\dot{n}_{H_2}+\dot{n}_{CO_2,loss}\right)}{\dot{n}_{FG}}\right] \qquad \textbf{Equation 23}$$

2.2.8.5.2.2. Methanation reaction

Overall the Sabatier reaction is exothermic (see equation 26), and several reactions play a role in the methanation process [50], [60] although the exact reaction mechanism is still under discussion [50]. The most widely accepted mechanism is methanation via a combination of reversed endothermic water gas shift reaction (equation 27) [50], [60] and exothermic CO methanation [50] (also known as CO hydrogenation reaction [60]) (equation 28). Finally, the boudouard reaction (equation 29), which is an undesirable reaction resulting in carbon formation also takes part [60]. The equilibrium constant for the reaction at constant temperature and pressure can be determined using equation 24 and equation 25 respectively [50].

$$K_p = \frac{Y_{H_2O}^2 Y_{CH_4}}{Y_{CO_2} Y_{H_2}^4}\left(\frac{P}{P^O}\right)^{-2} \qquad \textbf{Equation 24}$$

$$K_p = exp\left(-\frac{\Delta G_T^0}{R_u T}\right) \qquad \textbf{Equation 25}$$

Though the reaction overall favours lower temperatures (see Table 2); kinetic limitations necessitate operation at higher temperatures [50] within the range of (190℃ - 550℃) [59] enabled by the Haldor TopsØe – PK-7R [49], [50], [59] nickel-based catalyst mentioned in section 2.2.8.5.2.1.

Table 2: K_p values for Sabatier reaction between the temperatures of $400K$ - $1000K$ [50].

Temperature		Kp
[K]	[°C]	[-]
400	127	2.70Ex12
600	327	7.15Ex4
800	527	7.70
1000	727	0.03

$$CO_2(g) + 4H_2 \leftrightarrow CH_4\,(g) + H_2O \qquad \Delta H^{O}_{reaction} = -165\left(\frac{kJ}{mol}\right) \qquad \textbf{Equation 26}$$

$$CO_2(g) + H_2(g) \leftrightarrow CO\,(g) + H_2O(g) \qquad \Delta H^{O}_{reaction} = +41.2\left(\frac{kJ}{mol}\right) \qquad \textbf{Equation 27}$$

$$CO(g) + 3H_2 \leftrightarrow CH_4\,(g) + H_2O \qquad \Delta H^{O}_{reaction} = -206.4\left(\frac{kJ}{mol}\right) \qquad \textbf{Equation 28}$$

$$2CO(g) \rightarrow C(s) + CO_2(g) \qquad \Delta H^{O}_{reaction} = -172.5\left(\frac{kJ}{mol}\right) \qquad \textbf{Equation 29}$$

2.2.9. Exergy analysis

2.2.9.1. Significance of the second law

Plant efficiency can be determined using characterisation of state properties determined from an energy analysis using the first law of thermodynamics. This law states that: energy cannot be created or destroyed; only transferred i.e.(energy is conserved). This law does not consider the second law of thermodynamics which states: the entropy of an isolated system (the system and surrounding) is forever increasing. An amount of work is lost as this happens that cannot be harnessed using any means derived from the technology in our present day. Accounting for this, transforms the "energy" analysis to what is called an "exergy" analysis, which allows us not only to more accurately determine what plant layouts are most efficient; it's also a tool with which sections in the plant and their accompanying process units can be accurately ranked according to irreversibility: irreversibility is a measure of the amount of work destroyed to reach a desired outcome. It can help determine which areas are most wasteful and which areas have the greatest potential for improvement. The work output that isn't destroyed as a result of entropy production is called the heat or mass flow exergy content, availability or useful work content [24].

2.2.9.2. Carnot efficiency; equilibrium & reversibility

There exists an upper limit to the amount of work (which in this case is called usable work or exergy) an amount of heat accepted or rejected by a system can do called the Carnot efficiency. This limit is dependent on the temperature disparity between the thermal reservoir that rejects the heat and the ambient environment. Equation 30 is a means of determining this Carnot efficiency, and equation 31 is a means of using the Carnot efficiency to determine the amount of usable work that can be harnessed from heat flow "Q" [24].

$$\eta_{carnot} = \frac{T_H - T_0}{T_H} \qquad \textbf{Equation 30}$$

$$W_{usable} = Q\left[\frac{T_H - T_0}{T_H}\right] \qquad \textbf{Equation 31}$$

Where: T_H is the temperature at which the heat is delivered, T_0 is the prevailing ambient temperature and Q is the quantity in heat delivered. This Carnot efficiency was developed through the conception of an idealised power cycle that transmits heat from a hot reservoir to

a working fluid through a conducting surface i.e.(an idealised Rankine cycle). As the fluid goes round the cycle; it goes through a series of processes that are infinitesimally close to equilibrium. This makes the idealised process perfectly efficient and its work output an idealised maximum for the quantity of heat accepted by the working fluid [61]. It can also by extension be used to determine the amount of usable work attainable from a quantity of heat (Q) transmitted through a conducting surface [24].

Reversibility is the reason we characterise the equilibrium processes that the fluid goes through as being perfectly efficient. Reversibility can be thought of as the maximum amount of work attainable after achieving a particular change in state, and the work losses that occur on route to reaching the final state are called exergy losses. These exergy loses destroy the work potential or the useable work content of all the matter and heat streams coming to and from the system.

Formally, these un-retrievable work flows are caused by: solid fluid friction i.e.(viscous dissipation from unrestrained expansion and dissipative processes), mechanical or electrical hysteresis, ohmic resistance and heat transfer over a finite temperature difference. The quantity in work potential that isn't destroyed is called the stream exergy content; and is a measure of the maximum amount of work that can be harnessed from the said stream [24].

The fraction of work that isn't usable is destroyed as a result of an increase in entropy of the isolated system (which is combination of the system and the surroundings). Equation 32 (which is the product of the entropy production of the isolated system (ΔS_{isol}), and the prevailing ambient temperature, T_0) is an expression for determining the fraction of work or heat destroyed as a result entropy production for a system [24].

$$W_R = (T_0)\,\Delta S_{isol} \qquad \textbf{Equation 32}$$

2.2.9.3. Energy balance for a control region

The first law of thermodynamics states that the energy is conserved; and that there exists a property called internal energy (U) whose change in value for a system not in motion is given by the difference between the heating done to the system (Q) and the work done by the system (W) (see equation 33) [24], [31], [61], [62].

$$\Delta U = Q - W \qquad \textbf{Equation 33}$$

This property can be evaluated for an infinitesimal part of the system using the differential form of equation 33; which is equation 34 [24], [31], [61], [62].

$$dE = \delta Q - \delta W$$ **Equation 34**

Note that "δ" here is used in place of the differential operator "d" to indicate that both Q and W cannot be evaluated without information on the process path [24]: in other words, work and heat are not state variables.

For a system undergoing an infinitesimal process as it moves through a control region it is assumed that the control region (CR) can undergo a change in volume, and the work done by the system on the control region to bring about this change in volume is labelled δW_{CS} (see figure 34). The change in energy of the control region will be labelled dE_{CR}. Additional forms of work that can be done by the system are: Shaft work δW_X and net displacement work $P_e v_e dm_e - P_e v_e dm_e$ [24].

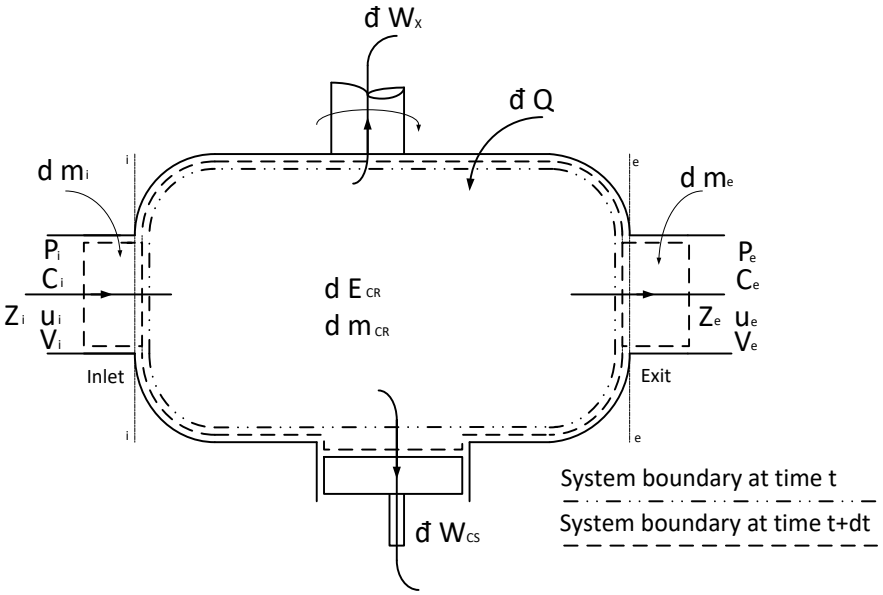


Figure 34: Movement of a system through a control region. This diagram is adapted from a similar one in Kotas [24].

When one takes into consideration the change in kinetic and potential energies in the system before combining these into equation 34 you get equation 35 [24]:

$$\delta Q - \delta W_X - \delta W_{CS} = dE_{CR} + \left[(U_e + P_e v_e) + \frac{1}{2}C_e^2 + g_E Z_e\right] dm_e$$

$$- \left[(U_i + P_i v_i) + \frac{1}{2}C_i^2 + g_E Z_i\right] dm_i$$ **Equation 35**

Once you take into consideration the definition of specific enthalpy ($h = u + Pv$) and substitute this into equation 35, divide by dt and express in a rate basis we get equation 36 [24]:

$$\delta Q - \delta W_X - \delta W_{CS} = \left[h_e + \frac{1}{2}C_e^2 + g_E Z_e\right]\dot{m}_e - \left[h_i + \frac{1}{2}C_i^2 + g_E Z_i\right]\dot{m}_i + \frac{dE_{CR}}{dt} \qquad \textbf{Equation 36}$$

If you replace δQ with the sum of all heat flows entering and leaving the system $\left(\sum_r \dot{Q}_r\right)$, and for the sake of generality assume that there are also several streams of matter entering and leaving the system; you get equation 37 [24].

$$\sum_r \dot{Q}_r - \delta W_X - \delta W_{CS} = \sum_{OUT} \dot{m}_e \left[h_e + \frac{1}{2}C_e^2 + g_E Z_e\right]\dot{m}_e$$

$$- \sum_{IN} \dot{m}_i \left[h_i + \frac{1}{2}C_i^2 + g_E Z_e\right]\dot{m}_i + \frac{dE_{CR}}{dt} \qquad \textbf{Equation 37}$$

2.2.9.4. Entropy production rate for a control region

The second law of thermodynamics states that there is a property called entropy (S) whose change for an isolated system (the system and its surroundings) is always greater than or equal to zero [24] (see equation 38).

$$(\Delta S)_{ISOL} \geq 0 \qquad \textbf{Equation 38}$$

Applying this to the control region pictured in figure 35 and you get equation 39. This equation is an expression stating that the entropy production in an isolated system ($\delta \Pi$) is equal to the sum of the entropy changes of its constituent parts which are: the inlet matter reservoir (dS_{IMR}) (this is the reservoir from which matter flows come from), the control region (dS_{CR}), the outlet matter reservoir (dS_{EMR}) (this is the matter reservoir to which matter is fed from the control region), the thermal energy reservoir (dS_{TER}) (this is the reservoir that exchanges heat with the control region) and the mechanical energy reservoir (this is the reservoir that the control region dose work to or has work done to it) [24].

$$\delta \Pi = dS_{CR} + dS_{IMR} + dS_{EMR} + dS_{TER} + dS_{MER} \geq 0 \qquad \textbf{Equation 39}$$

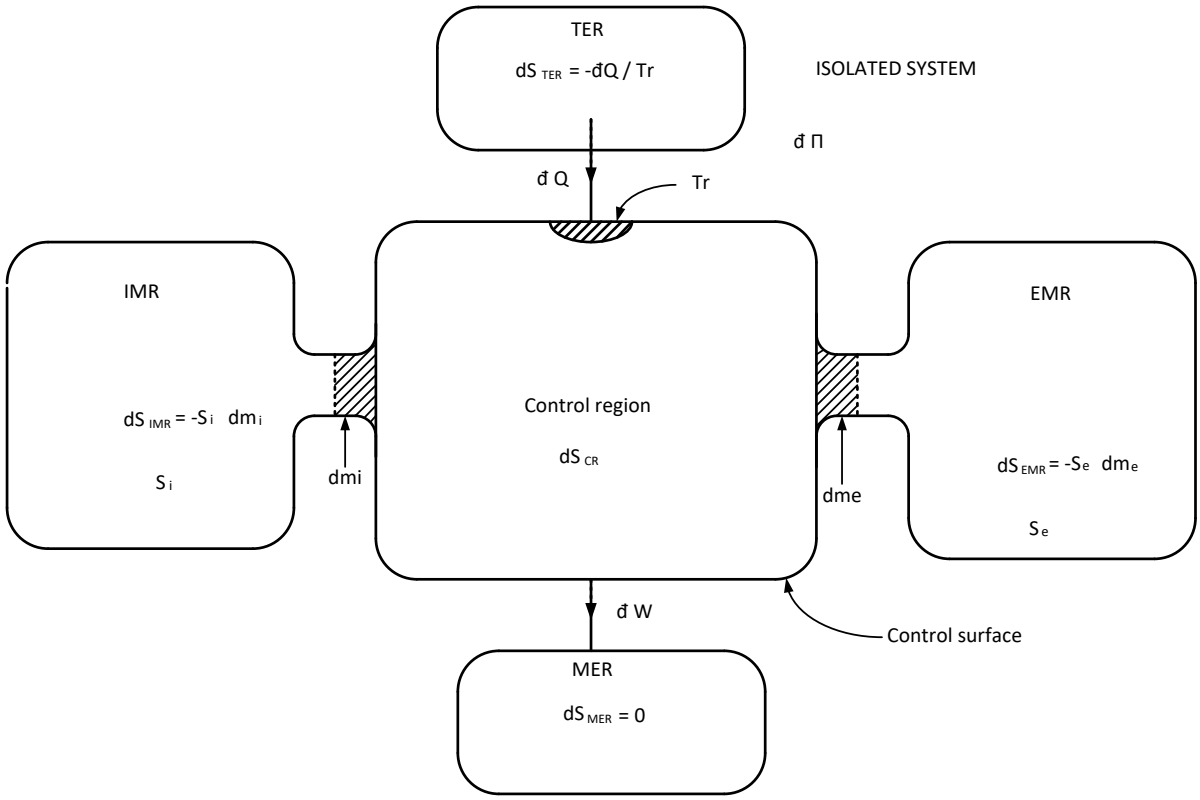


Figure 35: Entropy production in a control region. The diagram is adapted from a similar one in Kotas [24].

Assuming the mechanical exergy reservoir does not experience an increase in entropy ($dS_{MER} = 0$), and writing the terms in equation 52 as; $dS_{IMR} = -s_i dm_i$, $dS_{EMR} = s_e dm_e$, $dS_{TER} = -\frac{\delta Q_r}{T_r}$ we get equation 40 [24].

$$\delta \Pi = dS_{CR} + S_e dm_e - S_i dm_i - \frac{\delta Q_r}{T_r} \geq 0 \qquad \textbf{Equation 40}$$

When you take into consideration that there may be several streams flowing into and out of the control region, and this region could be interacting with several reservoirs and dividing by the time interval dt you get equation 41 [24].

$$\dot{\Pi} = \frac{dS_{CR}}{dt} + \sum_{OUT}(S_e \dot{m}_e) - \sum_{IN}(S_i \dot{m}_i) - \sum_r \frac{\dot{Q}_r}{T_r} \geq 0 \qquad \textbf{Equation 41}$$

Multiplying equation 41 by T_0 to determine irreversibility or restoring work $\left((T_0 \Delta S)_{ISOL} = W_R = \dot{I}\right)$ and substituting equation 42 into this equation you get equation 43 [24].

$$T_0 \sum_r \frac{\dot{Q}_r}{T_r} \equiv \sum_r \dot{Q}_r - \sum_r \left(\dot{Q}_r \frac{T_r - T_0}{T_r}\right) \qquad \textbf{Equation 42}$$

$$\sum_r \dot{Q}_r = T_0 \frac{dS_{CR}}{dt} + \sum_{OUT}(T_0 S_e \dot{m}_e) - \sum_{IN}(T_0 S_i \dot{m}_i) + \sum_r \left(\dot{Q}_r \frac{T_r - T_0}{T_r}\right) - T_0 \dot{I}$$ **Equation 43**

2.2.9.5. Chemical exergy

The chemical exergy of a stream of matter is defined as the maximum amount of work one can harness from the said stream when each of its components are brought from the environmental state (ambient temperature $[T_0]$ and pressure$[P_0]$) to the dead state: the dead state is characterized by thermal equilibrium (where the stream is at the ambient environmental temperature $[T_0]$) and chemical equilibrium (here each component exists in its environmental chemical state (as a reference substance or substances [24]) and partial pressure $[P_{00}]$) with the environment. To calculate the chemical exergy of a reference substance at the environmental state one can use equation 44 [24].

$$\tilde{\varepsilon}_0 = \tilde{R} T_0 \ln \frac{P_0}{P_{00}}$$ **Equation 44**

Equation 45 is an expression for determining the chemical exergy content of a material stream [24].

$$\tilde{\varepsilon}_{0M} = \sum_i x_i \tilde{\varepsilon}_{0i} + \tilde{R} T_0 \sum_i x_i \ln x_i$$ **Equation 45**

The term to the right of equation 45 $\left(\tilde{R} T_0 \sum_i x_i \ln x_i\right)$ represents the amount of work that needs to be done to get each gas mixture component to the environmental state. This work requirement is always negative since we are trying to determine the exergy content of the combined mixture at the environmental state for each component (An amount of work has to be done to compress each component from its initial state; which is only a fraction of the total environmental state pressure of the mixture), this can be considered the exergy of mixing and represents the amount of work destroyed upon mixing with the environment. The term to the left $(\sum_i x_i \tilde{\varepsilon}_{0i})$ represents the change in exergy of a pure component as it moves from the environmental state to the dead state. Values of standard chemical exergy for several reference species can be found in literature [24]. Equation 45 is means of calculating the chemical exergy content of an ideal solution. When dealing with real solutions (solutions in which there will be a change in volume or enthalpy upon mixing) one has to use equation 46 which incorporates the activity coefficient (γ_i) [24].

$$\tilde{\varepsilon}_{0M} = \sum_i x_i \tilde{\varepsilon}_{0i} + \tilde{R} T_0 \sum_i x_i \ln \gamma_i x_i$$ **Equation 46**

2.2.9.6. Physical exergy

By definition the physical exergy of a flow of matter is the maximum amount of work one can harness from it when the said stream is brought from its initial state to the environmental state by physical processes involving only thermal interaction with the environment. The environmental state is characterised by thermal equilibrium (where the stream is at the ambient environmental temperature; T_0) and isolated stream (the stream by definition cannot exchange matter with the environment) mechanical equilibrium (where the total stream pressure is one atmosphere; P_0) with the environment. Equation 47 is a simplified form of the first expression in equation 49 and equation 50, for a single component system [24]. All variables should be in SI units.

$$\varepsilon_{ph} = (h_i - h_0) - T_0(s_i - s_0) \qquad \textbf{Equation 47}$$

Where:

- ε_{ph} = physical exergy of a stream
- h_i = initial enthalpy of the stream
- h_0 = environmental state enthalpy of the stream
- T_0 = ambient temperature
- s_i = initial stream entropy
- s_0 = environmental state stream entropy

The term to the left can also be viewed as the total heat the flow of matter accepts or rejects, whilst the term to the right is a determination of the quantity of work the system destroys as it accepts or rejects the very same heat. This colligates with the general expression for determining the exergy destroyed of an isolated system (equation 38), only in that case it is the total amount in non-retrievable work in the system as whole.

2.2.9.7. Irreversibility around a control region

For equations 43 and 37, If you assume that the kinetic and potential energy terms are negligible, that the process is at steady state $\left(\frac{dE_{CR}}{dt} = \frac{dS_{CR}}{dt} = 0\right)$, that the control region cannot undergo a change in volume ($\delta W_{CS} = 0$) and equate equation 43 to equation 37 by eliminating the term $\sum_r \dot{Q}_r$ you get equation 48 [24].

$$T_0 \dot{\Pi} = \dot{I} = \sum_{IN} \dot{m}_i (h_i - T_o S_i) - \sum_{OUT} \dot{m}_e (h_e - T_o S_e) + \sum_r \left(\dot{Q}_r \frac{T_r - T_0}{T_r}\right) - \delta W_X \qquad \textbf{Equation 48}$$

However equation 48 is only suitable if one takes the environmental state as a basis for all mass flows; a more accurate measure will be based on the dead state which takes into consideration the chemical exergy's of all constituents entering and leaving the control region as well. This can be accomplished by incorporating equation 45 for ideal solutions, or equation 46 for real solutions into equation 48; giving equation 49 and equation 50 [24]. All variables should be in SI units.

Equation 49

$$T_0 \dot{\Pi} = \dot{I} = \sum_{IN} \dot{m}_i (h_i - T_o S_i) + \dot{m}_i \sum_i x_i \tilde{\varepsilon}_{0i} + \dot{m}_i \tilde{R} T_0 \sum_i x_i \ln x_i - \sum_{OUT} \dot{m}_e (h_e - T_o S_e) + \dot{m}_e \sum_e x_e \tilde{\varepsilon}_{0e} + \dot{m}_e \tilde{R} T_0 \sum_e x_e \ln x_e + \sum_r \left(\dot{Q}_r \frac{T_r - T_0}{T_r} \right) - \delta W_X$$

Equation 50

$$T_0 \dot{\Pi} = \dot{I} = \sum_{IN} \dot{m}_i (h_i - T_o S_i) + \dot{m}_i \sum_i x_i \tilde{\varepsilon}_{0i} + \dot{m}_i \tilde{R} T_0 \sum_i x_i \ln \gamma_i x_i - \sum_{OUT} \dot{m}_e (h_e - T_o S_e) + \dot{m}_e \sum_e x_e \tilde{\varepsilon}_{0e} + \dot{m}_e \tilde{R} T_0 \sum_e x_e \ln \gamma_e x_e + \sum_r \left(\dot{Q}_r \frac{T_r - T_0}{T_r} \right) - \delta W_X$$

Equation 49 is the equation to use when calculating the irreversibility around a control region when working with ideal solutions, and equation 50 is the equation to use when calculating the irreversibility around a control region when working with real solutions.

2.2.9.8. Exergy and flow-sheeting simulators

A more convenient means of determining the exergy content of material streams in flow-sheet simulators such as ASPEN plus was developed by Hinderink, et al, [63]. Unlike the method developed by Kotas [24], this method separates the material stream into its pure unmixed components at the initial stream conditions (T, P) before determination of the physical and chemical exergies. This separates the exergy of mixing term from the chemical exergy and greatly simplifies the calculation of total stream exergy for flow-sheet simulators. So when using this method the total exergy content of a material stream is divided into three distinct components: the exergy of mixing ($\dot{E}_{mix}$), the physical exergy ($\dot{E}_{ph}$) and the chemical exergy ($\dot{E}_{ch}$) [63] (see equation 51).

$$\dot{E}_{tot} = \dot{E}_{ch} + \dot{E}_{ph} + \dot{E}_{mix} \qquad \textbf{Equation 51}$$

2.2.9.8.1. Exergy of mixing

First the stream at its initial conditions (T, P) is separated out into its pure unmixed components at conditions (T, P) using the exergy of mixing. Much like the exergy of mixing in equations 45 and equation 46, it too is always negative (see equation 52) [42], [63]. All variables should be in SI units.

$$\dot{E}_{mix} = \left[\dot{F}h - \sum_i^n(\dot{F}_i h_i)\right] - T_0\left[\dot{F}s - \sum_i^n(\dot{F}_i s_i)\right] \quad \textbf{Equation 52}$$

Where, $\dot{F}$ is the total stream molar flow, $\dot{F}_i$ is the component molar flow, h is the total stream enthalpy, h_i is the component molar enthalpy, s is the total stream molar entropy and s_i is the component molar entropy.

It is because the stream is separated out into its pure components that you can ignore the activity coefficient when using this method.

2.2.9.8.2. Physical exergy

Then the physical exergy of the pure unmixed components is determined as each component moves from processes conditions (T, P) to the environmental state (T_0, P_0) using equation 53 [42], [63]. All variables should be in SI units.

$$\dot{E}_{ph} = \left[\sum_i^n(\dot{F}_i h_i) - \sum_i^n(\dot{F}_{0,i} h_{0,i})\right] - T_0\left[\sum_i^n(\dot{F}_i s_i) - \sum_i^n(\dot{F}_{0,i} s_{0,i})\right] \quad \textbf{Equation 53}$$

Where, $h_{0,i}$ and $s_{0,i}$ are the component enthalpy and entropy at reference conditions (T_0, P_0) respectively.

2.2.9.8.3. Chemical exergy

Then the change in chemical exergy is determined as each of the pure unmixed reference components go from the environmental state (T_0, P_0) to the dead state (T_0, P_{00}). Here, $e^0_{ch,i}$ is the standard chemical exergy [24], [42], [63] which can be determined using Equation 44 [24], [63] or it can be acquired from the literature [24]. Please note that the chemical exergy here is for reference species whose chemical exergy is known. A means for determining the chemical exergy of non-reference species can be found in Kotas [24].

$$\dot{E}_{ch} = \sum_i^n(\dot{F}_i e^0_{ch,i}) \quad \textbf{Equation 54}$$

2.2.9.8.4. Benefits of the methodology

With this method you do not need to find the activity coefficients (γ_i) for each component in a stream, neither do you need to assume the stream is an ideal solution. ASPEN is able to return the pure component properties of each constituent in a mixture along with the properties of the mixture as whole. This allows one to determine the exergy of mixing accurately through simple subtraction. When dealing with multi-phase streams each phase is dealt with separately before their exergy contents are summed together to give the total stream exergy. Separation of streams with a liquid and gas phase can be accomplished by simply flashing the stream at the processes conditions (T, P). Another benefit of using this method is that by dealing with pure processes components its more accurate, since thermodynamic properties such as entropy and enthalpy change of pure components can more accurately be determined than those of a mixture from state to state [5]. A method for applying this to multi-phase streams in ASPEN plus is proposed in chapter 6.

References

[1] Houghton JT *et al.*, “Climate Change 2001: The Scientific Basis,” 2001.

[2] R. J. Petit *et al.*, “Climate and atmospheric history of the past 420,000 years from the Vostok ice core, Antarctica,” *Nature*, vol. 399, pp. 429–413, 1999.

[3] O. Edenhofer *et al.*, “Climate Change 2014: Mitigation of Climate Change,” *Work. Gr. III Contrib. to Fifth Assess. Rep. Intergov. Panel Clim. Chang.*, vol. 3, pp. 1–1435, 2014.

[4] IEA (International energy agency), “World Energy Outlook 2013,” Paris, France, 2013.

[5] Intergovernmental Panel on Climate Change, “Renewable Energy Sources and Climate Change Mitigation Special Report of the Intergovernmental Panel on Climate Change,” 2012.

[6] M. Bailera, P. Lisbona, L. M. Romeo, and S. Espatolero, “Power to Gas projects review: Lab, pilot and demo plants for storing renewable energy and CO2,” *Renew. Sustain. Energy Rev.*, vol. 69, no. October 2016, pp. 292–312, 2017.

[7] H. Chen, T. Ngoc, W. Yang, C. Tan, and Y. Li, “Progress in electrical energy storage system : A critical review,” *Prog. Nat. Sci.*, vol. 19, no. 3, pp. 291–312, 2009.

[8] EU Commission, “”Winning the battle against global climate change”,” Brussels, 2005.

[9] J. Herold, S. Rüster, and C. Von Hirschhausen, “Carbon capture, transport and storage in Europe: A problematic energy bridge to nowhere?,” 2010.

[10] E. S. Rubin and H. Zhai, “The Cost of Carbon Capture and Storage for Natural Gas Combined Cycle Power Plants,” *Environ. Sci. Technol.*, no. 46, pp. 3076–3084, 2015.

[11] IEAGHG, “CO2 CAPTURE AT GAS FIRED POWER PLANTS,” 2012.

[12] J. M. Beér, “High efficiency electric power generation: The environmental role,” *Prog. Energy Combust. Sci.*, vol. 33, no. 2, pp. 107–134, 2006.

[13] B. J. Wittebrood, “System design and thermody namic evaluation of natural gas combined cycle (NGCC) systems including carbon capture & storage (CCS) and metal hydride based hydrogen storage .,” 2015.

[14] R. Kehlhofer, *Combined-Cycle Gas and Steam Turbine Power Plants*. 1997.

[15] M. Gazzani, E. Macchi, and G. Manzolini, “CO 2 capture in natural gas combined cycle with SEWGS . Part A : Thermodynamic performances,” *Int. J. Greenh. Gas Control*, vol. 12, pp. 493–501, 2013.

[16] DOE/NETL, “Carbon Capture Approaches for Natural Gas Combined Cycle Systems,” 2010.

[17] R. Soundararajan, “Efficiency loss analysis for oxy- combustion CO2 capture process,” 2011.

[18] L. Balling and S. AG, “Flexible future for combined cycle,” *Mod. Power Syst.*, vol. 30, no. 12, pp. 61–65, 2010.

[19] International Energy Agengy, “Combining Bioenergy with CCS,” 2011.

[20] C. Gough and P. Upham, “Biomass energy with carbon capture and storage (BECCS): a review,” 2010.

[21] E. M. W. Smeets, A. P. C. Faaij, I. M. Lewandowski, and W. C. Turkenburg, “A bottom-up assessment and review of global bio-energy potentials to 2050,” *Prog. Energy Combust. Sci.*, vol. 33, no. 1, pp. 56–106, 2006.

[22] S. Danje, “Fast pyrolysis of corn residues for energy production,” Stellenbosch University, 2011.

[23] Q. Zhu, “High-efficiency power generation – review of alternative systems,” pp. 1–120, 2015.

[24] T. J. Kotas, *The Exergy Method of Thermal Plant Analysis*. Essex: Butterworths, 1985.

[25] K. Burnard and S. Bhattacharya, “Power generation from coal: Ongoing Developments and Outlook,” 2011.

[26] Coal Industry Advisory Board, “‘Power Generation from Coal: Measuring and Reporting Efficiency Performance and CO2 Emissions,’” Paris, 2010.

[27] S. Hough, “Supercritical Rankine Cycle,” pp. 1–11, 2009.

[28] Q. Zhu, “Developments in fluidised bed combustion technology,” 2013.

[29] D. Kumar Mohanty, V. K. Venkatesh BITS Pilani K Birla Goa Campus, Z. Nagar, and G. -, “Performance Analysis of a Combined Cycle Gas Turbine Under Varying Operating Conditions,” *Mech. Eng. An Int. J. (MEIJ)*, vol. 1, no. 2, pp. 11–25, 2014.

[30] D. P. Hanak, C. Biliyok, H. Yeung, and R. Bia??ecki, “Heat integration and exergy analysis for a supercritical high-ash coal-fired power plant integrated with a post-combustion carbon capture process,” *Fuel*, vol. 134, pp. 126–139, 2014.

[31] Y. A. Cengel and M. A. Boles, *Thermodynamics: An Engineering Approach*. 2006.

[32] W. Liu, F. Wen, and Y. Xue, “Power-to-gas technology in energy systems : current status and prospects of potential operation strategies,” *J. Mod. Power Syst. Clean Energy*, vol. 5, no. 3, pp. 439–450, 2017.

[33] DOE/NETL, “Cost and Performance Baseline for Fossil Energy Plants,” 2007.

[34] O. Bolland and H. Undrum, “A novel methodology for comparing CO2 capture options for

natural gas-fired combined cycle plants," *ELSEVIER*, vol. 7, pp. 901–911, 2003.

[35] A. Skorek-osikowska, J. Kotowicz, and K. Janusz-szyman, "Comparison of the Energy Intensity of the Selected CO 2 -Capture Methods Applied in the Ultra-supercritical Coal Power Plants," *Energy & Fuels*, vol. 26, pp. 6509–6517, 2012.

[36] K. Almås, "Coal-fired Power Plants based on Oxy-combustion with Carbon Capture : Combustion Conditions and Water Consumption," Norwegian University of Science and Technology, 2012.

[37] M. Kanniche, R. Gros-Bonnivard, P. Jaud, J. Valle-Marcos, J. M. Amann, and C. Bouallou, "Pre-combustion, post-combustion and oxy-combustion in thermal power plant for CO2 capture," *Appl. Therm. Eng.*, vol. 30, no. 1, pp. 53–62, 2010.

[38] A. W. Dowling, C. Balwani, Q. Gao, and L. T. Biegler, "Equation-oriented optimization of cryogenic systems for coal oxycombustion power generation," *Energy Procedia*, vol. 63, no. November, pp. 421–430, 2014.

[39] IEAGHG, "OXYFUEL COMBUSTION OF PULVERISED COAL," 2010.

[40] J. Ciferno *et al.*, "Pulverized Coal Oxycombustion Power Plants Volume 1 : Bituminous Coal to Electricity Final Report," 2008.

[41] J. Amann, M. Kanniche, and C. Bouallou, "Natural gas combined cycle power plant modified into an O2 /CO2 cycle for CO2 capture," *Energy Convers. Manag.*, vol. 50, no. 3, pp. 510–521, 2009.

[42] C. Fu and T. Gundersen, "Exergy Analysis and Heat Integration of a Coal-Based Oxy-combustion Power Plant," *Energy & Fuels*, vol. 27, pp. 7138–7149, 2013.

[43] Y. Hu, "CO2 capture from oxy-fuel combustion power plants," KTH Royal Institue of Technology, 2011.

[44] M. Simo, C. J. Brown, and V. Hlavacek, "Simulation of pressure swing adsorption in fuel ethanol production process," vol. 32, pp. 1635–1649, 2008.

[45] J. Guan and X. Hu, "Simulation and analysis of pressure swing adsorption : ethanol drying process by the electrical analogue," vol. 31, pp. 31–35, 2003.

[46] T. Roth, P. Kreis, and A. Górak, "Process analysis and optimisation of hybrid processes for the dehydration of ethanol," *Chem. Eng. Res. Des.*, vol. 91, no. 7, pp. 1171–1185, 2013.

[47] C. A. Cardona and O. J. Sanchez, "Fuel ethanol production: Process design trends and integration opportunities," *Bioresour. Technol.*, vol. 98, pp. 2415–2457, 2007.

[48] R. Turton, R. C. Bailie, W. B. Whiting, and J. A. Shaeiwitz, *Analysis, Synthesis and Design of*

Chemical Processes. Boston: Pearson Education, Inc, 2009.

[49] M. Bailera, P. Lisbona, L. M. Romeo, and S. Espatolero, "Power to Gas-biomass oxycombustion hybrid system: Energy integration and potential applications," *Appl. Energy*, vol. 167, pp. 221–229, 2016.

[50] J. Agerborg and E. Lingehed, "Integration of Power-to-Gas in Gasendal and GoBiGas," *Publications.Lib.Chalmers.Se*, pp. 1–70, 2013.

[51] T. Gur, M, "Environmental Science materials and systems : challenges and prospects for large-scale grid storage," *Energy Environ. Sci.*, vol. 11, no. 11, pp. 2696–2767, 2018.

[52] P. M. Diéguez, A. Ursúa, P. Sanchis, C. Sopena, E. Guelbenzu, and L. M. Gandía, "Thermal performance of a commercial alkaline water electrolyzer: Experimental study and mathematical modeling," *Int. J. Hydrogen Energy*, vol. 33, no. 24, pp. 7338–7354, 2008.

[53] A. S. Tijani, N. A. B. Yusup, and A. H. A. Rahim, "Mathematical Modelling and Simulation Analysis of Advanced Alkaline Electrolyzer System for Hydrogen Production," *Procedia Technol.*, vol. 15, pp. 798–806, 2014.

[54] J. E. O'Brien, M. G. McKellar, E. A. Harvego, and C. M. Stoots, "High-temperature electrolysis for large-scale hydrogen and syngas production from nuclear energy - summary of system simulation and economic analyses," *Int. J. Hydrogen Energy*, vol. 35, no. 10, pp. 4808–4819, 2010.

[55] X. Luo, J. Wang, M. Dooner, and J. Clarke, "Overview of current development in electrical energy storage technologies and the application potential in power system operation," *Appl. Energy*, vol. 137, pp. 511–536, 2015.

[56] Y. Redissi and C. Bouallou, "Valorization of carbon dioxide by co-electrolysis of CO2/H2O at high temperature for syngas production," *Energy Procedia*, vol. 37, pp. 6667–6678, 2013.

[57] Y. Zheng *et al.*, "A review of high temperature co-electrolysis of H 2 O and CO 2 to produce sustainable fuels using solid oxide electrolysis cells (SOECs): advanced materials and technology," *Chem. Soc. Rev.*, vol. 46, no. 5, pp. 1427–1463, 2017.

[58] Y. Luo, Y. Shi, W. Li, and N. Cai, "Comprehensive modeling of tubular solid oxide electrolysis cell for co-electrolysis of steam and carbon dioxide," *Energy*, vol. 70, pp. 420–434, 2014.

[59] S. K. Hoekman, A. Broch, C. Robbins, and R. Purcell, "International Journal of Greenhouse Gas Control CO 2 recycling by reaction with renewably-generated hydrogen," vol. 4, pp. 44–50, 2010.

[60] N. Kuehn, B. Hamilton, Allen, A. Kyle, M. Woods, and W.-C. Yang, "Carbon Capture

Approaches for Natural Gas Combined Cycle Systems," 2011.

[61] J. Wallace, F and A. Linning, W, *Basic Engineering Thermodynamics*. Birmingham: Pitman publishing, 1970.

[62] A. C. Wallshaw, *THERMODYNAMICS FOR ENGINEERS*. Birmingham, 1963.

[63] A. P. Hinderink, F. P. J. M. Kerkhof, A. B. K. Lie, J. De Swaan Arons, and H. J. Van Der Kooi, "Exergy analysis with a flowsheeting simulator - I. Theory; calculating exergies of material streams," *Chem. Eng. Sci.*, vol. 51, no. 20, pp. 4693–4700, 1996.

3. Modelling, design, and Optimization of NGCC and NGGC Pre-combustion Capture power plant

3.1. Methodology

3.1.1. NGCC flow-sheet model

The NGCC power plant simulated in this work is based on the work of Wittebrood [2] and the DOE/NETL [4] report. The steam cycle was based on the work of Wittebrood [2]. The flow-sheeting software package used to simulate the power plant is ASPEN plus (V8.4). The Peng-Robinson thermodynamic property package, and the IAPWS-95 free water method were used.

3.1.1.1. NGCC Process description

3.1.1.1.1. Gas turbine and Rankine hierarchy

Figure 36 is an image of the ASPEN plus flow sheet for the baseline NGCC power plant simulated in this work. Important stream data for all material streams can be found in appendix A. System boundary GT surrounds the topping gas turbine cycle and system boundary SC surrounds the bottom rankine cycle. Stream AIR (which represents the incoming air used as oxidant) and stream NG (which represents the natural gas feed) are mixed and fed into unit operation COMB: COMB is an RGIBBS reactor meant to simulate the combustion of natural gas with an oxidant. The combustion products from unit operation COMB then report to the gas turbine (labelled GTURBINE). The work output from the gas turbine is labelled W-GT. The hot flue gasses leave the gas turbine via stream G4 before being fed into the rankine cycle hierarchy labelled RANKINE. The hot flue gasses then generate additional electricity within the rankine cycle: the electrical work flows resulting from this are labelled W-HPST (work output for high pressure steam turbine), W-MPST (work output for medium pressure steam turbine) and W-LPST (work output for the low pressure steam turbine). Once all the thermal energy of the hot flue gas is spent, the gas escapes through the stack; this is represented by rankine cycle product stream STACK. The work streams leaving the RANKINE hierarchy, represent the work outputs from the high pressure steam turbine (W-HPST), the intermediate pressure steam turbine (W-MPST) and the low pressure steam turbine (W-LPST) which are all combined in the work mixer block (block SSWORK) to produce the combined steam cycle work stream (stream SS-WORK) before being combined with the gas turbine work stream (W-

GT) in the work mixer block TOTWORK to give the total NGCC power plant work output (stream TOT-WORK).

3.1.1.1.2. Steam cycle and HRSG hierarchy

Within the RANKINE hierarchy is the HRSG hierarchy which contains the steam cycle. Figure 37 is an image of the flow sheet one will find inside the RANKINE hierarchy block. Hot flue gasses (stream G4) enter the HRSG where they heat low pressure (stream SS64-IN [this is just stream SS64]), intermediate pressure (stream SS56-IN [this is just stream SS56]) and high pressure (stream 10-IN [this is just stream 10]) water flows from the steam cycle water pumps to conditions needed for them to generate the required mechanical energy once they are fed to the high pressure (HP), intermediate pressure (MP) and low pressure (LP) steam turbines. The high pressure (pumps water to 120bar), intermediate pressure (pumps water to 32bar) and low pressure (pumps water to 5bar) pumps were simulated using ASPEN plus PUMP unit operations and the high pressure (HP), intermediate pressure (MP) and low pressure turbines were simulated using APSEN plus turbine blocks. Once all the energy in the steam is spent, it reports to the cooling tower (CTOWER) which has been simulated using a heating block before reporting to the initial steam cycle pump (C-PUMP) which raises the water pressure to 1.5bar before it is directed to the HRSG as SS33IN (this is really stream SS33) where it is pre-heated before exiting the HRSG as stream 9-OUT (this is really stream 9) and is split into requisite stream flows needed for the high pressure, intermediate pressure and low pressure sections of the HRSG; re-initiating the cycle. Important stream data for all material streams can be found in appendix A.

Figure 38 is a diagram of the steam cycle within the HSRG hierarchy. The steam cycle is composed of three pressurised water flows (a high pressure (HP), intermediate pressure (IP) and low pressure (LP) stream) that flow counter currently to the flue gas that contains the heat rejected by the gas turbine. Each stream is initially heated by economisers (the high pressure stream has 3 [heat exchanger blocks HECL, HECM and HECH], the intermediate pressure stream has 2 [heat exchanger blocks MECL and MECM] and the low pressure stream has 1 [heat exchanger block LECL]) to its saturation temperature at the specified stream pressure. Once that is done the stream then enters an evaporator that vaporises it (heat exchanger block HPEV is the high pressure stream evaporator, heat exchanger MPEV is the intermediate pressure stream evaporator and heat exchanger LPEV is the low pressure stream evaporator) before reporting to heat exchangers that take it to the final required turbine inlet conditions

(heat exchanger block SUP1for the high pressure steam, heat exchanger blocks SUP2 and RH for the intermediate pressure steam and heat exchanger block SUP3 for the low pressure steam). The HP and IP pressure turbine outlet streams then combine with the streams from super heaters at pressure levels immediately below them before reporting to the lower pressure turbine. The steam reporting from the LP turbine then flows to a condenser operating at 48mbar. Important stream data for all material streams can be found in appendix A.

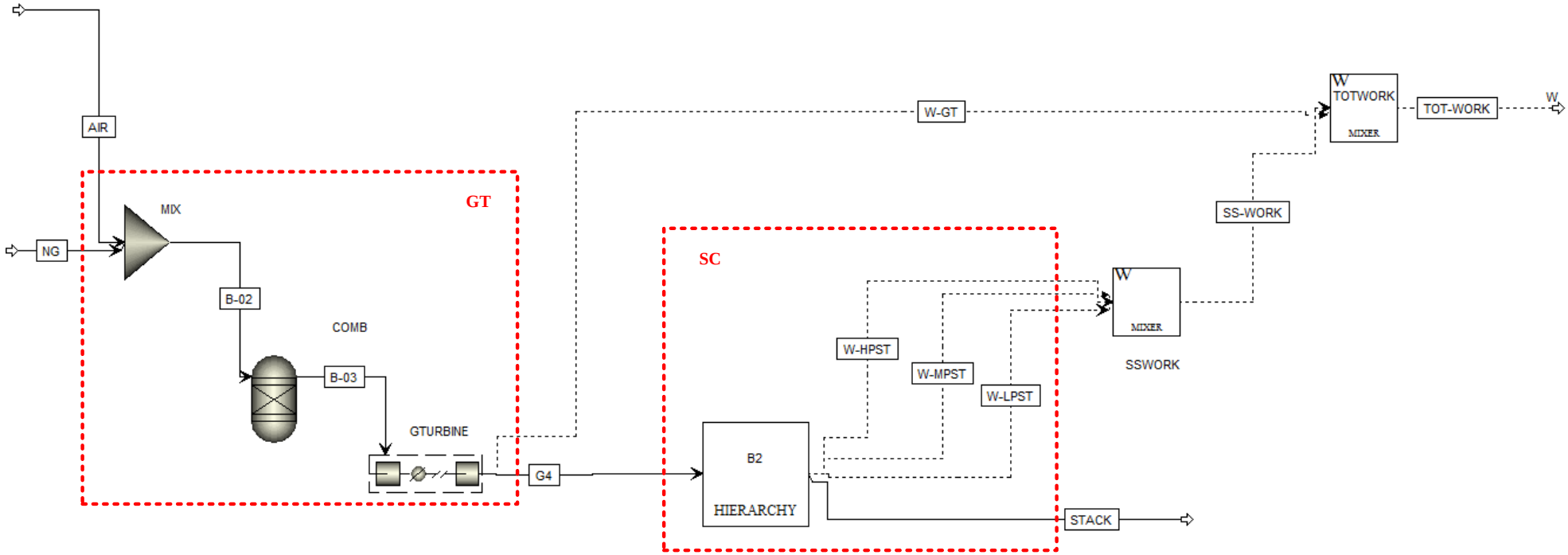


Figure 36: Flow-sheet of NGCC baseline power plant. GT: system boundary around gas turbine; SC: system boundary around bottom Rankine cycle (Important stream information can be found in appendix A).

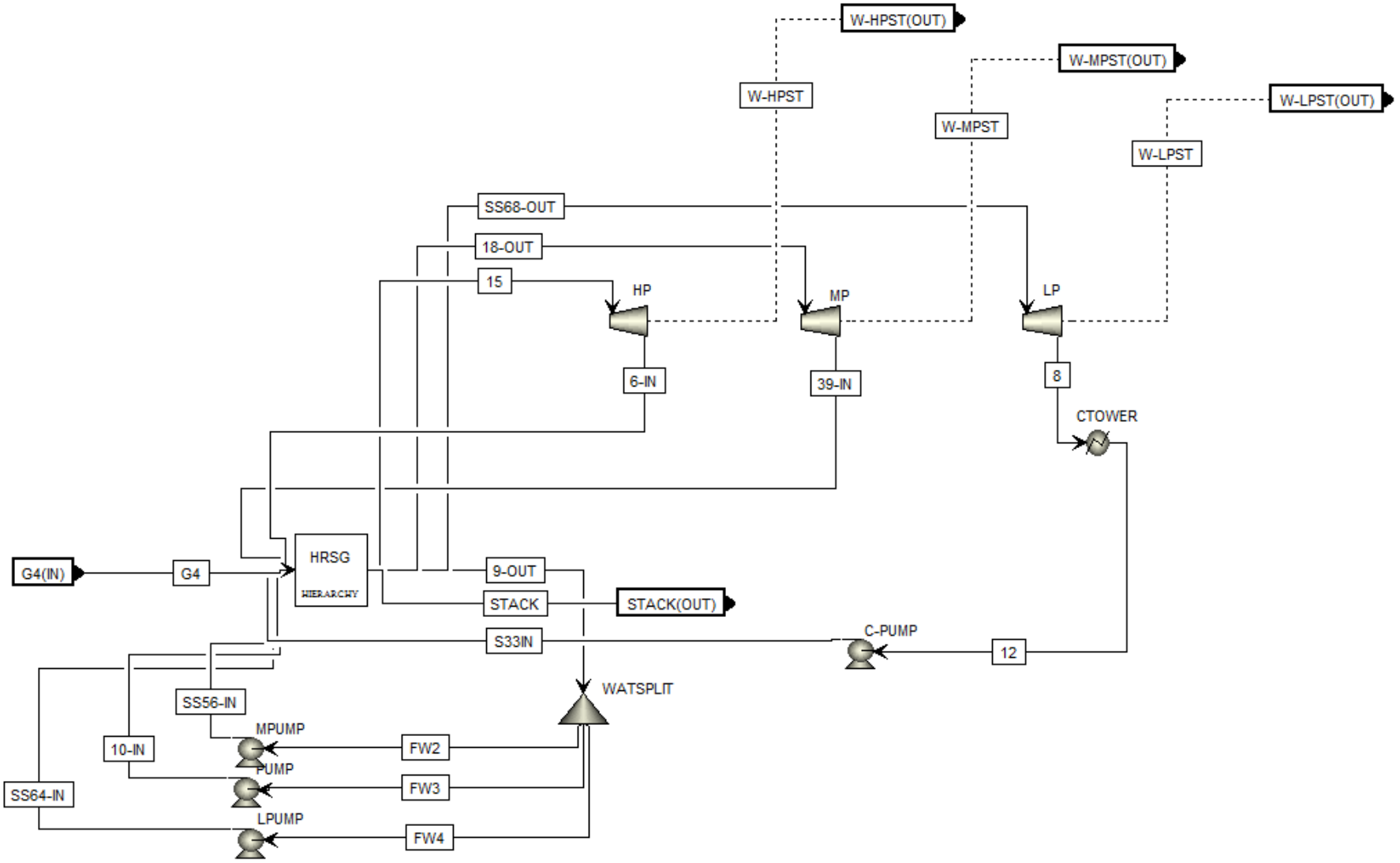


Figure 37: Rankine hierarchy ASPEN-plus flow sheet (Important stream information can be found in appendix A)**.**

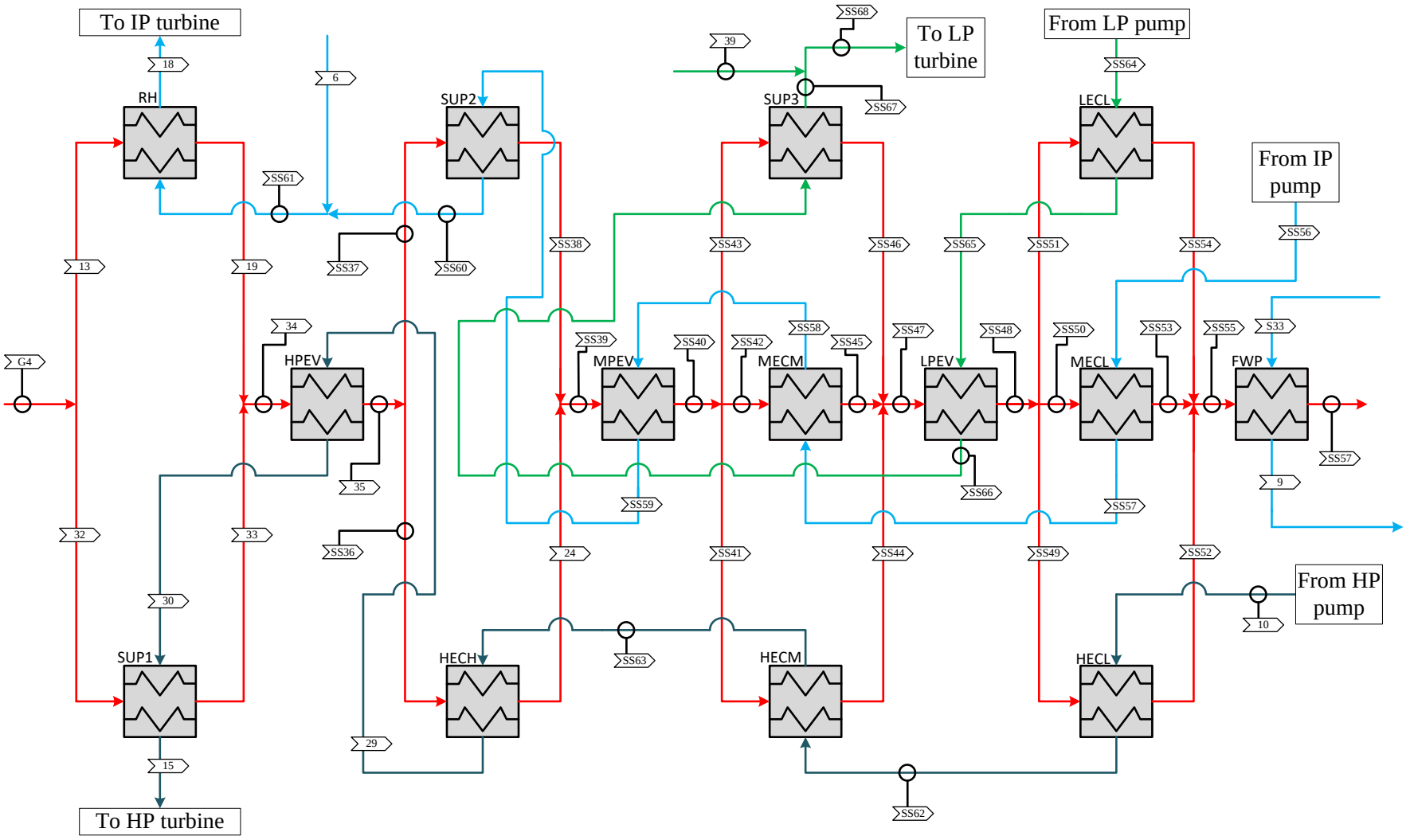


Figure 38: Diagram of ASPEN plus flow-sheet for the steam cycle within the HRSG hierarchy (Important stream information for the baseline and the pre-combustion capture NGCC power plant can be found in appendix A and in appendix B respectively).

3.1.1.2. NGCC performance summary and steam cycle optimization

3.1.1.2.1. Natural gas and air feed characteristics

Table 3 lists the molar compositions of all the important species within the South African natural gas fed to the power plant. The composition of the natural gas feed was acquired from the SASOL website [1]. Table 4 is a list of the molar compositions of the chemical species in the air fed to the plant.

Table 3: Molar composition of methane feed.

Component	Mole percentage
Nitrogen	2.06
Carbon dioxide	0.00
Methane	94.28
Ethane	2.03
Propane	0.83
i-Butane	0.21
n-Butane	0.24
i-Pentane	0.07
n-Pentane	0.06
neo Pentane	0.01
Hexane	0.06
Heptane	0.12
Octane	0.02
Nonane	0.00

Table 4: Molar composition of air feed.

Species	Mole percentage
Water	0.99
Nitrogen	77.31
Oxygen	20.74
Carbon dioxide	0.04
Argon	0.92
Neon	0.00
Helium	0.00
Methane	0.00

3.1.1.2.2. Computational specifications

3.1.1.2.2.1. Gas turbine

The gas turbine is a large scale “F class” 50 Hz type gas turbine with an expected net power output of between 280 MW-285 MW. It is based on the performance data of the GE 9371F and SIEMENS STG-4000F gas turbine [2]. It was assumed that the gas turbine is comprised of 4 turbine stages, is air cooled and has between 13 and 15 compressor stages [3]. Sadly, no one has yet modelled a utility scale gas turbine for NGCC comprehensively through ASPEN plus and compared it with what is said in the literature. Through sensitivity analysis it was found that the appropriate pressure ratio required to have the exhaust gasses come out of the turbine at 1.25bar is 0.4825 and that the required isentropic efficiency is around 0.5321. To simulate a turbine with exhaust gasses leaving its tail end at 630℃ each turbine stage was cooled to 630℃. The outputs reported for the said turbine class are net outputs which take into consideration the compression work requirements for the incoming air much like was done in the DOE/NETL [4] report. When air enters a gas turbine it is compressed in-situ by the torque generated as the fuel and oxidant are combusted further down coaxially.

3.1.1.2.2.2. Turbo machinery units

Table 5 contains the computational specifications for the turbo machinery units.

Table 5: Specifications for the turbines and the compressors

Steam turbine	
Isentropic efficiency of HP/IP/LP steam turbines	0.9/0.9/0.88
Steam turbine mechanical efficiency	0.996
HP turbine inlet pressure [bar]	120
IP turbine inlet pressure [bar]	32
LP turbine inlet pressure [bar]	5
Compressors	
Isentropic / mechanical efficiency of compressors	0.82/0.97
Condenser pressure [bar]	0.048
Condenser outlet tmperature [°C]	26

3.1.1.3. Steam cycle design and optimization

This section describes how it is that the steam cycle was designed and optimized within each setup before presenting the results of the optimization. The evaporators for all three steam pressure levels (HP, IP and LP) had to be optimized in order to ensure the steady state results within each unit would have saturated water coming in (vapour fraction = 0, liquid fraction = 1 at T_{sat}) and saturate steam coming out (vapour fraction = 1, liquid fraction = 0 at T_{sat}) and that the water moving through the unit remained at the saturation temperature (T_{sat}). This is refinement on the work of Wittebrood [2] and the DOE/NETL [4]. It is also very important when conducting a heat integration study to know exactly what the demand is across the steam cycle in order to accurately predict the magnitude of the improvements to the overall performance that come with heat integration.

With the initial economisers that each steam pressure level moves through one simply needs to input the initial and final temperature of either the hot or the cold stream moving through the heat exchanger. However this will not work for the evaporators since the temperature through the evaporator remains constant at the saturation temperature (T_{sat}); so what one needs to do is calculate the heat duty across the unit instead and provide that as input in the evaporator heat exchanger block. This was achieved by producing a process flow sheet of a heat exchanger with a cold stream with the same stream pressure as the water flow whose saturation temperature you want to determine. Then, using a hot stream, the duty across the heat exchanger is increased until the cold stream in the unit operation begins to boil: this happens when the temperature of the water in the unit remains constant and the vapour fraction begins to increase. The temperature at which the water remains constant is the saturation temperature (T_{sat}). Once you have T_{sat}, one can calculate the heat duty, or enthalpy of vaporisation ($\Delta\bar{H}_{vap}$) as the difference between the enthalpy of the saturated vapour (H_{vap}), and the enthalpy of the saturated liquid (H_{liqiud}) (see equation 55).

$$heat\ duty\ [Watts] = \Delta\bar{H}_{vap}[Watts] = \dot{M}\left[\frac{kg}{sec}\right]\left(H_{vap}\left[\frac{J}{kg}\right] - H_{liqiud}\left[\frac{J}{kg}\right]\right) \qquad \textbf{Equation 55}$$

To ensure that one can check that the results across each evaporator are correct without compromising each run and therefore the assessment; heater blocks need to be placed at streams headed toward the turbines that keep the overall cycle results as they should be whilst the evaporator is being designed. Once you have inputted the appropriate heat duty into all three evaporators the heater blocks can then be removed.

Using this method the mass flow of water through the steam cycle was adjusted whilst adhering to the steam cycle constraints for a pinch point of 10℃ or higher and a steam vapour fraction reporting to the condenser of more than 0.88.

3.1.2. NGCC pre-combustion capture flow-sheet model

The sections that follow contain the pre-combustion capture power plant process description, design, optimization and overall performance assessment. The GHR-ATR-SEWGS retrofit was modelled in the same manner as that of Wittebrood [2]. The oxy-combustion air separation unit (ASU) characteristics are based on the work of Fu and Gundersen [10]. The overall results obtained (without the ASU) were compared with those in the DOE/NETL [4] report. The ASU and SEWGS capture unit were not simulated in great detail; with only their major products and energy consumptions being taken into account. Important stream data for all material streams can be found in appendix B.

3.1.2.1. NGCC pre-combustion capture process description

The NGCC pre-combustion capture power plant flow-sheet (figure 40) has a gas turbine (GT) and a Rankine steam cycle hierarchy (SC) system boundary much like the baseline NGCC power plant (figure 36). Where they differ is that the pre-combustion capture power plant has retrofitted to it the air separation unit (system boundary ASU) and reformer (system boundary GHR-ATR-SEWG). The reason the air separation unit was included is to ensure a pure stream of hydrogen reports to the gas turbine. This makes the power plant more flexible as the hydrogen can easily be diverted to onsite storage for later use in the event the power plant needs to run at part load. Important stream data for all material streams can be found in appendix B.

3.1.2.1.1. GHR-ATR-SEWGS and ASU

Figure 39 is the ASPEN flow sheet within the CCS hierarchy surrounded by the GHR-ATR-SEWG system boundary. The process takes in oxygen (95 mole% pure) from stream OP-5, high pressure steam from stream STEAM and natural gas from stream NG. The HP steam in stream STEAM is fed to the GHR and the SEWGS unit, the oxygen (stream OP-5) is fed to the ATR and the natural gas is mixed with stream STEAMATR (0.677 of stream STEAM by mass)

to form stream CC-2 which then reports to the GHR. Stream CC-2 is fed into the GHR along with a proportion of the heat evolved from the ATR to partially convert the incoming stream to syngas as stream CC-3 which then reports to the ATR along with the oxygen stream (stream OP-5). The ATR then converts its entire feed to syngas before its products are sent to HEATX which cools the hot syngas to 420℃ and uses the heat released to provide the process heat needed for the GHR. Stream CC-5 is cooled in heat exchanger REFCOOL to 310℃, before its products report to the SEWGS unit as stream CC-6. The products from the SEWGS unit are then cooled to 36℃ to condense out any excess water as stream CC-9, and the rest of the dry syngas (stream CC-8) then reports to a splitter (unit operation CCU-1) that then separates out the hydrogen (stream CC-10) from the CO_2 (stream CC-11). The hydrogen is then re-heated to 302℃ before reporting to the gas turbine as stream CC-H2. The CO_2 separated out from the hydrogen in unit operation CCU-1 (stream CC-11) then gets flashed to ambient conditions by unit operation CCU-2 to condense out any excess water which is removed as stream CC-14. Stream CC-14 then combines with the condensed water in stream CC-9 to form stream CC-15 which then leaves the hierarchy. The CO_2 in stream CC-13 then gets compressed by a five stage CO_2 compressor with intercooling (CO2-COMP) [each compression stage has a pressure ratio of 2.3959 and is cooled to 298.15K] to 80bar before leaving the hierarchy as stream P-101. The GHR, ATR and SEWGS were modelled using RGibbs reactors. Unit operations HEATX, REFCOOL and B3 were modelled using heater blocks. Unit operations GOOLING and CCU-2 are flash blocks. Important stream data for all material streams can be found in appendix B.

The air separation unit (ASU) flow-sheet lies within the main capture plant flow-sheet (Figure 40) ASU system boundary. Ambient air comes in (stream AIR) and is split into streams OP-1, which is directed to the gas turbine and stream OP-2, which is directed to the ASU. Stream OP-2 is compressed to 5.6bar in the three stage air separation unit compressor (ASU-COMP) [each compression stage has a pressure ratio of 1.768 and is cooled to 298.15K], and the resulting stream of compressed gas is called OP-3. OP-3 then has its Oxygen (95 mole %) and Nitrogen separated out as streams OP-5 and OP-4 respectively. Important stream data for all material streams can be found in appendix B.

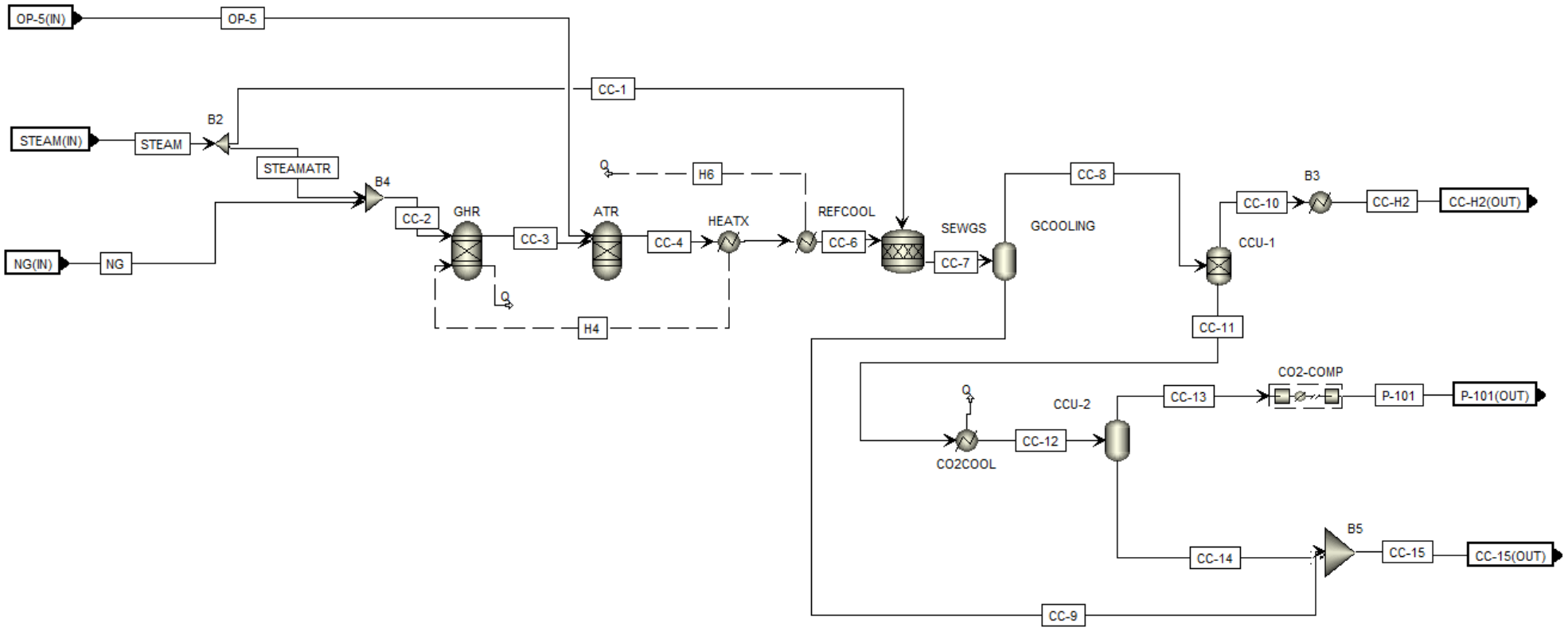


Figure 39: ASPEN flow-sheet for auto thermal reformer, gas heated reformer SEWGS retrofit which lies in hierarchy within the system boundary GHR-ATR-SEWG in Figure 29 (Important stream information can be found in appendix B).

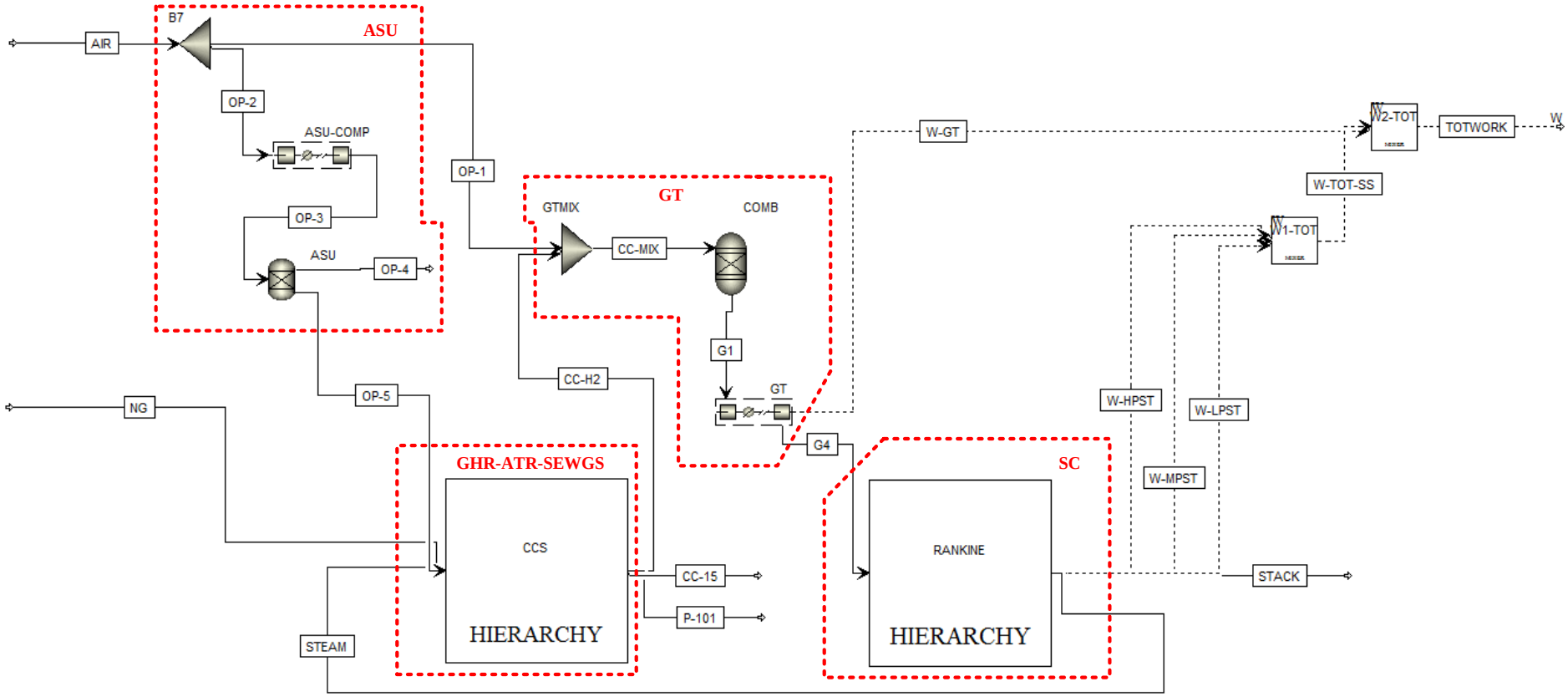


Figure 40: Flow-sheet of pre-combustion capture NGCC power plant. GHR-ATR-SEWGS is the system boundary around the gas heated reformer (GHR), auto thermal reformer (ATR) sorbent enhanced water gas shift (SEWGS) flow-sheet. ASU is the system boundary surrounding the air separation unit (Important stream information can be found in appendix B).

3.2. Results

3.2.1. NGCC Results

It was determined that the saturation temperatures for water flows moving through the steam cycle were: 152.83℃ at 5 bar (LP), 237℃ at 32 bar (IP) and 324℃ at 120 bar (HP), which is in agreement with the results of Wittebrood [2]. The heat duties across the low pressure evaporator (LPEV), the intermediate pressure evaporator (MPEV) and the high pressure evaporator (HPEV) were 31.48 MW, 17.53 MW and 98.6 MW respectively (stream flows can be found in appendix A). Figure 41 displays the temperature profiles across all heat exchangers in the baseline NGCC power plant steam cycle, with the heat duty in the horizontal axis, and the temperature within each heat exchanger in the retrofitted power plant steam cycle in the vertical axis. The temperature profiles of the water flows are in blue and those of the flue gasses are in red.

Table 6 contains the power plant performance summary for the baseline NGCC power plant. Other auxiliaries include: the condensate pumps, boiler feed-water pumps, amine system auxiliaries, CO_2 compression, circulating water pump, ground water pump, cooling tower fans, SCR, gas turbines auxiliaries, steam turbine auxiliaries, miscellaneous balance of plant and transformer losses [4]. The higher heating value [HHV] thermal efficiency of the plant was found to be 53.52% and the lower heating value [LHV] thermal efficiency of the plant was found to be 59.32%. This is in agreement with the findings in the DOE/NETL report which determined this efficiency to be 55.7%. The NGCC baseline power plant HHV efficiency is around 13% higher than that of a pulverised coal power plant**.** This answers the first research question.

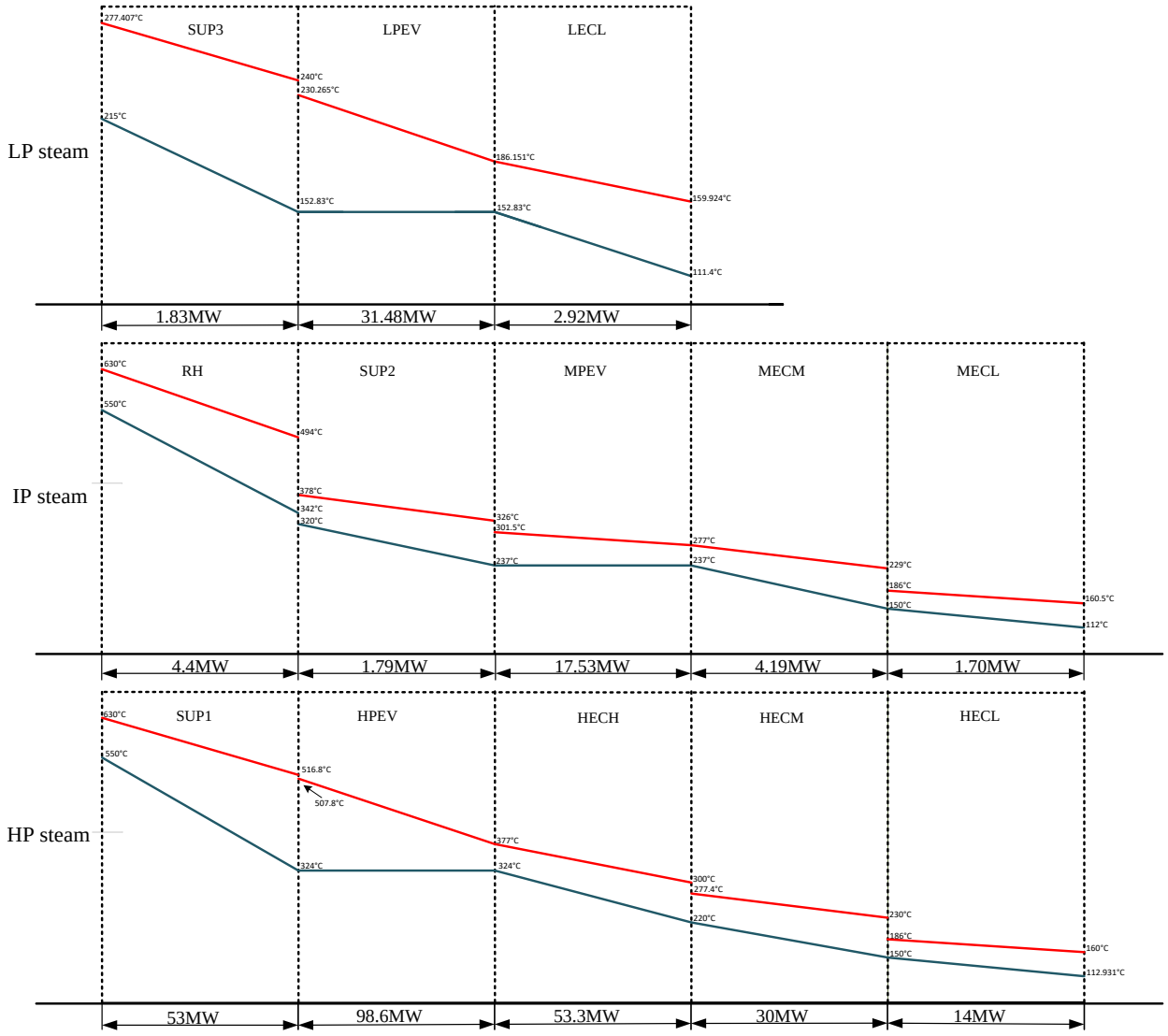


Figure 41: Steam cycle heat load and temperature diagram for the baseline NGCC power plant. Please note that the figures proportions have been intentionally distorted across the horizontal axis for clarity (refer to figure 38 and important stream data for all material streams can be found in appendix A).

Table 6: NGCC power plant performance summary.

Property / attribute	
Fuel feed rate (kg/s)	15.5
Net GT output (MW)	293.05
HP ST output (MW)	28.69
MP ST output (MW)	45.78
LP ST output (MW)	73.00
Net ST output (MW)	147.48
TOTAL output (MW)	440.53
Additional plant axuxilaries [NETL] (MW)	-7.072
CH4 [HHV] (MJ/kg)	52.26
CH4 [LHV] (MJ/kg)	47.14
Thermal input [HHV](MW)	809.95
Thermal input [LHV](MW)	730.69
Plant efficiency [HHV] %	53.52
Plant efficiency [LHV]%	59.32

3.2.2. NGCC pre-combustion capture results

Figure 43 is the flow-sheet within the RANKINE hierarchy of the NGCC, CCS power plant. The RANKINE hierarchy flow-sheet within the capture plant is almost identical to the flow-sheet lying in the RANKINE hierarchy within the baseline NGCC power plant (Figure 37), with the only difference being that 34% of the steam that is directed to the intermediate pressure (MP) turbine (stream 18-OUT; this is just stream 18) is instead diverted to provide steam for the GHR-ATR-SEWGS hierarchy. The reason this stream was selected is that its conditions lie closest to the steam conditions required for the GHR-ATR-SEWGS hierarchy which are: a moderately high pressures of around 25bar (the intermediate pressure steam pressure lies closet to what is required at 32bar) and temperatures of between 350℃ and 550℃ (see literature review section titled “Pre-combustion capture SEWGS on NGCC power plants). As a result the entire steam cycle had to be designed and optimised a second time in the same manner as was outlined in section 3.1.1.3.

Because the pressure levels in the steam cycle don't change, the saturation temperatures remain unchanged as well: 152.83℃ for the low pressure steam (LP), 237℃ for the intermediate pressure steam (IP) and 324℃ for the high pressure steam (HP) . Upon optimization it was found that the heat duty across the low pressure evaporator (LPEV), the intermediate pressure evaporator (MPEV) and the high pressure evaporator (HPEV) are 24.6 MW, 13.7 MW and 77 MW respectively. Figure 42 displays the temperature profiles across all heat exchangers in the NGCC pre-combustion capture power plant team cycle, with the heat duty in the horizontal axis, and the temperature within each heat exchanger in the retrofitted power plant steam cycle in the vertical axis. The temperature profiles of the water flows are in blue and those of the flue gasses are in red.

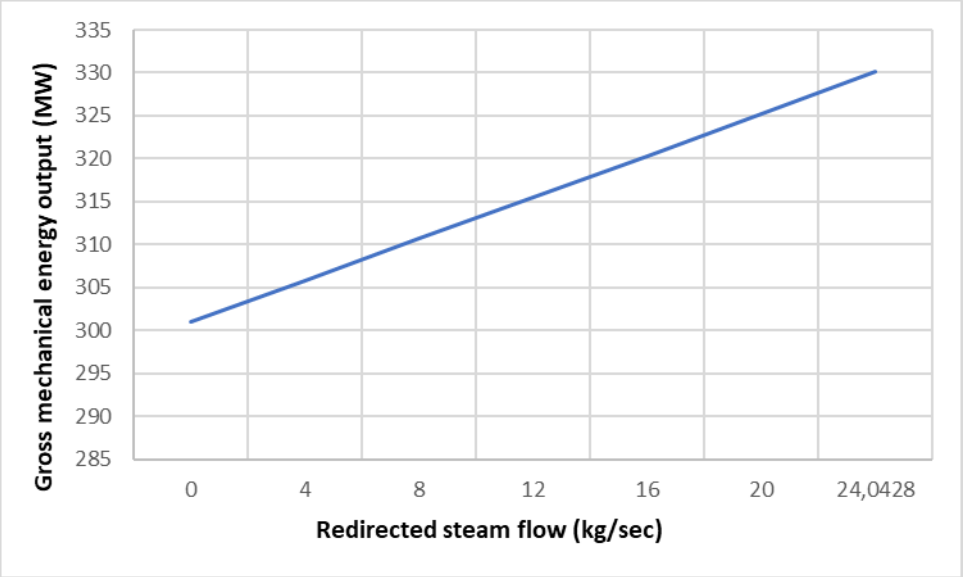
The plant performance summary for the pre-combustion capture NGCC power plant is shown in table 7. The additional auxiliaries include: fuel gas compression, condensate pumps, boiler feed-water pumps, circulating water pump, ground water pumps, cooling tower fans, SCR, gas tribune auxiliaries, steam turbine auxiliaries, miscellaneous balance of plant and transformer losses. The HHV efficiency of the pre-combustion capture NGCC power plant is 29.92% which is 12.48% lower than that which was reported in the DOE/NETL report of 42.4%. The LHV efficiency is 33.17%, which is 13.83% lower than that which was reported in the DOE/NETL report of 47%. This answers the second research question.

Additionally, a study was conducted that looked at how the the gross mechanical work output would be affected if there were no steam extraction. This was done incrementally, until all the steam that originally reported to the reformer was instead directed to the intermediate pressure turbine, just like in the baseline power plant. When this was done the gross power output increased form 300.95 MW to 330.08 MW. The results are presented in
table 3.2.2a and figure 3.2.2a.

Table 3.2.2a: Table of redirected HRSG water verses gross mechanical energy output.

Redirected steam (kg/sec)	Power output (MW)
0	300.95
4	305.8
8	310.64
12	315.49
16	320.34
20	325.18
24.0428	330.08

Figure 3.2.2a: Figure of redirected HRSG water verses gross mechanical energy output.



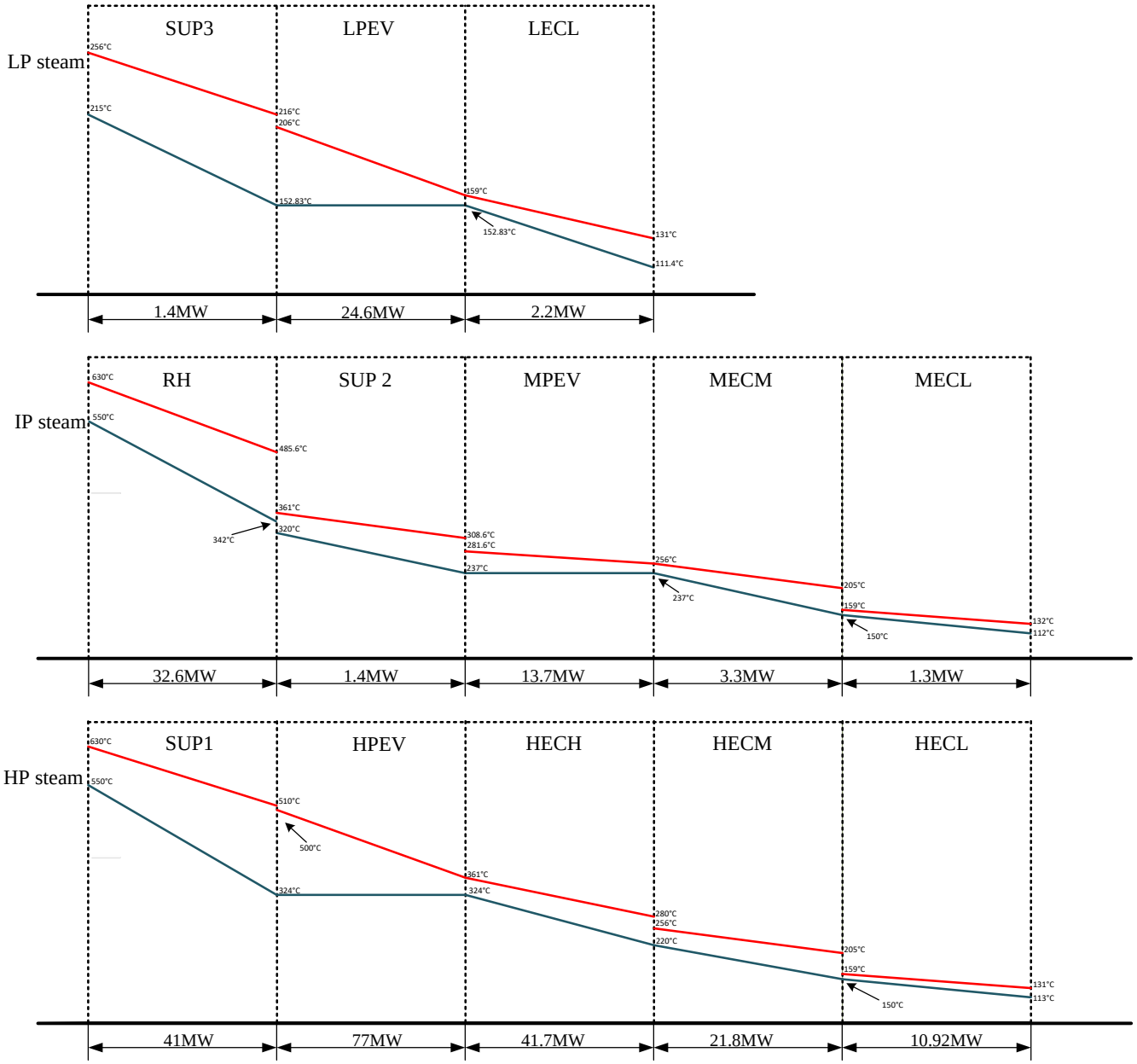


Figure 42: Steam cycle heat load versus temperature diagram for the pre-combustion capture NGCC power plant. Please note that the figures proportions have been intentionally distorted in the horizontal axis for the sake of clarity (refer to figure 38, stream information can be found in appendix B).

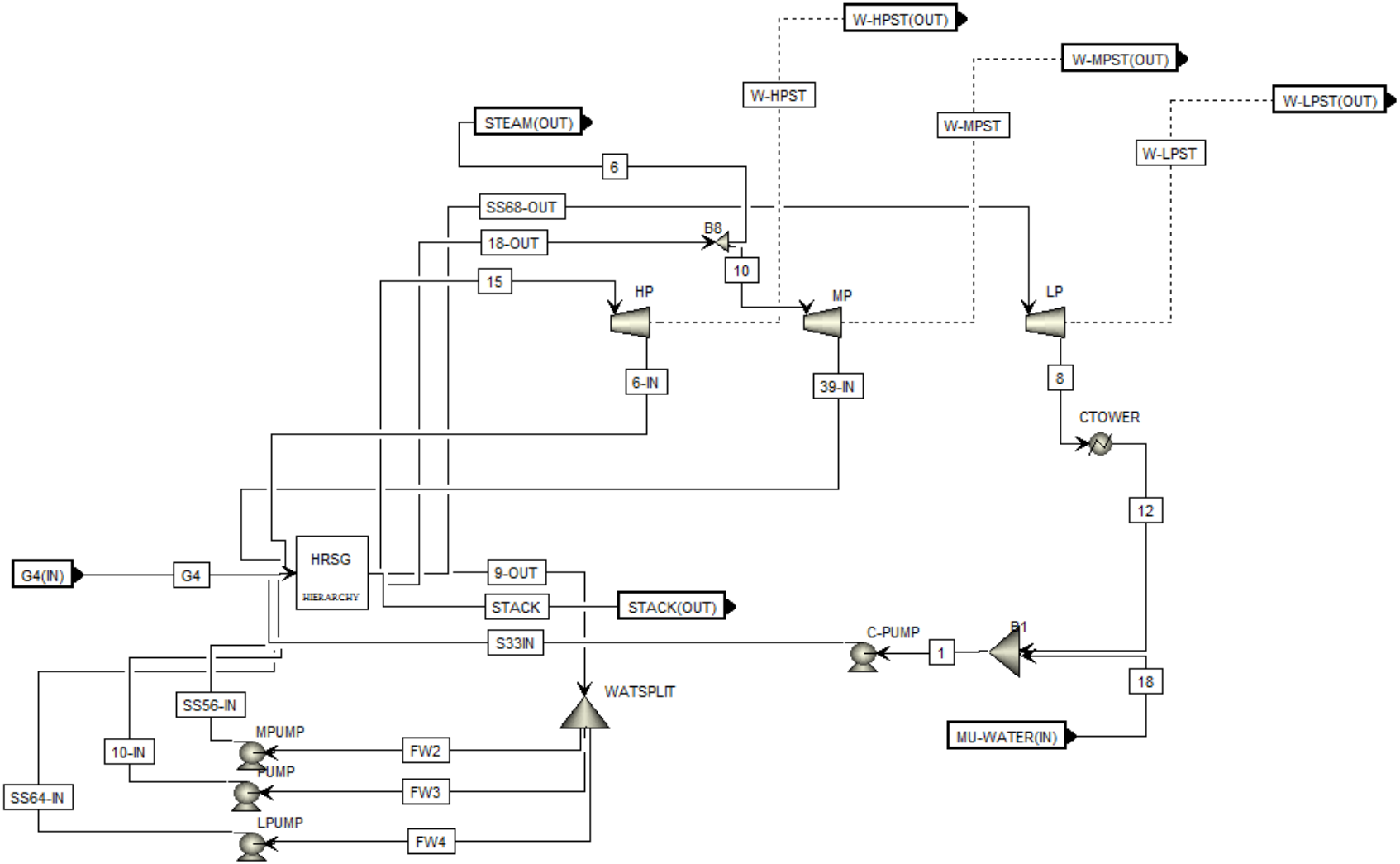


Figure 43: ASPEN Flow-sheet within the RANKINE hierarchy of the pre-combustion capture NGCC power plant (Important stream information can be found in appendix B).

Table 7: Plant performance summary for the NGCC, CCS power plant

Property / attribute	
Fuel feed rate (kg/s)	15.5
Net GT output (MW)	189.08
HP ST output (MW)	22.42
MP ST output (MW)	23.60
LP ST output (MW)	40.09
Net ST output (MW)	86.09
TOTAL output (MW)	300.95
Additional plant axuxilaries [NETL] (MW)	-29.14
CO2 compressor (MW)	-13.42
ASU compressor (MW)	-16.04
CH4 [HHV] (MJ/kg)	52.26
CH4 [LHV] (MJ/kg)	47.14
Thermal input [HHV] (MW)	809.95
Thermal input [LHV] (MW)	730.69
Plant efficiency [HHV] %	29.92
Plant efficiency [LHV]%	33.17

3.3. Discussion

3.3.1. NGCC results discussion

Among the reasons for the superiority of the NGCC power plant is that it utilises gas turbine power generation. This overcomes the exergy losses (see chapter on exergy) associated with transmitting heat across a finite temperature difference by using the flue gasses themselves as working fluid in the combustion turbine. The nature of the working fluid in the combustion turbine also contributes; being a gas, there is no need to overcome the sensible heat barrier and destroy work potential before reaching saturation and producing the vapour that ultimately turns the turbine. Natural gas is also a higher quality fuel than coal; with a lower carbon to hydrogen ratio and a higher calorific value. The setup recovers what exergy remains in the hot flue gasses from the gas turbine exhaust by directing the exhaust from the gas turbine to a bottom Rankine cycle that makes use of its remaining thermal exergy content in a steam cycle.

The triple pressure system utilised in the steam cycle is also very effective at making the most of the exergy contained in the flue gasses. This is because the different pressurised steam flows only mix when exhaust fluid from higher pressure steam turbines mixes with steam headed for steam turbines at pressure levels immediately below them making more use of the exergy contained in each stream. This is very different from steam cycles in conventional power plants that mix exhaust fluid from several steam turbine outlets (all at different pressure) to heat boiler feed water [5]–[7]. This is because of the drop in overall exergy whenever substances are mixed [8], [9].

The simulated plant dose have a high mole fraction in oxygen in the flue gas exhaust however; and as a recommendation it is suggested that the power plant is optimised to reduce this wastage as it should reduce work losses.

3.3.2. NGCC pre-combustion capture results discussion

The disparity in the HHV and the LHV efficiencies determined in this research of 29.9% and 33.17%, with those that were reported in the DOE/NETL [4] report of 42.4% and 47% respectively, cannot be laid upon the fact that the pre-combustion capture gas fired power plant simulated in the DOE/NETL [4] report does not have an ASU. This is because the demand of the ASU compressor is relatively small at 16 MW. The disparity came about because the steam cycle HRSG flow-sheet for an NGCC pre-combustion capture power plant fitted with SEWGS, that provides steam to the upstream pre-combustion capture unit has yet to be modelled in as much detail as it has in this thesis. This is backed by the exergy analysis conducted on the capture plant in chapter 6, which found that the steam extracted for the GHR-ATR-SEWGS unit has an exergy content of 35 MW. This is very high when you consider the fact that the flue gasses that report to the Rankine cycle only have an exergy content of 171.95 MW before heat transfer, with 29.65 MW being lost through irreversibility and 22.41 MW escaping through the stack. This leaves only 119.89 MW, therefore as much as 29.19% of the work potential leaves with the extracted steam leaving only 84.89 MW for power generation which matches the results obtained very closely (amount of power generated by the steam turbines in table 7 is 86.09 MW). Additionally, it was determined from the study conducted to determine how it is that the total mechanical energy output would be affected if no steam were extracted from the HRSG for the pre-combustion capture retrofit that the gross mechanical energy output would

increase by 29.13 MW from 300.95 MW to 330.08 MW. This is very close to the 35 MW predicted from the exergy analysis, with the discrepancy likely being the result of turbine inefficiency and the difficulty associated with extracting all the available exergy as a mass stream moves toward the dead state.

This is proof that the proposed method for conducting exergy analysis using ASPEN plus, as well as the method developed for design and optimization of HRSG's are very accurate. The technique developed for HRSG design and optimization could be implemented on a thermal power plant setup generating electricity from any hydrocarbon feed or waste stream with a single, or multi-pressure HRSG. It will especially prove useful for fossil fuel power plants that utilise HRSG steam extraction to provide the necessary steam for their CCS retrofits as well as geothermal, and combined heat and power plants. It can also be used to determine the efficiency of nuclear power plants with greater accuracy through simulation. This is a long-standing problem that has made research of power plant setups very difficult. There is much potential for heat integration between the GHR-ATR-SEWGS and the steam cycle though; with the flash unit after the SEWGS unit possessing as much as 42,291MW of exergy. The larger than expected efficiency penalty makes the retrofitted power plant very good candidate for heat integration with the high temperature heat from a PtG retrofit.

References

[1] (SASOL), “NATURAL GAS,” 2018. [Online]. Available: http://www.sasol.co.za/products/gas/natural-gas.

[2] B. J. Wittebrood, “System design and thermody namic evaluation of natural gas combined cycle (NGCC) systems including carbon capture & storage (CCS) and metal hydride based hydrogen storage .,” 2015.

[3] (Linkedin), “h class gass turbines: further developments,” 2019. [Online]. Available: https://www.linkedin.com/pulse/h-class-gas-turbines-further-developments-vlad-rosen.

[4] DOE/NETL, “Carbon Capture Approaches for Natural Gas Combined Cycle Systems,” 2010.

[5] K. Almås, “Coal-fired Power Plants based on Oxy-combustion with Carbon Capture : Combustion Conditions and Water Consumption,” Norwegian University of Science and Technology, 2012.

[6] R. Soundararajan, “Oxy-combustion coal based power plants with CO2 capture : Process integration approach to reduce capture penalty,” Norwegian University of Science and Technology, 2015.

[7] T. H. Zeiner, “Process Integration Potentials in Coal- based Power Plants using Oxy-combustion,” Norwegian University of Science and Technology, 2012.

[8] T. J. Kotas, *The Exergy Method of Thermal Plant Analysis*. Essex: Butterworths, 1985.

[9] A. P. Hinderink, F. P. J. M. Kerkhof, A. B. K. Lie, J. De Swaan Arons, and H. J. Van Der Kooi, “Exergy analysis with a flowsheeting simulator - I. Theory; calculating exergies of material streams,” *Chem. Eng. Sci.*, vol. 51, no. 20, pp. 4693–4700, 1996.

[10] C. Fu and T. Gundersen, “Exergy Analysis and Heat Integration of a Coal-Based Oxy-combustion Power Plant,” *Energy & Fuels*, vol. 27, pp. 7138–7149, 2013.

4. Modelling, design & simulation of LTE & HTCE PtG processes

4.1. Methodology

4.1.1. PtG flow-sheet model

Both the HTCE and LTE electrolyser models were developed in a similar manner to the model which was developed in the work of Redissi and Bouallou [2] using the results reported by Luo, et al, [1]. The methanation unit that follows the electrolyser was developed in a similar manner to models of Agerborg and Lingehed [7], Hoekman, et al, [6] and Bailera, et al, [4].

4.1.1.1. PtG process description

4.1.1.1.1. Electrolyser process description

Figure 44 shows the electrolyser model for both the HTCE and LTE unit. It composed of an initial heat exchanger (WATER–HX) that heats the incoming feed (stream EL-1) to the temperature required for electrolysis before it is fed to the RSTOIC block as stream EL-2. The RSTOICH block is meant to simulate the electrolyser in both the HTCE and LTE cases. Once the incoming feed has reacted it then reports to splitter block as electrolyser product stream EL-3. The less desirable products (stream P-103) then leave as a stream of oxygen (for LTE) or oxygen and water for (HTCE) at the electrolyser conditions. The desirable products then leave in stream P-102 as a stream of either hydrogen (for LTE) or syngas for (HTCE), at the electrolyser conditions. The reason the products are separated cleanly at the electrolyser conditions is because the gasses evolve from different electrolyser compartments in reality. And so the work output from the splitter needs to be ignored for it to resemble an electrolyser closely.

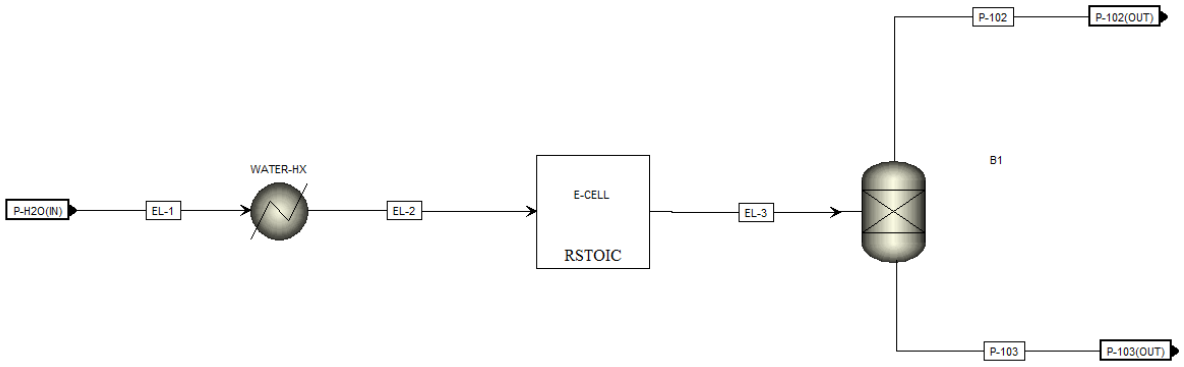


Figure 44: Generic ASPEN plus flow-sheet for both the HTCE and LTE eletrolyser.

4.1.1.1.1.1. HTCE electrolyser characteristics

The model developed in this thesis is a tubular solid oxide electrolysis cell, and the electrolyser characteristics used to develop this model are shown in table 8 [1]. In this study, only the main reaction was taken into consideration (equation 57 [2]); the reversible water gas shift reaction (equation 56) was ignored. The electrolyser in the HTCE model will be fed an equimolar feed in water and CO_2 $\left(n_{CO_2}/n_{H_2} = 1\right)$ as was the case in the research conducted by Luo, et al, [1]. Equation 58 is used to determine the hydrogen conversion (ξ_{H_2}), equation 59 is used to determine the carbon monoxide conversion (ξ_{CO}) and equation 60 is used to determine the syngas conversion (ξ_{tot}). Where $q_{H_2}^{out}$ represents the molar flow of hydrogen out of the electrolyser, $q_{H_2O}^{in}$ represents the molar flow of water into the electrolyser, q_{CO}^{out} represents the molar flow in carbon monoxide out of the electrolyser and $q_{CO_2}^{in}$ represents the molar flow of carbon dioxide into the electrolyser.

Table 8: Electrolyser characterises for HTCE [1].

Electrolyser characteristics	
Temperature [°C]	700
Hydrogen conversion %	52.16
Carbon monoxide conversion %	39.32
Syngas conversion %	48.3
Efficiency %	58.8

$$2CO_2(g) + H_2 \leftrightarrow \ CO(g) + H_2O$$ **Equation 56**

$$H_2O + CO_2 \rightarrow H_2 + CO + O_2$$ **Equation 57**

$$\xi_{H_2} = \frac{q_{H_2}^{out}}{q_{H_2O}^{in}}$$ **Equation 58**

$$\xi_{CO} = \frac{q_{CO}^{out}}{q_{CO_2}^{in}}$$ **Equation 59**

$$\xi_{tot} = \frac{q_{H_2}^{out} + q_{CO}^{out}}{q_{H_2O}^{in} + q_{CO_2}^{in}}$$ **Equation 60**

4.1.1.1.1.2. LTE electrolyser characteristics

For electrolysis conducted at low temperature the electrolyser is fed only water; which it then splits into H_2 at the cathode (equation 61) and O_2 at the anode (equation 62) [3]. The combined cell reaction is given in equation 63. Water conversion is above 99.9% [4], and the temperature at which electrolysis is conducted is 80℃ [3], [4].

$$Cathode: 2H_2O_{(l)} + 2e^- \rightarrow H_{2(g)} + 2OH^-_{(aq)}$$ **Equation 61**

$$Anode: \ 2OH^-_{(aq)} \ \rightarrow 1/2\ O_{2(g)} + H_2O_{(l)} + 2e^-$$ **Equation 62**

$$Overall\ reaction: H_2O(l) \rightarrow H_{2(g)} + 1/2\ O_{2(g)}$$ **Equation 63**

4.1.1.1.2. Methanation unit process decryption

Figure 45 is a diagram of the electrolyser retrofitted to a generic diagram of a methanation unit composed of several Sabatier reactors. The methanation unit receives renewable hydrogen (stream P-102) from the electrolyser and CO_2 (stream P-101) from an industrial emission source to produce methane via Sabatier reactors. The incoming feed then gets heated to 468.15K in heater blocks (PU-01, PU-04, PU-07 etc…) before it's fed to a Sabatier reactor (These have been modelled on RGibbs reactors: unit operations PU-02, PU-05, PU-08 etc…). The products from each Sabatier reactor then get flashed to ambient conditions in flash blocks before getting recycled back into the reactor for temperature control (the temperature must be between 450℃ and 200℃) and improved conversion. Once the methane stream reaches a quality suitable for pipeline transportation (95 mole%) it then reports to the PtG compressor PTG-COMP were it is then compressed to 65 bar in a 5 stage compressor with intercooling

(each stage is cooled to 298.15K). A final product methane pressure of 65 bar was chosen in order to investigate the energy penalty associated with methane storage in metallic organic frameworks (MOFs) [5], and final product methane pressure of 5 bar was chosen in order to investigate the energy penalty associated generating a methane stream ready for pipeline transport.

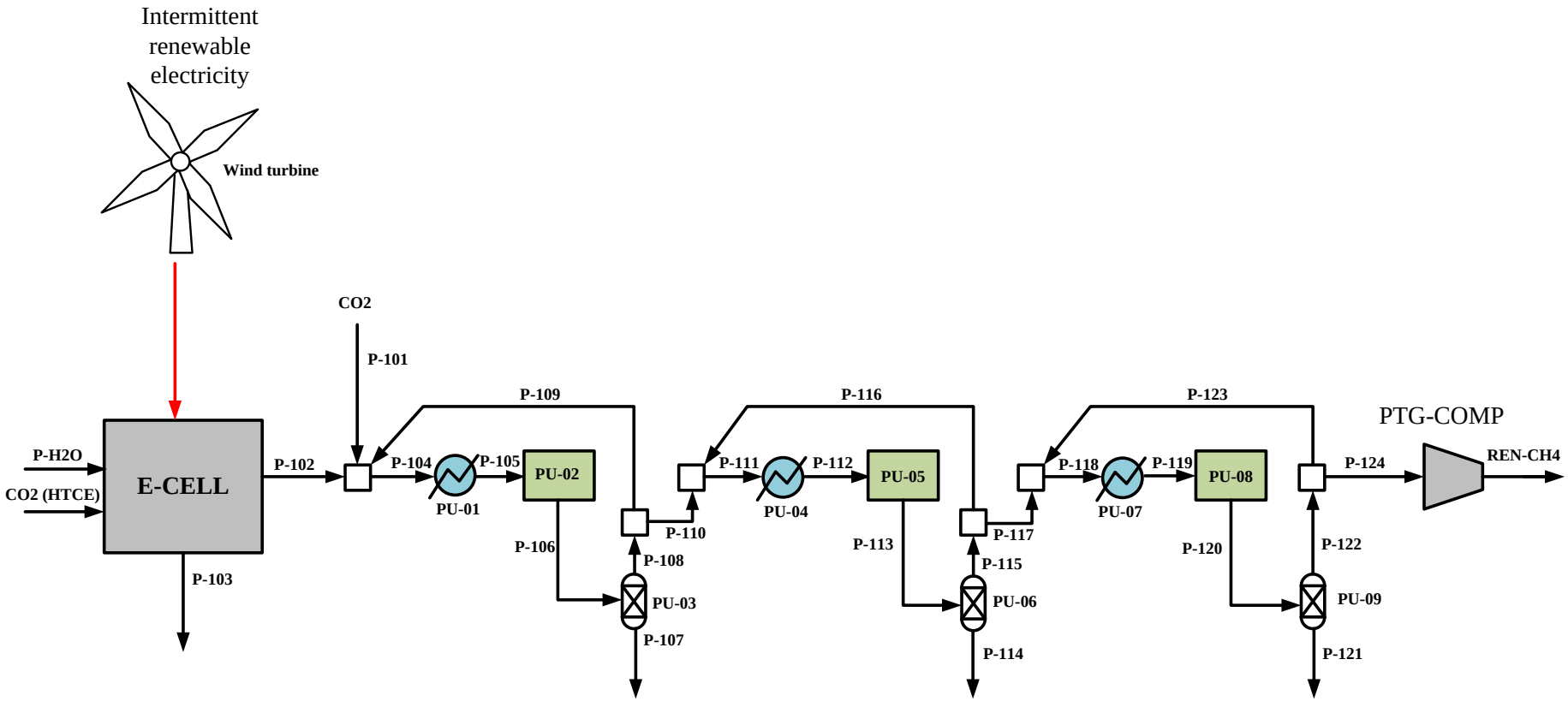


Figure 45: Generic diagram of a PtG setup.

The reactions that can take place across the Sabatier reactor are: methanation of CO_2 (equation 64), the reverse water gas shift reaction (equation 65), methanation of CO (equation 66) and the boudouard reaction (equation 67).

$$CO_2(g) + 4H_2 \leftrightarrow CH_4\,(g) + H_2O \qquad \Delta H^{O}_{reaction} = -165\left(\frac{kJ}{mol}\right) \qquad \textbf{Equation 64}$$

$$CO_2(g) + H_2(g) \leftrightarrow CO\,(g) + H_2O(g) \qquad \Delta H^{O}_{reaction} = +41.2\left(\frac{kJ}{mol}\right) \qquad \textbf{Equation 65}$$

$$CO(g) + 3H_2 \leftrightarrow CH_4\,(g) + H_2O \qquad \Delta H^{O}_{reaction} = -206.4\left(\frac{kJ}{mol}\right) \qquad \textbf{Equation 66}$$

$$2CO(g) \rightarrow C(s) + CO_2(g) \qquad \Delta H^{O}_{reaction} = -172.5\left(\frac{kJ}{mol}\right) \qquad \textbf{Equation 67}$$

4.1.1.1.3. Results

4.1.1.1.3.1. HTCE PtG results

The amount in water fed to the electrolyser was used as a basis for comparison between the LTE and HTCE electrolyser. To achieve this, the ratio of CH_4/H_2O (CH_4 fed to the NGCC plant and H_2O fed to the electrolyser) needs to remain the same in both models for the sake of the heat integration study. Preliminary calculations indicated that in order for the PtG, HTCE retrofit to have the same ratio in CH_4/H_2O at the feed as that of the PtG,LTE retrofit, 65.75 (kg/s) of H_2O had to be fed to the HTCE electrolyser. Therefore 160.61 (kg/sec) of CO_2 was needed for an equimolar 3.65 (kmols/sec) feed in both CH_4 and H_2O. The power plant only produced 40.068 (kg/sec) of CO_2; which then meant the remaining 120.55 (kg/sec) of CO_2 would have to come from an external emission source (this could be an industrial or power utility emission source).

Figure 46 is a graph charting syngas conversion (across the horizontal axis) against the H_2, CO and CO_2 mole fractions in the desired product stream from the electrolyser for an equimolar feed in H_2O and CO_2 to the unit. Table 9 shows the stream results across all streams in the HTCE electrolyser, among the results is the composition of the stream reporting to the methanation unit from the electrolyser at the reported conversion in syngas of 43.8% (stream P-102 in figure 45) (please note that stream EX-CO2 in this case represents stream CO2 (HTCE) in figure 45). Looking at figure 46 it's clear that initially the CO_2 molar composition is very high, before it slowly begins fall at a decreasing rate until its slightly higher than the

CO and H_2 mole factions in the product stream. The mole fraction of CO_2, CO and H_2 from the product stream are 0.39, 0.31 and 0.30 respectively.

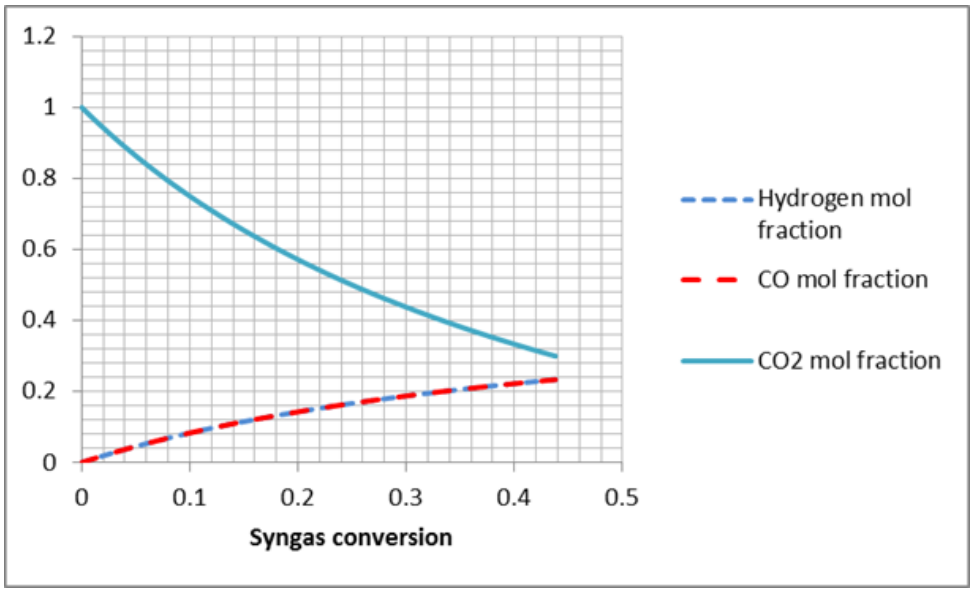


Figure 46: Graph charting syngas conversion against the CO, H_2 and CO_2 mole fraction in the product stream from the HTCE electrolyser for an equimolar feed in H_2O and CO_2.

Table 9: Stream results across HTCE electrolyser. Stream P102 (see figure 45) is the stream that reports to the methanation unit form the electrolyser (Important stream information can also be found in appendix C).

	Eletrolyser stream results				
	Feed			Products	
	P-101	P-H2O	EX-CO2	P-103	P-102
Molar flow [kmol/sec]	0.92	3.63	2.74	3.63	5.25
Mass flow [kg/sec]	110.52	180.15	332.52	241.40	381.80
Temperature (K)	301.15	298.15	298.15	973.15	973.15
Pressure (Pa)	8000000	101325	15000000	101325	101325
Vapour fraction (V)	1	0	0	1	1
Liquid fraction (L)	0	1	1	0	0
Mole percentages					
Carbon dioxide	95.87	0.00	100	0.00	38.80
Carbon monoxide	4.13	0.00	0.00	0.00	30.96
Water	0.00	100	0.00	56.20	0.00
Oxygen	0.00	0.00	0.00	43.80	0.00
Hydrogen	0.00	0.00	0.00	0.00	30.24

Figure 47 is a graph charting the recycle fraction (in the horizontal axis) against methane composition in the stream leaving the first Sabatier reactor and the temperature of the unit (in the vertical axis). The feed to the methanation unit is that which was predicted for the HTCE electrolyser hydrogen product (stream P-102 in table 9). As expected, the temperature drops as the recycle fraction increases until you get to a point where the methane composition begins to asymptote at around 21 mole % (see table 10) and a unit operating temperature of around 313℃. This occurs at the maximum recycle fraction of 0.9. The final process layout for the methanation unit in HTCE is shown in figure 49: it has a single Sabatier reactor with a recycle fraction of 90% and a unit operating temperature of 313℃.

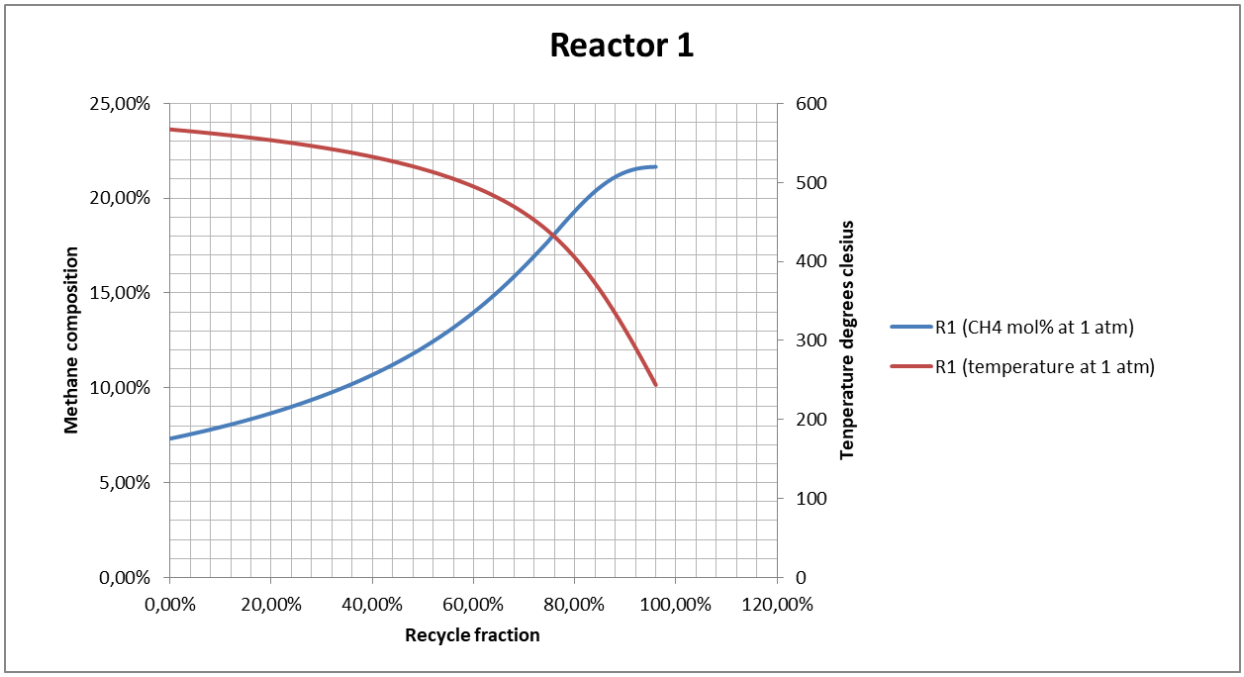


Figure 47: Graph plotting Sabatier rector recycle fraction against unit operation temperature and product methane composition in the first and only Sabatier reactor for HTCE (unit PU-02 in figure 45). Data can be found in appendix C.

Table 10: Stream characteristics of the product from the first Sabatier reactor in the HTCE PtG setup

	P-110
Molar flow [kmol/sec]	3.68
Mass flow [kg/sec]	381.80
Temperature (K)	298.15
Pressure (Pa)	101325
Vapour fraction (V)	1
Liquid fraction (L)	0
Mole percentages	
Carbon dioxide	76.53
Carbon monoxide	1.68
Water	0.23
Oxygen	0.00
Hydrogen	0.18
Methane	21.38

Figure 48 and figure 49 are the final flow-sheets for the HTCE electrolyser and the PtG, HTCE process respectively. And figure 50 is the ASPEN plus flow sheet for the entire retrofitted NGCC pre-combustion capture, HTCE PtG setup. Stream results can be found in appendix C.

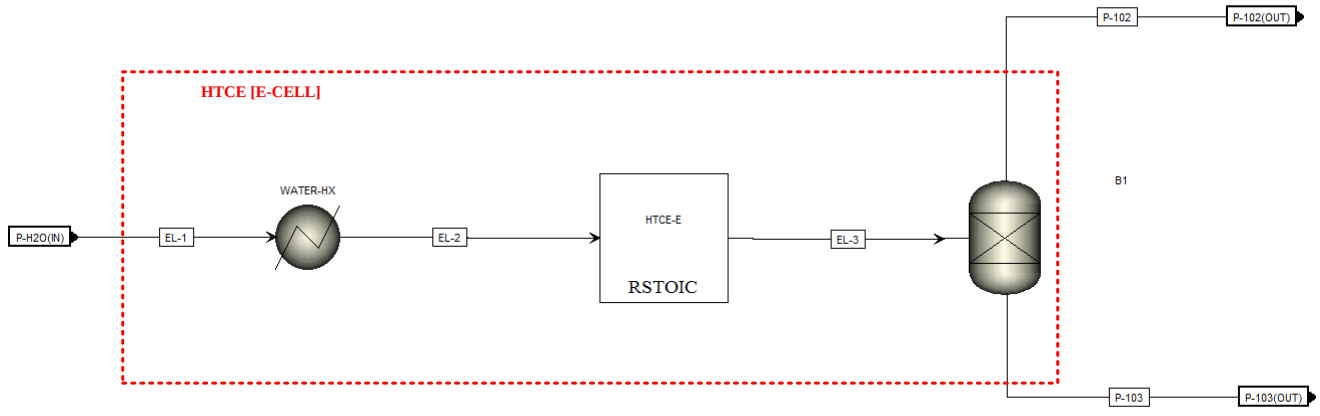


Figure 48: Flow-sheet for HTCE electrolyser.

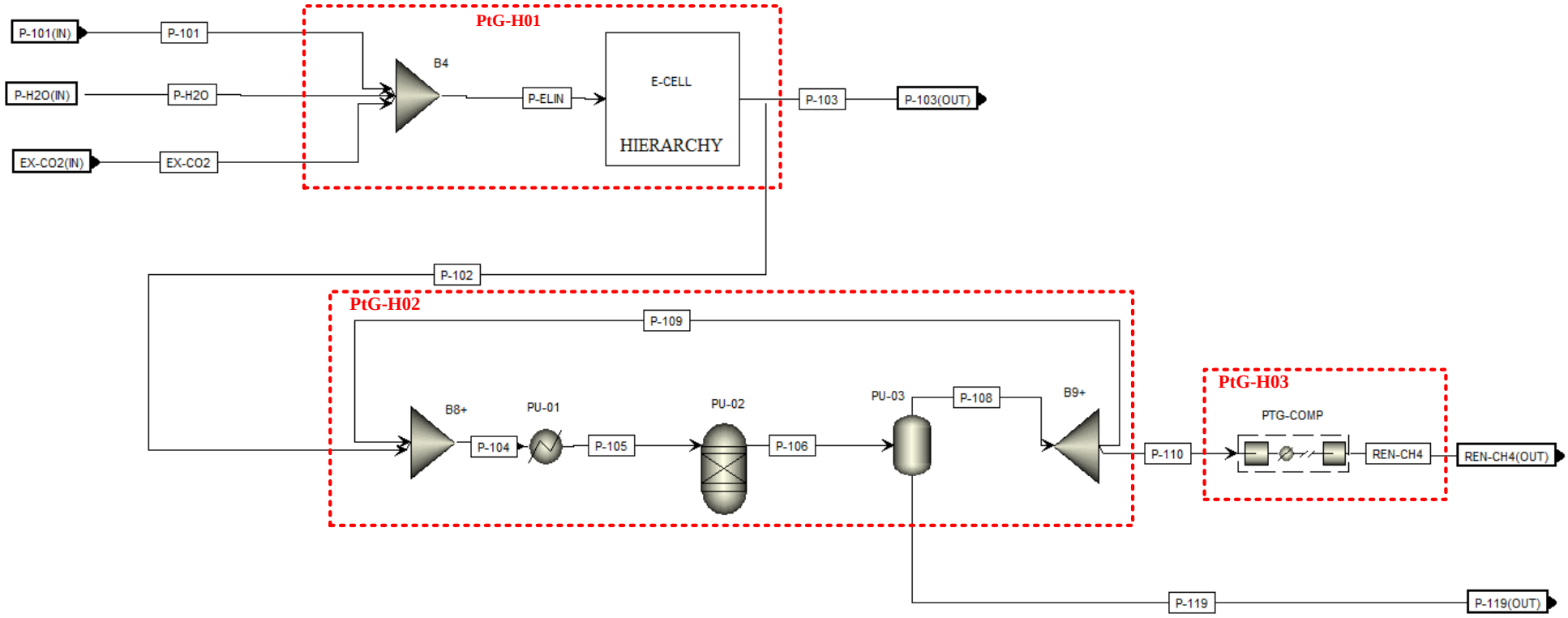


Figure 49: Final flow-sheet for HTCE PtG retrofit.

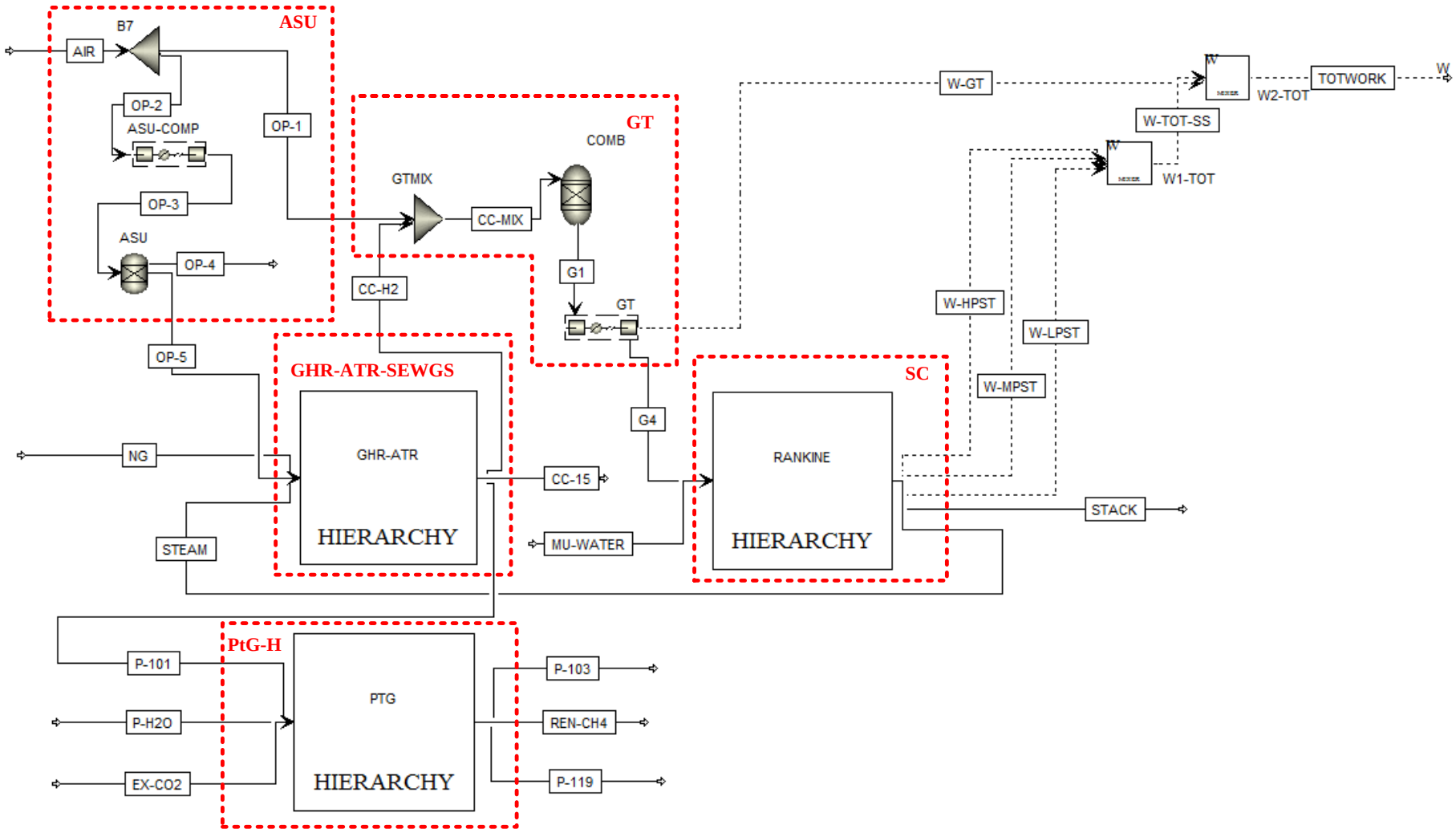


Figure 50: Final flow-sheet for entire NGCC, CCS power plant retrofitted with HTCE, PtG. The system boundary PtG-H surrounds the HTCE hierarchy PTG retrofit which contains the flow-sheet in figure 49.

4.1.1.1.3.2. LTE PtG results

Table 11 contains the stream results across the LTE electrolyser. The flow of water to the unit was adjusted so the molar flow in hydrogen from the unit is 4 times the molar flow of CO_2 [0.89 $(kmol/sec)$] added to three times the molar flow of CO [0.04 $(kmol/sec)$] coming from the capture plant. So the flow in water to the electrolyser and the flow in hydrogen from the eletrolyser would need to be 3.7 $(kmol/sec)$. This was to ensure there was enough hydrogen to methanate the CO_2 and CO in the flue gasses from the capture plant according to equation 64 and equation 66.

Table 11: Stream results across the LTE electrolyser (Important stream information can also be found in appendix D).

	Eletrolyser stream results		
	Feed	Products	
	P-H2O	P-103	P-102
Molar flow [kmol/sec]	3.70	1.85	3.70
Temperature (K)	298.15	353.15	353.15
Pressure (Pa)	101325	101325	101325
Vapour fraction (V)	0	1	1
Liquid fraction (L)	1	0	0
Mole percentages			
Carbon dioxide	0.00	0.00	0.00
Carbon monoxide	0.00	0.00	0.00
Water	100	0.002	0.00
Oxygen	0.00	99.98	0.00
Hydrogen	0.00	0.00	100

Figure 51 is a graph charting the recycle fraction in the horizontal axis against methane composition in the stream leaving the first Sabatier reactor and the temperature of the unit in the vertical axis. The feed to the methanation unit is that which was predicted for the LTE electrolyser hydrogen product (stream P-102 in table 11). The temperature drops as the recycle fraction increases until it reaches 436.16℃ for a product methane mole fraction of 70.87% and a maximum recycle fraction of 0.9. This product then reported to the second Sabatier reactor (unit PU-05 in figure 45), for which a similar graph was produced in figure 52. The methane product in the second reactor had a methane composition of 93.25 mol%, this occurred for a Sabatier reactor recycle fraction of 0.78 and a unit operation temperature of 259℃. Figure 53 combines the results charting recycle fraction against methane composition and reactor

temperature in both Sabatier reactors. The stream results across the LTE PtG process can be viewed in table 12, and the final flow-sheet for the PtG, LTE retrofit can be seen in figure 55. The flowsheet for the entire retrofitted NGCC pre-combustion capture LTE, PtG setup can be seen figure 56.

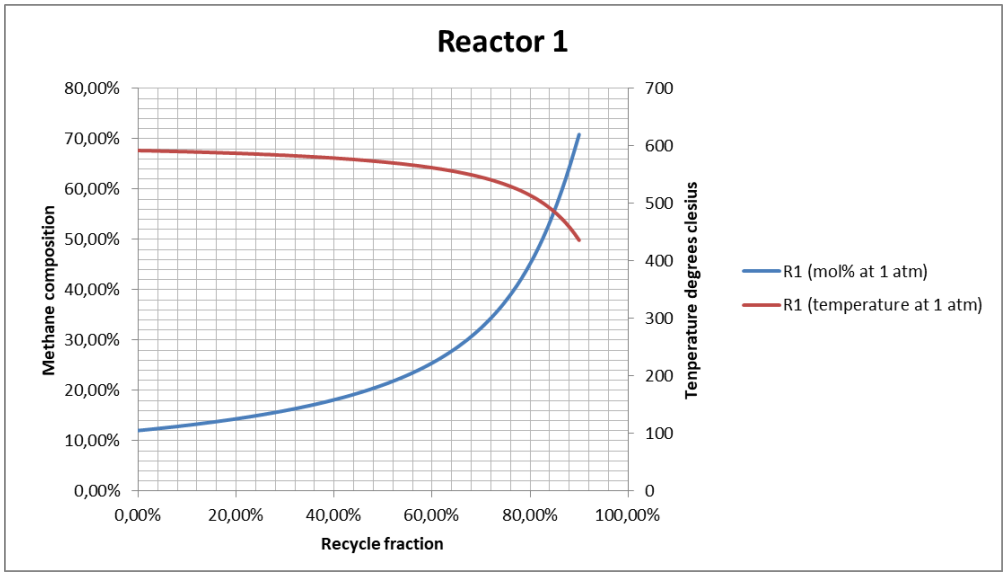


Figure 51: Graph plotting Sabatier rector recycle fraction against unit operation temperature and product methane composition in the first Sabatier reactor for LTE PtG (unit PU-02 in figure 45). Data can be found in appendix D.

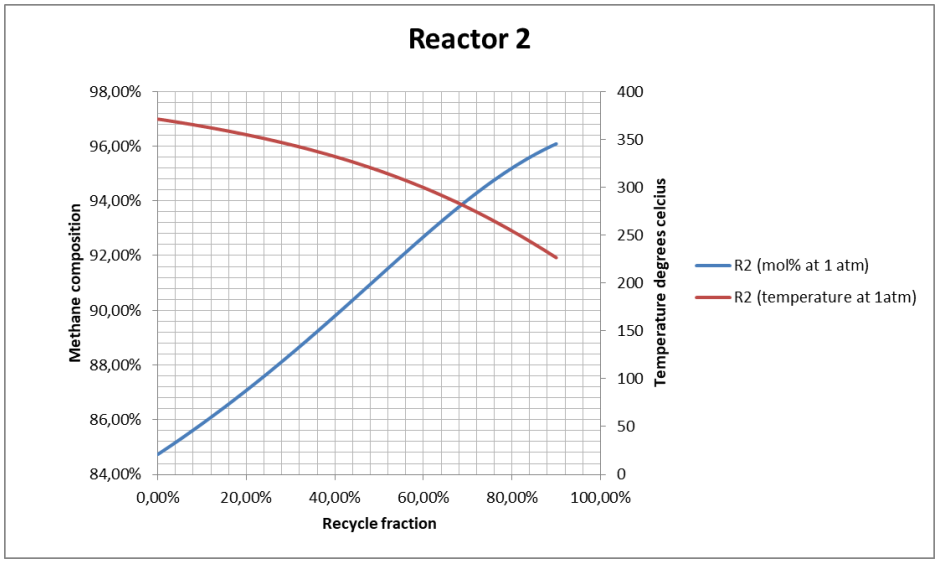


Figure 52: Graph plotting Sabatier rector recycle fraction against unit operation temperature and product methane composition in the second Sabatier reactor for LTE PtG (unit PU-05 in figure 45). Data can be found in appendix D.

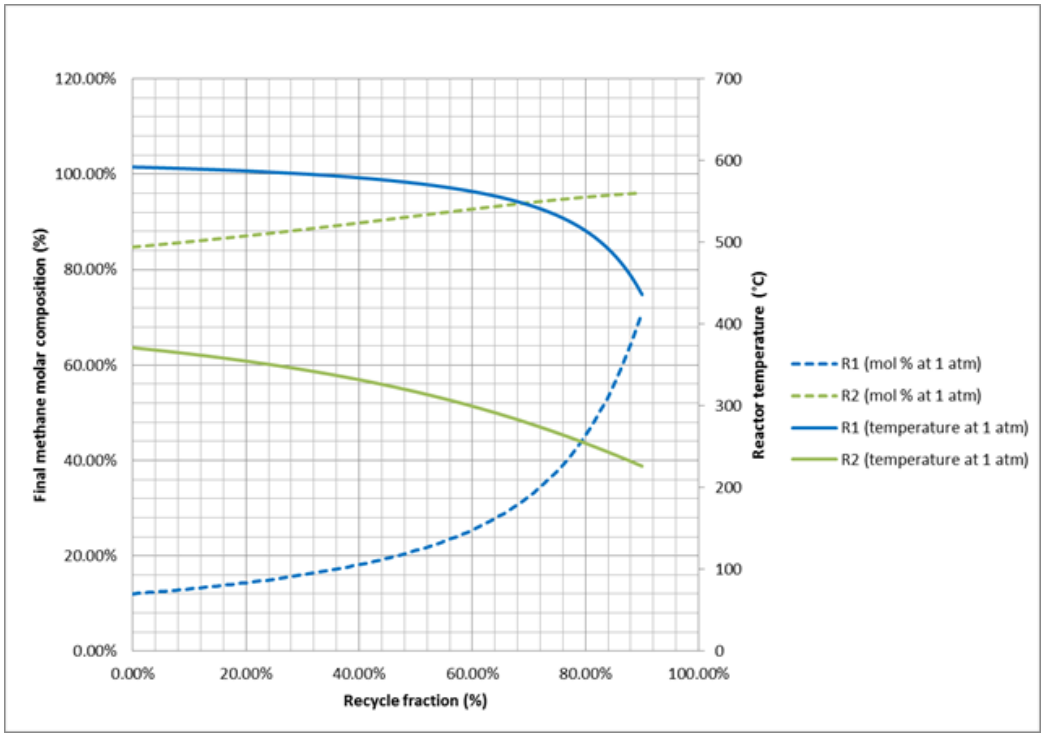


Figure 53: This graph combines the results from the first Sabatier reactor (Figure 51) with those of the second one (Figure 52). Data can be found in appendix D

Table 12: Table containing the stream result for the products emanating from the LTE PtG methanation unit.

	PtG stream results				
	Feed		Products		
	P-H2O	P-101	P-103	P-119	REN-NG
Molar flow [kmol/sec]	3.70	0.92	1.85	1.78	0.99
Temperature (K)	298.15	298.15	353.15	298.15	298.15
Pressure (Pa)	101325	8000000	101325	101325	6500000
Vapour fraction (V)	0	1	1	0	0.97
Liquid fraction (L)	1	0	0	1	0.03
Mole percentages					
Carbon dioxide	0.00	95.87	0.00	0.00	0.00
Carbon monoxide	0.00	4.13	0.00	0.00	0.00
Water	100	0.00	0.02	100	2.58
Oxygen	0.00	0.00	99.98	0.00	0.00
Hydrogen	0.00	0.00	0.00	0.00	4.17
Methane	0.00	0.00	0.00	0.00	93.25

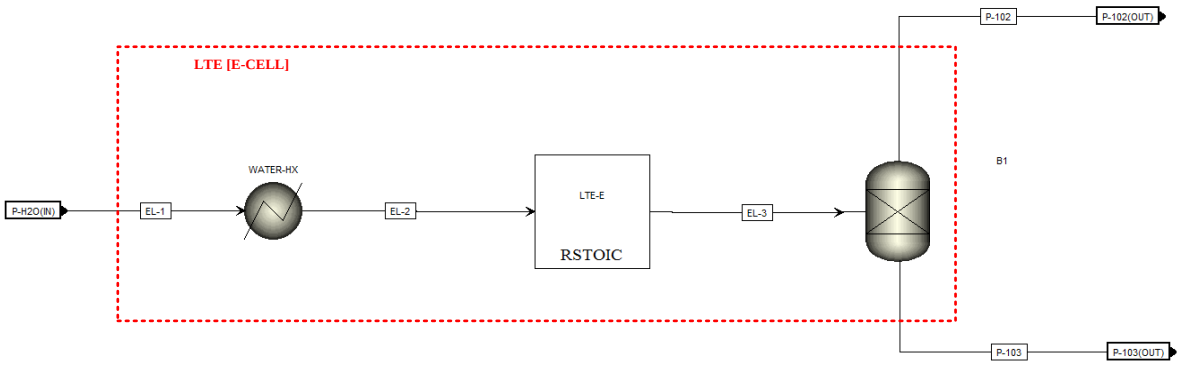


Figure 54: Final flow-sheet for the LTE electrolyser.

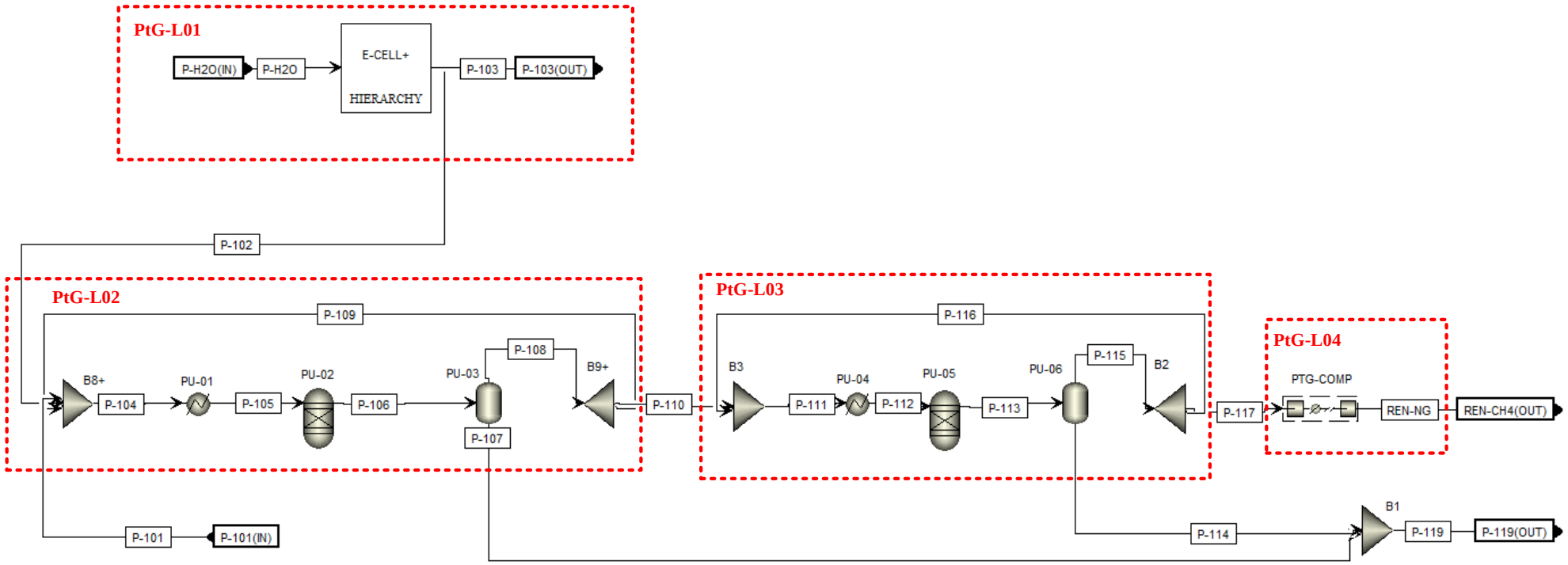


Figure 55: Final flow-sheet for LTE PtG retrofit (Important stream information can be found in appendix C)

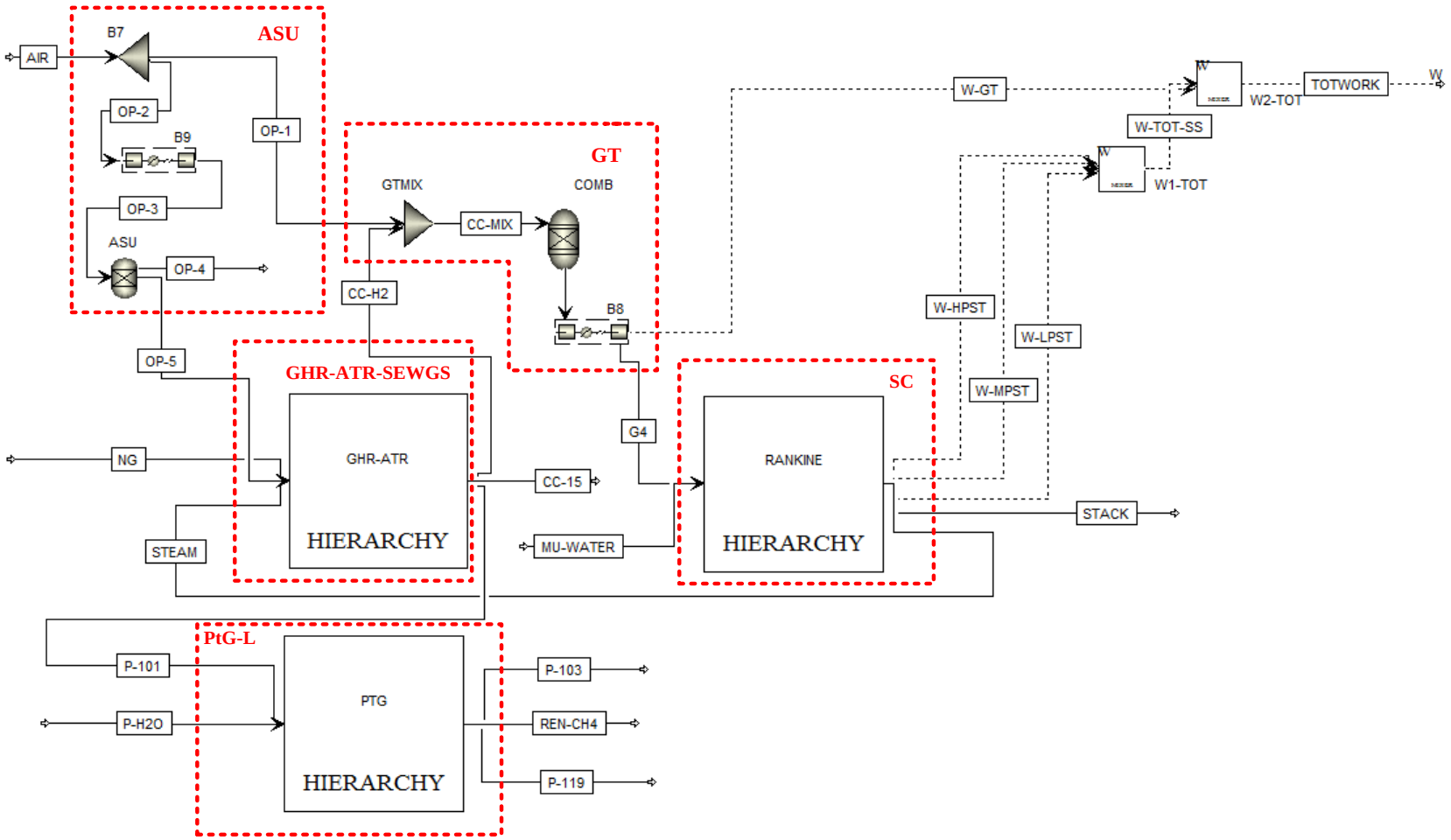


Figure 56: final flow-sheet of NGCC power plant retrofitted with SEWGS CCS and LTE PtG. The system boundary PtG-L surrounds the LTE hierarchy PTG retrofit which contains the flow-sheet in figure 55.

4.1.1.1.4. Discussion

Looking at figure 46 (HTCE electrolyser results), the reason the CO_2 mole fraction starts at 1 is because initially nothing reacts in the electrolyser, and the reason the CO_2 mole fraction then reduces is because as the syngas conversion begins to rise, the CO_2 gets used up and the H_2 and CO mole fractions begin to increase. The H_2 and CO mole fractions are identical for all syngas conversions because they are produced in an equimolar ratio according to equation 57.

One of the reasons the methane composition rises as the recycle fraction increases across the Sabatier reactors for both HTCE and LTE is because a portion of the product gets removed (water is condensed out) before recycling which gives the unreacted feed multiple passes which increases conversion. Another reason for it is that the temperature drops upon recycling which promotes methanation as the reaction is exothermic.

The reason the methane composition across the first Sabatier reactor in the HTCE PtG process begins to asymptote around a CH_4 composition of 21% is because all the hydrogen was exhausted. Evidence of this can be found in the table 10, which contains the molar composition of the stream emanating from this Sabatier reactor. This composition in methane is too low for transportation and storage in pipeline networks which require a composition in methane of around 95 mol%. It is however recommended that another study be conducted on the processes that takes the RWGS reaction into consideration which might change the outcome. Therefore, the syngas stream fed to the methanation unit described in the results requires a higher H_2 mole fraction: which answers research question 3 for the HTCE PtG NGCC CCS process.

The LTE PtG process did manage to produce a final product stream with a CH_4 composition high enough (93.25 mol%) for transport and storage in pipeline networks making it superior to HTCE for this purpose: which answers research question 5. And the syngas stream fed to the methanation unit described in the results was at the appropriate conditions: which answers research question 3 for the LTE PtG NGCC CCS process.

References

[1] Y. Luo, Y. Shi, W. Li, and N. Cai, “Comprehensive modeling of tubular solid oxide electrolysis cell for co-electrolysis of steam and carbon dioxide,” *Energy*, vol. 70, pp. 420–434, 2014.

[2] Y. Redissi and C. Bouallou, “Valorization of carbon dioxide by co-electrolysis of CO2/H2O at high temperature for syngas production,” *Energy Procedia*, vol. 37, pp. 6667–6678, 2013.

[3] P. M. Diéguez, A. Ursúa, P. Sanchis, C. Sopena, E. Guelbenzu, and L. M. Gandía, “Thermal performance of a commercial alkaline water electrolyzer: Experimental study and mathematical modeling,” *Int. J. Hydrogen Energy*, vol. 33, no. 24, pp. 7338–7354, 2008.

[4] M. Bailera, P. Lisbona, L. M. Romeo, and S. Espatolero, “Power to Gas-biomass oxycombustion hybrid system: Energy integration and potential applications,” *Appl. Energy*, vol. 167, pp. 221–229, 2016.

[5] Y. He, W. Zhou, G. Qian, and B. Chen, “Methane storage in metal-organic frameworks,” *Chem. Soc. Rev.*, pp. 1–23, 2014.

[6] S. K. Hoekman, A. Broch, C. Robbins, and R. Purcell, “International Journal of Greenhouse Gas Control CO 2 recycling by reaction with renewably-generated hydrogen,” vol. 4, pp. 44–50, 2010.

[7] J. Agerborg and E. Lingehed, “Integration of Power-to-Gas in Gasendal and GoBiGas,” *Publications.Lib.Chalmers.Se*, pp. 1–70, 2013.

5. Heat integration study on NGCC Pre-combustion capture HTCE and LTE PtG setups

In this section a heat integration study was conducted to determine to what degree the heat from the methanation units in both LTE and HTCE could be used to overcome the efficiency penalty that comes with the GHR-ATR-SEWGS retrofit.

5.1. Methodology

The following are steps taken in the heat integration study for a minimum temperature difference of 10℃:

1. Determine the supply temperatures for the compression heat assuming the compressor has 2 compression stages with intercooling (each compression stage is cooled to 298.15K) as well as the heat sources in the methanation unit.
2. Determine which heat sinks can be integrated with these heat sources within the PtG retrofit and the NGCC capture plant steam cycle (figure 42).
3. Draw the grand composite curve (GCC) and determine the minimum hot and cold utility upon integration.
4. Determine the increase in mechanical work output that would come with heat integration using figure 42 and the pre-combustion capture plant appendix.

5.1.1. HTCE PtG heat integration methodology

The heat sources within the HTCE PtG retrofit include, stream P-106 and the power to gas compressor (see table 13, table 14 and figure 49). It was determined that these heat sources could be integrated with the cold streams moving through heat exchangers HECL and HECM within the pre-combustion capture NGCC power plant steam cycle (see table 14 and figure 42). There is no heat source in the setup that can supply heat at temperatures required by the HTCE electrolyser. So the heat duty across heat exchanger WATER-HX of 379.78MW, was instead used directly in the efficiency estimates.

Table 13: Inlet and outlet temperatures, heat duties, compression ratios, CP values and compression work for the PtG compressor compression stages in HTCE.

PTG-COMP						
Stage number	$T_{in}\ [Kelvin]$	$T_{out}\ [Kelvin]$	$\Delta H\ [MW]$	$Comp\ ratio$	$CP\ [MW/°C]$	Comp work req [*MW*]
Stage 1	492.77	298.15	-29.89	8.01	0.15	58.88
Stage 2	498.42	298.15	-37.54	8.01	0.19	

Table 14: Inlet and out let temperatures, heat duties and CP values for all the heat sinks and heat sources in the methanation unit in HTCE.

PtG				
Sabatier reactor heat sources				
Stream name	$T_{in}\ [Kelvin]$	$T_{out}\ [Kelvin]$	$\Delta H\ [MW]$	$CP\ [MW/°C]$
P-106	586.30	298.15	-452.18	0.77
Sabatier reactor heat sinks				
Stream name	$T_{in}\ [Kelvin]$	$T_{out}\ [Kelvin]$	$\Delta H\ [MW]$	$CP\ [MW/°C]$
P-104	387.35	468.15	127.83	0.56
Steam cycle heat sinks				
Stream name	$T_{in}\ [Kelvin]$	$T_{out}\ [Kelvin]$	$\Delta H\ [MW]$	$CP\ [MW/°C]$
HELC	386.15	423.15	10.92	0.30
HECM	423.15	493.15	21.8	0.31

5.1.2. LTE, PtG heat integration methodology

The heat sources within the LTE PtG retrofit include; the PtG compressor (PTG-COMP), stream P-106 and stream P-113 (see figure 55, table 15, and table 16). It was determined that they could be integrated with streams P-104, P-111 and EL-1 within the LTE PtG retrofit (see figure 55 and figure 54) and the cold streams in heat exchangers HELC, HECM and HECH in the pre-combustion capture NGCC power plant steam cycle (see figure 38 and figure 42).

The initial and final temperatures, heat duties and CP values for the integrated streams can be found in table 16. The inlet and outlet temperatures, heat duties, compression ratios and CP values for each of the compression stages can be found in table 15.

Table 15: Inlet and out let temperatures, heat duties, compression ratios and CP values for the PtG compressor compression stages in LTE PtG retrofit.

PTG-COMP						
Stage number	$T_{in}\ [Kelvin]$	$T_{out}\ [Kelvin]$	$\Delta H\ [MW]$	$Comp\ ratio$	$CP\ [MW/°C]$	Comp work req [MW]
Stage 1	497.52	298.15	-7.97	8	0.04	15.82
Stage 2	496.69	298.15	-8,63	8	0.04	

Table 16: Inlet and out let temperatures, heat duties and CP values for all the heat sinks and heat sources in the methanation unit in LTE PtG retrofit.

PtG				
Sabatier reactor heat sources				
Stream name	$T_{in}\ [Kelvin]$	$T_{out}\ [Kelvin]$	$\Delta H\ [MW]$	$CP\ [MW/°C]$
P-106	709.73	298.15	-315.13	0.77
P-113	492.56	298.15	-83.12	0.43
Sabatier reactor heat sinks				
Stream name	$T_{in}\ [Kelvin]$	$T_{out}\ [Kelvin]$	$\Delta H\ [MW]$	$CP\ [MW/°C]$
P-104	296.90	468.15	95.30	0.56
P-111	296.66	468.15	66.88	0.39
Steam cycle heat sinks				
Stream name	$T_{in}\ [Kelvin]$	$T_{out}\ [Kelvin]$	$\Delta H\ [MW]$	$CP\ [MW/°C]$
HECL	386.15	423.15	10.92	0.30
HECM	423.15	493.15	21.8	0.31
HECH	493.15	597.15	41.7	0.40
Eletrolyzer heat sinks				
Stream name	$T_{in}\ [Kelvin]$	$T_{out}\ [Kelvin]$	$\Delta H\ [MW]$	$CP\ [MW/°C]$
EL-1	298.15	353.15	16.62	0.30

5.2. Results

5.2.1. HTCE PtG heat integrations results

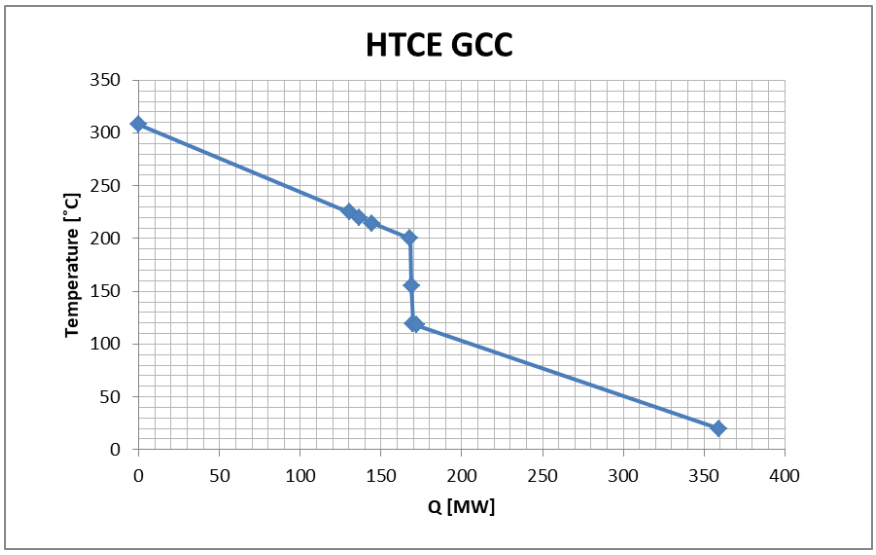


Figure 57: GCC for PtG HTCE retrofit heat integration with NGCC, CCS steam cycle.

GCC results indicate that there would be no hot utility requirement for the streams integrated. We know that the contribution made by the low-pressure steam turbines to the total work output within the capture plant comes to 40MW (see table 7). So assuming linearity between the total work output through the turbines and steam molar flow through them; one can deduce that the contribution made to the work output through the low pressure turbine by stream SS67 in the steam cycle (see figure 38) for the pre-combustion capture plant should be around 7.78MW. Using the heat duties that were plotted in figure 42, one can determine what would happen if the flue gasses that would ordinarily flow through the high pressure economisers (HECH and HECM) were to instead be directed to the heat exchangers in the low pressure section of the HRSG (heat exchangers LECL, LEPV and SUP3): the increase in output that would results within the low pressure section would be around 9.028 MW. Additionally, we have around 50MW in cold utility required for the flue gasses according figure 57, which can be delivered at a temperature of around 277℃. If this heat were also directed to the LP HRSG heat exchangers; an additional 13.8 MW in mechanical energy could be generated. These actions would increase the mechanical energy from the low-pressure turbine to 62.91MW. The effect that this and the heat duty across HTCE electrolyser would have on the efficiency of the pre-combustion capture plant is shown in the plant performance summary in table 17. The heat integration would reduce the HHV and LHV efficiency of the of the capture plant to -14.15%

and -15.68% respectively. This answers research question 6 for the HTCE PtG, NGCC, CCS setup.

Table 17: Plant performance summary of pre-combustion capture power plant upon heat integration with HTCE PtG retrofit

Property / attribute	
Fuel feed rate (kg/s)	15.5
Net GT output (MW)	214.86
HP ST output (MW)	22.42
MP ST output (MW)	23.59
LP ST output (MW)	62.91
Net ST output (MW)	108.92
TOTAL output (MW)	323.77
Electrolyser heat duty [MW]	-379.78
Additional plant axuxilaries [NETL] (MW)	-29.14
CO2 compressor (MW)	-13.42
ASU compressor (MW)	-16.04
CH4 [HHV] (MJ/kg)	52.26
CH4 [LHV] (MJ/kg)	47.14
Thermal input [HHV] (MW)	809.95
Thermal input [LHV] (MW)	730.69
Plant efficiency [HHV] %	-14.15
Plant efficiency [LHV]%	-15.68

5.2.2. LTE PtG heat integration results

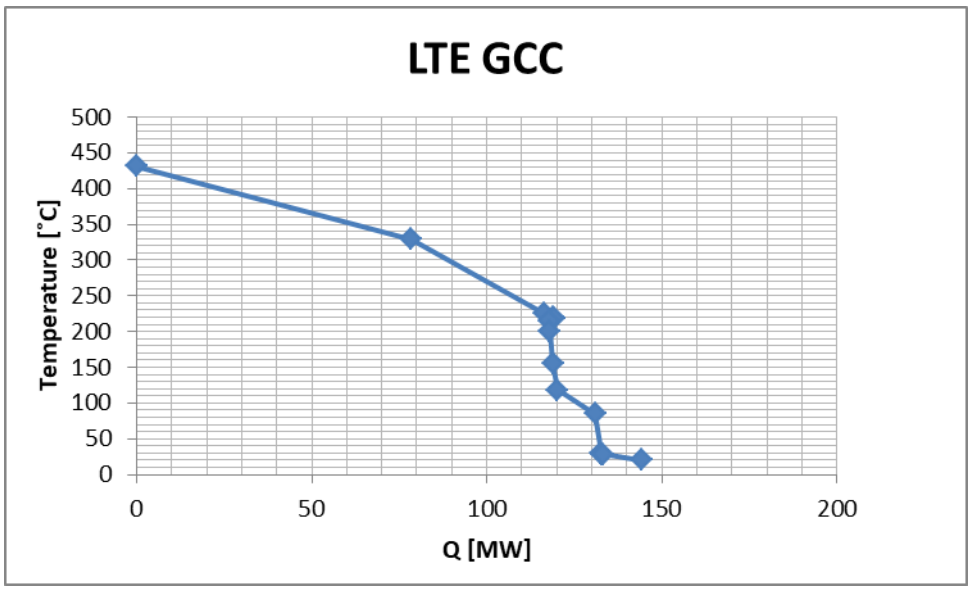


Figure 58: GCC for PtG LTE heat integration with NGCC, CCS steam cycle heat sinks.

The same procedure that was followed for the HTCE heat integration study was implemented here. This time, flue gasses from three high pressure economisers (HECH, HECM and HECL) would be directed to the heat exchangers in the low-pressure section of the HRSG (heat exchangers LECL, LEPV and SUP3). The increase in output within the low-pressure turbines would come to 20.53MW. The additional cold utility required in this case comes to 93MW at 277℃, which should result in an increase in output of 25.66MW when directed to the LP HRSG heat exchangers. These actions would increase the output from the low-pressure turbines to 86.280MW. The effect that this would have on the NGCC pre-combustion capture power plant performance is summarized in table 18. The actions would increase the HHV efficiency of the of the capture plant by 5.703% to 35.625% and increase the LHV efficiency of the capture plant by 6.322% to 39.490%. This answers research question 6 for the LTE PtG, NGCC, CCS setup.

Table 18: Plant performance summary for the pre-combustion capture NGCC power plant upon heat integration with its LTE PtG retrofit

Property / attribute	
Fuel feed rate (kg/s)	15.50
Net GT output (MW)	214.86
HP ST output (MW)	22.42
MP ST output (MW)	23.60
LP ST output (MW)	86.28
Net ST output (MW)	132.29
TOTAL output (MW)	347.14
Additional plant axuxilaries [NETL] (MW)	-29.14
CO2 compressor (MW)	-13.42
ASU compressor (MW)	-16.04
CH4 [HHV] (MJ/kg)	52.26
CH4 [LHV] (MJ/kg)	47.14
Thermal input [HHV] (MW)	809.95
Thermal input [LHV] (MW)	730.69
Plant efficiency [HHV] %	35.62
Plant efficiency [LHV]%	39.49

5.3. Discussion

5.3.1. HTCE & LTE PtG heat integration results discussion

When fully integrated, the HTCE PtG processes reduces the NGCC pre-combustion capture power plant overall efficiency due to the high demand of the electrolyser. This heat demand is so high that it is greater than the amount in mechanical work generated by the entire capture plant, even upon integrating the Sabatier reaction heat (see table 17). The outcome would be made worse if one were to consider instead the calorific value of the fuel burned to supply the heat needed to raise the temperature of the electrolyser. Therefore, HTCE PtG, and other variants of the processes that produce products other than methane should be seen predominantly as a means of processing CO_2 and not as a source of heat.

When fully integrated the LTE PtG process is able to enhance the efficiency of the pre-combustion capture NGCC power plant due to the a greater amount of available heat in its Sabatier reactors, as well as a much lower demand from its electrolyser. This integrated setup could be used for baseload power supply, or as a more renewable adaptation to traditional peaker plants. The flexibility that comes with gas turbine power generation is what would make this integration affective; allowing an operator to accurately adjust the output from the power plant very rapidly with little wastage or deficit. This peaker plant would use what would otherwise be waste heat from renewable energy generation during off peak hours, to produce electricity during peak hours of demand. During low demand hours when excess renewable energy is being generated, the renewable hydrogen could be stored in tanks before it is then released during high demand peak hours when there is a short fall in renewable power generation and fed to the setup. The pre-combustion capture setup could supplement fuel used to generate electricity with the heat generated in the Sabatier reactors during the high demand, peak hours as it converted the excess renewable hydrogen to methane for storage in pipeline networks.

6. PtG - NGCC performance & exergy analysis

6.1. Methodology

6.1.1. Proposed method for flow-sheet simulators

This section will focus on how one can go about collecting the information required from ASPEN plus to perform the evaluation: serving as a methodology section for the exergy analysis. A hurdle to overcome when determining the physical exergy of material streams using the method developed by Hinderink, et al, [1]; is how one can conduct the evaluation for a stream with multiple phases. The best way to go about doing it, is to conduct the evaluation on each phase separately, and this can be achieved by simply separating the said phases out i.e.(for gas liquid phases this can be done using a flash block). When one does this, the expressions for determining the chemical exergy, physical exergy, and exergy of mixing for flow-sheet simulators need to be altered to give equations 70, 69 and 68 respectively. All variables should be in SI units.

Equation 68

$$\dot{E}_{mix} = F\{L([h^l - (\sum x_i\, h_i^l)] - T_0[S^l - (\sum x_i\, S_i^l)]) + V([h^v - (\sum y_i\, h_i^v)] - T_0[S^v - (\sum y_i\, S_i^v)])\}_{T,P}$$

Equation 69

$$\dot{E}_{ph} = F\left[L\left((\sum x_i h_i^l) - T_0(\sum x_i\, S_i^l)\right) + V\left((\sum y_i h_i^v) - T_0(\sum y_i\, S_i^v)\right)\right]_{T,P} - F\left[L\left((\sum x_i h_i^l) - T_0(\sum x_i\, S_i^l)\right) + V\left((\sum y_i\, h_i^v) - T_0(\sum y_i\, S_i^v)\right)\right]_{T_0,P_0}$$

$$\dot{E}_{ch} = F\left[L(\sum x_i Ex_{ch,i}^l) + V(\sum y_i Ex_{ch,i}^v)\right]_{T_0,P_0}$$ **Equation 70**

Where: L represents the stream liquid fraction, V represents the stream vapour fraction, x_i represents the component mole fraction in the liquid phase, y_i represents the component mole fraction in the vapour phase, h^l represents the combined stream enthalpy in the liquid phase, h_i^l represents the component stream enthalpy in the liquid phase, h^v represents the combined stream enthalpy in the vapour phase, h_i^v represents the component stream enthalpy in the vapour phase, S^l represents the combined stream entropy in the liquid phase, S_i^l represents the component stream entropy in the liquid phase, S^v represents the combined stream entropy in the vapour phase, S_i^v represents the component stream entropy in the vapour phase, $Ex_{ch,i}^l$ is

the chemical exergy of component I in the liquid phase and $Ex^{v}_{ch,i}$ is the chemical exergy of component I in the vapour phase.

To determine material stream physical exergy using equation 68, equation 69 and equation 70, the stream of interest would need to be flashed once at stream conditions (T, P), before being mixed and returned to ambient conditions and then flashed again at ambient conditions. Additionally, since the evaluation may be conducted on a cycle; you need to ensure that the process of collecting the data does not interfere with the very cycle results the evaluation is dependent on. So if you alter the flow-sheet by adding a flash block for the sake of collecting data; you need to return the stream to its initial conditions if both the simulation results and by extension the data collected are not to be affected. This can be achieved using a heater block which you can instruct to return the stream to its initial conditions before feeding it back to the external process. If one ignores the net-work or heating required to alter the stream within each of the said units (the flash blocks and the heater blocks); you can then use the setup to collect data from the said stream with confidence since each of the properties that we are evaluating are state variables who's values are not dependent on the path taken by a process.

This can be achieved through ASPEN plus using the flow-sheet shown in figure 59. The flow-sheet is comprised of 6 process units: 2 flash blocks, 2 mixers and 2 heater blocks. Unit operation [FLASH-1] is meant to flash the stream at the process conditions (T, P) before both phases are mixed using unit operation [EX-01]. The stream emanating from mixer [EX-01] is called [EX-02]. [EX-02] is then heated or cooled to reach the environmental state (T_0, P_0) using the heater block [T0,P0], and the resulting stream is called [T0, P0-M]. [T0, P0-M] is then flashed at the environmental state by flash block [FLASH-2] before being mixed by unit operation [EX-03] to make stream [EX-04]. Stream [EX-04] is then returned to the initial stream process conditions (T, P) by heater block $[T, P]$ before being returned to the external process as stream [RETURN]: this is done in order to make sure that the evaluation does not alter the overall process results with each successive run as mentioned before.

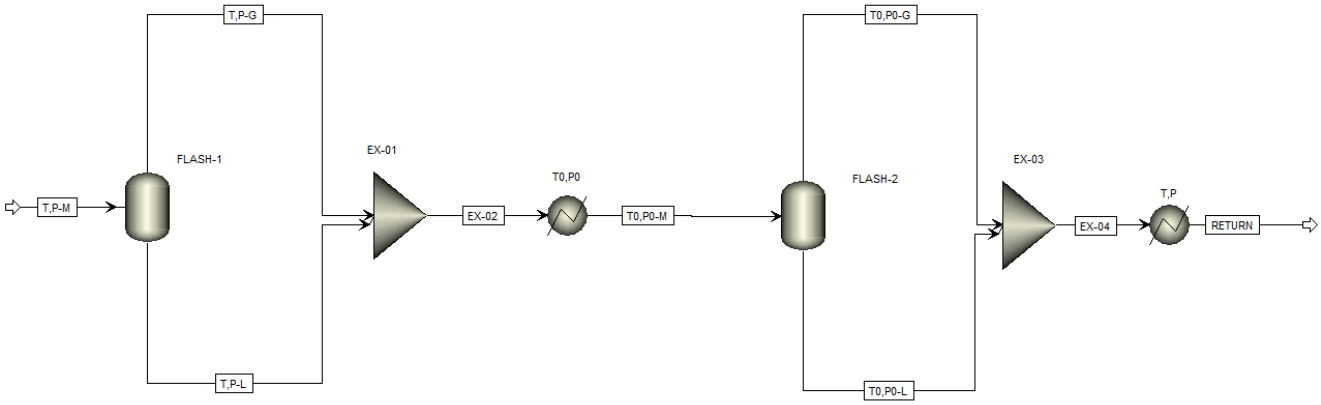


Figure 59: figure used to collect data required for evaluating the exergy content of a stream possessing both liquid and gaseous phases.

Streams [T, P-M] and stream [T0, P0-M] can be used to get the stream molar flow (F), and the liquid (L) and vapour (V) fractions from the stream at conditions (T, P) and (T_0, P_0) respectively. Stream [T, P-G] and stream [T, P-L] are the separate vapor and liquid flows respectively for the stream at conditions (T, P), and stream [T0, P0-G] and stream [T0, P0-L] are the separate vapor and liquid flows respectively for the stream at conditions $(T0, P0)$. These streams can be used to acquire the following properties at conditions (T, P) and $(T0, P0)$: the liquid enthalpy (h^l), liquid entropy (S^l), vapor enthalpy (h^v), vapor entropy (S^v), the mole fractions of each species in the liquid phase (x_i), the mole fractions each species in the vapor phase (y_i), the component enthalpies of each species in the liquid phase $\left(h_i^l\right)$ and vapor phase (h_i^v) and the component entropies of each species in the liquid $\left(S_i^l\right)$ and vapor phases (S_i^v).

The chemical exergy's of all species (in the liquid phase $\left(Ex_{ch,i}^l\right)$ and the vapor phase $\left(Ex_{ch,i}^v\right)$) can be acquired or determined using methods outlined in in the text**.**

The method outlined above can also by extension be used to determine the pressure and thermal exergy components of a stream. The pressure exergy component of a stream is by definition the maximum amount of work one can harness from a reversible isothermal process in which the stream moves form its process conditions of (T, P) to the environmental state pressure of 1 atmosphere at the original stream temperature (T, P_0). The thermal exergy component of stream is the maximum amount of work one can harness from a stream undergoing an isobaric process in which it moves from its initial process conditions (T, P) to the ambient environmental temperature at the original stream pressure (T_0, P). Because both pressure and thermal exergy components involve usable work harnessed as a stream moves to the

environmental state for only the pressure or the temperature; they do not account for the chemical exergy component of the total stream exergy. So from equation 69 and equation 68 comes equation 71 and equation 72 which are expressions for determining the thermal and pressure exergy components of a flow of matter respectively. The expression $\dot{E}_{mix}$ represents the stream exergy of mixing as it was defined in equation 68. All variables should be in SI units.

Equation 71

$$\dot{E}^T = \dot{E}_{mix} + F\left[L\left(\left(\sum x_i h_i^l\right) - T_0\left(\sum x_i\, S_i^l\right)\right) + V\left(\left(\sum y_i h_i^v\right) - T_0\left(\sum y_i\, S_i^v\right)\right)\right]_{T,P} - F\left[L\left(\left(\sum x_i h_i^l\right) - T_0\left(\sum x_i\, S_i^l\right)\right) + V\left(\left(\sum y_i\, h_i^v\right) - T_0\left(\sum y_i\, S_i^v\right)\right)\right]_{T_0,P}$$

Equation 72

$$\dot{E}^P = \dot{E}_{mix} + F\left[L\left(\left(\sum x_i h_i^l\right) - T_0\left(\sum x_i\, S_i^l\right)\right) + V\left(\left(\sum y_i h_i^v\right) - T_0\left(\sum y_i\, S_i^v\right)\right)\right]_{T,P} - F\left[L\left(\left(\sum x_i h_i^l\right) - T_0\left(\sum x_i\, S_i^l\right)\right) + V\left(\left(\sum y_i\, h_i^v\right) - T_0\left(\sum y_i\, S_i^v\right)\right)\right]_{T,P_0}$$

In order to accomplish this using the flow-sheet shown in figure 59; you need to ensure that the process units [T0, P0], and FLASH-2 are set to the environmental state temperature and original stream process pressure (T_0, P) for calculation of the thermal exergy component $\left(\dot{E}^T\right)$. For calculation of the stream pressure exergy component $\left(\dot{E}^P\right)$ you need to ensure that they are set to the environmental state pressure and the original stream temperature (T, P_0).

An example on how the exergy analysis was conducted is provided in appendix E. Appendix E contains the stream results as well a table used to conduct the exergy analysis on stream CC-H2 in the pre-combustion capture NGCC power plant.

6.2. Results

6.2.1. NGCC & NGCC pre-combustion capture power plant exergy analysis results

Table 19 shows the exergy contents of the important streams leading in and out of the system boundaries in the baseline NGCC power plant (see figure 36). Table 20 contains the irreversibilities around the system boundaries within the baseline NGCC power plant as well the total irreversibility around the power plant as a whole. Figure 60 is a pie chart showing the distribution of irreversibilities around this same power plant. The irreversibility around the gas turbine came to 264.97 MW and that around the steam cycle came to 51.20 MW. The gas turbine was responsible for the majority (84%) of the irreversibility within the power plant.

Table 19: Exergy contents of mass and work streams flowing to and from system boundaries within the baseline NGCC power plant depicted in the ASPEN flow-sheet in figure 36.

Stream name	Stream exergy [MW]
AIR	0.00
NG	768.45
G4	232.61
STACK	33.93
W-HPST	28.69
W-MPST	45.78
W-HPST	73.00

Table 20: Irreversibilities around system boundaries steam cycle (SC) and gas turbine (GT) in the baseline NGCC power plant in figure 36.

System boundary	Irreversiblity [MW]
GT	264.97
SC	51.20
Total	316.18

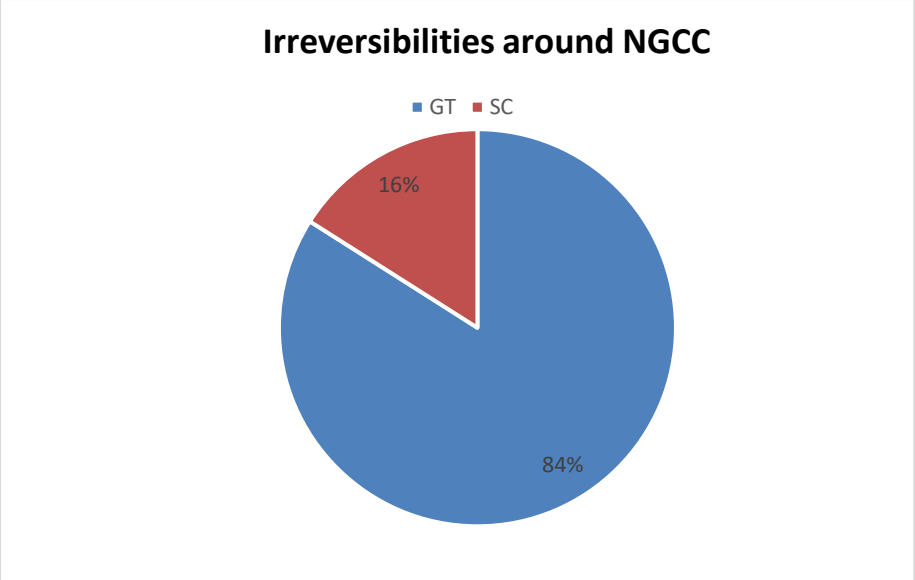


Figure 60: Distribution of irreversibilities in the NGCC power plant in figure 36.

Table 22 shows the exergy contents of the important streams leading in and out of the system boundaries in the pre-combustion capture NGCC power plant (see figure 40). The exergy contents of the heat streams alongside the unit operation names are for the net heat duties for the unit operations. In conducting the assessment, it was assumed that the temperature at which the heat was supplied to unit operation B3 was identical to that of the high pressure and intermediate pressure steam of 550℃. Table 21 contains the irreversibilities around the system boundaries within the pre-combustion capture NGCC power plant as well the total irreversibility around the power plant as a whole. Figure 61 is a pie chart showing the distribution of irreversibilities around this same power plant. Much like the baseline power plant the gas turbine is responsible for contributing to most of the irreversibility around the power plant (78%). The steam cycles contribution of 8% is much lower than it was in the baseline power plant. The exergy content of the intermediate pressure steam extracted for the reforming process (stream STEAM in figure 43) is significant at 35MW, especially when you consider that the exergy content of the flue gasses that report to the Rankine cycle is only 171.95MW, the exergy content of the flue gasses that leave with the stack is 22.41MW and that the exergy destroyed within the steam cycle is 29.65MW. This leaves a total of 119.89MW which is transferred to the working fluid of which 35MW leaves with the extracted intermediate pressure steam in stream STEAM. This amounts to 29.19% of the exergy content transferred and explains why it is that the efficiency penalty that comes with the retrofit is much higher than expected.

Table 21: Irreversibilities around major system boundaries in pre-combustion capture NGCC power plant seen in figure 40.

System boundary	Irreversiblity [MW]
ASU	2.57
GT	293.44
SC	29.65
GHR-ATR-SEWGS	48.65
Total	374.31

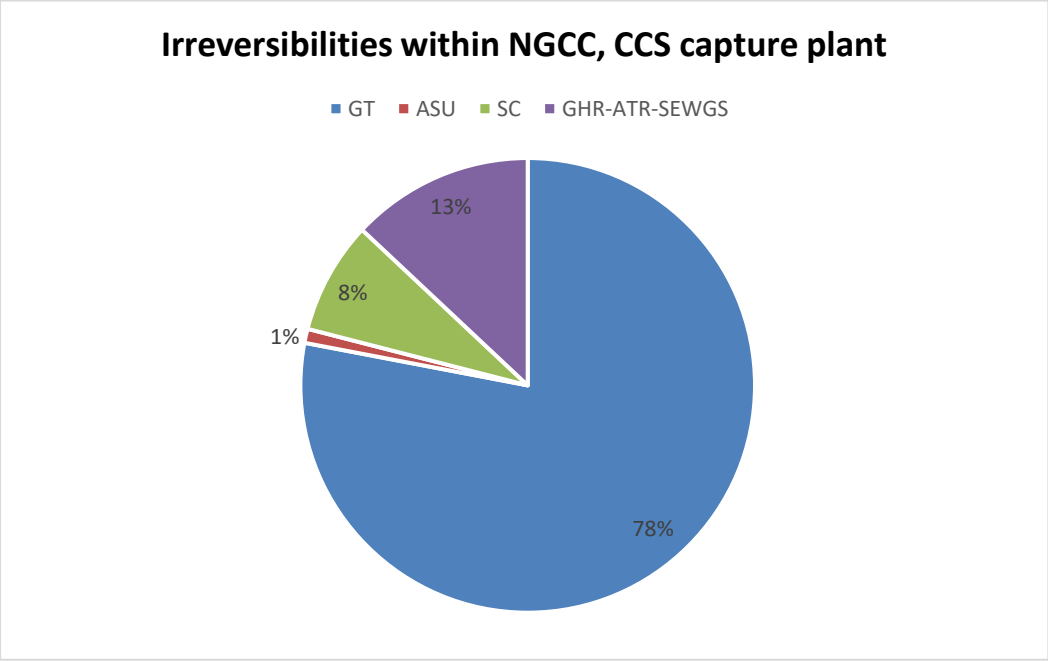


Figure 61: Distribution of irreversibilities in the pre-combustion capture NGCC power plant seen in figure 40.

Table 22: Exergy contents of mass, work and heat streams flowing to and from system boundaries within the pre-combustion capture NGCC power plant seen in figure 40.

Mass stream name	Stream exergy [MW]
P-101	37.16
CC-H2	679.27
AIR	0.00
OP-4	8.67
OP-1	0.97
OP-5	3.82
CC-MIX	633.37
G4	171.95
NG / CH4	768.63
STEAM	35.00
CC-15	0.41
MU-WATER	1.20
STACK	22.41
Work stream name	Stream exergy [MW]
ASU-COMP	16.04
CO2 COMP	13.42
W-GT	214.86
W-HPST	22.42
W-MPST	23.59
W-LPST	40.09
Heat stream unit ope	Stream exergy [MW]
GHR	6.49
REFCOOL	6.36
CO2COOL	0.09
CCU-2	0.00
SEWGS	8.69
GCOOLING	42.29
ATR	5.36
B3	13.70

6.2.2. HTCE PtG performance & exergy analysis results

Table 23 is a table displaying the first law thermodynamic efficiency of the PtG, HTCE retrofit. Please note that the evaluation only takes the H_2 and CH_4 components of the product streams into account and does not consider other products from the process like CO that have calorific value. Also note that what is meant by "LHV of product" or "HHV of product" is that the assessment is made based on the LHV or HHV of the product gasses. Only the LHV efficiencies will be stated; the others can be read off the table. It was assumed that heat was supplied to the heat sinks at a temperature of 586.3K (the temperature of Sabatier reactor PU-02). The LHV efficiency of the electrolyser is 31.49%, and that of the entire PtG process is 42.21% with methane storage and 43.45% without methane storage (heat released not included). The net electrical duty of the electrolyser was found to be 842.27 MW, and the overall net duty of the electrolyser (electrical energy and heat) was found to be 1222.05 MW. When one considers the heat released the value of the efficiency of the entire PtG process becomes 74.31% with methane storage and 76.49% without methane storage (heat released included). Table 25 is a table containing the exergy efficiency of the PtG, HTCE retrofit. The figures in megawatts associated with each stream represent the exergy of the said streams and the streams labelled QEX followed by the name of unit operation represent the flow in exergy of the heat fed to or from a unit operation. The exergy efficiency of the electrolyser is 87.07%, and that of the entire PtG process is 84% with methane storage and 87% without methane storage. This answers research question 4 for the HTCE, PtG setup.

Table 23: First law thermodynamic efficiency of the PtG HTCE retrofit

Eletrolyzer efficiency (first law)	
Eletrolyzer net duty [MW]	842.27
QEX (WATER-HX) [MW]	379.78
Hydrogen flow [kg/sec]	3.20
Efficiency [LHV] % (Only H2 as product)	31.49
Efficiency [HHV] % (Only H2 as product)	37.24
Eletrical efficiency [HHV] % (only H2 as product)	54.03
PtG efficiency (first law)	
Eletrolyzer net duty [MW]	842.27
Q (WATER-HX) [MW]	379.78
Q (PU-01) [MW]	127.83
Q (PU-03) [MW]	-452.18
PTG-COMP (Net work with methane storage) [MW]	58.85
PTG-COMP (Net work without methane storage) [MW]	18.79
CH4 flow [kg/sec]	12.61
Efficiency [LHV of product] % with methane stroage {Heat realeased not included}	42.21
Efficiency [LHV of product] % with methane storage {Heat realeased included}	74.31
Efficiency [LHV of product] % without methane stroage {Heat realeased not included}	43.45
Efficiency [LHV of product] % without methane storage {Heat realeased included}	76.49
Efficiency [HHV of product] % {Heat realeased not included}	46.76
Efficiency [HHV of product] % {Heat realeased included}	78.86

Table 24 shows the irreversibilities around the system boundaries in the PtG, HTCE retrofit and figure 62 shows the proportion the irreversibility's around each system boundary contribute to the overall process irreversibility (system boundary PtG-H in figure 50) for the case with methane storage. Table 22 shows that the irreversibility's around system boundaries PtG-H01, PtG-H02, PtG-H03 in figure 49 sum up to equal the irreversibility around the entire process. This answers research question 7 for the HTCE, PtG setup.

Table 24: Irreversibility's around system boundaries within the PtG HTCE retrofit.

System boundary	Irreversibility [MW]
PtG-H01	145.42
PtG-H02	30.23
PtG-H03	23.64
PtG-H	199.28

Table 25: Exergy efficiency of the PtG HTCE retrofit

Eletrolyzer exergy efficiency (2nd law)	
Eletrolyzer net duty [MW]	842.27
QEX (WATER-HX) [MW]	186.65
P-101 [MW]	37.16
EX-CO2 [MW]	55.17
P-102 [MW]	917.06
P-H2O [MW]	3.26
P-103 [MW]	62.03
Exergy efficiency % (eletrolyzer)	87.07
PtG efficiency (2nd law)	
Eletrolyzer net duty [MW]	842.27
P-101 [MW]	37.16
P-H2O [MW]	3.26
P-103 [MW]	62.03
QEX (WATER-HX) [MW]	186.65
QEX (PU-01) [MW]	62.83
QEX (PU-03) [MW]	222.23
PTG-COMP (with methane storage) (Net work) [MW]	58.85
PTG-COMP (without methane storage) (Net work) [MW]	18.79
REN-CH4 [MW]	762.64
EX-CO2 [MW]	55.17
Exergy efficiency % with methane storgae (PtG)	84
Exergy efficiency % without methane storgae (PtG)	86.80

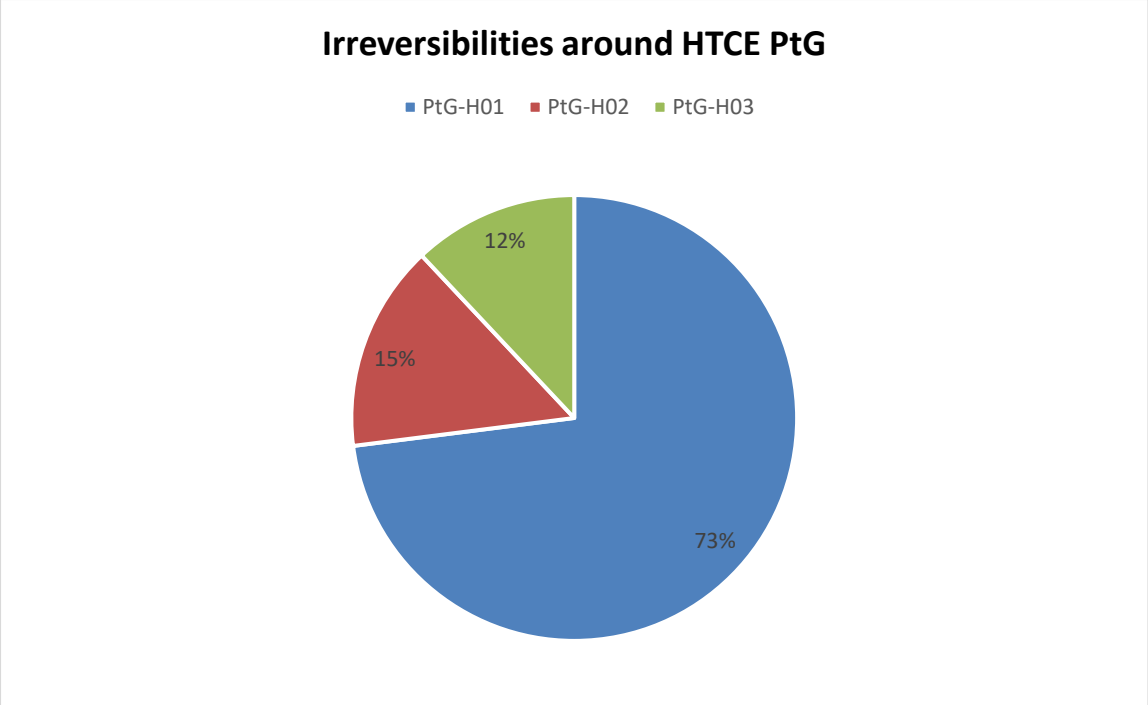


Figure 62: Proportion in irreversibility's around the PtG, HTCE retrofit.

6.2.3. LTE PtG performance & exergy analysis results

Table 27 is a table displaying the first law thermodynamic efficiency of the PtG, LTE retrofit. Please note that what is meant by "LHV of product" or "HHV of product" is that the assessment is made based on the LHV or HHV of the product gasses. It was assumed that heat was supplied to the heat sinks at a temperature of 709,729K (the temperature of Sabatier reactor PU-02). Please note that only the LHV efficiencies will be stated; the others can be read off the table. The LHV efficiency of the LTE electrolyser was found to be 83.52%, much higher than the 31.49% efficiency of the HTCE electrolyser. The net electrical demand of the LTE electrolyser is 1057.09MW and the overall net duty (electrical and heat demand) is 1073.7MW.

The LHV efficiency of the entire PtG process is 87.79% when one takes into consideration the heat released from the process (with methane storage). When you don't take into consideration the heat released from the processes the LHV efficiency of the entire processes is 55.95% with methane storage and 56.34% without methane storage. This 55.95% LHV is similar to that which was made as a rough estimated in the literature of 55%.

Table 28 contains the exergy efficiency of the PtG, LTE retrofit. The figures in megawatts associated with each stream name represent the exergy of the said streams and the streams

labelled QEX followed by the name of unit operation represent the flow in exergy of the heat fed to or from a unit operation. The exergy efficiency of the electrolyser is 83%, which is lower than the exergy efficiency of the HTCE electrolyser which is 94.86%. The exergy efficiency of the entire PtG process is 83.71% with methane storage and 84.30% without methane storage. This answers research question 4 for the LTE, PtG setup.

Table 26 contains the irreversibility's around the LTE, PtG retrofit system boundaries. Much like the HTCE retrofit the electrolyser is responsible for the largest share in irreversibility. Much like the HTCE results the irreversibility's within each subsection add up to equal the irreversibility of the of the entire PtG retrofit as a whole. These results are also displayed in a pie chart (figure 63). This answers research question 7 for the LTE, PtG setup.

Table 26: Irreversibility's around system boundaries within the PtG LTE retrofit.

System boundary	Irreversibility [MW]
PtG-L01	179.44
PtG-L02	2.16
PtG-L03	12.58
PtG-L04	3.75
PtG-L	197.92

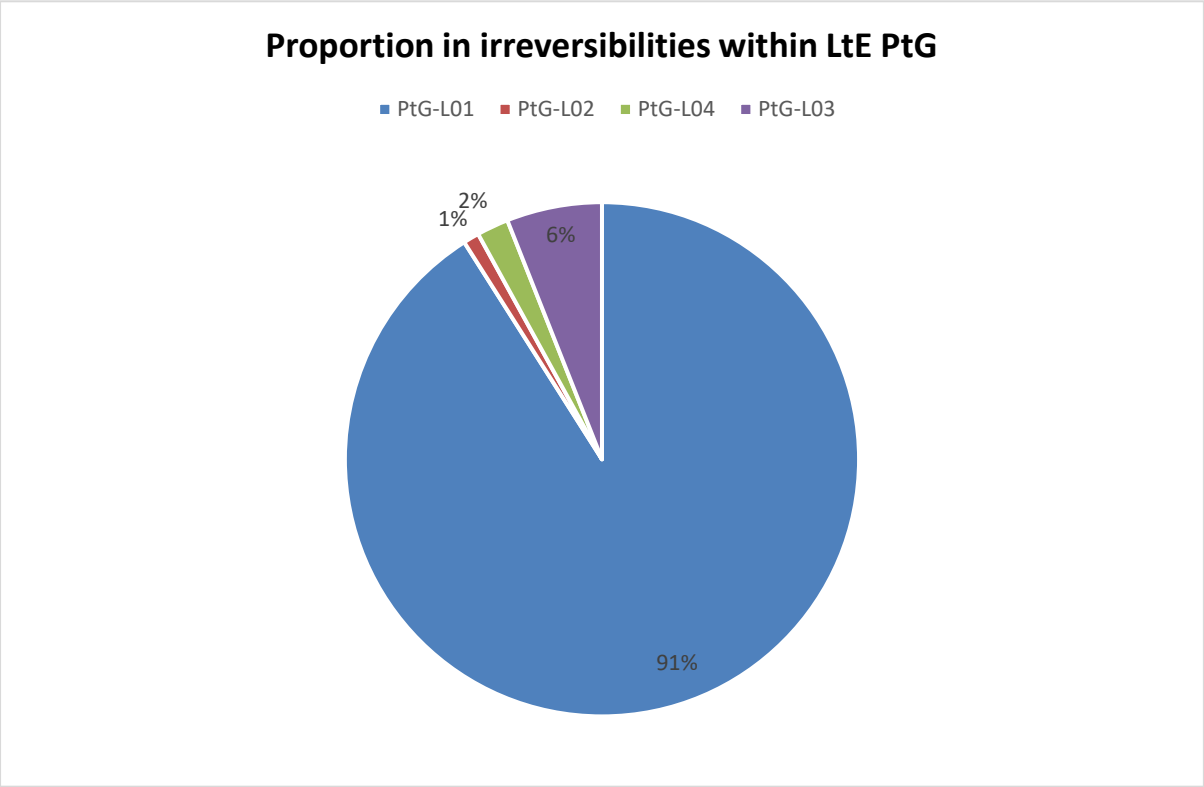
Table 27: First law thermodynamic efficiency of the PtG LTE retrofit

Eletrolyzer efficiency (first law)	
Eletrolyzer net duty [MW]	1057.09
Q (WATER-HX) [MW]	16.62
Hydrogen flow [kg/sec]	7.46
Efficiency [LHV] %	83.52
Efficiency [HHV] %	98.78
PtG efficiency (first law)	
Eletrolyzer net duty [MW]	1057.09
Q (WATER-HX) [MW]	16.62
Q (PU-01) [MW]	95.29
Q (PU-03) [MW]	-315.13
Q (PU-04) [MW]	66.88
Q (PU-06) [MW]	-82.67
PTG-COMP with methane storage (Net work) [MW]	13.49
PTG-COMP without methane storage (Net work) [MW]	4.99
CH4 flow [kg/sec]	14.83
Efficiency [LHV of product] % (Heat realeased included)	87.79
Efficiency [HHV of product] % (Heat realeased included)	93.83
Efficiency with methane storage [LHV of product] % (Heat realeased not included)	55.95
Efficiency without methane storage [LHV of product] % (Heat realeased not included)	56.34

Table 28: Exergy efficiencies of the for the LTE, PtG process

Eletrolyzer exergy efficiency (2nd law)	
Eletrolyzer net duty [MW]	1057.09
QEX (WATER-HX) [MW]	9.64
P-102 [MW]	883.03
P-H2O [MW]	3.33
P-103 [MW]	7.59
Exergy efficiency (eletrolyzer)	83.23
PtG efficiency (2nd law)	
Eletrolyzer net duty [MW]	1057.09
P-101 [MW]	37.16
P-H2O [MW]	3.33
P-103 [MW]	7.59
P-119 [MW]	1.61
QEX (WATER-HX) [MW]	9.64
QEX (PU-01) [MW]	55.26
QEX (PU-03) [MW]	182.75
QEX (PU-04) [MW]	38.78
QEX (PU-06) [MW]	32.54
PTG-COMP with methane storage (Net work) [MW]	13.49
PTG-COMP without methane storage (Net work) [MW]	4.99
REN-CH4 [MW]	792.35
Exergy efficiency with methane storage (PtG)	83.71
Exergy efficiency without methane storage (PtG)	84.30

Figure 63: Proportion in irreversibility's around the PtG, LTE retrofit.



6.3. Discussion

6.3.1. NGCC & NGCC pre-combustion capture power plant exergy analysis results discussion.

The reason that the gas turbine was responsible for the majority (84%) of the irreversibility within the NGCC power plant (see figure 60) is because the gas turbine is where combustion takes place. This is also the reason that this unit contributes to the majority of the irreversibility within the pre-combustion capture power plant (see figure 61). This irreversibility can be reduced by increasing the number of intercooled turbine stages whilst making use of the heat evolved from each stage. The LTE electrolyser efficiency of 83.52% is similar to the efficiency of a polymer exchange membrane (PEM) electrolyser which is anywhere between 65-82% [4]. For the NGCC pre-combustion capture plant, the steam cycles contribution of 8% is much lower than it was in the baseline power plant. This could be attributed to the fact that the fuel lost much of its chemical exergy in the upstream reformer as it was converted form CH_4 to H_2. It could also be attributed to the fact that H_2 is a higher quality fuel than CH_4; with a higher chemical exergy content per mole. This reduces the amount in flue gases that result from combustion which then reducing the losses in exergy associated with viscous dissipation. To reduce the larger than expected losses that come with steam extraction within the setup; it is recommended that the significant amount in exergy contained in the heat evolved from the GHR-ATR-SEWGS be put to use (see table 22).

6.3.2. HTCE PtG performance & exergy analysis results discussion.

The reason the HTCE electrolyser has the highest exergy efficiency within the HTCE PtG setup, is that there are no heat streams that leave its system boundary (PtG-H02); all exergy leaves as stream mass flow exergy that leaves with the electrolyser product. For the same process product specification and electrolyser conversion it is recommended that the electrolyser temperature be lowered to improve efficiency. The electrolyser exergy efficiency is larger than its first law LHV efficiency for a similar reason: when the first law LHV or HHV efficiency of the electrolyser is determined it is not customary to account for the sensible heat that leaves with an undesired product. Something else which contributed to the first law

efficiency of the entire processes being higher than that of the electrolyser, and is likely chiefly responsible for the exergy efficiency of the entire process being slightly higher than that of the electrolyser; is the pressure-based exergy that was carried in the high pressure CO_2 stream. As a recommendation it is suggested that this stream of CO_2 be directed to a gas turbine which should expand it to one atmosphere before feeding it to the methanation unit. This will make better use of the pressure-based exergy carried in with the stream. The greatest amount of irreversibility is around the electrolyser (system boundary PtG-H01) and this can be attributed to the fact that it has to accomplish the energy intensive task of having to split water and in this case has to be raised to a very high temperature of 700℃. As a recommendation it is suggested that the process be conducted at lower temperatures for the same product specifications and electrolyser conversion to reduce irreversibility. The exergy efficiency of the process is very low, especially when considering its low conversion. The large proportion in CO_2 in the product gas needs to be separated out even if it were to be used as a fuel. Additionally, there is not enough hydrogen to completely react with the CO in the methanation unit if the reaction were to go to completion in the electrolyser. As it is the setup fails to produce a product with a high enough mol% in methane for transport and storage in pipeline networks but might be useful as a means of producing a syngas feed for other processes. The results could change if the RWGS reaction were to be taken into consideration. This should be prioritized in future studies.

6.3.3. LTE PtG performance & exergy analysis results discussion

The likely reason that the HTCE electrolysers exergy efficiency is higher than that of the LTE electrolyser efficiency, is the fact stream exergy takes into consideration the available work or exergy contained in the sensible heat leaving with the electrolyser product and the fact that the reaction in the HTCE electrolyser never went to completion. This is backed both by the higher first law LHV efficiency of the LTE electrolyser (though the assessment did not take CO into consideration for the HTCE electrolyser), and the fact that the overall energy consumption of the HTCE electrolyser is higher than that of the LTE electrolyser despite the fact that the overall reaction never went to completion. Often it is claimed that electrolysis conducted at higher temperature is more efficient. However, this is only true if one only takes into consideration the electrical efficiency of the electrolyser, which increases with rising temperature, but only at the expense of the overall efficiency. The electrolyser thermoneutral voltage, which occurs

at ambient conditions, is further evidence that operation at lower temperature is more efficient; since this is considered as the reversible potential. The following simplified analogy illustrates how it is that efficiencies are improved at lower temperatures.

In processes that deal with fluids, irreversibility is reduced the closer a process comes to being an equilibrium or pseudo equilibrium process. Equilibrium processes are closest to being reversible because they do not possess the intensive property gradients associated with non-equilibrium processes. These gradients (whether they be temperature gradients, pressure gradients etc…) will promote the diffusion of matter until a fluid completely equilibrates and becomes uniform. If a change in state is the desired goal, its best to alter all properties apart from the one which needs to be altered. So if you want to alter the temperature you need to make sure that other properties apart from the temperature such as the pressure remain constant as the process takes place to minimize irreversibility and the same applies to the pressure. Hence why it is the thermal exergy component of a fluid stream is determined at constant pressure and the pressure exergy component of a fluid stream is determined at constant temperature. In instances in which a reaction is the desired end (much like in water electrolysis), its best if the fluid properties within the reactor remain constant throughout unit. Very high or low temperature processes are also more likely to have pockets of disequilibrium; creating regions of non-uniformity due the difficulty that comes with heating a fluid evenly in a reaction vessel. Figure 64 illustrates this with a very simple analogy for a fluid undergoing a reaction through a cylindrical reactor or pipe, similar to the HTCE electrolyser in this thesis as fluid moves from point A in the cylinder to point B. The diagram depicts a situation in which reactor temperature is raised using a heating element that runs down the centre of the cylinder pipe. This results in the cylinder through which the fluid flows being cooler at its outer circumference (blue lines), and gradually getting hotter near its centre (yellow, followed by orange, followed by red lines): this causes the fluid to diffuse toward the pipe walls, increasing the length of the path it needs to take as well as the losses associated with movement such as viscous dissipation. The bottom arrow represents the direction the energy contained in the fluid takes from the initial state (point A in red) to the final state (point B in red). As can be seen from the diagram the greater the non-uniformity of the temperature of the fluid; the more the path it needs to take is lengthened and the more the energy contained in the fluid is directed away from the desired path (which is point B in red) which results in work or exergy losses.

This same principal applies if the fluid is going through a change of state (from low to high pressure, or from low to high temperature for example). It explains why it is that increasing the

number stages with intercooling in a compressor is more efficient and reduces irreversibility. It explains why it is that increasing the number of reboilers in a distillation column increase efficiency and reduces irreversibility since the processes has more stages: the fluid is at equilibrium for longer as the operating line sits closer to the equilibrium curve [2], [3]. It also explains why it is that electrochemical conversion is more efficient than a conventional reaction or combustion: electrochemical reactions are able to take place at very constant and moderate state properties.

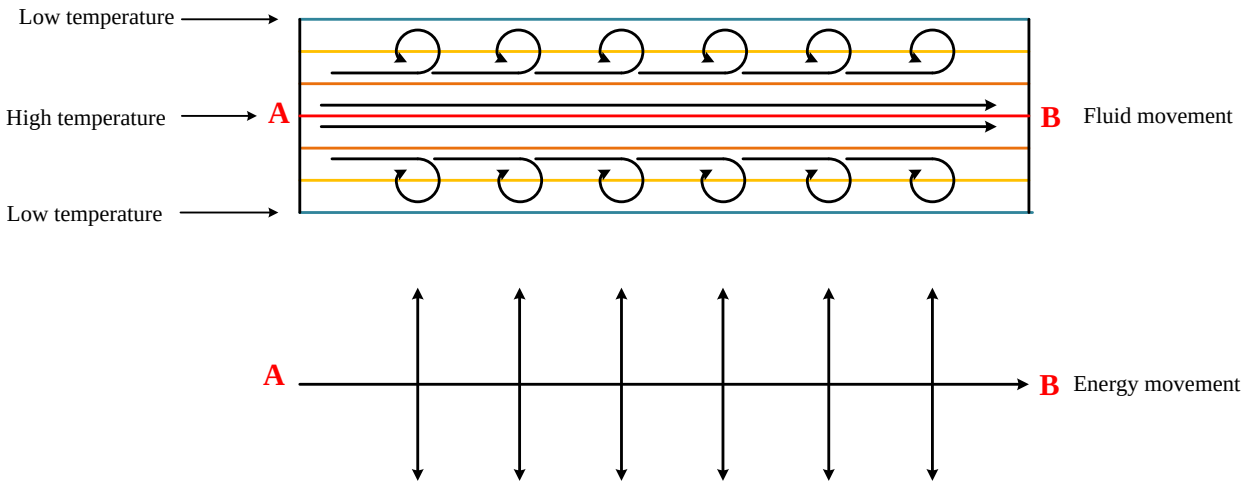


Figure 64: Figure depicting irreversible change of state or a reaction, in a fluid moving through a pipe from point A to point B, with a non-uniform temperature at pipe cross sectional face.

What is more, people often neglect the fuel required to raise the temperature of the electrolyser to temperatures as high as is required in HTCE: so if the calorific content of the fuel burned were to be taken into consideration and not just the resultant heat (which still needs to be transmitted via heat exchange to water); HTCE would be proven to be even less efficient.

The likely reason that the exergy efficiency of the entire LTE PtG process is higher than that of the LTE electrolyser is the pressure based exergy contained in the high pressure carbon dioxide feed coming in with stream P-101 which for LTE was fed to the methanation unit. Much like the LTE PtG processes it is recommended that this stream be fed to a gas turbine that should recover the pressure based exergy of the stream by expanding it to 1 atmosphere of pressure before feeding it to the Methanation unit.

The results from the research we have conducted indicate that LTE PtG should prove competitive with other methods for storing renewable electricity over longer, seasonal time

frames in regions with access to pre-existing natural gas pipeline networks. The high temperature methanation heat offers much opportunity for heat integration. A stumbling block that the process has to overcome is the high cost of water electrolysers, but this should be offset by the fact that a single unit should have limitless capacity; held back only by the volume of gas that can be stored onsite.

References

[1] A. P. Hinderink, F. P. J. M. Kerkhof, A. B. K. Lie, J. De Swaan Arons, and H. J. Van Der Kooi, “Exergy analysis with a flowsheeting simulator - I. Theory; calculating exergies of material streams,” *Chem. Eng. Sci.*, vol. 51, no. 20, pp. 4693–4700, 1996.

[2] T. J. Kotas, *The Exergy Method of Thermal Plant Analysis*. Essex: Butterworths, 1985.

[3] C. Fu and T. Gundersen, “Using exergy analysis to reduce power consumption in air separation units for oxy-combustion processes,” *Energy*, vol. 44, no. 1, pp. 60–68, 2012.

[4] M. Gur, Turgut, “Review of electrical energy storage technologies, materials and systems: challenges and prospects for large-scale grid storage,” *Energy Environ. Sci.*, vol. 11, no. 11, pp. 2696–2767, 2018.

Appendix A

Stream results for baseline NGCC power plant in figure 24

Stream name	AIR	B-02	B-03	G4	NG	STACK
Molar flow [kmol/sec]	22,29307	23,19226	23,22253	23,22253	0,8991922	23,22253
Temperature (K)	298,15	298,1463	1270,78	903,15	298,15	374,6126
Pressure (Pa)	101325	101325	2310000	125199	101325	125199
Vapour fraction (V)	1	1	1	1	1	1
Liquid fraction (L)	0	0	0	0	0	0
Exergy [MW]	0			232,614	768,452	33,933
Mole percentages						
H2O	0,990%	0,952%	8,797%	8,797%	0,000%	8,797%
N2	77,309%	74,391%	74,281%	74,281%	2,060%	74,281%
O2	20,742%	19,938%	11,920%	11,920%	0,000%	11,920%
NO2	0,000%	0,000%	0,001%	0,001%	0,000%	0,001%
NO	0,000%	0,000%	0,026%	0,026%	0,000%	0,026%
H2	0,000%	0,000%	0,000%	0,000%	0,000%	0,000%
CO	0,000%	0,000%	0,000%	0,000%	0,000%	0,000%
CO2	0,037%	0,035%	4,089%	4,089%	0,000%	4,089%
Ar	0,920%	0,884%	0,883%	0,883%	0,000%	0,883%
Ne	0,002%	0,002%	0,002%	0,002%	0,000%	0,002%
He	0,000%	0,000%	0,000%	0,000%	0,000%	0,000%
CH4	0,000%	3,656%	0,000%	0,000%	94,289%	0,000%
C2H6	0,000%	0,079%	0,000%	0,000%	2,030%	0,000%
C3H8	0,000%	0,032%	0,000%	0,000%	0,830%	0,000%
n-Butane	0,000%	0,009%	0,000%	0,000%	0,240%	0,000%
n-Pentane	0,000%	0,002%	0,000%	0,000%	0,060%	0,000%
Hexane	0,000%	0,002%	0,000%	0,000%	0,060%	0,000%
Heptane	0,000%	0,005%	0,000%	0,000%	0,120%	0,000%
Octane	0,000%	0,001%	0,000%	0,000%	0,020%	0,000%
Nonane	0,000%	0,000%	0,000%	0,000%	0,000%	0,000%
i-Butane	0,000%	0,008%	0,000%	0,000%	0,210%	0,000%
neo-Pentane	0,000%	0,000%	0,000%	0,000%	0,010%	0,000%
i-Pentane	0,000%	0,003%	0,000%	0,000%	0,070%	0,000%

Stream results for baseline NGCC power plant in figure 24

Stream name	15	6	8	9	10	12
Molar flow [kmol/sec]	4,490632	4,490632	5,817284	5,817284	4,490632	5,817284
Temperature (K)	823,1499	617,7281	309,1831	384,5532	386,0807	298,15
Pressure (Pa)	12000000	3200000	5000	150000	12000000	101325
Vapour fraction (V)	1	1	0,9064108	0	0	0
Liquid fraction (L)	0	0	0,0935892	1	1	1
Exergy [MW]						
Mole percentages						
H2O	100,000%	100,000%	100,000%	100,000%	100,000%	100,000%
N2	0,000%	0,000%	0,000%	0,000%	0,000%	0,000%
O2	0,000%	0,000%	0,000%	0,000%	0,000%	0,000%
NO2	0,000%	0,000%	0,000%	0,000%	0,000%	0,000%
NO	0,000%	0,000%	0,000%	0,000%	0,000%	0,000%
H2	0,000%	0,000%	0,000%	0,000%	0,000%	0,000%
CO	0,000%	0,000%	0,000%	0,000%	0,000%	0,000%
CO2	0,000%	0,000%	0,000%	0,000%	0,000%	0,000%
Ar	0,000%	0,000%	0,000%	0,000%	0,000%	0,000%
Ne	0,000%	0,000%	0,000%	0,000%	0,000%	0,000%
He	0,000%	0,000%	0,000%	0,000%	0,000%	0,000%
CH4	0,000%	0,000%	0,000%	0,000%	0,000%	0,000%
C2H6	0,000%	0,000%	0,000%	0,000%	0,000%	0,000%
C3H8	0,000%	0,000%	0,000%	0,000%	0,000%	0,000%
n-Butane	0,000%	0,000%	0,000%	0,000%	0,000%	0,000%
n-Pentane	0,000%	0,000%	0,000%	0,000%	0,000%	0,000%
Hexane	0,000%	0,000%	0,000%	0,000%	0,000%	0,000%
Heptane	0,000%	0,000%	0,000%	0,000%	0,000%	0,000%
Octane	0,000%	0,000%	0,000%	0,000%	0,000%	0,000%
Nonane	0,000%	0,000%	0,000%	0,000%	0,000%	0,000%
i-Butane	0,000%	0,000%	0,000%	0,000%	0,000%	0,000%
neo-Pentane	0,000%	0,000%	0,000%	0,000%	0,000%	0,000%
i-Pentane	0,000%	0,000%	0,000%	0,000%	0,000%	0,000%

Stream results for baseline NGCC power plant in figure 24

Stream name	18	39	FW2	FW3	FW4	G4
Molar flow [kmol/sec]	5,017963	5,017963	0,5273301	4,490632	0,7993215	23,22253
Temperature (K)	823,1502	566,7806	384,5532	384,5532	384,5532	903,15
Pressure (Pa)	3200000	500000	150000	150000	150000	125199
Vapour fraction (V)	1	1	0	0	0	1
Liquid fraction (L)	0	0	1	1	1	0
Exergy [MW]						
Mole percentages						
H2O	100,000%	100,000%	100,000%	100,000%	100,000%	8,797%
N2	0,000%	0,000%	0,000%	0,000%	0,000%	74,281%
O2	0,000%	0,000%	0,000%	0,000%	0,000%	11,920%
NO2	0,000%	0,000%	0,000%	0,000%	0,000%	0,001%
NO	0,000%	0,000%	0,000%	0,000%	0,000%	0,026%
H2	0,000%	0,000%	0,000%	0,000%	0,000%	0,000%
CO	0,000%	0,000%	0,000%	0,000%	0,000%	0,000%
CO2	0,000%	0,000%	0,000%	0,000%	0,000%	4,089%
Ar	0,000%	0,000%	0,000%	0,000%	0,000%	0,883%
Ne	0,000%	0,000%	0,000%	0,000%	0,000%	0,002%
He	0,000%	0,000%	0,000%	0,000%	0,000%	0,000%
CH4	0,000%	0,000%	0,000%	0,000%	0,000%	0,000%
C2H6	0,000%	0,000%	0,000%	0,000%	0,000%	0,000%
C3H8	0,000%	0,000%	0,000%	0,000%	0,000%	0,000%
n-Butane	0,000%	0,000%	0,000%	0,000%	0,000%	0,000%
n-Pentane	0,000%	0,000%	0,000%	0,000%	0,000%	0,000%
Hexane	0,000%	0,000%	0,000%	0,000%	0,000%	0,000%
Heptane	0,000%	0,000%	0,000%	0,000%	0,000%	0,000%
Octane	0,000%	0,000%	0,000%	0,000%	0,000%	0,000%
Nonane	0,000%	0,000%	0,000%	0,000%	0,000%	0,000%
i-Butane	0,000%	0,000%	0,000%	0,000%	0,000%	0,000%
neo-Pentane	0,000%	0,000%	0,000%	0,000%	0,000%	0,000%
i-Pentane	0,000%	0,000%	0,000%	0,000%	0,000%	0,000%

Stream results for baseline NGCC power plant in figure 24

Stream name	S33	SS56	SS64	SS68	STACK	13
Molar flow [kmol/sec]	5,817284	0,5273301	0,7993215	5,817284	23,22253	9,193132
Temperature (K)	298,1532	385,2489	384,6229	556,0591	374,6126	903,15
Pressure (Pa)	150000	3200000	500000	500000	125199	125199
Vapour fraction (V)	0	0	0	1	1	1
Liquid fraction (L)	1	1	1	0	0	0
Exergy [MW]						
Mole percentages						
H2O	100,000%	100,000%	100,000%	100,000%	8,797%	8,797%
N2	0,000%	0,000%	0,000%	0,000%	74,281%	74,281%
O2	0,000%	0,000%	0,000%	0,000%	11,920%	11,920%
NO2	0,000%	0,000%	0,000%	0,000%	0,001%	0,001%
NO	0,000%	0,000%	0,000%	0,000%	0,026%	0,026%
H2	0,000%	0,000%	0,000%	0,000%	0,000%	0,000%
CO	0,000%	0,000%	0,000%	0,000%	0,000%	0,000%
CO2	0,000%	0,000%	0,000%	0,000%	4,089%	4,089%
Ar	0,000%	0,000%	0,000%	0,000%	0,883%	0,883%
Ne	0,000%	0,000%	0,000%	0,000%	0,002%	0,002%
He	0,000%	0,000%	0,000%	0,000%	0,000%	0,000%
CH4	0,000%	0,000%	0,000%	0,000%	0,000%	0,000%
C2H6	0,000%	0,000%	0,000%	0,000%	0,000%	0,000%
C3H8	0,000%	0,000%	0,000%	0,000%	0,000%	0,000%
n-Butane	0,000%	0,000%	0,000%	0,000%	0,000%	0,000%
n-Pentane	0,000%	0,000%	0,000%	0,000%	0,000%	0,000%
Hexane	0,000%	0,000%	0,000%	0,000%	0,000%	0,000%
Heptane	0,000%	0,000%	0,000%	0,000%	0,000%	0,000%
Octane	0,000%	0,000%	0,000%	0,000%	0,000%	0,000%
Nonane	0,000%	0,000%	0,000%	0,000%	0,000%	0,000%
i-Butane	0,000%	0,000%	0,000%	0,000%	0,000%	0,000%
neo-Pentane	0,000%	0,000%	0,000%	0,000%	0,000%	0,000%
i-Pentane	0,000%	0,000%	0,000%	0,000%	0,000%	0,000%

Stream results for baseline NGCC power plant in figure 24

Stream name	19	24	29	30	32	33
Molar flow [kmol/sec]	9,193132	22,09789	4,490632	4,490632	14,0294	14,0294
Temperature (K)	766,8472	573,4201	596,8897	596,8909	903,15	789,9459
Pressure (Pa)	125199	125199	12000000	12000000	125199	125199
Vapour fraction (V)	1	1	0	1	1	1
Liquid fraction (L)	0	0	1	0	0	0
Exergy [MW]						
Mole percentages						
H2O	8,797%	8,797%	100,000%	100,000%	8,797%	8,797%
N2	74,281%	74,281%	0,000%	0,000%	74,281%	74,281%
O2	11,920%	11,920%	0,000%	0,000%	11,920%	11,920%
NO2	0,001%	0,001%	0,000%	0,000%	0,001%	0,001%
NO	0,026%	0,026%	0,000%	0,000%	0,026%	0,026%
H2	0,000%	0,000%	0,000%	0,000%	0,000%	0,000%
CO	0,000%	0,000%	0,000%	0,000%	0,000%	0,000%
CO2	4,089%	4,089%	0,000%	0,000%	4,089%	4,089%
Ar	0,883%	0,883%	0,000%	0,000%	0,883%	0,883%
Ne	0,002%	0,002%	0,000%	0,000%	0,002%	0,002%
He	0,000%	0,000%	0,000%	0,000%	0,000%	0,000%
CH4	0,000%	0,000%	0,000%	0,000%	0,000%	0,000%
C2H6	0,000%	0,000%	0,000%	0,000%	0,000%	0,000%
C3H8	0,000%	0,000%	0,000%	0,000%	0,000%	0,000%
n-Butane	0,000%	0,000%	0,000%	0,000%	0,000%	0,000%
n-Pentane	0,000%	0,000%	0,000%	0,000%	0,000%	0,000%
Hexane	0,000%	0,000%	0,000%	0,000%	0,000%	0,000%
Heptane	0,000%	0,000%	0,000%	0,000%	0,000%	0,000%
Octane	0,000%	0,000%	0,000%	0,000%	0,000%	0,000%
Nonane	0,000%	0,000%	0,000%	0,000%	0,000%	0,000%
i-Butane	0,000%	0,000%	0,000%	0,000%	0,000%	0,000%
neo-Pentane	0,000%	0,000%	0,000%	0,000%	0,000%	0,000%
i-Pentane	0,000%	0,000%	0,000%	0,000%	0,000%	0,000%

Stream results for baseline NGCC power plant in figure 24

Stream name	34	35	SS36	SS37	SS38	SS39
Molar flow [kmol/sec]	23,22253	23,22253	22,09789	1,124637	1,124637	23,22253
Temperature (K)	780,8167	649,8039	649,8039	649,8039	599,0869	574,6666
Pressure (Pa)	125199	125199	125199	125199	125199	125199
Vapour fraction (V)	1	1	1	1	1	1
Liquid fraction (L)	0	0	0	0	0	0
Exergy [MW]						
Mole percentages						
H2O	8,797%	8,797%	8,797%	8,797%	8,797%	8,797%
N2	74,281%	74,281%	74,281%	74,281%	74,281%	74,281%
O2	11,920%	11,920%	11,920%	11,920%	11,920%	11,920%
NO2	0,001%	0,001%	0,001%	0,001%	0,001%	0,001%
NO	0,026%	0,026%	0,026%	0,026%	0,026%	0,026%
H2	0,000%	0,000%	0,000%	0,000%	0,000%	0,000%
CO	0,000%	0,000%	0,000%	0,000%	0,000%	0,000%
CO2	4,089%	4,089%	4,089%	4,089%	4,089%	4,089%
Ar	0,883%	0,883%	0,883%	0,883%	0,883%	0,883%
Ne	0,002%	0,002%	0,002%	0,002%	0,002%	0,002%
He	0,000%	0,000%	0,000%	0,000%	0,000%	0,000%
CH4	0,000%	0,000%	0,000%	0,000%	0,000%	0,000%
C2H6	0,000%	0,000%	0,000%	0,000%	0,000%	0,000%
C3H8	0,000%	0,000%	0,000%	0,000%	0,000%	0,000%
n-Butane	0,000%	0,000%	0,000%	0,000%	0,000%	0,000%
n-Pentane	0,000%	0,000%	0,000%	0,000%	0,000%	0,000%
Hexane	0,000%	0,000%	0,000%	0,000%	0,000%	0,000%
Heptane	0,000%	0,000%	0,000%	0,000%	0,000%	0,000%
Octane	0,000%	0,000%	0,000%	0,000%	0,000%	0,000%
Nonane	0,000%	0,000%	0,000%	0,000%	0,000%	0,000%
i-Butane	0,000%	0,000%	0,000%	0,000%	0,000%	0,000%
neo-Pentane	0,000%	0,000%	0,000%	0,000%	0,000%	0,000%
i-Pentane	0,000%	0,000%	0,000%	0,000%	0,000%	0,000%

Stream results for baseline NGCC power plant in figure 24

Stream name	SS40	SS41	SS42	SS43	SS44	SS45
Molar flow [kmol/sec]	23,22253	18,87271	2,819979	1,529839	18,87271	2,819979
Temperature (K)	550,5548	550,5548	550,5548	550,5548	502,7685	502,4186
Pressure (Pa)	125199	125199	125199	125199	125199	125199
Vapour fraction (V)	1	1	1	1	1	1
Liquid fraction (L)	0	0	0	0	0	0
Exergy [MW]						
Mole percentages						
H2O	8,797%	8,797%	8,797%	8,797%	8,797%	8,797%
N2	74,281%	74,281%	74,281%	74,281%	74,281%	74,281%
O2	11,920%	11,920%	11,920%	11,920%	11,920%	11,920%
NO2	0,001%	0,001%	0,001%	0,001%	0,001%	0,001%
NO	0,026%	0,026%	0,026%	0,026%	0,026%	0,026%
H2	0,000%	0,000%	0,000%	0,000%	0,000%	0,000%
CO	0,000%	0,000%	0,000%	0,000%	0,000%	0,000%
CO2	4,089%	4,089%	4,089%	4,089%	4,089%	4,089%
Ar	0,883%	0,883%	0,883%	0,883%	0,883%	0,883%
Ne	0,002%	0,002%	0,002%	0,002%	0,002%	0,002%
He	0,000%	0,000%	0,000%	0,000%	0,000%	0,000%
CH4	0,000%	0,000%	0,000%	0,000%	0,000%	0,000%
C2H6	0,000%	0,000%	0,000%	0,000%	0,000%	0,000%
C3H8	0,000%	0,000%	0,000%	0,000%	0,000%	0,000%
n-Butane	0,000%	0,000%	0,000%	0,000%	0,000%	0,000%
n-Pentane	0,000%	0,000%	0,000%	0,000%	0,000%	0,000%
Hexane	0,000%	0,000%	0,000%	0,000%	0,000%	0,000%
Heptane	0,000%	0,000%	0,000%	0,000%	0,000%	0,000%
Octane	0,000%	0,000%	0,000%	0,000%	0,000%	0,000%
Nonane	0,000%	0,000%	0,000%	0,000%	0,000%	0,000%
i-Butane	0,000%	0,000%	0,000%	0,000%	0,000%	0,000%
neo-Pentane	0,000%	0,000%	0,000%	0,000%	0,000%	0,000%
i-Pentane	0,000%	0,000%	0,000%	0,000%	0,000%	0,000%

Stream results for baseline NGCC power plant in figure 24

Stream name	SS46	SS47	SS48	SS49	SS50	SS51
Molar flow [kmol/sec]	1,529839	23,22253	23,22253	17,56494	2,157284	3,500299
Temperature (K)	513,1937	503,4135	459,2988	459,2988	459,2988	459,2988
Pressure (Pa)	125199	125199	125199	125199	125199	125199
Vapour fraction (V)	1	1	1	1	1	1
Liquid fraction (L)	0	0	0	0	0	0
Exergy [MW]						
Mole percentages						
H2O	8,797%	8,797%	8,797%	8,797%	8,797%	8,797%
N2	74,281%	74,281%	74,281%	74,281%	74,281%	74,281%
O2	11,920%	11,920%	11,920%	11,920%	11,920%	11,920%
NO2	0,001%	0,001%	0,001%	0,001%	0,001%	0,001%
NO	0,026%	0,026%	0,026%	0,026%	0,026%	0,026%
H2	0,000%	0,000%	0,000%	0,000%	0,000%	0,000%
CO	0,000%	0,000%	0,000%	0,000%	0,000%	0,000%
CO2	4,089%	4,089%	4,089%	4,089%	4,089%	4,089%
Ar	0,883%	0,883%	0,883%	0,883%	0,883%	0,883%
Ne	0,002%	0,002%	0,002%	0,002%	0,002%	0,002%
He	0,000%	0,000%	0,000%	0,000%	0,000%	0,000%
CH4	0,000%	0,000%	0,000%	0,000%	0,000%	0,000%
C2H6	0,000%	0,000%	0,000%	0,000%	0,000%	0,000%
C3H8	0,000%	0,000%	0,000%	0,000%	0,000%	0,000%
n-Butane	0,000%	0,000%	0,000%	0,000%	0,000%	0,000%
n-Pentane	0,000%	0,000%	0,000%	0,000%	0,000%	0,000%
Hexane	0,000%	0,000%	0,000%	0,000%	0,000%	0,000%
Heptane	0,000%	0,000%	0,000%	0,000%	0,000%	0,000%
Octane	0,000%	0,000%	0,000%	0,000%	0,000%	0,000%
Nonane	0,000%	0,000%	0,000%	0,000%	0,000%	0,000%
i-Butane	0,000%	0,000%	0,000%	0,000%	0,000%	0,000%
neo-Pentane	0,000%	0,000%	0,000%	0,000%	0,000%	0,000%
i-Pentane	0,000%	0,000%	0,000%	0,000%	0,000%	0,000%

Stream results for baseline NGCC power plant in figure 24

Stream name	SS52	SS53	SS54	SS55	SS57	SS58
Molar flow [kmol/sec]	17,56494	2,157284	3,500299	23,22253	0,5273301	0,5273301
Temperature (K)	433,2145	433,6416	433,0718	433,2327	423,1499	510,2189
Pressure (Pa)	125199	125199	125199	125199	3200000	3200000
Vapour fraction (V)	1	1	1	1	0	0
Liquid fraction (L)	0	0	0	0	1	1
Exergy [MW]						
Mole percentages						
H2O	8,797%	8,797%	8,797%	8,797%	100,000%	100,000%
N2	74,281%	74,281%	74,281%	74,281%	0,000%	0,000%
O2	11,920%	11,920%	11,920%	11,920%	0,000%	0,000%
NO2	0,001%	0,001%	0,001%	0,001%	0,000%	0,000%
NO	0,026%	0,026%	0,026%	0,026%	0,000%	0,000%
H2	0,000%	0,000%	0,000%	0,000%	0,000%	0,000%
CO	0,000%	0,000%	0,000%	0,000%	0,000%	0,000%
CO2	4,089%	4,089%	4,089%	4,089%	0,000%	0,000%
Ar	0,883%	0,883%	0,883%	0,883%	0,000%	0,000%
Ne	0,002%	0,002%	0,002%	0,002%	0,000%	0,000%
He	0,000%	0,000%	0,000%	0,000%	0,000%	0,000%
CH4	0,000%	0,000%	0,000%	0,000%	0,000%	0,000%
C2H6	0,000%	0,000%	0,000%	0,000%	0,000%	0,000%
C3H8	0,000%	0,000%	0,000%	0,000%	0,000%	0,000%
n-Butane	0,000%	0,000%	0,000%	0,000%	0,000%	0,000%
n-Pentane	0,000%	0,000%	0,000%	0,000%	0,000%	0,000%
Hexane	0,000%	0,000%	0,000%	0,000%	0,000%	0,000%
Heptane	0,000%	0,000%	0,000%	0,000%	0,000%	0,000%
Octane	0,000%	0,000%	0,000%	0,000%	0,000%	0,000%
Nonane	0,000%	0,000%	0,000%	0,000%	0,000%	0,000%
i-Butane	0,000%	0,000%	0,000%	0,000%	0,000%	0,000%
neo-Pentane	0,000%	0,000%	0,000%	0,000%	0,000%	0,000%
i-Pentane	0,000%	0,000%	0,000%	0,000%	0,000%	0,000%

Stream results for baseline NGCC power plant in figure 24

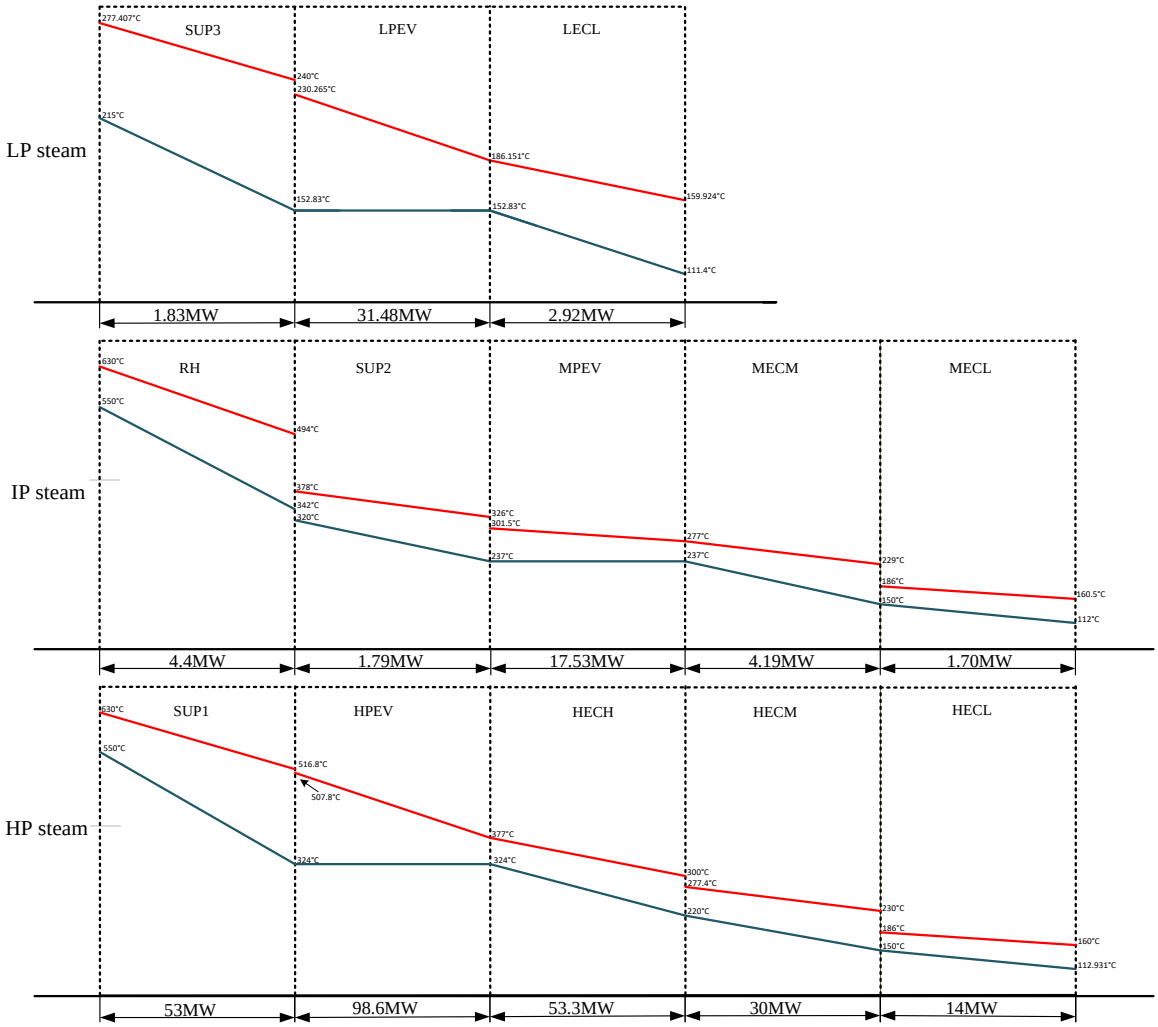
Stream name	SS59	SS60	SS61	SS62	SS63	SS65
Molar flow [kmol/sec]	0,5273301	0,5273301	5,017963	4,490632	4,490632	0,7993215
Temperature (K)	510,3455	593,1495	615,1412	423,1497	493,1497	425,9629
Pressure (Pa)	3200000	3200000	3200000	12000000	12000000	500000
Vapour fraction (V)	0,9979693	1	1	0	0	0
Liquid fraction (L)	0,00203065	0	0	1	1	1
Exergy [MW]						
Mole percentages						
H2O	100,000%	100,000%	100,000%	100,000%	100,000%	100,000%
N2	0,000%	0,000%	0,000%	0,000%	0,000%	0,000%
O2	0,000%	0,000%	0,000%	0,000%	0,000%	0,000%
NO2	0,000%	0,000%	0,000%	0,000%	0,000%	0,000%
NO	0,000%	0,000%	0,000%	0,000%	0,000%	0,000%
H2	0,000%	0,000%	0,000%	0,000%	0,000%	0,000%
CO	0,000%	0,000%	0,000%	0,000%	0,000%	0,000%
CO2	0,000%	0,000%	0,000%	0,000%	0,000%	0,000%
Ar	0,000%	0,000%	0,000%	0,000%	0,000%	0,000%
Ne	0,000%	0,000%	0,000%	0,000%	0,000%	0,000%
He	0,000%	0,000%	0,000%	0,000%	0,000%	0,000%
CH4	0,000%	0,000%	0,000%	0,000%	0,000%	0,000%
C2H6	0,000%	0,000%	0,000%	0,000%	0,000%	0,000%
C3H8	0,000%	0,000%	0,000%	0,000%	0,000%	0,000%
n-Butane	0,000%	0,000%	0,000%	0,000%	0,000%	0,000%
n-Pentane	0,000%	0,000%	0,000%	0,000%	0,000%	0,000%
Hexane	0,000%	0,000%	0,000%	0,000%	0,000%	0,000%
Heptane	0,000%	0,000%	0,000%	0,000%	0,000%	0,000%
Octane	0,000%	0,000%	0,000%	0,000%	0,000%	0,000%
Nonane	0,000%	0,000%	0,000%	0,000%	0,000%	0,000%
i-Butane	0,000%	0,000%	0,000%	0,000%	0,000%	0,000%
neo-Pentane	0,000%	0,000%	0,000%	0,000%	0,000%	0,000%
i-Pentane	0,000%	0,000%	0,000%	0,000%	0,000%	0,000%

Stream results for baseline NGCC power plant in figure 24

Stream name	SS66	SS67
Molar flow [kmol/sec]	0,7993215	0,7993215
Temperature (K)	425,9632	488,1502
Pressure (Pa)	500000	500000
Vapour fraction (V)	1	1
Liquid fraction (L)	0	0
Exergy [MW]		
Mole percentages		
H2O	100,000%	100,000%
N2	0,000%	0,000%
O2	0,000%	0,000%
NO2	0,000%	0,000%
NO	0,000%	0,000%
H2	0,000%	0,000%
CO	0,000%	0,000%
CO2	0,000%	0,000%
Ar	0,000%	0,000%
Ne	0,000%	0,000%
He	0,000%	0,000%
CH4	0,000%	0,000%
C2H6	0,000%	0,000%
C3H8	0,000%	0,000%
n-Butane	0,000%	0,000%
n-Pentane	0,000%	0,000%
Hexane	0,000%	0,000%
Heptane	0,000%	0,000%
Octane	0,000%	0,000%
Nonane	0,000%	0,000%
i-Butane	0,000%	0,000%
neo-Pentane	0,000%	0,000%
i-Pentane	0,000%	0,000%

Turbine work outputs for baseline NGCC power plant in figure 24

Gas turbine	
GT work output [MW]	270,863906
Steam turbine work outputs	
W-HPST [MW]	28,6929864
W-MPST [MW]	45,775729
W-HPST [MW]	73,0078722



Steam cycle heat load and temperature diagram for the baseline NGCC power plant in figure 24. Please note that the diagrams proportions have been intentionally distorted across the horizontal axis for clarity.

Appendix B

Stream results for the pre-combustion capture NGCC power plant in figure 29.

Stream name	AIR	CC-15	CC-H2	CC-MIX	G4	MU-WATER
Molar flow [kmol/sec]	18,11779	0,4407491	2,717355	18,58937	17,25589	1,334573
Temperature (K)	298,15	309,15	575,15	338,9954	903,15	298,15
Pressure (Pa)	101325	1290000	3070000	101325	122435	101325
Vapour fraction (V)	1	0	1	1	1	0
Liquid fraction (L)	0	1	0	0	0	1
Exergy [MW]	0	0,412768304	679,2698357	633,3738772	171,9501952	1,2011157
Mole percentages						
H2O	0,99%	100,00%	0,55%	0,93%	16,65%	100,00%
N2	77,31%	0,00%	0,68%	66,11%	71,16%	0,00%
O2	20,74%	0,00%	0,00%	17,71%	11,10%	0,00%
NO2	0,00%	0,00%	0,00%	0,00%	0,00%	0,00%
NO	0,00%	0,00%	0,00%	0,00%	0,11%	0,00%
H2	0,00%	0,00%	98,13%	14,35%	0,00%	0,00%
CO	0,00%	0,00%	0,00%	0,00%	0,00%	0,00%
CO2	0,04%	0,00%	0,00%	0,03%	0,13%	0,00%
Ar	0,92%	0,00%	0,00%	0,79%	0,85%	0,00%
Ne	0,00%	0,00%	0,00%	0,00%	0,00%	0,00%
He	0,00%	0,00%	0,00%	0,00%	0,00%	0,00%
CH4	0,00%	0,00%	0,63%	0,09%	0,00%	0,00%
C2H6	0,00%	0,00%	0,00%	0,00%	0,00%	0,00%
C3H8	0,00%	0,00%	0,00%	0,00%	0,00%	0,00%
n-Butane	0,00%	0,00%	0,00%	0,00%	0,00%	0,00%
n-Pentane	0,00%	0,00%	0,00%	0,00%	0,00%	0,00%
Hexane	0,00%	0,00%	0,00%	0,00%	0,00%	0,00%
Heptane	0,00%	0,00%	0,00%	0,00%	0,00%	0,00%
Octane	0,00%	0,00%	0,00%	0,00%	0,00%	0,00%
Nonane	0,00%	0,00%	0,00%	0,00%	0,00%	0,00%
i-Butane	0,00%	0,00%	0,00%	0,00%	0,00%	0,00%
neo-Pentane	0,00%	0,00%	0,00%	0,00%	0,00%	0,00%
i-Pentane	0,00%	0,00%	0,00%	0,00%	0,00%	0,00%

Stream results for the pre-combustion capture NGCC power plant in figure 29.

Stream name	NG	OP-1	OP-2	OP-3	OP-4	OP-5
Molar flow [kmol/sec]	0,8991922	15,87201	2,245772	2,245772	1,779947	0,465825
Temperature (K)	298,15	298,15	298,15	298,15	298,15	283,3149
Pressure (Pa)	110000	101325	101325	560000	560000	140000
Vapour fraction (V)	1	1	1	0,9949199	0,9923121	1
Liquid fraction (L)	0	0	0	0,00508011	0,0076879	0
Exergy [MW]	768,634717	0,971805877			8,670034694	3,823765025
Mole percentages						
H2O	0,00%	0,99%	0,99%	0,99%	1,25%	0,00%
N2	2,06%	77,31%	77,31%	77,31%	97,54%	0,00%
O2	0,00%	20,74%	20,74%	20,74%	0,00%	100,00%
NO2	0,00%	0,00%	0,00%	0,00%	0,00%	0,00%
NO	0,00%	0,00%	0,00%	0,00%	0,00%	0,00%
H2	0,00%	0,00%	0,00%	0,00%	0,00%	0,00%
CO	0,00%	0,00%	0,00%	0,00%	0,00%	0,00%
CO2	0,00%	0,04%	0,04%	0,04%	0,05%	0,00%
Ar	0,00%	0,92%	0,92%	0,92%	1,16%	0,00%
Ne	0,00%	0,00%	0,00%	0,00%	0,00%	0,00%
He	0,00%	0,00%	0,00%	0,00%	0,00%	0,00%
CH4	94,29%	0,00%	0,00%	0,00%	0,00%	0,00%
C2H6	2,03%	0,00%	0,00%	0,00%	0,00%	0,00%
C3H8	0,83%	0,00%	0,00%	0,00%	0,00%	0,00%
n-Butane	0,24%	0,00%	0,00%	0,00%	0,00%	0,00%
n-Pentane	0,06%	0,00%	0,00%	0,00%	0,00%	0,00%
Hexane	0,06%	0,00%	0,00%	0,00%	0,00%	0,00%
Heptane	0,12%	0,00%	0,00%	0,00%	0,00%	0,00%
Octane	0,02%	0,00%	0,00%	0,00%	0,00%	0,00%
Nonane	0,00%	0,00%	0,00%	0,00%	0,00%	0,00%
i-Butane	0,21%	0,00%	0,00%	0,00%	0,00%	0,00%
neo-Pentane	0,01%	0,00%	0,00%	0,00%	0,00%	0,00%
i-Pentane	0,07%	0,00%	0,00%	0,00%	0,00%	0,00%

Stream results for the pre-combustion capture NGCC power plant in figure 29.

Stream name	P-101	STACK	STEAM	CC-1	CC-2	CC-3
Molar flow [kmol/sec]	0,9243006	17,25589	1,334573	0,4306247	1,80314	2,175113
Temperature (K)	298,15	342,5613	823,15	823,15	533,9662	939,35
Pressure (Pa)	8000000	122435	3200000	3200000	110000	2500000
Vapour fraction (V)	1	1	1	1	1	1
Liquid fraction (L)	0	0	0	0	0	0
Exergy [MW]	37,16015895	22,41303095	34,99746616			
Mole percentages						
H2O	0,00%	16,65%	100,00%	100,00%	50,13%	27,48%
N2	0,00%	71,16%	0,00%	0,00%	1,03%	0,85%
O2	0,00%	11,10%	0,00%	0,00%	0,00%	0,00%
NO2	0,00%	0,00%	0,00%	0,00%	0,00%	0,00%
NO	0,00%	0,11%	0,00%	0,00%	0,00%	0,00%
H2	0,00%	0,00%	0,00%	0,00%	0,00%	28,39%
CO	4,13%	0,00%	0,00%	0,00%	0,00%	3,02%
CO2	95,87%	0,13%	0,00%	0,00%	0,00%	5,53%
Ar	0,00%	0,85%	0,00%	0,00%	0,00%	0,00%
Ne	0,00%	0,00%	0,00%	0,00%	0,00%	0,00%
He	0,00%	0,00%	0,00%	0,00%	0,00%	0,00%
CH4	0,00%	0,00%	0,00%	0,00%	47,02%	34,72%
C2H6	0,00%	0,00%	0,00%	0,00%	1,01%	0,00%
C3H8	0,00%	0,00%	0,00%	0,00%	0,41%	0,00%
n-Butane	0,00%	0,00%	0,00%	0,00%	0,12%	0,00%
n-Pentane	0,00%	0,00%	0,00%	0,00%	0,03%	0,00%
Hexane	0,00%	0,00%	0,00%	0,00%	0,03%	0,00%
Heptane	0,00%	0,00%	0,00%	0,00%	0,06%	0,00%
Octane	0,00%	0,00%	0,00%	0,00%	0,01%	0,00%
Nonane	0,00%	0,00%	0,00%	0,00%	0,00%	0,00%
i-Butane	0,00%	0,00%	0,00%	0,00%	0,10%	0,00%
neo-Pentane	0,00%	0,00%	0,00%	0,00%	0,00%	0,00%
i-Pentane	0,00%	0,00%	0,00%	0,00%	0,03%	0,00%

Stream results for the pre-combustion capture NGCC power plant in figure 29.

Stream name	CC-4	CC-5	CC-6	CC-7	CC-8	CC-9
Molar flow [kmol/sec]	3,65178	3,65178	3,65178	4,082405	3,641656	0,4407491
Temperature (K)	1323,15	693,15	583,15	701,55	309,15	309,15
Pressure (Pa)	2500000	2500000	2500000	2500000	1290000	1290000
Vapour fraction (V)	1	1	1	1	1	0
Liquid fraction (L)	0	0	0	0	0	1
Exergy [MW]						
Mole percentages						
H2O	20,55%	20,55%	20,55%	11,16%	0,41%	100,00%
N2	0,51%	0,51%	0,51%	0,45%	0,51%	0,00%
O2	0,00%	0,00%	0,00%	0,00%	0,00%	0,00%
NO2	0,00%	0,00%	0,00%	0,00%	0,00%	0,00%
NO	0,00%	0,00%	0,00%	0,00%	0,00%	0,00%
H2	53,16%	53,16%	53,16%	65,32%	73,23%	0,00%
CO	20,91%	20,91%	20,91%	0,94%	1,05%	0,00%
CO2	4,40%	4,40%	4,40%	21,71%	24,33%	0,00%
Ar	0,00%	0,00%	0,00%	0,00%	0,00%	0,00%
Ne	0,00%	0,00%	0,00%	0,00%	0,00%	0,00%
He	0,00%	0,00%	0,00%	0,00%	0,00%	0,00%
CH4	0,47%	0,47%	0,47%	0,42%	0,47%	0,00%
C2H6	0,00%	0,00%	0,00%	0,00%	0,00%	0,00%
C3H8	0,00%	0,00%	0,00%	0,00%	0,00%	0,00%
n-Butane	0,00%	0,00%	0,00%	0,00%	0,00%	0,00%
n-Pentane	0,00%	0,00%	0,00%	0,00%	0,00%	0,00%
Hexane	0,00%	0,00%	0,00%	0,00%	0,00%	0,00%
Heptane	0,00%	0,00%	0,00%	0,00%	0,00%	0,00%
Octane	0,00%	0,00%	0,00%	0,00%	0,00%	0,00%
Nonane	0,00%	0,00%	0,00%	0,00%	0,00%	0,00%
i-Butane	0,00%	0,00%	0,00%	0,00%	0,00%	0,00%
neo-Pentane	0,00%	0,00%	0,00%	0,00%	0,00%	0,00%
i-Pentane	0,00%	0,00%	0,00%	0,00%	0,00%	0,00%

Stream results for the pre-combustion capture NGCC power plant in figure 29.

Stream name	CC-10	CC-11	CC-12	CC-13	CC-14	P-101
Molar flow [kmol/sec]	2,717355	0,9243006	0,9243006	0,9243006	0	0,9243006
Temperature (K)	309,15	289,15	323,15	323,15	0	298,15
Pressure (Pa)	1290000	140000	110000	110000	110000	8000000
Vapour fraction (V)	0,9984374	1	1	1	0	1
Liquid fraction (L)	0,00156265	0	0	0	0	0
Exergy [MW]						
Mole percentages						
H2O	0,55%	0,00%	0,00%	0,00%	0,00%	0,00%
N2	0,68%	0,00%	0,00%	0,00%	0,00%	0,00%
O2	0,00%	0,00%	0,00%	0,00%	0,00%	0,00%
NO2	0,00%	0,00%	0,00%	0,00%	0,00%	0,00%
NO	0,00%	0,00%	0,00%	0,00%	0,00%	0,00%
H2	98,13%	0,00%	0,00%	0,00%	0,00%	0,00%
CO	0,00%	4,13%	4,13%	4,13%	0,00%	4,13%
CO2	0,00%	95,87%	95,87%	95,87%	0,00%	95,87%
Ar	0,00%	0,00%	0,00%	0,00%	0,00%	0,00%
Ne	0,00%	0,00%	0,00%	0,00%	0,00%	0,00%
He	0,00%	0,00%	0,00%	0,00%	0,00%	0,00%
CH4	0,63%	0,00%	0,00%	0,00%	0,00%	0,00%
C2H6	0,00%	0,00%	0,00%	0,00%	0,00%	0,00%
C3H8	0,00%	0,00%	0,00%	0,00%	0,00%	0,00%
n-Butane	0,00%	0,00%	0,00%	0,00%	0,00%	0,00%
n-Pentane	0,00%	0,00%	0,00%	0,00%	0,00%	0,00%
Hexane	0,00%	0,00%	0,00%	0,00%	0,00%	0,00%
Heptane	0,00%	0,00%	0,00%	0,00%	0,00%	0,00%
Octane	0,00%	0,00%	0,00%	0,00%	0,00%	0,00%
Nonane	0,00%	0,00%	0,00%	0,00%	0,00%	0,00%
i-Butane	0,00%	0,00%	0,00%	0,00%	0,00%	0,00%
neo-Pentane	0,00%	0,00%	0,00%	0,00%	0,00%	0,00%
i-Pentane	0,00%	0,00%	0,00%	0,00%	0,00%	0,00%

Stream results for the pre-combustion capture NGCC power plant in figure 29.

Stream name	STEAM	STEAMATR	8	12	15	18
Molar flow [kmol/sec]	1,334573	0,903948	3,210531	3,210531	3,508577	3,920586
Temperature (K)	823,15	823,15	309,1831	298,15	823,15	823,15
Pressure (Pa)	3200000	3200000	5000	101325	12000000	3200000
Vapour fraction (V)	1	1	0,904254	0	1	1
Liquid fraction (L)	0	0	0,095746	1	0	0
Exergy [MW]						
Mole percentages						
H2O	100,00%	100,00%	100,00%	100,00%	100,00%	100,00%
N2	0,00%	0,00%	0,00%	0,00%	0,00%	0,00%
O2	0,00%	0,00%	0,00%	0,00%	0,00%	0,00%
NO2	0,00%	0,00%	0,00%	0,00%	0,00%	0,00%
NO	0,00%	0,00%	0,00%	0,00%	0,00%	0,00%
H2	0,00%	0,00%	0,00%	0,00%	0,00%	0,00%
CO	0,00%	0,00%	0,00%	0,00%	0,00%	0,00%
CO2	0,00%	0,00%	0,00%	0,00%	0,00%	0,00%
Ar	0,00%	0,00%	0,00%	0,00%	0,00%	0,00%
Ne	0,00%	0,00%	0,00%	0,00%	0,00%	0,00%
He	0,00%	0,00%	0,00%	0,00%	0,00%	0,00%
CH4	0,00%	0,00%	0,00%	0,00%	0,00%	0,00%
C2H6	0,00%	0,00%	0,00%	0,00%	0,00%	0,00%
C3H8	0,00%	0,00%	0,00%	0,00%	0,00%	0,00%
n-Butane	0,00%	0,00%	0,00%	0,00%	0,00%	0,00%
n-Pentane	0,00%	0,00%	0,00%	0,00%	0,00%	0,00%
Hexane	0,00%	0,00%	0,00%	0,00%	0,00%	0,00%
Heptane	0,00%	0,00%	0,00%	0,00%	0,00%	0,00%
Octane	0,00%	0,00%	0,00%	0,00%	0,00%	0,00%
Nonane	0,00%	0,00%	0,00%	0,00%	0,00%	0,00%
i-Butane	0,00%	0,00%	0,00%	0,00%	0,00%	0,00%
neo-Pentane	0,00%	0,00%	0,00%	0,00%	0,00%	0,00%
i-Pentane	0,00%	0,00%	0,00%	0,00%	0,00%	0,00%

Stream results for the pre-combustion capture NGCC power plant in figure 29.

Stream name	FW2	FW3	FW4	6	9	10
Molar flow [kmol/sec]	0,4120085	3,508577	0,6245181	3,508577	4,545104	3,508577
Temperature (K)	384,5535	384,5535	384,5535	617,7283	384,5535	386,1594
Pressure (Pa)	150000	150000	150000	3200000	150000	12000000
Vapour fraction (V)	0	0	0	1	0	0
Liquid fraction (L)	1	1	1	0	1	1
Exergy [MW]						
Mole percentages						
H2O	100,00%	100,00%	100,00%	100,00%	100,00%	100,00%
N2	0,00%	0,00%	0,00%	0,00%	0,00%	0,00%
O2	0,00%	0,00%	0,00%	0,00%	0,00%	0,00%
NO2	0,00%	0,00%	0,00%	0,00%	0,00%	0,00%
NO	0,00%	0,00%	0,00%	0,00%	0,00%	0,00%
H2	0,00%	0,00%	0,00%	0,00%	0,00%	0,00%
CO	0,00%	0,00%	0,00%	0,00%	0,00%	0,00%
CO2	0,00%	0,00%	0,00%	0,00%	0,00%	0,00%
Ar	0,00%	0,00%	0,00%	0,00%	0,00%	0,00%
Ne	0,00%	0,00%	0,00%	0,00%	0,00%	0,00%
He	0,00%	0,00%	0,00%	0,00%	0,00%	0,00%
CH4	0,00%	0,00%	0,00%	0,00%	0,00%	0,00%
C2H6	0,00%	0,00%	0,00%	0,00%	0,00%	0,00%
C3H8	0,00%	0,00%	0,00%	0,00%	0,00%	0,00%
n-Butane	0,00%	0,00%	0,00%	0,00%	0,00%	0,00%
n-Pentane	0,00%	0,00%	0,00%	0,00%	0,00%	0,00%
Hexane	0,00%	0,00%	0,00%	0,00%	0,00%	0,00%
Heptane	0,00%	0,00%	0,00%	0,00%	0,00%	0,00%
Octane	0,00%	0,00%	0,00%	0,00%	0,00%	0,00%
Nonane	0,00%	0,00%	0,00%	0,00%	0,00%	0,00%
i-Butane	0,00%	0,00%	0,00%	0,00%	0,00%	0,00%
neo-Pentane	0,00%	0,00%	0,00%	0,00%	0,00%	0,00%
i-Pentane	0,00%	0,00%	0,00%	0,00%	0,00%	0,00%

Stream results for the pre-combustion capture NGCC power plant in figure 29.

Stream name	13	19	24	29	30	32
Molar flow [kmol/sec]	6,831113	6,831113	16,42021	3,508577	3,508577	10,42478
Temperature (K)	903,15	758,7566	553,4286	596,8894	596,8909	903,15
Pressure (Pa)	122435	122435	122435	12000000	12000000	122435
Vapour fraction (V)	1	1	1	0	1	1
Liquid fraction (L)	0	0	0	1	0	0
Exergy [MW]						
Mole percentages						
H2O	16,65%	16,65%	16,65%	100,00%	100,00%	16,65%
N2	71,16%	71,16%	71,16%	0,00%	0,00%	71,16%
O2	11,10%	11,10%	11,10%	0,00%	0,00%	11,10%
NO2	0,00%	0,00%	0,00%	0,00%	0,00%	0,00%
NO	0,11%	0,11%	0,11%	0,00%	0,00%	0,11%
H2	0,00%	0,00%	0,00%	0,00%	0,00%	0,00%
CO	0,00%	0,00%	0,00%	0,00%	0,00%	0,00%
CO2	0,13%	0,13%	0,13%	0,00%	0,00%	0,13%
Ar	0,85%	0,85%	0,85%	0,00%	0,00%	0,85%
Ne	0,00%	0,00%	0,00%	0,00%	0,00%	0,00%
He	0,00%	0,00%	0,00%	0,00%	0,00%	0,00%
CH4	0,00%	0,00%	0,00%	0,00%	0,00%	0,00%
C2H6	0,00%	0,00%	0,00%	0,00%	0,00%	0,00%
C3H8	0,00%	0,00%	0,00%	0,00%	0,00%	0,00%
n-Butane	0,00%	0,00%	0,00%	0,00%	0,00%	0,00%
n-Pentane	0,00%	0,00%	0,00%	0,00%	0,00%	0,00%
Hexane	0,00%	0,00%	0,00%	0,00%	0,00%	0,00%
Heptane	0,00%	0,00%	0,00%	0,00%	0,00%	0,00%
Octane	0,00%	0,00%	0,00%	0,00%	0,00%	0,00%
Nonane	0,00%	0,00%	0,00%	0,00%	0,00%	0,00%
i-Butane	0,00%	0,00%	0,00%	0,00%	0,00%	0,00%
neo-Pentane	0,00%	0,00%	0,00%	0,00%	0,00%	0,00%
i-Pentane	0,00%	0,00%	0,00%	0,00%	0,00%	0,00%

Stream results for the pre-combustion capture NGCC power plant in figure 29.

Stream name	SS36	SS37	SS38	SS39	SS40	SS41
Molar flow [kmol/sec]	16,42021	0,8356809	0,8356809	17,25589	17,25589	14,02369
Temperature (K)	634,5225	634,5225	581,5519	554,7946	529,1344	529,1344
Pressure (Pa)	122435	122435	122435	122435	122435	122435
Vapour fraction (V)	1	1	1	1	1	1
Liquid fraction (L)	0	0	0	0	0	0
Exergy [MW]						
Mole percentages						
H2O	16,65%	16,65%	16,65%	16,65%	16,65%	16,65%
N2	71,16%	71,16%	71,16%	71,16%	71,16%	71,16%
O2	11,10%	11,10%	11,10%	11,10%	11,10%	11,10%
NO2	0,00%	0,00%	0,00%	0,00%	0,00%	0,00%
NO	0,11%	0,11%	0,11%	0,11%	0,11%	0,11%
H2	0,00%	0,00%	0,00%	0,00%	0,00%	0,00%
CO	0,00%	0,00%	0,00%	0,00%	0,00%	0,00%
CO2	0,13%	0,13%	0,13%	0,13%	0,13%	0,13%
Ar	0,85%	0,85%	0,85%	0,85%	0,85%	0,85%
Ne	0,00%	0,00%	0,00%	0,00%	0,00%	0,00%
He	0,00%	0,00%	0,00%	0,00%	0,00%	0,00%
CH4	0,00%	0,00%	0,00%	0,00%	0,00%	0,00%
C2H6	0,00%	0,00%	0,00%	0,00%	0,00%	0,00%
C3H8	0,00%	0,00%	0,00%	0,00%	0,00%	0,00%
n-Butane	0,00%	0,00%	0,00%	0,00%	0,00%	0,00%
n-Pentane	0,00%	0,00%	0,00%	0,00%	0,00%	0,00%
Hexane	0,00%	0,00%	0,00%	0,00%	0,00%	0,00%
Heptane	0,00%	0,00%	0,00%	0,00%	0,00%	0,00%
Octane	0,00%	0,00%	0,00%	0,00%	0,00%	0,00%
Nonane	0,00%	0,00%	0,00%	0,00%	0,00%	0,00%
i-Butane	0,00%	0,00%	0,00%	0,00%	0,00%	0,00%
neo-Pentane	0,00%	0,00%	0,00%	0,00%	0,00%	0,00%
i-Pentane	0,00%	0,00%	0,00%	0,00%	0,00%	0,00%

Stream results for the pre-combustion capture NGCC power plant in figure 29.

Stream name	SS42	SS43	SS44	SS45	SS46	SS47
Molar flow [kmol/sec]	2,095433	1,136773	14,02369	2,095433	1,136773	17,25589
Temperature (K)	529,1344	529,1344	478,3746	478,0446	489,3602	479,0589
Pressure (Pa)	122435	122435	122435	122435	122435	122435
Vapour fraction (V)	1	1	1	1	1	1
Liquid fraction (L)	0	0	0	0	0	0
Exergy [MW]						
Mole percentages						
H2O	16,65%	16,65%	16,65%	16,65%	16,65%	16,65%
N2	71,16%	71,16%	71,16%	71,16%	71,16%	71,16%
O2	11,10%	11,10%	11,10%	11,10%	11,10%	11,10%
NO2	0,00%	0,00%	0,00%	0,00%	0,00%	0,00%
NO	0,11%	0,11%	0,11%	0,11%	0,11%	0,11%
H2	0,00%	0,00%	0,00%	0,00%	0,00%	0,00%
CO	0,00%	0,00%	0,00%	0,00%	0,00%	0,00%
CO2	0,13%	0,13%	0,13%	0,13%	0,13%	0,13%
Ar	0,85%	0,85%	0,85%	0,85%	0,85%	0,85%
Ne	0,00%	0,00%	0,00%	0,00%	0,00%	0,00%
He	0,00%	0,00%	0,00%	0,00%	0,00%	0,00%
CH4	0,00%	0,00%	0,00%	0,00%	0,00%	0,00%
C2H6	0,00%	0,00%	0,00%	0,00%	0,00%	0,00%
C3H8	0,00%	0,00%	0,00%	0,00%	0,00%	0,00%
n-Butane	0,00%	0,00%	0,00%	0,00%	0,00%	0,00%
n-Pentane	0,00%	0,00%	0,00%	0,00%	0,00%	0,00%
Hexane	0,00%	0,00%	0,00%	0,00%	0,00%	0,00%
Heptane	0,00%	0,00%	0,00%	0,00%	0,00%	0,00%
Octane	0,00%	0,00%	0,00%	0,00%	0,00%	0,00%
Nonane	0,00%	0,00%	0,00%	0,00%	0,00%	0,00%
i-Butane	0,00%	0,00%	0,00%	0,00%	0,00%	0,00%
neo-Pentane	0,00%	0,00%	0,00%	0,00%	0,00%	0,00%
i-Pentane	0,00%	0,00%	0,00%	0,00%	0,00%	0,00%

Stream results for the pre-combustion capture NGCC power plant in figure 29.

Stream name	SS48	SS49	SS50	SS51	SS52	SS53
Molar flow [kmol/sec]	17,25589	13,05193	1,603006	2,600957	13,05193	1,603006
Temperature (K)	432,2446	432,2446	432,2446	432,2446	404,5846	405,0374
Pressure (Pa)	122435	122435	122435	122435	122435	122435
Vapour fraction (V)	1	1	1	1	1	1
Liquid fraction (L)	0	0	0	0	0	0
Exergy [MW]						
Mole percentages						
H2O	16,65%	16,65%	16,65%	16,65%	16,65%	16,65%
N2	71,16%	71,16%	71,16%	71,16%	71,16%	71,16%
O2	11,10%	11,10%	11,10%	11,10%	11,10%	11,10%
NO2	0,00%	0,00%	0,00%	0,00%	0,00%	0,00%
NO	0,11%	0,11%	0,11%	0,11%	0,11%	0,11%
H2	0,00%	0,00%	0,00%	0,00%	0,00%	0,00%
CO	0,00%	0,00%	0,00%	0,00%	0,00%	0,00%
CO2	0,13%	0,13%	0,13%	0,13%	0,13%	0,13%
Ar	0,85%	0,85%	0,85%	0,85%	0,85%	0,85%
Ne	0,00%	0,00%	0,00%	0,00%	0,00%	0,00%
He	0,00%	0,00%	0,00%	0,00%	0,00%	0,00%
CH4	0,00%	0,00%	0,00%	0,00%	0,00%	0,00%
C2H6	0,00%	0,00%	0,00%	0,00%	0,00%	0,00%
C3H8	0,00%	0,00%	0,00%	0,00%	0,00%	0,00%
n-Butane	0,00%	0,00%	0,00%	0,00%	0,00%	0,00%
n-Pentane	0,00%	0,00%	0,00%	0,00%	0,00%	0,00%
Hexane	0,00%	0,00%	0,00%	0,00%	0,00%	0,00%
Heptane	0,00%	0,00%	0,00%	0,00%	0,00%	0,00%
Octane	0,00%	0,00%	0,00%	0,00%	0,00%	0,00%
Nonane	0,00%	0,00%	0,00%	0,00%	0,00%	0,00%
i-Butane	0,00%	0,00%	0,00%	0,00%	0,00%	0,00%
neo-Pentane	0,00%	0,00%	0,00%	0,00%	0,00%	0,00%
i-Pentane	0,00%	0,00%	0,00%	0,00%	0,00%	0,00%

Stream results for the pre-combustion capture NGCC power plant in figure 29.

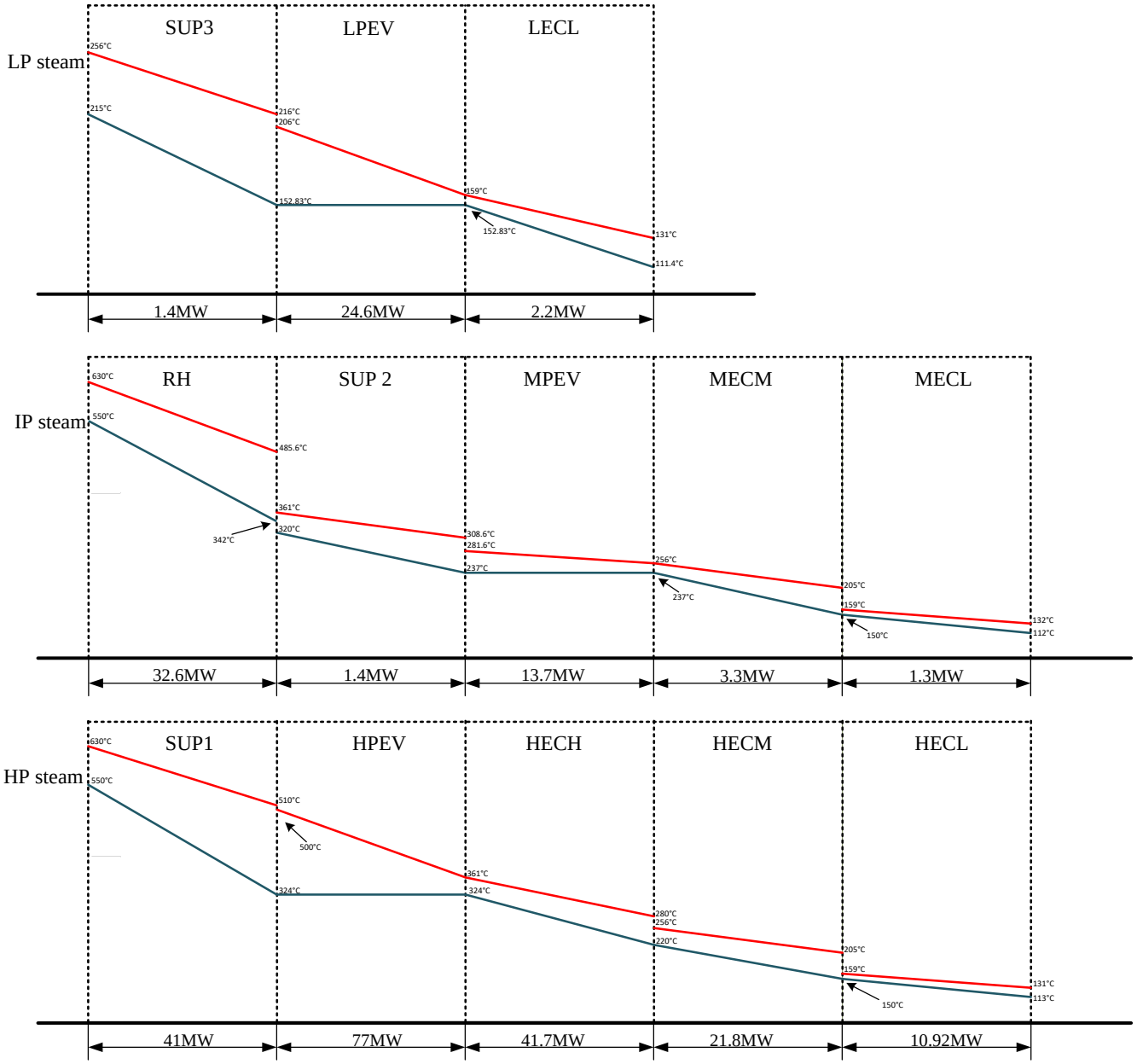
Stream name	SS54	SS55	SS56	SS57	SS58	SS59
Molar flow [kmol/sec]	2,600957	17,25589	0,4120085	0,4120085	0,4120085	0,4120085
Temperature (K)	404,4397	404,6048	385,3128	423,2148	510,2188	510,3455
Pressure (Pa)	122435	122435	3200000	3200000	3200000	3200000
Vapour fraction (V)	1	1	0	0	0	0,9996942
Liquid fraction (L)	0	0	1	1	1	0,000305838
Exergy [MW]						
Mole percentages						
H2O	16,65%	16,65%	100,00%	100,00%	100,00%	100,00%
N2	71,16%	71,16%	0,00%	0,00%	0,00%	0,00%
O2	11,10%	11,10%	0,00%	0,00%	0,00%	0,00%
NO2	0,00%	0,00%	0,00%	0,00%	0,00%	0,00%
NO	0,11%	0,11%	0,00%	0,00%	0,00%	0,00%
H2	0,00%	0,00%	0,00%	0,00%	0,00%	0,00%
CO	0,00%	0,00%	0,00%	0,00%	0,00%	0,00%
CO2	0,13%	0,13%	0,00%	0,00%	0,00%	0,00%
Ar	0,85%	0,85%	0,00%	0,00%	0,00%	0,00%
Ne	0,00%	0,00%	0,00%	0,00%	0,00%	0,00%
He	0,00%	0,00%	0,00%	0,00%	0,00%	0,00%
CH4	0,00%	0,00%	0,00%	0,00%	0,00%	0,00%
C2H6	0,00%	0,00%	0,00%	0,00%	0,00%	0,00%
C3H8	0,00%	0,00%	0,00%	0,00%	0,00%	0,00%
n-Butane	0,00%	0,00%	0,00%	0,00%	0,00%	0,00%
n-Pentane	0,00%	0,00%	0,00%	0,00%	0,00%	0,00%
Hexane	0,00%	0,00%	0,00%	0,00%	0,00%	0,00%
Heptane	0,00%	0,00%	0,00%	0,00%	0,00%	0,00%
Octane	0,00%	0,00%	0,00%	0,00%	0,00%	0,00%
Nonane	0,00%	0,00%	0,00%	0,00%	0,00%	0,00%
i-Butane	0,00%	0,00%	0,00%	0,00%	0,00%	0,00%
neo-Pentane	0,00%	0,00%	0,00%	0,00%	0,00%	0,00%
i-Pentane	0,00%	0,00%	0,00%	0,00%	0,00%	0,00%

Stream results for the pre-combustion capture NGCC power plant in figure 29.

Stream name	SS60	SS61	SS62	SS63	SS64	SS65
Molar flow [kmol/sec]	0,4120085	3,920586	3,508577	3,508577	0,6245181	0,6245181
Temperature (K)	593,1495	615,1413	423,2294	493,2294	384,629	425,963
Pressure (Pa)	3200000	3200000	12000000	12000000	500000	500000
Vapour fraction (V)	1	1	0	0	0	0
Liquid fraction (L)	0	0	1	1	1	1
Exergy [MW]						
Mole percentages						
H2O	100,00%	100,00%	100,00%	100,00%	100,00%	100,00%
N2	0,00%	0,00%	0,00%	0,00%	0,00%	0,00%
O2	0,00%	0,00%	0,00%	0,00%	0,00%	0,00%
NO2	0,00%	0,00%	0,00%	0,00%	0,00%	0,00%
NO	0,00%	0,00%	0,00%	0,00%	0,00%	0,00%
H2	0,00%	0,00%	0,00%	0,00%	0,00%	0,00%
CO	0,00%	0,00%	0,00%	0,00%	0,00%	0,00%
CO2	0,00%	0,00%	0,00%	0,00%	0,00%	0,00%
Ar	0,00%	0,00%	0,00%	0,00%	0,00%	0,00%
Ne	0,00%	0,00%	0,00%	0,00%	0,00%	0,00%
He	0,00%	0,00%	0,00%	0,00%	0,00%	0,00%
CH4	0,00%	0,00%	0,00%	0,00%	0,00%	0,00%
C2H6	0,00%	0,00%	0,00%	0,00%	0,00%	0,00%
C3H8	0,00%	0,00%	0,00%	0,00%	0,00%	0,00%
n-Butane	0,00%	0,00%	0,00%	0,00%	0,00%	0,00%
n-Pentane	0,00%	0,00%	0,00%	0,00%	0,00%	0,00%
Hexane	0,00%	0,00%	0,00%	0,00%	0,00%	0,00%
Heptane	0,00%	0,00%	0,00%	0,00%	0,00%	0,00%
Octane	0,00%	0,00%	0,00%	0,00%	0,00%	0,00%
Nonane	0,00%	0,00%	0,00%	0,00%	0,00%	0,00%
i-Butane	0,00%	0,00%	0,00%	0,00%	0,00%	0,00%
neo-Pentane	0,00%	0,00%	0,00%	0,00%	0,00%	0,00%
i-Pentane	0,00%	0,00%	0,00%	0,00%	0,00%	0,00%

Stream results for the pre-combustion capture NGCC power plant in figure 29.

Stream name	SS66	SS67	SS68	39
Molar flow [kmol/sec]	0,6245181	0,6245181	3,210531	2,586013
Temperature (K)	425,9632	488,1502	551,5941	566,7804
Pressure (Pa)	500000	500000	500000	500000
Vapour fraction (V)	0,9999013	1	1	1
Liquid fraction (L)	9,86778E-05	0	0	0
Exergy [MW]				
Mole percentages				
H2O	100,00%	100,00%	100,00%	100,00%
N2	0,00%	0,00%	0,00%	0,00%
O2	0,00%	0,00%	0,00%	0,00%
NO2	0,00%	0,00%	0,00%	0,00%
NO	0,00%	0,00%	0,00%	0,00%
H2	0,00%	0,00%	0,00%	0,00%
CO	0,00%	0,00%	0,00%	0,00%
CO2	0,00%	0,00%	0,00%	0,00%
Ar	0,00%	0,00%	0,00%	0,00%
Ne	0,00%	0,00%	0,00%	0,00%
He	0,00%	0,00%	0,00%	0,00%
CH4	0,00%	0,00%	0,00%	0,00%
C2H6	0,00%	0,00%	0,00%	0,00%
C3H8	0,00%	0,00%	0,00%	0,00%
n-Butane	0,00%	0,00%	0,00%	0,00%
n-Pentane	0,00%	0,00%	0,00%	0,00%
Hexane	0,00%	0,00%	0,00%	0,00%
Heptane	0,00%	0,00%	0,00%	0,00%
Octane	0,00%	0,00%	0,00%	0,00%
Nonane	0,00%	0,00%	0,00%	0,00%
i-Butane	0,00%	0,00%	0,00%	0,00%
neo-Pentane	0,00%	0,00%	0,00%	0,00%
i-Pentane	0,00%	0,00%	0,00%	0,00%



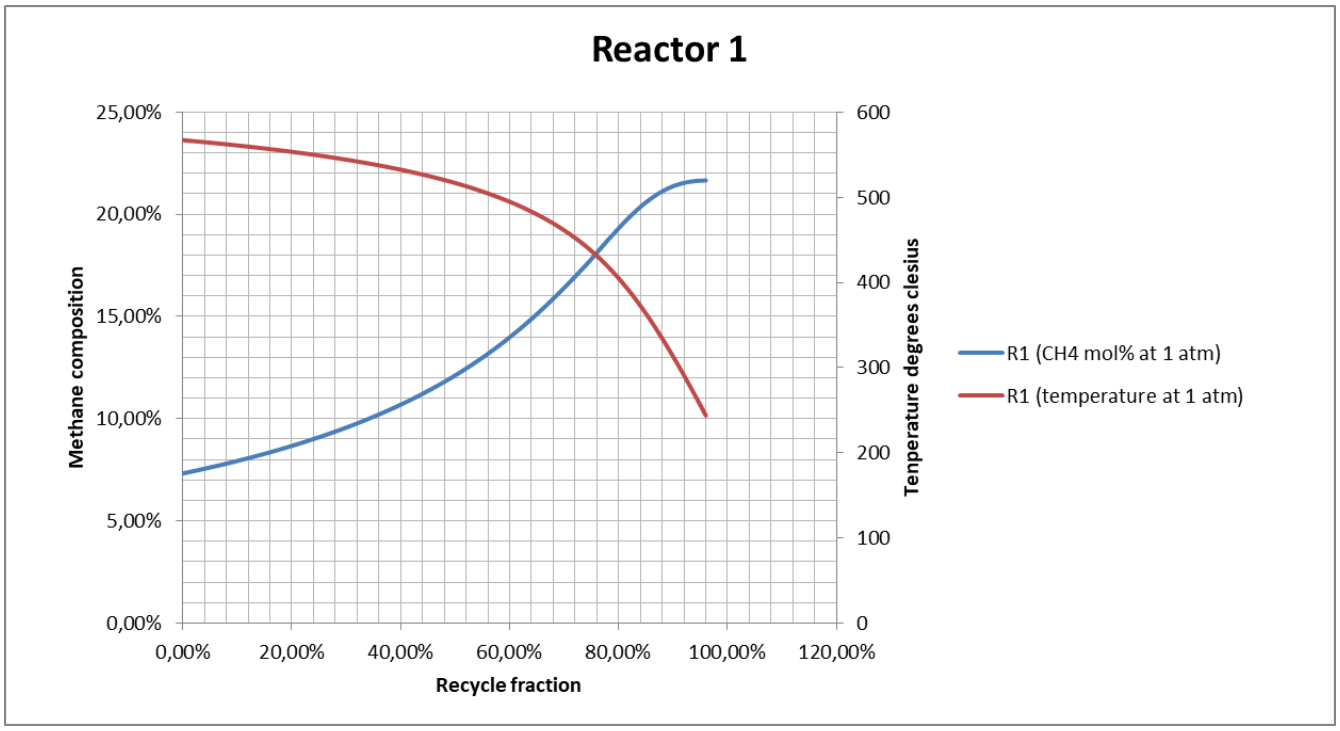
Steam cycle heat load and temperature diagram for the pre-combustion capture NGCC power plant in figure 29. Please note that the diagrams proportions have been intentionally distorted in the horizontal plain for the sake of clarity.

Turbine and compression work outputs for pre-combustion capture NGCC power plant in figure 29.

Gas turbine work ouput	
Work output [MW]	214,855437
Steam cycle work outputs	
W-LPST [MW]	40,0861058
W-MPST [MW]	23,5905708
W-HPST [MW]	22,4181313
CO2 COMP	
Net work [MW]	13,4216371
ASU-COMP	
Net work [MW]	16,0386692

Appendix C

Graph charting recycle fraction against methane composition and reactor temperature for the first Sabatier reactor (unit operation PU-02 in figure 48) in the HTCE PtG retrofit



Recycle fraction against methane composition and reactor temperature for the first Sabatier reactor (unit operation PU-02 in figure 48) in the HTCE PtG retrofit

Sabatier reactor 1 (unit operation PU-02)		
Recycle fraction	CH4 composition	Temperature
0,00%	7,32%	567,12455
0,97%	7,38%	566,566502
1,94%	7,43%	565,999442
2,91%	7,49%	565,423124
3,88%	7,55%	564,83729
4,85%	7,61%	564,241673
5,82%	7,67%	563,635993
6,79%	7,73%	563,019992
7,76%	7,79%	562,393286
8,73%	7,85%	561,755688
9,70%	7,91%	561,106781
10,67%	7,98%	560,446252
11,64%	8,05%	559,773769
12,61%	8,11%	559,088941

13,58%	8,18%	558,391421
14,55%	8,25%	557,680763
15,52%	8,32%	556,956617
16,49%	8,40%	556,218598
17,46%	8,47%	555,465992
18,43%	8,54%	554,698418
19,40%	8,62%	553,915782
20,37%	8,70%	553,117286
21,34%	8,78%	552,302053
22,31%	8,86%	551,469959
23,28%	8,94%	550,620272
24,25%	9,03%	549,752396
25,22%	9,11%	548,865673
26,19%	9,20%	547,959397
27,16%	9,29%	547,032848
28,13%	9,38%	546,085261
29,10%	9,48%	545,115596
30,07%	9,57%	544,124377
31,04%	9,67%	543,108197
32,01%	9,77%	542,06945
32,98%	9,88%	541,00436
33,95%	9,98%	539,913158
34,92%	10,09%	538,792017
35,89%	10,20%	537,646473
36,86%	10,31%	536,469735
37,83%	10,42%	535,258373
38,80%	10,54%	534,020531
39,77%	10,66%	532,745572
40,74%	10,78%	531,435509
41,71%	10,91%	530,089023
42,68%	11,04%	528,703809
43,65%	11,17%	527,277856
44,62%	11,31%	525,809945
45,59%	11,44%	524,293316
46,56%	11,59%	522,73803
47,53%	11,73%	521,130934
48,50%	11,88%	519,472519
49,47%	12,04%	517,760026
50,44%	12,19%	515,990532
51,41%	12,35%	514,161895
52,38%	12,52%	512,271278
53,35%	12,69%	510,312407
54,32%	12,86%	508,28464
55,29%	13,04%	506,18303
56,26%	13,23%	504,006253

57,23%	13,42%	501,742811
58,20%	13,61%	499,392783
59,17%	13,81%	496,947942
60,14%	14,01%	494,408666
61,11%	14,22%	491,763059
62,08%	14,44%	489,005846
63,05%	14,66%	486,129443
64,02%	14,88%	483,128527
64,99%	15,12%	479,99368
65,96%	15,35%	476,713898
66,93%	15,60%	473,281179
67,90%	15,85%	469,68263
68,87%	16,10%	465,911408
69,84%	16,36%	461,951388
70,81%	16,62%	457,788907
71,78%	16,89%	453,412831
72,75%	17,16%	448,794238
73,72%	17,44%	443,941105
74,69%	17,72%	438,810154
75,66%	18,01%	433,332311
76,63%	18,31%	427,558282
77,60%	18,61%	421,465538
78,57%	18,90%	415,054444
79,54%	19,18%	408,295303
80,51%	19,46%	401,195224
81,48%	19,73%	393,734315
82,45%	19,99%	385,913017
83,42%	20,23%	377,724938
84,39%	20,45%	369,174015
85,36%	20,66%	360,285754
86,33%	20,85%	351,013078
87,30%	21,02%	341,422802
88,27%	21,16%	331,525646
89,24%	21,29%	321,331173
90,00%	21,38%	313,152147
90,21%	21,40%	310,863502
91,18%	21,48%	300,144495
92,15%	21,55%	289,200199
93,12%	21,60%	278,048373
94,09%	21,63%	266,728729
95,06%	21,65%	255,257454
96,03%	21,66%	243,656237

Stream result for HTCE PtG flow-sheet in figure 48

Stream name	EX-CO2	P-101	P-102	P-103	P-104	P-105
Molar flow [kmol/sec]	2,739076	0,9243007	5,251215	3,625202	38,35723	38,35723
Temperature (K)	298,15	301,15	973,15	973,15	387,3512	468,15
Pressure (Pa)	15000000	8000000	101325	101325	101325	101325
Vapour fraction (V)	0	1	1	1	1	1
Liquid fraction (L)	1	0	0	0	0	0
Exergy [MW]	55,16499064	37,16015895	917,0615996	62,03		
Mole percentages						
H2O	0,00%	0,00%	0,00%	56,20%	0,20%	0,20%
N2	0,00%	0,00%	0,00%	0,00%	0,00%	0,00%
O2	0,00%	0,00%	0,00%	43,80%	0,00%	0,00%
NO2	0,00%	0,00%	0,00%	0,00%	0,00%	0,00%
NO	0,00%	0,00%	0,00%	0,00%	0,00%	0,00%
H2	0,00%	0,00%	30,24%	0,00%	4,29%	4,29%
CO	0,00%	4,13%	30,96%	0,00%	5,69%	5,69%
CO2	100,00%	95,87%	38,80%	0,00%	71,37%	71,37%
Ar	0,00%	0,00%	0,00%	0,00%	0,00%	0,00%
Ne	0,00%	0,00%	0,00%	0,00%	0,00%	0,00%
He	0,00%	0,00%	0,00%	0,00%	0,00%	0,00%
CH4	0,00%	0,00%	0,00%	0,00%	18,45%	18,45%
C2H6	0,00%	0,00%	0,00%	0,00%	0,00%	0,00%
C3H8	0,00%	0,00%	0,00%	0,00%	0,00%	0,00%
n-Butane	0,00%	0,00%	0,00%	0,00%	0,00%	0,00%
n-Pentane	0,00%	0,00%	0,00%	0,00%	0,00%	0,00%
Hexane	0,00%	0,00%	0,00%	0,00%	0,00%	0,00%
Heptane	0,00%	0,00%	0,00%	0,00%	0,00%	0,00%
Octane	0,00%	0,00%	0,00%	0,00%	0,00%	0,00%
Nonane	0,00%	0,00%	0,00%	0,00%	0,00%	0,00%
i-Butane	0,00%	0,00%	0,00%	0,00%	0,00%	0,00%
neo-Pentane	0,00%	0,00%	0,00%	0,00%	0,00%	0,00%
i-Pentane	0,00%	0,00%	0,00%	0,00%	0,00%	0,00%

Stream result for HTCE PtG flow-sheet in figure 48

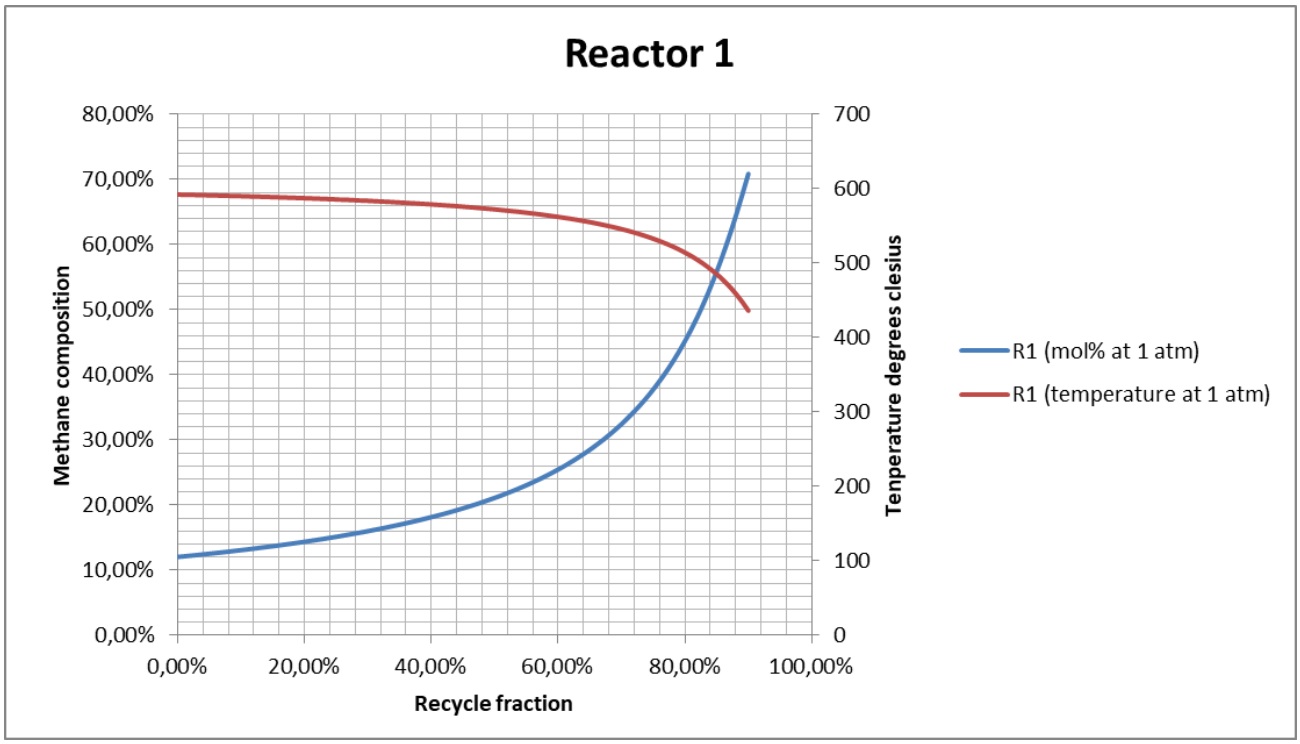
Stream name	P-106	P-108	P-109	P-110	P-119	P-ELIN
Molar flow [kmol/sec]	36,78446	36,78446	33,10601	3,678446	0	7,288578
Temperature (K)	586,3014	298,15	298,15	298,15	0	210,3535
Pressure (Pa)	101325	101325	101325	101325	101325	101325
Vapour fraction (V)	1	1	1	1	0	0,5026217
Liquid fraction (L)	0	0	0	0	0	0,4973784
Exergy [MW]				727,423402		86,28634137
Mole percentages						
H2O	0,23%	0,23%	0,23%	0,23%	0,00%	49,74%
N2	0,00%	0,00%	0,00%	0,00%	0,00%	0,00%
O2	0,00%	0,00%	0,00%	0,00%	0,00%	0,00%
NO2	0,00%	0,00%	0,00%	0,00%	0,00%	0,00%
NO	0,00%	0,00%	0,00%	0,00%	0,00%	0,00%
H2	0,18%	0,18%	0,18%	0,18%	0,00%	0,00%
CO	1,68%	1,68%	1,68%	1,68%	0,00%	0,52%
CO2	76,53%	76,53%	76,53%	76,53%	0,00%	49,74%
Ar	0,00%	0,00%	0,00%	0,00%	0,00%	0,00%
Ne	0,00%	0,00%	0,00%	0,00%	0,00%	0,00%
He	0,00%	0,00%	0,00%	0,00%	0,00%	0,00%
CH4	21,38%	21,38%	21,38%	21,38%	0,00%	0,00%
C2H6	0,00%	0,00%	0,00%	0,00%	0,00%	0,00%
C3H8	0,00%	0,00%	0,00%	0,00%	0,00%	0,00%
n-Butane	0,00%	0,00%	0,00%	0,00%	0,00%	0,00%
n-Pentane	0,00%	0,00%	0,00%	0,00%	0,00%	0,00%
Hexane	0,00%	0,00%	0,00%	0,00%	0,00%	0,00%
Heptane	0,00%	0,00%	0,00%	0,00%	0,00%	0,00%
Octane	0,00%	0,00%	0,00%	0,00%	0,00%	0,00%
Nonane	0,00%	0,00%	0,00%	0,00%	0,00%	0,00%
i-Butane	0,00%	0,00%	0,00%	0,00%	0,00%	0,00%
neo-Pentane	0,00%	0,00%	0,00%	0,00%	0,00%	0,00%
i-Pentane	0,00%	0,00%	0,00%	0,00%	0,00%	0,00%

Stream result for HTCE PtG flow-sheet in figure 48

Stream name	P-H2O	REN-CH4
Molar flow [kmol/sec]	3,625202	3,678446
Temperature (K)	298,15	298,15
Pressure (Pa)	101325	6500000
Vapour fraction (V)	0	1
Liquid fraction (L)	1	0
Exergy [MW]	3,2626818	762,64
Mole percentages		
H2O	100,00%	0,23%
N2	0,00%	0,00%
O2	0,00%	0,00%
NO2	0,00%	0,00%
NO	0,00%	0,00%
H2	0,00%	0,18%
CO	0,00%	1,68%
CO2	0,00%	76,53%
Ar	0,00%	0,00%
Ne	0,00%	0,00%
He	0,00%	0,00%
CH4	0,00%	21,38%
C2H6	0,00%	0,00%
C3H8	0,00%	0,00%
n-Butane	0,00%	0,00%
n-Pentane	0,00%	0,00%
Hexane	0,00%	0,00%
Heptane	0,00%	0,00%
Octane	0,00%	0,00%
Nonane	0,00%	0,00%
i-Butane	0,00%	0,00%
neo-Pentane	0,00%	0,00%
i-Pentane	0,00%	0,00%

Appendix D

Graph charting recycle fraction against methane composition and reactor temperature for the first Sabatier reactor (unit operation PU-02 in figure 53) in the LTE PtG retrofit



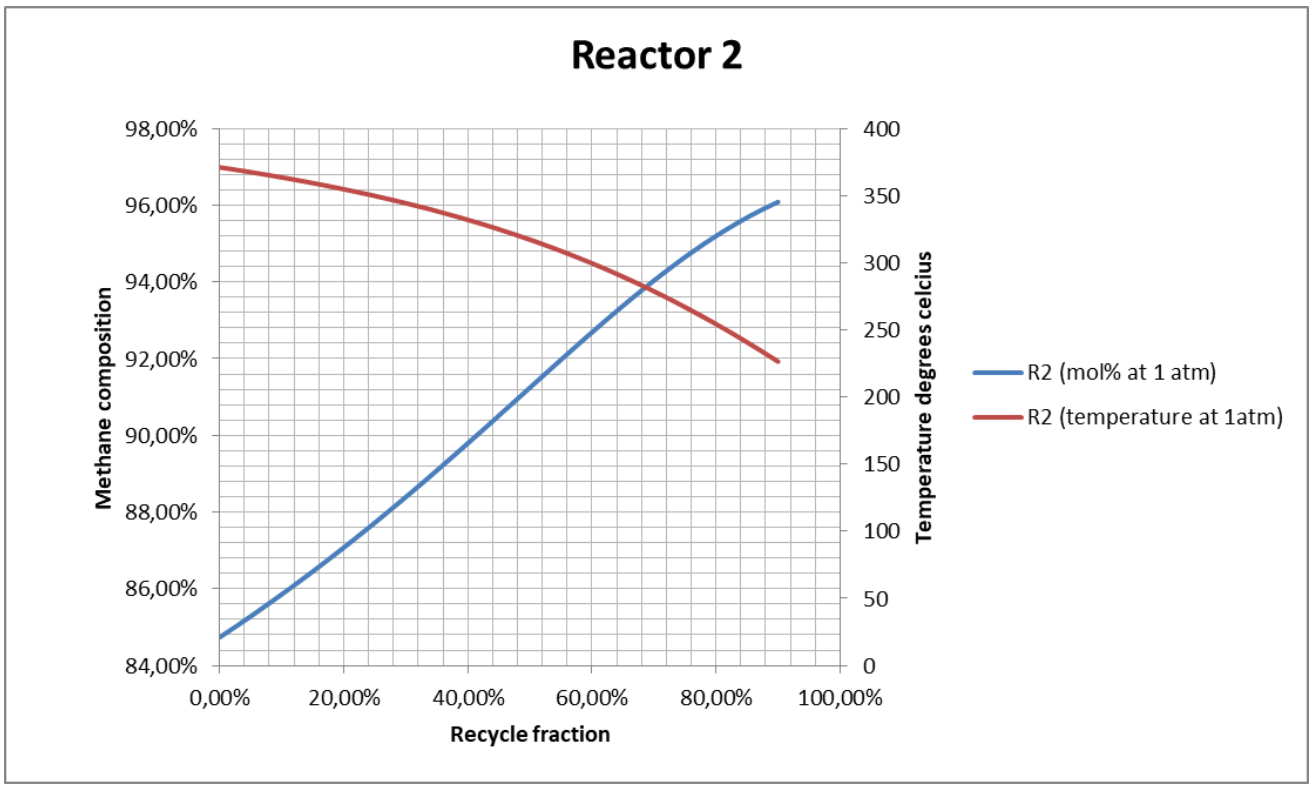
Recycle fraction against methane composition and reactor temperature for the first Sabatier reactor (unit operation PU-02 in figure 53) in the LTE PtG retrofit

Sabatier reactor 1 (unit operation PU-02)		
Recycle fraction	CH4 composition	Temperature
0,00%	12,03%	592,126094
0,91%	12,12%	591,953734
1,82%	12,21%	591,777743
2,73%	12,30%	591,598021
3,64%	12,39%	591,414464
4,55%	12,48%	591,226968
5,45%	12,57%	591,035395
6,36%	12,67%	590,839673
7,27%	12,77%	590,639673
8,18%	12,87%	590,435227
9,09%	12,97%	590,226243
10,00%	13,07%	590,012581
10,91%	13,18%	589,79409
11,82%	13,29%	589,570637

12,73%	13,40%	589,342024
13,64%	13,51%	589,107971
14,55%	13,62%	588,868804
15,45%	13,74%	588,623899
16,36%	13,86%	588,373157
17,27%	13,98%	588,11666
18,18%	14,10%	587,853772
19,09%	14,23%	587,584499
20,00%	14,36%	587,308683
20,91%	14,49%	587,025842
21,82%	14,62%	586,736802
22,73%	14,76%	586,439415
23,64%	14,90%	586,134862
24,55%	15,05%	585,822646
25,45%	15,20%	585,502389
26,36%	15,35%	585,173931
27,27%	15,50%	584,836288
28,18%	15,66%	584,489807
29,09%	15,82%	584,134176
30,00%	15,99%	583,76887
30,91%	16,16%	583,392964
31,82%	16,34%	583,007691
32,73%	16,52%	582,611067
33,64%	16,70%	582,20291
34,55%	16,89%	581,783372
35,45%	17,08%	581,351276
36,36%	17,28%	580,906511
37,27%	17,49%	580,44961
38,18%	17,70%	579,977461
39,09%	17,92%	579,491461
40,00%	18,14%	578,990976
40,91%	18,37%	578,474891
41,82%	18,61%	577,941233
42,73%	18,85%	577,390937
43,64%	19,10%	576,822512
44,55%	19,36%	576,236413
45,45%	19,63%	575,628153
46,36%	19,90%	575,002561
47,27%	20,19%	574,35336
48,18%	20,48%	573,68113
49,09%	20,79%	572,986649
50,00%	21,10%	572,266081
50,91%	21,43%	571,518474
51,82%	21,76%	570,743524
52,73%	22,11%	569,939383

53,64%	22,48%	569,10277
54,55%	22,85%	568,235217
55,45%	23,25%	567,331798
56,36%	23,65%	566,391464
57,27%	24,07%	565,412119
58,18%	24,51%	564,390946
59,09%	24,97%	563,32779
60,00%	25,45%	562,213269
60,91%	25,95%	561,052084
61,82%	26,47%	559,837364
62,73%	27,01%	558,564586
63,64%	27,58%	557,23094
64,55%	28,18%	555,82997
65,45%	28,80%	554,360466
66,36%	29,46%	552,811759
67,27%	30,15%	551,185731
68,18%	30,87%	549,472506
69,09%	31,63%	547,657774
70,00%	32,43%	545,74537
70,91%	33,28%	543,714922
71,82%	34,18%	541,565468
72,73%	35,12%	539,283006
73,64%	36,13%	536,8528
74,55%	37,19%	534,261392
75,45%	38,32%	531,49433
76,36%	39,52%	528,535211
77,27%	40,80%	525,361804
78,18%	42,16%	521,942227
79,09%	43,61%	518,265254
80,00%	45,16%	514,291616
80,91%	46,82%	509,987229
81,78%	48,51%	505,522431
81,82%	48,59%	505,313766
82,73%	50,49%	500,223314
83,64%	52,52%	494,671113
84,55%	54,69%	488,576052
85,45%	57,01%	481,889616
86,36%	59,48%	474,522697
87,27%	62,10%	466,375762
88,18%	64,89%	457,352006
89,09%	67,81%	447,321061
90,00%	70,87%	436,15822

Graph charting recycle fraction against methane composition and reactor temperature for the second Sabatier reactor (unit operation PU-05 in figure 53)



Recycle fraction against methane composition and reactor temperature for the second Sabatier reactor (unit operation PU-05 in figure 53) in the LTE PtG retrofit

Sabatier reactor 2 (unit operation PU-05)		
Recycle fraction	CH4 composition	Temperature
0,00%	84,74%	371,144409
0,91%	84,83%	370,509104
1,82%	84,93%	369,864888
2,73%	85,03%	369,211595
3,64%	85,13%	368,549054
4,55%	85,23%	367,877095
5,45%	85,33%	367,195537
6,36%	85,44%	366,504183
7,27%	85,54%	365,802906
8,18%	85,64%	365,091459
9,09%	85,75%	364,369679
10,00%	85,86%	363,637359
10,91%	85,96%	362,894307
11,82%	86,07%	362,140316
12,73%	86,18%	361,375181
13,64%	86,29%	360,598689

14,55%	86,40%	359,810625
15,45%	86,51%	359,010812
16,36%	86,62%	358,198974
17,27%	86,73%	357,374846
18,18%	86,85%	356,538212
19,09%	86,96%	355,688894
20,00%	87,08%	354,826639
20,91%	87,19%	353,95111
21,82%	87,31%	353,062231
22,73%	87,43%	352,159477
23,64%	87,54%	351,242973
24,55%	87,66%	350,311898
25,45%	87,78%	349,366757
26,36%	87,90%	348,40626
27,27%	88,02%	347,431626
28,18%	88,15%	346,441029
29,09%	88,27%	345,434991
30,00%	88,39%	344,412835
30,91%	88,52%	343,374555
31,82%	88,64%	342,319782
32,73%	88,77%	341,248008
33,64%	88,89%	340,159536
34,55%	89,02%	339,053369
35,45%	89,15%	337,93
36,36%	89,28%	336,787804
37,27%	89,41%	335,627617
38,18%	89,53%	334,448124
39,09%	89,66%	333,250017
40,00%	89,79%	332,032407
40,91%	89,92%	330,795263
41,82%	90,06%	329,538492
42,73%	90,19%	328,260354
43,64%	90,32%	326,9622
44,55%	90,45%	325,642341
45,45%	90,58%	324,30137
46,36%	90,71%	322,938672
47,27%	90,85%	321,553826
48,18%	90,98%	320,146527
49,09%	91,11%	318,716404
50,00%	91,24%	317,263091
50,91%	91,38%	315,786186
51,82%	91,51%	314,285742
52,73%	91,64%	312,760906
53,64%	91,77%	311,211563
54,55%	91,91%	309,63737

55,45%	92,04%	308,037984
56,36%	92,17%	306,413085
57,27%	92,30%	304,762372
58,18%	92,43%	303,08553
59,09%	92,56%	301,382248
60,00%	92,69%	299,652228
60,91%	92,81%	297,89396
61,82%	92,94%	296,109764
62,73%	93,07%	294,297872
63,64%	93,19%	292,458554
64,55%	93,32%	290,591452
65,45%	93,44%	288,694694
66,36%	93,56%	286,769908
67,27%	93,68%	284,816707
68,18%	93,80%	282,833145
69,09%	93,92%	280,823259
70,00%	94,04%	278,782234
70,91%	94,15%	276,712098
71,82%	94,27%	274,612434
72,73%	94,38%	272,482875
73,64%	94,49%	270,32402
74,55%	94,59%	268,134924
75,45%	94,70%	265,916625
76,36%	94,80%	263,667127
77,27%	94,91%	261,388453
78,18%	95,01%	259,080254
79,09%	95,10%	256,7413
80,00%	95,20%	254,372894
80,91%	95,29%	251,974511
81,82%	95,38%	249,546383
82,73%	95,47%	247,08893
83,64%	95,56%	244,601666
84,55%	95,64%	242,084657
85,45%	95,72%	239,539565
86,36%	95,80%	236,964165
87,27%	95,87%	234,360265
88,18%	95,95%	231,727918
89,09%	96,02%	229,066826
90,00%	96,09%	226,377184

Stream result for LTE PtG flow-sheet in figure 53

Stream name	P-101	P-102	P-103	P-104	P-105	P-106
Molar flow [kmol/sec]	0,9243006	3,70057	1,850655	15,63903	15,63903	13,90754
Temperature (K)	298,15	353,15	353,15	294,0529	468,15	709,7293
Pressure (Pa)	8000000	101325	101325	101325	101325	101325
Vapour fraction (V)	1	1	1	1	1	1
Liquid fraction (L)	0	0	0	0	0	0
Exergy [MW]	37,16015895	883,0341478	7,588256216			
Mole percentages						
H2O	0,00%	0,00%	0,02%	1,82%	1,82%	14,28%
N2	0,00%	0,00%	0,00%	0,00%	0,00%	0,00%
O2	0,00%	0,00%	99,98%	0,00%	0,00%	0,00%
NO2	0,00%	0,00%	0,00%	0,00%	0,00%	0,00%
NO	0,00%	0,00%	0,00%	0,00%	0,00%	0,00%
H2	0,00%	100,00%	0,00%	39,08%	39,08%	19,26%
CO	4,13%	0,00%	0,00%	0,70%	0,70%	0,56%
CO2	95,87%	0,00%	0,00%	8,59%	8,59%	3,65%
Ar	0,00%	0,00%	0,00%	0,00%	0,00%	0,00%
Ne	0,00%	0,00%	0,00%	0,00%	0,00%	0,00%
He	0,00%	0,00%	0,00%	0,00%	0,00%	0,00%
CH4	0,00%	0,00%	0,00%	49,82%	49,82%	62,25%
C2H6	0,00%	0,00%	0,00%	0,00%	0,00%	0,00%
C3H8	0,00%	0,00%	0,00%	0,00%	0,00%	0,00%
n-Butane	0,00%	0,00%	0,00%	0,00%	0,00%	0,00%
n-Pentane	0,00%	0,00%	0,00%	0,00%	0,00%	0,00%
Hexane	0,00%	0,00%	0,00%	0,00%	0,00%	0,00%
Heptane	0,00%	0,00%	0,00%	0,00%	0,00%	0,00%
Octane	0,00%	0,00%	0,00%	0,00%	0,00%	0,00%
Nonane	0,00%	0,00%	0,00%	0,00%	0,00%	0,00%
i-Butane	0,00%	0,00%	0,00%	0,00%	0,00%	0,00%
neo-Pentane	0,00%	0,00%	0,00%	0,00%	0,00%	0,00%
i-Pentane	0,00%	0,00%	0,00%	0,00%	0,00%	0,00%

Stream result for LTE PtG flow-sheet in figure 53

Stream name	P-107	P-108	P-109	P-110	P-111	P-112
Molar flow [kmol/sec]	1,669569	12,23797	11,01416	1,223797	10,14527	10,14527
Temperature (K)	298,15	298,15	298,15	298,15	298,1487	468,15
Pressure (Pa)	101325	101325	101325	101325	101325	101325
Vapour fraction (V)	0	1	1	1	0,9999984	1
Liquid fraction (L)	1	0	0	0	1,59338E-06	0
Exergy [MW]	1,50213415			789,0457815		
Mole percentages						
H2O	100,00%	2,58%	2,58%	2,58%	2,58%	2,58%
N2	0,00%	0,00%	0,00%	0,00%	0,00%	0,00%
O2	0,00%	0,00%	0,00%	0,00%	0,00%	0,00%
NO2	0,00%	0,00%	0,00%	0,00%	0,00%	0,00%
NO	0,00%	0,00%	0,00%	0,00%	0,00%	0,00%
H2	0,00%	21,89%	21,89%	21,89%	6,30%	6,30%
CO	0,00%	0,64%	0,64%	0,64%	0,08%	0,08%
CO2	0,00%	4,15%	4,15%	4,15%	0,50%	0,50%
Ar	0,00%	0,00%	0,00%	0,00%	0,00%	0,00%
Ne	0,00%	0,00%	0,00%	0,00%	0,00%	0,00%
He	0,00%	0,00%	0,00%	0,00%	0,00%	0,00%
CH4	0,00%	70,74%	70,74%	70,74%	90,53%	90,53%
C2H6	0,00%	0,00%	0,00%	0,00%	0,00%	0,00%
C3H8	0,00%	0,00%	0,00%	0,00%	0,00%	0,00%
n-Butane	0,00%	0,00%	0,00%	0,00%	0,00%	0,00%
n-Pentane	0,00%	0,00%	0,00%	0,00%	0,00%	0,00%
Hexane	0,00%	0,00%	0,00%	0,00%	0,00%	0,00%
Heptane	0,00%	0,00%	0,00%	0,00%	0,00%	0,00%
Octane	0,00%	0,00%	0,00%	0,00%	0,00%	0,00%
Nonane	0,00%	0,00%	0,00%	0,00%	0,00%	0,00%
i-Butane	0,00%	0,00%	0,00%	0,00%	0,00%	0,00%
neo-Pentane	0,00%	0,00%	0,00%	0,00%	0,00%	0,00%
i-Pentane	0,00%	0,00%	0,00%	0,00%	0,00%	0,00%

Stream result for LTE PtG flow-sheet in figure 53

Stream name	P-113	P-114	P-115	P-116	P-117	P-119
Molar flow [kmol/sec]	10,02807	0,1153165	9,912758	8,921474	0,9912758	1,784885
Temperature (K)	491,6755	298,15	298,15	298,15	298,15	298,15
Pressure (Pa)	101325	101325	101325	101325	101325	101325
Vapour fraction (V)	1	0	1	1	1	0
Liquid fraction (L)	0	1	0	0	0	1
Exergy [MW]		0,103760181			782,6092795	1,605886438
Mole percentages						
H2O	3,71%	100,00%	2,58%	2,58%	2,58%	100,00%
N2	0,00%	0,00%	0,00%	0,00%	0,00%	0,00%
O2	0,00%	0,00%	0,00%	0,00%	0,00%	0,00%
NO2	0,00%	0,00%	0,00%	0,00%	0,00%	0,00%
NO	0,00%	0,00%	0,00%	0,00%	0,00%	0,00%
H2	4,12%	0,00%	4,17%	4,17%	4,17%	0,00%
CO	0,00%	0,00%	0,00%	0,00%	0,00%	0,00%
CO2	0,00%	0,00%	0,00%	0,00%	0,00%	0,00%
Ar	0,00%	0,00%	0,00%	0,00%	0,00%	0,00%
Ne	0,00%	0,00%	0,00%	0,00%	0,00%	0,00%
He	0,00%	0,00%	0,00%	0,00%	0,00%	0,00%
CH4	92,18%	0,00%	93,25%	93,25%	93,25%	0,00%
C2H6	0,00%	0,00%	0,00%	0,00%	0,00%	0,00%
C3H8	0,00%	0,00%	0,00%	0,00%	0,00%	0,00%
n-Butane	0,00%	0,00%	0,00%	0,00%	0,00%	0,00%
n-Pentane	0,00%	0,00%	0,00%	0,00%	0,00%	0,00%
Hexane	0,00%	0,00%	0,00%	0,00%	0,00%	0,00%
Heptane	0,00%	0,00%	0,00%	0,00%	0,00%	0,00%
Octane	0,00%	0,00%	0,00%	0,00%	0,00%	0,00%
Nonane	0,00%	0,00%	0,00%	0,00%	0,00%	0,00%
i-Butane	0,00%	0,00%	0,00%	0,00%	0,00%	0,00%
neo-Pentane	0,00%	0,00%	0,00%	0,00%	0,00%	0,00%
i-Pentane	0,00%	0,00%	0,00%	0,00%	0,00%	0,00%

Stream result for LTE PtG flow-sheet in figure 53

Stream name	P-H2O	REN-NG
Molar flow [kmol/sec]	3,70094	0,9912758
Temperature (K)	298,15	298,15
Pressure (Pa)	101325	6500000
Vapour fraction (V)	0	0,9749666
Liquid fraction (L)	1	0,0250334
Exergy [MW]	3,330846	792,3476809
Mole percentages		
H2O	100,00%	2,58%
N2	0,00%	0,00%
O2	0,00%	0,00%
NO2	0,00%	0,00%
NO	0,00%	0,00%
H2	0,00%	4,17%
CO	0,00%	0,00%
CO2	0,00%	0,00%
Ar	0,00%	0,00%
Ne	0,00%	0,00%
He	0,00%	0,00%
CH4	0,00%	93,25%
C2H6	0,00%	0,00%
C3H8	0,00%	0,00%
n-Butane	0,00%	0,00%
n-Pentane	0,00%	0,00%
Hexane	0,00%	0,00%
Heptane	0,00%	0,00%
Octane	0,00%	0,00%
Nonane	0,00%	0,00%
i-Butane	0,00%	0,00%
neo-Pentane	0,00%	0,00%
i-Pentane	0,00%	0,00%

Appendix E

Table E1 contains the stream results to the hydrogen stream emanating from the GHR-ATR-SEWGS retrofit in figure 40. All the relevant stream properties such as the, total and component stream entropies, the total and component stream enthalpies and the mole fractions of all species can be read off the table at the stream (T, P) and ambient conditions (T_0, T_0) for both the liquid and gaseous phases. Table E2 was the table used to conduct the exergy analysis: included in the table are contributions that each of the species made to the stream physical exergy (Fraction E_{xph}) and the chemical exergy (Fraction E_{xchem}).

Table E1: Table containing the stream results for the hydrogen stream reporting to the combustion turbine in the NGCC pre-combustion capture power plant (stream CC-H2 in figure 40).

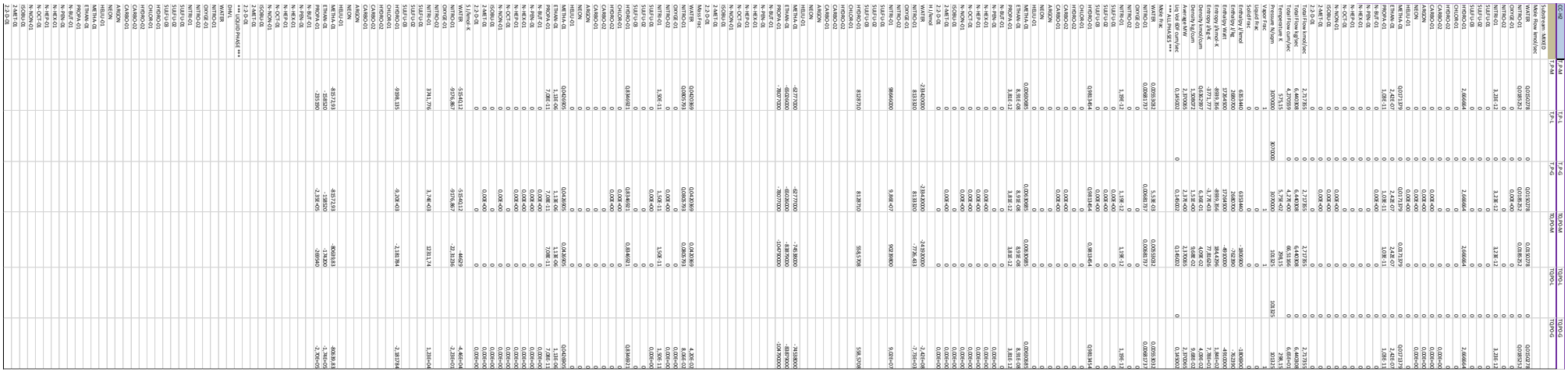


Table E2: Table used to conduct the exergy analysis on the hydrogen stream reporting to the combustion turbine in the NGCC pre-combustion capture power plant (stream CC-H2 in figure 40).

	CC-H2	T,P					CC-H2	T0,P0					
	F(Kmol/s) =	2,717355					F(Kmol/s) =	2,717355					
	Liquid			Vapour			Liquid			Vapour			
	Xi	hliq (J/Kmol)	Sliq(J/Kmol.K)	Yi	hvap(J/Kmol)	svap(J/Kmol.K)	Xi	hliq (J/Kmol)	Sliq(J/Kmol.K)	Yi	hvap(J/Kmol)	svap(J/Kmol.K)	Species
H2O	0	0	0	5,53E-03	-233420000	-51540,12	0	0	0	0,00553032	-2,42E+08	-4,46E+04	H2O
N2	0	0	0	6,82E-03	8133320	-9176,867	0	0	0	0,00681737	-7,73E+03	-2,23E+01	N2
O2	0	0	0	0,00E+00	0	0	0	0	0	0	0,00E+00	0,00E+00	O2
NO2	0	0	0	0,00E+00	0	0	0	0	0	0	0,00E+00	0,00E+00	NO2
NO	0	0	0	1,19E-12	98646000	3741,776	0	0	0	1,1885E-12	9,02E+07	1,23E+04	NO
S	0	0	0	0,00E+00	0	0	0	0	0	0	0,00E+00	0,00E+00	S
SO2	0	0	0	0,00E+00	0	0	0	0	0	0	0,00E+00	0,00E+00	SO2
SO3	0	0	0	0,00E+00	0	0	0	0	0	0	0,00E+00	0,00E+00	SO3
H2	0	0	0	9,81E-01	8128710	-9198,135	0	0	0	0,9813454	5,59E+02	-2,18E+00	H2
CL2	0	0	0	0,00E+00	0	0	0	0	0	0	0,00E+00	0,00E+00	CL2
HCL	0	0	0	0,00E+00	0	0	0	0	0	0	0,00E+00	0,00E+00	HCL
CO	0	0	0	0,00E+00	0	0	0	0	0	0	0,00E+00	0,00E+00	CO
CO2	0	0	0	0,00E+00	0	0	0	0	0	0	0,00E+00	0,00E+00	CO2
Ar	0	0	0	0,00E+00	0	0	0	0	0	0	0,00E+00	0,00E+00	Ar
Ne	0	0	0	0,00E+00	0	0	0	0	0	0	0,00E+00	0,00E+00	Ne
He	0	0	0	0,00E+00	0	0	0	0	0	0	0,00E+00	0,00E+00	He
CH4	0	0	0	6,31E-03	-62777000	-81572,93	0	0	0	0,00630685	-7,45E+07	-8,06E+04	CH4
Ethane	0	0	0	8,91E-08	-65026000	-158520	0	0	0	8,911E-08	-8,39E+07	-1,74E+05	Ethane
Propane	0	0	0	3,81E-12	-78077000	-235190	0	0	0	3,8079E-12	-1,05E+08	-2,70E+05	Propane
N-butane	0	0	0	0,00E+00	0	0	0	0	0	0	0,00E+00	0,00E+00	N-butane
N-pentane	0	0	0	0,00E+00	0	0	0	0	0	0	0,00E+00	0,00E+00	N-pentane
N-hexane	0	0	0	0,00E+00	0	0	0	0	0	0	0,00E+00	0,00E+00	N-hexane
N-heptane	0	0	0	0,00E+00	0	0	0	0	0	0	0,00E+00	0,00E+00	N-heptane
N-octane	0	0	0	0,00E+00	0	0	0	0	0	0	0,00E+00	0,00E+00	N-octane
N-nonane	0	0	0	0,00E+00	0	0	0	0	0	0,00E+00	0,00E+00	0,00E+00	N-nonane
TOTAL	Hliq(J/Kmol) =	0			Hvap(J/Kmol) =	6353440							
	Sliq(J/Kmol.K) =	0			Svap(J/Kmol.K) =	-8939,356							
	L (T,P) =	0			V (T,P) =	1	L (T0,P0) =	0			V (T0,P0) =	1	
Species	êliquid(J/Kmol)	êvapour(J/Kmol)	F(Kmol/s)	L (T,P)	V (T,P)	L (T0, P0)	V (T0,P0)	Exph [MW]	Fraction Exph	Exchem [MW]	Fraction Exchem		Species
H2O	900000	9490000	2,717355	0	1	0	1	158702,2907	0,005370119	0	0,142614227	0,00021925	H2O
N2		720000	2,717355	0	1	0	1	201377,9158	0,006814163		0,013338154	2,05056E-05	N2
O2		3970000	2,717355	0	1	0	1	0	0		0	0	O2
NO2		56000000	2,717355	0	1	0	1	0	0		0	0	NO2
NO		89040000	2,717355	0	1	0	1	3,54005E-05	1,19787E-12		2,87561E-10	4,42086E-13	NO
S		781143628	2,717355	0	1	0	1	0	0		0	0	S
SO2		303500000	2,717355	0	1	0	1	0	0		0	0	SO2
SO3		225070000	2,717355	0	1	0	1	0	0		0	0	SO3
H2		238490000	2,717355	0	1	0	1	28986435,51	0,980833964		635,9726567	0,977719965	H2
CL2		117520000	2,717355	0	1	0	1	0	0		0	0	CL2
HCL		85950000	2,717355	0	1	0	1	0	0		0	0	HCL
CO		275430000	2,717355	0	1	0	1	0	0		0	0	CO
CO2		20140000	2,717355	0	1	0	1	0	0		0	0	CO2
Ar		11690000	2,717355	0	1	0	1	0	0		0	0	Ar
Ne		27120000	2,717355	0	1	0	1	0	0		0	0	Ne
He		30290000	2,717355	0	1	0	1	0	0		0	0	He
CH4		836510000	2,717355	0	1	0	1	206327,2768	0,006981638		14,33606687	0,022039719	CH4
Ethane		1504360000	2,717355	0	1	0	1	3,433112538	1,16169E-07		0,000364271	5,60016E-07	Ethane
Propane		2163190000	2,717355	0	1	0	1	0,000170438	5,76723E-12		2,23834E-08	3,44114E-11	Propane
N-butane		2818930000	2,717355	0	1	0	1	0	0		0	0	N-butane
N-pentane		3477050000	2,717355	0	1	0	1	0	0		0	0	N-pentane
N-hexane		4134590000	2,717355	0	1	0	1	0	0		0	0	N-hexane
N-heptane		4786300000	2,717355	0	1	0	1	0	0		0	0	N-heptane
N-octane		5440030000	2,717355	0	1	0	1	0	0		0	0	N-octane
N-nonane		6093550000	2,717355	0	1	0	1	0	0		0	0	N-nonane
	Exchem [W]	6,50E+08						29552846,42	1		650,4646759	1	
	Exchem [MW] =	6,50E+02											
	Exph [W]	2,96E+07											
	Exph [MW]	2,96E+01											
	Exmix [(W]	-7,48E+05											
	Exmix [MW]	-7,48E-01											
	TOT Ex [MW]	679,27											